

**Genome-wide ribosome profiling reveals a translational  
enhancer function for TDP-43 in cellular models of  
neurodegenerative disease**

Dissertation with the aim of achieving a doctoral degree at the  
Faculty of Mathematics, Informatics and Natural Sciences  
Department of Biology of Universität Hamburg

Submitted by Nagammal Neelagandan  
2019, Hamburg, Germany

**Examiners of the dissertation**

Dr. Kent Duncan

Prof. Dr. Christian Lohr

Date of Defense- 26.04.2019

## PUBLICATION

1. **Neelagandan N**, Gonnella G, Dang S, Janiesch PC, Miller KK, Kuchler K, Marques RF, Indenbirken D, Alawi M, Grundhoff A, Kurtz S, Duncan KE (2018) TDP-43 enhances translation of specific mRNAs linked to neurodegenerative disease. *Nucleic Acids Res* 2018 Oct 24. doi: 10.1093/nar/gky972.

# TABLE OF CONTENTS

ACKNOWLEDGEMENT .....	7
ABSTRACT .....	8
ZUSAMMENFASSUNG .....	10
1 INTRODUCTION .....	12
1.1 NEURODEGENERATIVE DISEASES .....	12
1.1.1 TDP-43 PROTEINOPATHY .....	12
1.2. RNA-BINDING PROTEINS .....	16
1.2.1 RBPs AND TRANSLATIONAL REGULATION IN DISEASE .....	17
1.3. TAR DNA BINDING PROTEIN 43 (TDP-43) .....	18
1.3.1 DOMAINS OF TDP-43 .....	19
1.3.2. PATIENT MUTATIONS IN TDP-43 .....	19
1.3.3. TDP-43 ALS MODELS .....	20
1.3.4. POST-TRANSLATIONAL MODIFICATIONS (PTMs) OF TDP-43 .....	21
1.3.5. POTENTIAL PATHOMECHANISMS OF TDP-43 .....	22
1.4 EUKARYOTIC TRANSLATION .....	26
1.4.1 TRANSLATION INITIATION .....	27
1.4.2. TRANSLATION ELONGATION .....	28
1.4.3 TRANSLATION TERMINATION AND RIBOSOME RECYCLING .....	30
1.5. TRANSLATIONAL REGULATION .....	31
1.5.1 TRANSLATIONAL CONTROL IN NEURODEGENERATIVE DISEASES .....	32
1.5.2. NON-CANONICAL TRANSLATION .....	32
1.6 METHODS TO STUDY TRANSLATION .....	33
1.6.1 POLYSOME PROFILING .....	34
1.6.2. RIBOSOME PROFILING .....	35
1.6.3. TRANSLATING RIBOSOME AFFINITY PURIFICATION .....	35
2. AIMS OF THE PROJECT .....	37
3. MATERIALS .....	38
3.1. CELL CULTURE MEDIUM AND REAGENTS .....	38
3.2. RIBOSOME PROFILING BUFFERS .....	38
3.3. POLYSOME PROFILING BUFFERS .....	39
3.4 UV-CLIP BUFFERS .....	40
3.5. WESTERN BLOT BUFFERS .....	40
3.6 SUBCELLULAR FRACTIONATION .....	41
3.7 PRIMERS .....	42
3.8 PLASMIDS USED .....	43

3.9 ANTIBODIES.....	44
4. METHODS .....	46
4.1. MN1 CELL CULTURING.....	46
4.2 PRIMARY NEURONAL CULTURE .....	47
4.3 PLASMID CLONING.....	48
4.4 SUBCELLULAR FRACTIONATION.....	48
4.5 RIBOSOME FOOTPRINT PROFILING .....	49
4.6 ANALYSIS OF THE RIBOSOME PROFILING DATA.....	53
4.7 POLYSOME PROFILING.....	54
4.8 RNA EXTRACTION AND qRT PCR.....	55
4.9 ANALYSIS OF THE FRACTION OF RIBOSOMES IN POLYSOMES .....	55
4.10. CROSSLINK IMMUNOPRECIPITATION.....	56
4.11 IMMUNOSTAINING .....	56
4.12 MICROSCOPY IMAGE ANALYSIS.....	57
4.13 LUCIFERASE ASSAYS .....	57
4.14 WESTERN BLOTTING .....	58
4.15 STATISTICAL ANALYSIS AND PLOTS.....	58
5. RESULTS.....	<b>Error! Bookmark not defined.</b>
5.1 TRANSIENT TRANSFECTION OF MN1 CELLS SHOW SIMILAR EXPRESSION LEVELS OF HUMAN TDP-43 AND TDP-43 <sup>A315T</sup> PROTEINS.....	58
5.2 HUMAN TDP-43 <sup>A315T</sup> PROTEIN HAVE SLIGHTLY HIGHER EXPRESSION LEVEL THAN HUMAN TDP-43 IN PRIMARY CORTICAL NEURON CULTURE .....	60
5.3 SUBCELLULAR FRACTIONATION SHOWS BOTH HUMAN WT TDP-43 AND TDP-43 <sup>A315T</sup> ARE MOSTLY NUCLEAR.....	61
5.4 OVEREXPRESSION OF HUMAN TDP-43 OR TDP-43 <sup>A315T</sup> PROTEIN DOES NOT LEAD TO A SIGNIFICANT EFFECT ON GENERAL TRANSLATION.....	63
5.5 RIBOSOME FOOTPRINT PROFILING ON MN1 CELLS AND PRIMARY CORTICAL NEURONS REVEALS TRANSLATIONAL TARGETS OF TDP-43 .....	65
5.6 POLYSOME PROFILING CONFIRMS THAT hTDP-43 <sup>A315T</sup> PROTEIN INCREASES RIBOSOME DENSITY ON Camta1, Mig12, AND Dennd4a mRNAs IN MN1 CELLS ....	70
5.7 ASSESSMENT OF ALTERED FUNCTIONAL EFFECTS OF MASTER REGULATORS IN CELLS EXPRESSING hTDP-43/hTDP-43 <sup>A315T</sup> .....	74
5.8 TDP-43 PROTEIN INTERACTS DIRECTLY WITH Camta1, Mig12, AND Dennd4a mRNAs.....	76
5.9 hTDP-43 AND hTDP-43 <sup>A315T</sup> ENHANCE TRANSLATION OF Camta1 AND Mig12 mRNAs VIA THEIR 5'UTRS .....	78
5.10 hTDP-43 <sup>A315T</sup> ENHANCES TRANSLATION OF Dennd4a mRNA THROUGH A SPECIFIC 3'UTR REGION.....	80
5.11 VALIDATION OF CAMTA1 AND MIG12 ANITIBODIES.....	83

5.12 hTDP-43 OVEREXPRESSION LEADS TO INCREASED CAMTA1 AND MIG12 PROTEIN LEVELS IN MN1 CELLS.....	84
5.13 hTDP-43 <sup>A315T</sup> EXPRESSION LEADS TO INCREASED MIG12 PROTEIN LEVELS IN PROCESSES OF PRIMARY CORTICAL NEURONS.....	89
5.14 MID1, A DISEASE-ASSOCIATED MIG12 BINDING PARTNER, MODIFIES TDP-43'S EFFECTS ON MIG12 PROTEIN.....	91
5.15 OPTIMIZATION OF RIBOSOME PROFILING PROTOCOL FOR BETTER DATA QUALITY.....	93
6. DISCUSSION.....	104
6.1 TDP-43 IS REGULATING TRANSLATION OF SPECIFIC mRNAs.....	104
6.2 CELL BASED MODELS TO STUDY EARLY EFFECTS OF WILDTYPE AND MUTANT hTDP-43.....	105
6.3 IDENTIFICATION OF NEW TRANSLATIONAL TARGET mRNAs OF HUMAN TDP-43 <sup>A315T</sup> PROTEIN.....	106
6.4 CAMTA1 AND DENND4A ARE WELL-KNOWN MASTER REGULATORS OF NEURODEGENERATION.....	106
6.5 EFFECT OF HUMAN TDP-43 PROTEIN ON TRANSLATIONAL STATUS OF OTHER MASTER REGULATORS OF NEURODEGENERATION.....	108
6.6 POTENTIAL ROLE OF MID1IP1/MIG12 IN NEURODEGENERATION.....	111
6.7 SUCCESSFUL VALIDATION OF TDP-43 TRANSLATIONAL TARGETS USING POLYSOME PROFILING.....	112
6.8 IDENTIFICATION OF mRNA REGIONS IMPORTANT FOR TDP-43 TRANSLATIONAL REGULATION.....	112
6.9 IMPACT OF ALTERED mRNA TRANSLATION ON ENCODED PROTEIN LEVELS CAN BE DYNAMICALLY REGULATED.....	114
6.10 EFFECTS OF ALTERED TRANSLATIONAL REGULATION OF TDP-43 TARGETS AND THEIR IMPLICATION IN NEURODEGENERATION.....	116
6.11 FURTHER OPTIMIZATION OF RIBOSOME PROFILING IS REQUIRED TO GET MORE INSIGHTS INTO TDP-43- MEDIATED TRANSLATIONAL REGULATION.....	118
7. FUTURE PERSPECTIVES.....	120
REFERENCES.....	123

# ACKNOWLEDGEMENT

First, I would like to whole-heartedly thank my supervisor Dr. Kent Duncan for giving me the chance to work on this project in his lab, for all his guidance, mentoring, helpful discussions and opportunities to visit international scientific conferences.

I would like to thank my Thesis committee members Prof. Dr. Christian Kubisch and Prof. Dr. Hans-Jürgen Kreienkamp for their advice during the thesis. I would like to thank Prof. Dr. Christian Lohr for agreeing to co-supervise this project along with Dr. Kent Duncan and evaluating this thesis. Next I would like to thank the collaborators, Prof. Dr. Stefan Kurtz, Dr. Giorgio Gonnella and Malik Alawi for their efforts and inputs on this project.

Many thanks to Deutscher Akademischer Austauschdienst (DAAD) for offering me the scholarship research grants (Doctoral Programmes in Germany) for the past 3.5 years. It was a great honor.

I would like to express my sincere thanks to Katrin KÜchler, for all her help and support with maintenance of the mouse lines, genotyping, cloning and writing my manuscript. I would like to thank Eva Kronberg for mouse care. Many thanks to Christoph Janiesch for helping me set up various assays in the lab for this project, data analysis, discussions, writing my manuscript and this thesis (in particular, assisting with the German language). Thanks to Christoph and Katrin for helping me out especially during the first few weeks getting settled in Hamburg. I would like to thank Dr. Aida Cardona, for all the private discussions we had about our results in lab and during lunch and coffee breaks. Thanks to other members of Neuronal Translational control group: Dr. Kawssar Harb, Rita Marques, Florian Stelzner for the discussions we had during our lab meetings.

My heartfelt thanks to Edda Thies from Prof. Dr. Matthias Kneussel's lab and Birgit Schwanke from Dr. Froylan Calderon de Anda's lab, for their advice on establishing mouse primary neuronal cultures. I would like to thank Robin Scharrenberg and Froylan Calderon de Anda for helpful advice on image analysis. Froylan Calderon de Anda also gave helpful comments during various stage of this project. Thanks to other members of the ZMNH. In particular to the members of the ZMNH PhD Program Dr. Sabine Fleischer, Dr. Irm Hermans-Borgmeyer, Dr. Guido Hermey and Dr. Anne Willing.

Big thanks to all my friends in Germany and elsewhere who made this experience lot more fun: Jaqueline Gutzki, Henning Kayser, Francesca Xompero, Smruti Sourav Rout, Aritra Mukhopadhyay, Nisha Agrawal, Preeti Pandey, Udhaya Ponraj, Aswini Krishnan, Priyadharshini Arunachalam, Sethu Krishna. Thanks to my cousin Narayanan Perumal who gave me constant support throughout my PhD.

This thesis would not have been possible without the support and love of my family who I dedicate this thesis to- my father Neelagandan Subramonian, my mother Parvathy Neelagandan, my husband Giriram Kumar, my in-laws Mohana Sundara Shanmugam and Lalitha Mohana Sundara Shanmugam. Thank you does not cover the expanse of my gratitude.

## ABSTRACT

Altered function of the RNA-binding protein Transactive Response (TAR) DNA-Binding Protein 43 (TDP-43) is implicated in the neurodegenerative diseases frontotemporal dementia (FTD) and amyotrophic lateral sclerosis (ALS). TDP-43 mutations are detected in many patients and the protein is one of the major components of the ubiquitinated inclusions that are characteristic pathological features of these diseases. During disease, the level of cytoplasmic TDP-43 is significantly increased in diseased neurons. This increase in cytoplasmic TDP-43 levels suggests a potentially important role in this cellular compartment. In spite of significant research, it remains unclear how altered TDP-43 function causes disease. Cell and animal models support a key role in disease for altered regulation of cellular RNAs in motor neurons by TDP-43, including effects on transcription, splicing and stability.

Proteomic studies have revealed that TDP-43 interacts with many cytoplasmic proteins almost all of which are involved in translation. Intriguingly, many of these interacting proteins are also found in stress granules, dynamic cellular ribonucleoprotein structures believed to be important for translational control. Recent work has also implicated TDP-43 in transport of mRNAs in neurons, a process that is typically linked to translational control. To date, only a handful of TDP-43 translational targets have been identified. Taken together, these observations support the idea that TDP-43 might regulate translation in the cytoplasm in healthy neurons and that altered translational control by TDP-43 could contribute to disease. However, there is little evidence for this idea to date. Although previous studies have revealed TDP-43's direct RNA targets and function in many aspects of mRNA metabolism, it remains unresolved which effects on gene expression are the key drivers of disease.

Here, I used ribosome profiling of motor neuron cell lines and primary cortical neurons to identify mRNAs whose translation is altered by a TDP-43 patient mutant protein. This revealed a subset of translational target mRNAs for mutant TDP43, including some affected in both cell types. I validated increased ribosome density by polysome profiling in *Camta1*, *Mig12* and *Dennd4a* mRNAs and demonstrated that these are direct TDP-43 binding targets by UV crosslink-IP. *Camta1* and *Dennd4a* mRNAs encode proteins directly linked to ALS and other neurodegenerative



diseases. Interestingly, I found that the impact of altered mRNA translation on levels of the encoded protein can be cell-type and cell-compartment specific. Furthermore, using dual luciferase assays, I have defined the mRNA regions which mediate this positive translational regulation by TDP-43. The 5'UTR was important for *Camta1* and *Mig12* mRNAs and 3'UTR for *Dennd4a* mRNA. These results reveal a previously unappreciated role for TDP-43 as an mRNA-specific translational enhancer and suggest that this function contributes to disease.

## ZUSAMMENFASSUNG

Eine veränderte Funktion des RNA-Bindeproteins Transactive Response (TAR) DNA-Binding Protein 43 (TDP43) steht in Verbindung zu den neurodegenerativen Erkrankungen Frontotemporale Demenz (FTG) und Amyotrophe Lateralsklerose (ALS). Mutationen in TDP-43 wurden bisher in vielen Patienten gefunden, und das Protein ist als eine der Hauptkomponenten der, für die oben genannten Krankheiten charakteristischen, ubiquitinierten Einschlüsse bekannt. Im Krankheitsverlauf steigt in erkrankten Neuronen der Spiegel an zytoplasmatischem TDP-43 signifikant an und spricht für eine möglicherweise wichtige Rolle von TDP-43 in diesem zellulären Kompartiment. Trotz erheblichem Forschungsaufwand ist weiterhin unklar, wie die veränderte Funktion von TDP-43 zur Ausbildung von Krankheiten beiträgt. Zellkultur- und Tiermodelle unterstützen die These, dass TDP-43 eine Schlüsselrolle in der veränderten Regulation (einschließlich Transkription, Splicing und Stabilität) zellulärer mRNAs in Motoneuronen einnimmt.

Proteomische Studien haben gezeigt, dass TDP-43 mit vielen zytoplasmatischen Proteinen interagiert, die größtenteils am Prozess der Translation beteiligt sind. Verblüffenderweise finden sich viele dieser Proteine auch in Stress Granules, dynamischen, zellulären Ribonukleoproteinstrukturen, denen man eine wichtige Rolle in der Translationskontrolle zuschreibt. Jüngste Arbeiten haben TDP-43 auch mit dem Transport von mRNAs in Neuronen in Verbindung gebracht, einem Prozess, der typischerweise ebenfalls in Zusammenhang mit Translationkontrolle gebracht wird. Nur wenige validierte Zielproteine von TDP-43 konnten bisher identifiziert werden. Zusammengefaßt läßt sich aufgrund der genannten Beobachtungen feststellen, dass TDP-43 möglicherweise als Translationsregulator im Zytoplasma gesunder Neuronen wirkt und durch veränderte Kontrolle der Translation zur Ausbildung von Krankheiten beiträgt. Nichtsdestotrotz gibt es bisher nur wenige Beweise für diese These. Obwohl vorherige Studien sowohl die direkten Ziel-RNAs von TDP-43 als auch dessen Funktionsweise in vielen Aspekten des RNA-Metabolismus aufdecken konnten, bleibt ungeklärt, welche Effekte auf die Genexpression die Hauptverursacher der genannten Krankheiten sein könnten.

Im Rahmen dieser Arbeit habe ich Ribosomales Profiling von moto- und kortikoneuronalen Zelllinien zwecks Identifizierung von mRNAs, deren Translation durch eine Patientenmutation in TDP-43 verändert ist, durchgeführt. Dadurch wurden eine Reihe translationaler Ziel-mRNAs identifiziert, einige davon in beiden der verwendeten Zelltypen. Darüber hinaus konnte eine erhöhte ribosomale Dichte für die mRNAs von *Camta1*, *Mig12* und *Dennd4a* validiert und zugleich durch Crosslink-IPs gezeigt werden, dass diese mRNAs direkt von TDP-43 gebunden werden. *Camta1* und *Dennd4a* mRNAs kodieren für Proteine, die direkt mit ALS und weiteren neurodegenerativen Erkrankungen in Verbindung stehen. Interessanterweise konnte ich zeigen, dass der Einfluss veränderter mRNA-Translation auf die daraus resultierenden Mengen der kodierten Proteine sowohl zelltyp- als auch zellkompartimentspezifisch sein kann. Desweiteren habe ich durch Luciferase-Messungen die Regionen der mRNA Sequenzen bestimmt, die die beobachteten positiven translationalen Regulierungen durch TDP-43 vermitteln. Diese waren im Fall der *Camta1* und *Mig12* mRNAs das 5'UTR und im Fall der *Dennd4a* mRNA das 3'UTR. Diese Ergebnisse demonstrieren eine bisher nicht ausreichend wahrgenommene Rolle von TDP-43 als einen mRNA-spezifischen Enhancer und legen nahe, dass diese Funktion zur Ausbildung genannter Erkrankungen beiträgt.

# **1 INTRODUCTION**

## **1.1 NEURODEGENERATIVE DISEASES**

Neurodegenerative diseases cover a wide spectrum of neurological disorders and are marked by progressive neuronal loss and atrophy. These disorders present different symptoms like cognitive impairment and motor dysfunction. Neurodegenerative disorders include diseases like Alzheimer's disease (AD), Parkinson's disease (PD), amyotrophic lateral sclerosis (ALS), Huntington's disease (HD), dementia with Lewy bodies (DLB), progressive supranuclear palsy (PSP), multiple system atrophy (MSA), corticobasal degeneration (CBD), frontotemporal dementia (FTD), spinocerebellar ataxia (SCA) disorders, and spinal muscular atrophy (SMA), among others. Some of the proposed mechanisms leading to cell death in many neurodegenerative diseases include mitochondrial dysfunction, oxidative stress, loss of growth factors, proteasomal dysfunction, autophagic/lysosomal dysfunction, excitotoxicity, protein aggregation, prion-like spread, and neuroinflammation (Gan et al. 2018).

### **1.1.1 TDP-43 PROTEINOPATHIES**

Neurodegenerative diseases linked to the deposition of TDP-43 are termed 'TDP-43 proteinopathies' and include Amyotrophic lateral sclerosis (ALS), Frontotemporal dementia (FTD), Alzheimer's disease (AD) (Youmans and Wolozin 2012; Davis et al. 2017), Parkinson's disease (PD) (Nakashima-Yasuda et al. 2007), and Huntington's disease (HD). These diseases display similar TDP-43 pathological manifestations in neurons and glia, including the accumulation of detergent-resistant, ubiquitinated or hyper phosphorylated TDP-43 inclusions in the cytoplasm, along with nuclear loss of the protein. In this section, diseases that have strong causal link with TDP-43 will be discussed in detail.

#### **1.1.1.1 AMYOTROPHIC LATERAL SCLEROSIS (ALS)**

ALS manifests with degeneration of upper motor neurons (UMN) and lower motor neurons (LMN) and is therefore also called Motor Neuron disease in the UK. In the US, it is also known as Lou Gehrig's disease, after a famous baseball player who died from ALS. In the European population, the prevalence is estimated to be 2.6-3 per 100,000 people. ALS shows a male bias, with 1.2-1.5 men for every woman. The

average age of onset is between 55 and 70 years, with death in most cases about 3-4 years after onset and primarily due to respiratory failure (reviewed in (van Es et al. 2017)). The disease starts with a focal onset weakness of a muscle, followed by a gradual spread to other muscles, leading to atrophy, paralysis and death. UMN degeneration leads to muscle stiffness and spasticity, whereas, LMN degeneration leads to spontaneous muscle twitching (fasciculation), which then results in atrophy.

ALS has been classified into familial ALS (fALS), which occurs in 10% of patients, and sporadic ALS (sALS), which occurs in the majority of cases. *SOD1* was the first gene whose mutation was found to be associated with ALS (Rosen et al. 1993). More than 170 ALS-linked missense mutations of *SOD1* have been reported. *SOD1* mutations occur in almost 20% of familial and rare sporadic ALS cases (Figure. 1). Currently, there are more than 30 genes found to be associated with ALS. It is generally believed that due to the existing genetic variation of disease, ALS could be a collection of diseases with similar symptoms.

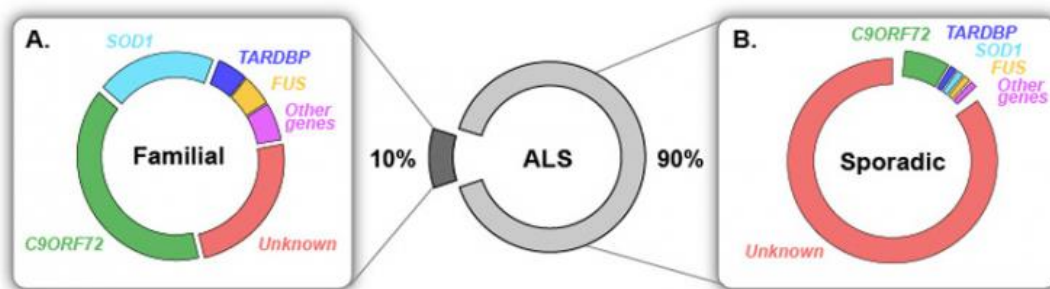


Figure 1: Known genetic causes of familial and sporadic ALS. 20% of fALS are due to mutations in *SOD1*. Mutations in TDP-43 and *FUS* account for ~5% of fALS each. Hexanucleotide repeat expansions in *C9ORF72* are the most common genetic cause of ALS accounting causing 40% of fALS and 7% of sALS. Figure adapted from (Laferriere and Polymenidou 2015).

Despite many preclinical studies for the last two decades, no effective treatments for the underlying cause have been identified. Riluzole, one of the two drugs used for treatment extends survival by three months on average. This drug is known to inhibit the excitotoxicity caused by the disease (Miller, Mitchell, and Moore 2012; Dharmadasa and Kiernan 2018). The free radical scavenger, Edaravone, was recently approved for ALS treatment by US Food and Drug Administration. This drug

is shown to be protective against the oxidative stress (Rothstein 2017; Ikeda and Iwasaki 2015).

TDP-43 was identified to be a major component of protein aggregates in ALS and in FTD in 2006 (Neumann et al. 2006; Arai et al. 2006). TDP-43-positive inclusions have subsequently been shown to be common to 97 % of ALS cases (Mackenzie et al. 2007; Turner et al. 2013). Following this, there were series of studies identifying many mutations in *TARDBP* gene causing both sporadic and familial forms of ALS (Sreedharan et al. 2008; Kabashi et al. 2008). Most patients with TDP-43 mutations display a classical ALS motor neuron phenotype without cognitive deficit, with some variability within families in the site and age of onset (Polymenidou and Cleveland 2017).

The discovery of TDP-43 mutations in ALS led to further studies identifying mutations in another DNA/RNA-binding protein called FUS/TLS (fused in sarcoma/ translocated in sarcoma) (Kwiatkowski et al. 2009). FUS predominantly localizes to the nucleus, whereas in ALS patients with FUS mutations, it is redistributed to the cytoplasm of affected cells where it accumulates and aggregates. ALS patients with FUS/TLS mutations display aggregates of FUS/TLS in the cytoplasm of neurons. Mutations in *FUS* account for ~5% of fALS. ALS patients with FUS/TLS mutations do not carry TDP-43 positive inclusions (Vance et al. 2009). This implies that neurodegenerative processes driven by FUS/TLS mutations are independent of TDP-43 aggregation.

	<b>Predominant pathology</b>	<b>Associated genes</b>
<b>Classic ALS</b>	TDP-43	ALS2, SETX, TARDBP, VAPB, CHMP2b, ANG, UBQLN2, OPTN, PFN1, TUBA4a, UNC13a, FIG4, ELP3, NEK1, C21orf2, SIGMAR1, DCTN1, MATR3, CHCHD10, VCP, hnRNPA1, hnRNPA2b1, NIPA1, SMN1, TBK1, ATXN2, MOBP, SARM1, UBQLN2, SQSTM1
<b>Classic ALS</b>	SOD1	SOD1
<b>Classic ALS</b>	FUS	FUS
<b>ALS with cognitive or behavioral impairment or comorbid FTD</b>	TDP-43	TARDBP, CHMP2b, TBK1, UBQLN2, SQSTM1, DCTN1, UNC13a

<b>Classic ALS, ALS-FTD, FTD</b>	TDP-43, p62, dipeptide repeats, RNA foci	C9orf72
----------------------------------	--	---------

Table1: Genes and pathology of ALS from (van Es et al. 2017)

In 2011, a major breakthrough discovery led to the identification of GGGGCC hexanucleotide repeat expansion in C9orf72 gene as the most common cause of ALS and FTD (Renton et al. 2011; DeJesus-Hernandez et al. 2011). In healthy controls, the typical repeat length is shorter than 25 units, but in ALS or FTD patients it goes up to 800-4400 units (Gijssels et al. 2012; DeJesus-Hernandez et al. 2011). There are three primary mechanisms through which the C9orf72 hexanucleotide repeat expansion has been known to cause neurodegeneration: 1. loss of function of C9orf72 gene due to reduced C9orf72 protein level; 2. formation of RNA foci and generation of expanded toxic RNA species; and 3. formation of aggregates of dipeptide repeat proteins (reviewed in (Haeusler, Donnelly, and Rothstein 2016). Although there has been a significant advancement in understanding ALS biology and pathophysiology, disease management by a curative therapy is lacking due to the multifactorial nature of the disease.

### 1.1.1.2 FRONTOTEMPORAL DEMENTIA

Frontotemporal dementia (FTD) is a cluster of syndromes that result from degeneration of the frontal and temporal lobes resulting in changes in behavior, language, executive control and often motor symptoms. The core spectrum of FTD disorders includes: behavioral variant FTD (bvFTD), nonfluent/agrammatic variant primary progressive aphasia (nfvPPA), and semantic variant PPA (svPPA) (reviewed in (Olney, Spina, and Miller 2017). There are three major inclusion pathologies have been identified in FTD patients, FTD-tau, FTD-TDP, FTD-FUS. Besides this, there are other disorders within the FTD spectrum that include FTD with motor neuron disease (FTD-MND), progressive supranuclear palsy syndrome (PSP-S) and corticobasal syndrome (CBS). FTD and ALS are considered as two extremes of a clinical continuum.

<b>Main clinical characteristics</b>		
<b>FTLD</b>	bvFTD	Disinhibition, apathy, lack of emotional concern, hyper orality, stereotypic behavior and executive dysfunction
	PNFA	Labored speech, agrammatism with relatively spared comprehension Comprehension deficits, naming errors with fluent speech
	SD	
<b>FTLD-MND-like</b>		FTLD with minor motor system dysfunction
<b>FTLD-ALS</b>		Meeting the diagnostic criteria of both FTLD and ALS
<b>ALSci</b>		ALS with minor cognitive impairment
<b>ALSbi</b>		ALS with minor behavioral impairment
<b>ALS</b>		Muscle weakness, hyperreflexia, spasticity, atrophy and fasciculations

Table 2: Diagnostic categories of the FTLD-ALS disease spectrum (Table from (Van Langenhove, van der Zee, and Van Broeckhoven 2012). ALSbi - ALS with a mild behavioral impairment; ALSci - ALS with a mild cognitive impairment.

Abnormal accumulation of TDP-43 in neuronal and glial inclusions is the characteristic neuropathological feature in approximately 50% of FTD patients (FTLD-TDP) (Neumann et al. 2006; Arai et al. 2006). FTD-TDP has been classified into four groups (A, B, C, D) based on TDP-43 neuropathology (Mackenzie et al. 2011).

## 1.2. RNA-BINDING PROTEINS

RNAs associate with RNA-binding proteins (RBPs) throughout their lifetime to form complexes called ribonucleoproteins (RNPs). The binding is influenced by sequence and/or structural motifs in RNA. Some well-defined RNA binding domains (RBDs) include the RNA recognition motif (RRM), hnRNP K homology domain (KH) or DEAD box helicase domain. Besides these, RBPs are also known to bind to their RNA targets via non-canonical RNA-binding domains. Various functions have been attributed to these RNA-RBP associations. Some of these functions include modulation of mRNA expression, localization, splicing and translation (reviewed in (Singh et al. 2015; Hentze et al. 2018)), indicating that disruption of this association might be deleterious to the cells.



### 1.2.1 RBPs AND TRANSLATIONAL REGULATION IN DISEASE

Many RBPs regulate translation and are connected to diseases. One of the best studied RBPs known to be involved in translation regulation is FMRP. Misregulation of FMRP is implicated in FXS, a condition characterized by impaired cognitive, physical, emotional, and sensory function. FMRP associates with polysomes and represses translation of a subset of mRNAs (Darnell et al. 2011; Darnell and Klann 2013; Brown et al. 2001). Upon neuronal stimulation, levels of FMRP increase leading to an increase in translation of its target mRNAs indicating an activity-mediated response (Nalavadi et al. 2012).

Other proteins involved in translation regulation linking disease include hnRNP A2/B1, hnRNP C, and TDP-43. hnRNP A2/B1 and hnRNP C were shown to be translational enhancers in various studies (Lee et al. 2010; Kwon, Barbarese, and Carson 1999). TDP-43's role in translation will be discussed in detail in section 1.3.5.6. However, it is worth noting that all studies involving translation regulation by TDP-43 to date have indicated that the protein acts as translational repressor. An overview of major RBPs implicated in diseases and their role in translation regulation are shown in table 3.

RBP	Function	Disease	Reference
<b>FMRP</b>	Repressor	FXS	(Darnell et al. 2011; Kwon, Barbarese, and Carson 1999)
<b>hnRNP A2/B1</b>	Activator	ALS, FTLN	(Kwon, Barbarese, and Carson 1999)
<b>hnRNP C</b>	Activator	AD	(Lee et al. 2010)
<b>IGHMBP2</b>	Regulator	SMA	(de Planell-Saguer et al. 2009; Grohmann et al. 2001)
<b>Musashi</b>	Repressor	AD	(Okano, Imai, and Okabe 2002; Perry et al. 2012)
<b>SMN</b>	Putative repressor	SMA	(Piazzon et al. 2008)
<b>TDP-43</b>	Repressor	ALS, FTLN	(Lagier-Tourenne, Polymenidou, and Cleveland 2010)

Table 3: List of RBPs involved in translation and implicated in neurological diseases from (Kapeli and Yeo 2012). AD, Alzheimer's disease; ALS, Amyotrophic lateral sclerosis; FTL, Frontotemporal lobar dementia; FXS, Fragile X syndrome; SMA, Spinal muscular atrophy.

### **1.3. TAR DNA BINDING PROTEIN 43 (TDP-43)**

TDP-43 is a ubiquitously expressed DNA-/RNA- binding protein, first identified as a transcription factor binding to the Transactive response (TAR) element of HIV-1 DNA thereby repressing transcription (Ou et al. 1995). However, further studies have shown that TDP-43 binds RNA and regulates various steps of mRNA regulation, including splicing, translation, stability and transport (Fiesel et al. 2012; Fiesel et al. 2010; Buratti and Baralle 2001; Ayala et al. 2011).

TDP-43 is predominantly a nuclear protein. But this protein has NES and NLS domains which help in shuttling back and forth the cytoplasm. TDP-43's role in neurodegenerative diseases was established in the year 2006 when two studies identified ubiquitinated TDP-43 aggregates in ALS and FTD patients (Neumann et al. 2006; Arai et al. 2006). It has been shown that the TDP-43 accumulates in the cytoplasm during disease along with nuclear depletion. In addition, it was also shown that cytoplasmic localization alone can cause neuronal death (Barmada et al. 2010). This supports the hypothesis that TDP-43 might cause neurodegeneration by gain of cytoplasmic toxic function.

Later studies showed that RNA binding activity of TDP-43 is important for its toxicity (Voigt et al. 2010), and splicing misregulation occurs in disease (Tollervey et al. 2011; Polymenidou et al. 2011). These studies converge on the importance of mRNA regulation by TDP-43 and its impact on disease.

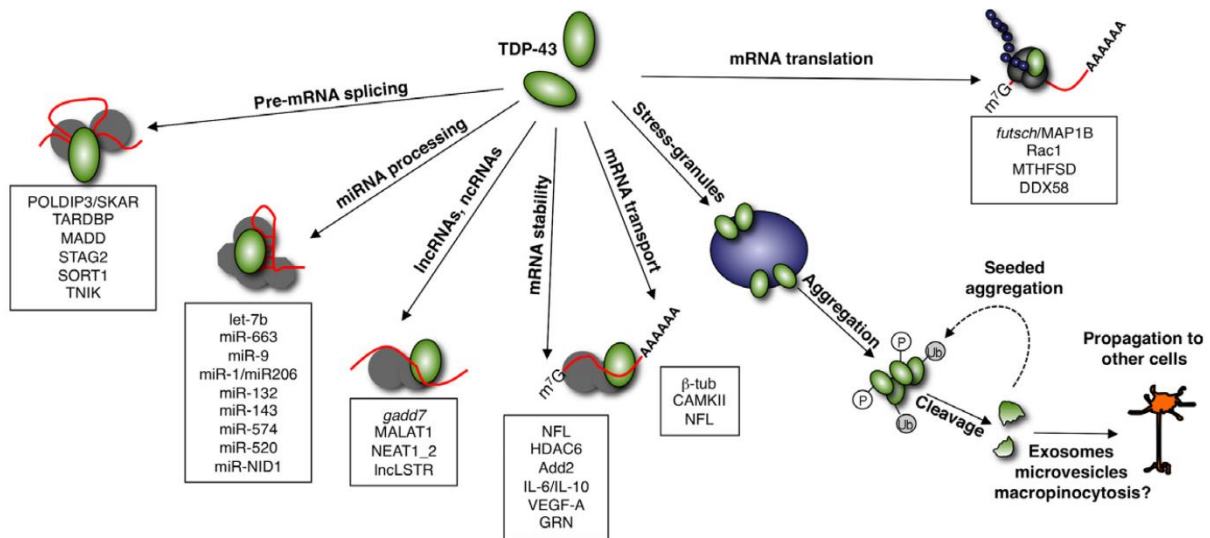


Figure 7: Schematic diagram of known TAR DNA binding protein 43 kDa (TDP-43) regulated cellular functions in the nuclear and cytoplasmic compartments. The boxes specify validated target genes for the corresponding functions indicated. Figure adapted from (Ratti and Buratti 2016).

### 1.3.1 DOMAINS OF TDP-43

TDP-43 is encoded by the *TARDBP* gene, located in the chromosomal region 1p36. This is a 414 amino acid protein (43 kDa) (Figure 7). TDP-43 protein has a nuclear localization signal (NLS) and nuclear export signal (NES), indicating that this protein shuttles between nucleus and cytoplasm. There are also two RNA recognition motifs (RRM1 and RRM2) facilitating the RNA binding activity of TDP-43. The C-terminal region which is called 'glycine rich region' (also called low complexity domain-LCD) is identified to be important for its interaction with other proteins (reviewed in (Lagier-Tourenne and Cleveland 2009)).

### 1.3.2. PATIENT MUTATIONS IN TDP-43

After the identification of TDP-43 as one of the major proteins found in the cytoplasmic aggregates of diseases like ALS and FTL, patients were screened for mutations in this protein (Sreedharan et al. 2008; Kabashi et al. 2008). These studies have resulted in more than 30 mutations of TDP-43, with most of them occurring in the C-terminal glycine-rich region. Mutant TDP-43 proteins, like the wild type protein, exhibit cytoplasmic accumulation and formation of aggregates.

In vitro studies on cultured motor neurons show that TDP-43 patient mutant proteins cause defective RNA processing and axonal transport (Arnold et al. 2013; Alami et al. 2014). It has also been shown that expressing patient mutant TDP-43 fails to rescue the motor neuronal defects caused by loss of endogenous protein (Kabashi et al. 2010; Alami et al. 2014).

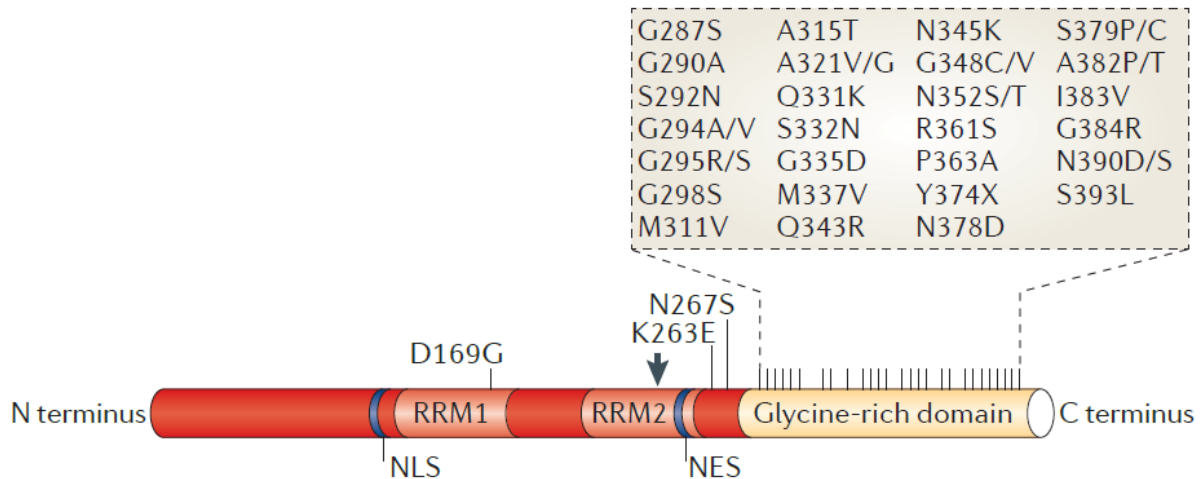


Figure 8: Schematic representation of TDP-43 protein with its domains and ALS-causing mutations. Most of the disease-causing mutations are found within or immediately adjacent to the glycine rich domain of the protein. Figure from (Lee, Lee, and Trojanowski 2012)

Numerous animal models have been established to study how these mutations alter the functions of TDP-43. These models have shown that toxicity driven by TDP-43 depends upon the transgene expression level, as the animals expressing higher TDP-43 levels exhibit stronger phenotypes than that of the ones expressing intermediate levels. The common observations from these animal models are axonal and/or neuronal degeneration, motor deficits and early lethality. Besides these, it has also been shown that both TDP-43 wild type and mutant protein can drive neurotoxicity and neurodegeneration when expressed at high level.

TDP-43 mutations account for 1-2% of the total ALS cases, but TDP-43 aggregates are found in patients without the mutation, suggesting that the disease phenotype occurs irrespective of TDP-43 mutations.

### 1.3.3. TDP-43 ALS MODELS

Studies so far have suggested that altered RNA metabolism in cytoplasm through a toxic gain of function and/or altered RNA metabolism through loss of function due to

nuclear depletion are major factors driving disease. Many rodent models have been generated to address this gain or loss of function component of TDP-43 driving disease. These models also cover various modes of TDP-43 expression: 1. Ubiquitous expression, 2. Neuron-specific expression and 3. Astrocyte-specific expression (to address non-cell autonomous effects) reviewed in (Philips and Rothstein 2015; Gendron and Petrucelli 2011).

One of the models which expresses human TDP-43 A315T mutant protein under control of the Prp promoter (Wegorzewska et al. 2009) shows selective degeneration of layer 5 cortical and motor neurons and these mice die around the age of 150 days. However, these animals did not exhibit TDP-43 cytoplasmic aggregates, suggesting that these are not required to cause TDP-43-mediated toxicity. Another mouse model, expressing wild type human TDP-43 protein under the Prp promoter (Xu et al. 2010) shows axonal and myelin degeneration and early lethality in homozygous state. These studies indicate that overexpression of not only the mutant protein but also the wild type human TDP-43 is toxic and leads to degenerative phenotypes. Another study has shown that TDP-43 dependent toxicity occurs does not require either nuclear clearing or formation of cytoplasmic aggregates (Arnold et al. 2013). Most importantly, none of the TDP-43-based animal models have been shown to replicate the extent of ALS phenotypes as seen in human patients due to lack of correlation between human and rodent ALS models seen in the pathology studies.

#### **1.3.4. POST-TRANSLATIONAL MODIFICATIONS (PTMs) OF TDP-43**

TDP-43 has been known to undergo some post-translational modifications (PTMs), especially in the aggregates. It has also been hypothesized that some of these modifications could explain the pathology (reviewed in (Buratti 2018)). Some of the most prevalent PTMs that are known to be associated with ALS/FTD are:

- Phosphorylation
- Ubiquitination
- Acetylation
- Cysteine oxidation
- Sumoylation
- Proteolytic cleavage to generate of C-terminal domain (CTD) fragments

Phosphorylation at serine, threonine and tyrosine residues within TDP-43 have been identified, of which serine 403,404,409 and 410 phosphorylation have been studied in detail (reviewed in (Gendron, Josephs, and Petrucelli 2010)). Casein kinase 1 has been identified as a likely candidate enzyme responsible for abnormal TDP-43 phosphorylation. In addition to this, another interesting link between disease and pTDP-43 comes from a C9orf72 mouse model (Schludi et al. 2017) which shows increased levels of phosphorylated TDP-43. Phosphorylation of TDP-43 has been shown to be involved in regulating its aggregation and oligomerization. Nevertheless, more studies are required to clearly define the impact of pTDP-43 on its physiological and pathological functions.

Another major PTM that has been frequently reported in ALS patients is proteolytic cleavage to generate CTD fragments with molecular weight of 20–25 kDa or 35 kDa. Some of the proteases that are shown to mediate TDP-43 cleavage include calpain, caspase 3, and caspase 4 (Yamashita et al. 2012; Dormann et al. 2009). Several lower molecular fragments have been described to occur due to combined caspase and calpain-cleavage after neurotoxic conditions and traumatic brain injury. Most of the ALS-causing mutations are found within these cleavage products. This region is important for hnRNP interactions and for mRNA splicing activity and studies have shown that overexpression of CTFs enhance aggregation of endogenous TDP-43. In addition to this, CTD has been reported to form amyloid-like  $\beta$ -sheet structures. Ubiquitination of aggregates in almost all affected patients represents the most characteristic feature of disease. In fact, the above mentioned three PTMs were the first identified PTMs of TDP-43 known to be associated with disease (Neumann et al. 2006; Arai et al. 2006).

### **1.3.5. POTENTIAL PATHOMECHANISMS OF TDP-43**

#### **1.3.5.1 pre-mRNA SPLICING**

TDP-43's nuclear function has been investigated by several groups so far, where splicing regulation in particular has been studied in great detail. It has been shown that TDP-43 acts as a repressor of cryptic splicing and that repression of TDP-43 leads to increased inclusion of cryptic exons in its targets (Ling et al. 2015). iCLIP studies have shown that TDP-43 binds to ~30% of the mouse transcriptome and that it has a significant impact on alternative splicing regulation (Tollervey et al. 2011;

Polymenidou et al. 2011). These studies have also shown that TDP-43 binds to tandem UG repeats or long clusters of UG repeat motifs. However, these UG repeat motifs are neither sufficient nor necessary for binding. These studies also show that pre-mRNA splicing is altered in disease, supporting the notion that loss of nuclear TDP-43 and associated effects on splicing would be a major disease driver (Tollervey et al. 2011; Polymenidou et al. 2011; Ling et al. 2015). Interestingly, another study also revealed that mild overexpression of hTDP-43 protein could lead to both loss- and gain-of-function effects on splicing of specific pre-mRNAs and identified mutant-specific events in mice expressing the patient mutant hTDP-43<sup>Q331K</sup> protein at a similar level to hTDP-43 (Arnold et al. 2013). In addition to this, most of the TDP-43 binding sites were identified to be intronic. However, in a recent study, TDP-43 LCDmut exhibited a gain of function phenotype, where the authors identified skipping of normally constitutively expressed exons (called skiptic exons) (Fratta et al. 2018). Additionally, TDP-43 is known to regulate its own transcript via splicing in its 3'UTR region leading to differential use of *TARDBP* alternative polyadenylation sites (Ayala et al. 2011). Importantly, this mechanism allows the autoregulation of *TARDBP* gene expression within cells to ultimately maintain TDP-43 protein levels within a physiological range.

#### **1.3.5.2. LncRNA AND ncRNA EXPRESSION**

Recent studies highlight emerging roles of misregulated long non-coding RNA (lncRNA) in aging and neurological disorders (Roberts, Morris, and Wood 2014; Grammatikakis et al. 2014). In line with this, TDP-43 has been shown to be directly binding *gadd7* lncRNA and affects TDP-43's interaction with cyclin-dependent kinase 6 (Cdk6) mRNA, resulting in Cdk6 mRNA degradation (Liu et al. 2012). In addition to this, TDP-43 has also been shown to be involved in expression of MALAT1 and NEAT1\_2 lncRNAs (Tollervey et al. 2011).

TDP-43 also directly interacts with other members of non-coding RNA (ncRNA) family and upon its knockdown expression level of ncRNAs are altered (Polymenidou et al. 2011). It has also been seen that TDP-43 binds to transcripts from Transposable Elements such as Short interspersed elements (SINE), Long interspersed elements (LINE), and Long terminal repeats (LTRs), and regulates their expression level (Li et al. 2012). However, the effect of altered regulation of ncRNAs in disease still remains to be understood and requires further studies.

### **1.3.5.3 NUCLEOCYTOPLASMIC TRANSPORT DEFECTS**

As mentioned earlier, TDP-43 mislocalizes to the cytoplasm in ALS and other neurodegenerative diseases. This could be due to impaired nuclear import of this protein which, in turn, suggests defective nucleocytoplasmic transport. A very recent TDP-43 aggregate interactome study shows enrichment of nuclear pore complex components and nucleocytoplasmic transport machinery (Chou et al. 2018). Furthermore, N2a cells expressing a TDP-43 C-terminal fragment exhibit an abnormal nuclear membrane. These findings were also replicated in primary cortical neurons and patient derived iPSCs expressing ALS associated mutant TDP-43. Additionally, brain tissues from sALS, TDP-ALS and C9orf72-ALS cases also exhibit nuclear pore defects (Chou et al. 2018). In ALS mutant SOD1 mouse models of ALS, alterations of NPC components include increased immunoreactivity of the nucleoporins GP210 and Nup205, the staining pattern of which reflects those in sALS patients (Shang et al. 2017). This indicates that a nucleocytoplasmic transport defect could be one of the common pathogenic features of ALS and FTD.

Additionally, some ALS- and FTD-associated mutations in FUS and hnRNP A1 were found in the NLS domains. Moreover, in a genetic screen performed in *Drosophila* to identify dominant modifiers of G<sub>4</sub>C<sub>2</sub> repeat-mediated toxicity, it was shown that loss of NUP50 strongly enhanced neurodegeneration (Freibaum et al. 2015).

### **1.3.5.4. miRNA PROCESSING**

TDP-43 is known to be involved in biogenesis of a subset of miRNA by interacting with Drosha complex in the nucleus and Dicer complex in the cytoplasm (Kawahara and Mieda-Sato 2012). Various studies have shown that depletion of TDP-43 leads to dysregulation of various miRNAs (King et al. 2014; Kawahara and Mieda-Sato 2012; Fan, Chen, and Chen 2014). Importantly, TDP-43 also regulates miRNAs that are implicated in cancer (Chen et al. 2017). However, how this regulation of miRNAs by TDP-43 causes disease is not well known.

### **1.3.5.5 ROLE OF TDP-43 IN STRESS GRANULES**

Stress granules (SGs) are membrane-less cytoplasmic assemblies of RNA/protein complexes formed during cellular stress. The role of SGs is to arrest translation of housekeeping genes, by sequestering their mRNAs, and to increase the selective translation of stress-responsive mRNAs facing the environmental insult. Following



stress removal, SGs dissolve and mRNA translation goes back to normal. The persistence of a stressful condition within cells is therefore considered as a major risk for inducing SGs to eventually become aberrant aggregates that are unable to be cleared by the protein quality system. One popular hypothesis is that SGs may facilitate formation of cytoplasmic aggregates in ALS.

Stress granules contain mRNAs that are translationally stalled along with translation initiation factors (eIF2, eIF3 and eIF4A/B/G). Other proteins commonly found to be in SGs include TIA1, PABP, and G3BP. TDP-43 has been shown to localize to SGs during various stress conditions including oxidative (arsenite), osmotic (sorbitol), ER (thapsigargin), heat, serum deprivation, proteasome inhibition (MG132), and mitochondrial stress (paraquat), where it co-localizes with SG markers (Liu-Yesucevitz et al. 2010; Freibaum et al. 2010; Dewey et al. 2011; Colombrita et al. 2009; McDonald et al. 2011). This implies that SGs play an important role in pathology of ALS. A recent study has shown that ALS-associated TIA1 alters the dynamics of SGs and it enhances the formation of TDP-43-containing SGs, which are less dynamic (Mackenzie et al. 2017).

TDP-43 knockdown has been shown to reduce oxidative stress-induced SG formation in HeLa cells by differentially regulating TIA1 and G3BP (McDonald et al. 2011). In addition to this, the same study also shows TDP-43 mutants display differential effects on SG dynamics. However, this is still unclear for majority of other TDP-43 mutants. Nevertheless, association of TDP-43 to SGs, which contain mRNAs whose translation is inhibited, hints that TDP-43 is involved in regulation of mRNA translation.

#### **1.3.5.6. TRANSLATIONAL REGULATION BY TDP-43**

Previous studies with cultured cells implicate TDP-43 in translation. Knocking down TDP-43 in HEK cells led to a global increase in translation, through indirect effects on SKAR (Fiesel et al. 2010) and cellular stress treatment was reported to lead to TDP-43 association with stalled ribosomes (Higashi et al. 2013). However, no specific mRNAs were examined in either of these studies. Indirect evidence that cytoplasmic TDP-43 could regulate translation of specific mRNAs comes from CLIP-Seq experiments demonstrating that TDP-43 binds to many mRNAs in their 3'UTR

(Tollervey et al. 2011; Polymenidou et al. 2011). There are other studies that show that other RBPs bind to 3'UTRs of their target mRNAs and regulate translation.

In *Drosophila*, TDP-43 negatively regulates translation of *futsch* (Coyne et al. 2014) and *hsc 70-4* (Coyne et al. 2017). Studies in cultured mammalian neurons also provide additional evidence for translational co-repression by TDP-43 and FMRP of Rac1, Map1b and GluR1 (GluA1) mRNAs (Majumder et al. 2016; Majumder et al. 2012). These directed studies with individual mRNAs indicate that TDP-43 can affect translation of specific mRNAs under certain circumstances. In addition to this TDP-43 has been shown to be implicated in regulation of mitochondrial mRNA translation (Wang et al. 2016). These studies indicate the need for a broader investigation of TDP-43's impact on translation in neurons and how it might contribute to neurodegenerative disease.

Furthermore, an in vivo study that performed genome-wide translating ribosome affinity purification on symptomatic TDP-43<sup>A315T</sup> mice revealed mRNAs with differential ribosome association in spinal motor neurons of mutant mice vs. controls. However, whether these differences reflect transcriptional or translational control remains to be determined. This study also identified DDX58 and MTHFSD as potential targets of TDP-43 that are misregulated in ALS (MacNair et al. 2016).

## **1.4 EUKARYOTIC TRANSLATION**

Translation is a tightly regulated step of gene expression and it is energetically demanding. Neurons are specialized cells which are dependent on spatial and temporal gene regulation due to their morphology and demands of synaptic plasticity. Recent studies have shown that dysregulated mRNA translation might lead to neurodegenerative diseases. Various RNA-binding proteins (RBPs) are known to regulate the process of translation. Translation is a cyclic process with steps of initiation, elongation, termination and ribosome recycling.

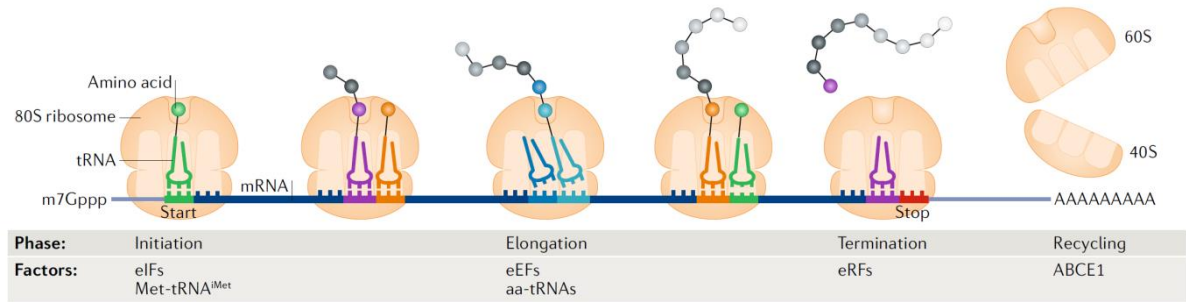


Figure 2: Overview of steps in translation. Translation involves complex coordination of eukaryotic translation factors, tRNAs, ribosomal subunits and mRNA to be translated. Figure adapted from (Schuller and Green 2018).

In eukaryotes, the majority of proteins are obtained from protein-coding genes in the nuclear genome and translated in the cytoplasm. A small subset of proteins is from the mitochondrial genome and is translated by the specialized protein synthesis machinery of the mitochondria.

Since my thesis focused on altered translational regulation, this section covers the major aspects of mammalian translation needed to appreciate my work.

### 1.4.1 TRANSLATION INITIATION

Most eukaryotic mRNAs undergo cap-dependent translation initiation. The canonical process of translation initiation begins with cap recognition. The small 40s ribosomal subunit binds to the initiator methionyl-tRNA (Met-tRNA<sup>i</sup>) in a ternary complex with GTP-bound eukaryotic initiation factor eIF2, along with other factors including eIF1, eIF1A, eIF5, and eIF3, to form the 43S preinitiation complex (PIC). This 43S PIC is recruited to the mRNA transcript at its m<sup>7</sup>G-cap by the eIF4F complex, which is composed of cap-binding protein eIF4E and scaffolding protein eIF4G, and RNA helicase eIF4A. eIF4B assists this process. The scaffolding protein eIF4G can also interact with poly(A) binding protein (PABP), facilitating circularization of the mRNA. This resulting complex moves along the 5'UTR of the transcript until a start codon in an optimal context is found in a process called 'ribosome scanning'.

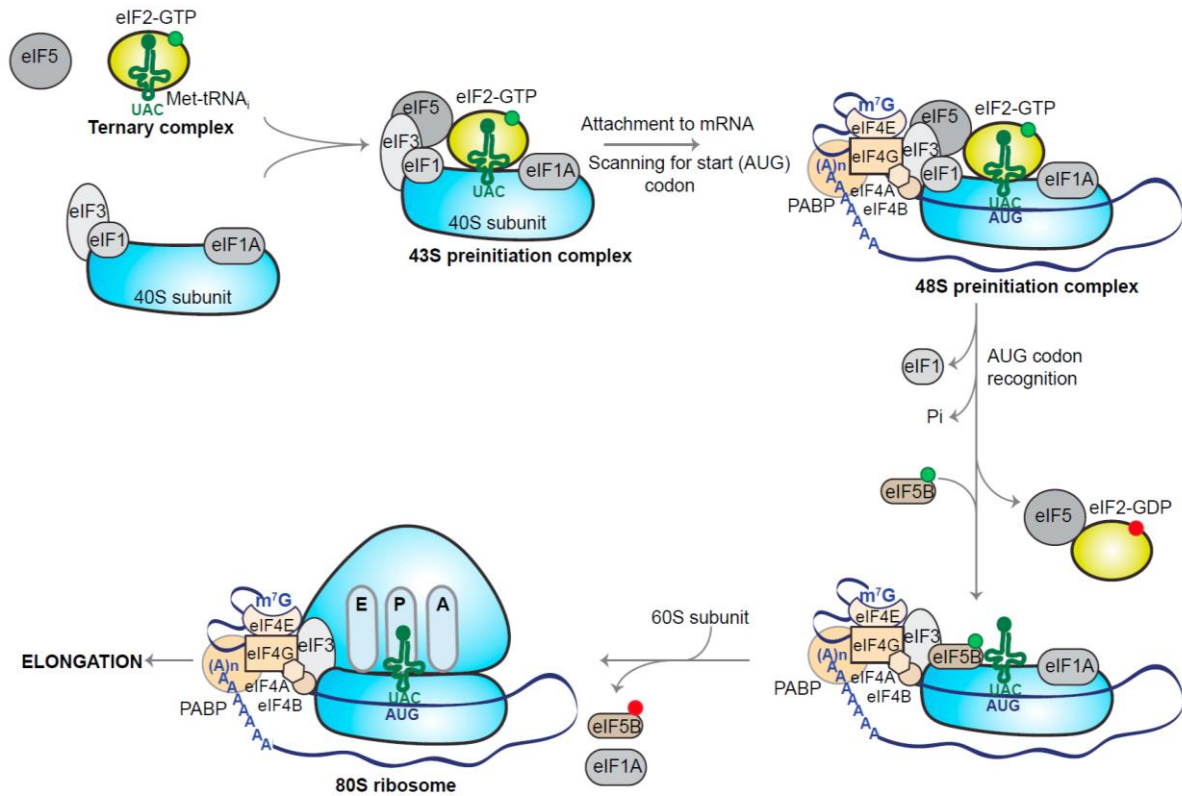


Figure 3: Eukaryotic Cap-Dependent Translation Initiation. Figure modified from (Kapur, Monaghan, and Ackerman 2017).

During this process of scanning, the 43s PIC will encounter a short stretch of nucleotide sequence flanking the start codon called 'Kozak sequence' that determines the association of 60S ribosomal subunit. The Kozak sequence consensus is (GCC)GCCRCCAUGG (Kozak 1987). Upon identification of a start codon, eIF2-GTP is hydrolyzed to eIF2-GDP, eIF1 is released and a new factor, eIF5B-GTP, associates with the complex. This is followed by hydrolysis of eIF5B-GTP to eIF5B-GDP allowing the large 60S ribosomal subunit to associate with the PIC to form a translationally active 80S initiation complex (Hinnebusch 2014).

### 1.4.2. TRANSLATION ELONGATION

Upon initiation, the Met-tRNA<sub>i</sub> is base paired to the AUG start codon and is placed in the peptidyl (P) site of the 80S ribosome. At this point, both the aminoacyl acceptor (A) site and the exit (E) site of the 80S ribosome are unoccupied. The second codon is placed at the A site and the corresponding tRNA is delivered by the eukaryotic elongation factor eEF1A-GTP. Cognate codon recognition by the tRNA triggers GTP hydrolysis and release of eEF1A-GDP from the tRNA. Next, peptide-bond formation

occurs, which transfers the peptide to the A-site tRNA, extending the nascent chain by one amino acid. Following this, the ribosome undergoes a major conformational change forming the so-called 'hybrid state'.

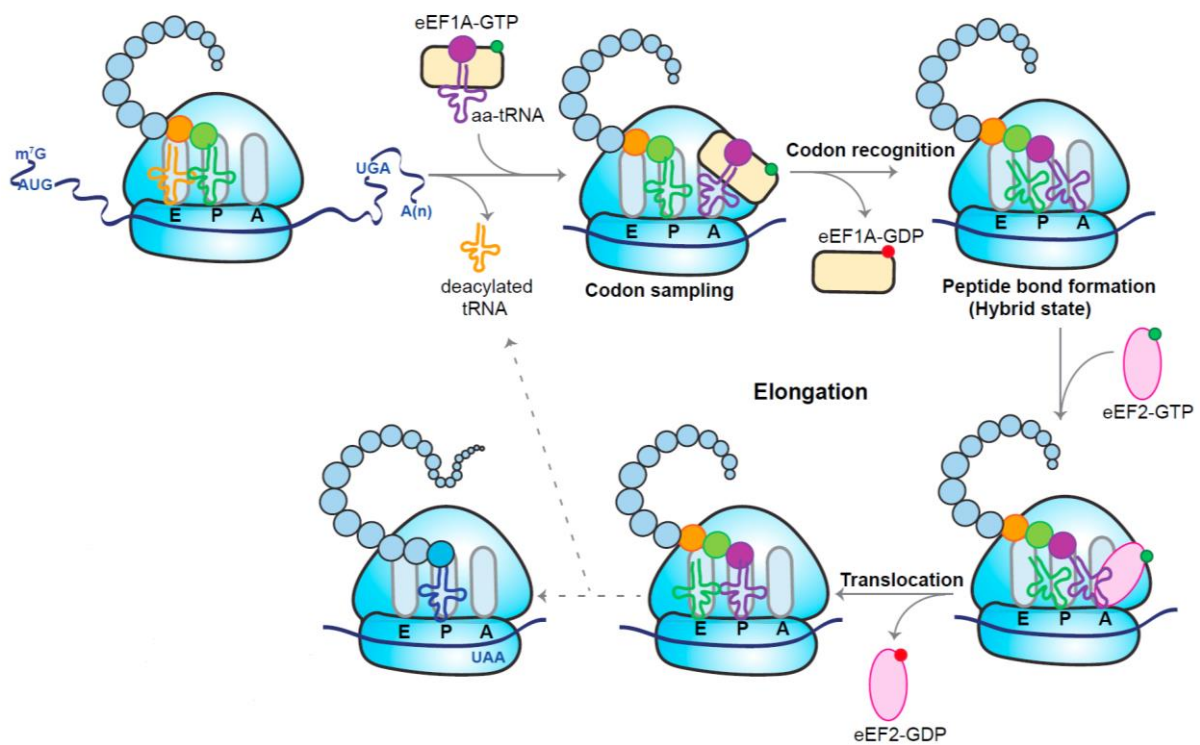


Figure 4: Eukaryotic Translation Elongation. Figure modified from (Kapur, Monaghan, and Ackerman 2017).

In this hybrid state, the amino acid acceptor stem of the tRNAs are in the E and P sites, while their anticodon loops remain in the P and A sites. The complete and stable translocation of the ribosome along the mRNA requires the entry of GTP-bound eEF2 into the A site. Binding of eEF2-GTP stabilizes the hybrid state, and promotes rapid GTP hydrolysis. The accompanying conformational changes reset the ribosome, with the deacylated tRNA released from the E site, the peptidyl-tRNA in the P site, and the vacant A site awaiting the next aminoacyl tRNA (reviewed in (Kapur, Monaghan, and Ackerman 2017; Dever and Green 2012)). This cycle is repeated until the elongating ribosome encounters a stop codon (UAA, UGA, or UAG) in the A site, triggering termination of translation.

### 1.4.3 TRANSLATION TERMINATION AND RIBOSOME RECYCLING

Eukaryotic translation termination is carried out by two release factors eRF1 and eRF3. eRF1, which is shaped similar to tRNA, is involved in stop codon recognition. Upon binding of the eRF1-eRF3-GTP ternary complex to the A-site, eRF1, which is the main catalytic factor of translation termination, triggers GTP hydrolysis and polypeptide release. Following this, ATP binding cassette protein 1 (ABCE1) interacts with eRF1 resulting in the splitting of 40S and 60S ribosomal subunits.

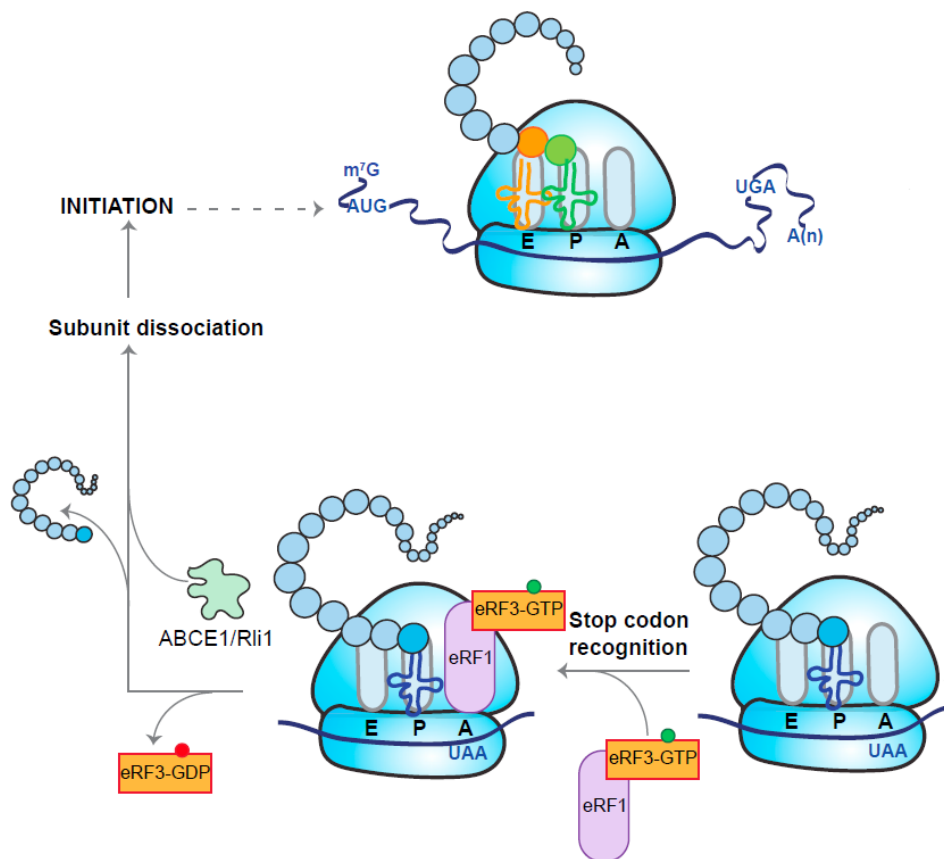


Figure 5: Eukaryotic Translation termination. Figure modified from (Kapur, Monaghan, and Ackerman 2017).

Finally, dissociation of the tRNA and mRNA from the 40S ribosome occurs via the action of numerous proteins, including some of the translation initiation factors, and the components are regenerated for another cycle of translation (Dever and Green 2012). Thus, accurate decoding of mRNA into protein requires tight coordination among ribosomes, elongation factors, tRNA molecules and the mRNA transcript itself.

## 1.5. TRANSLATIONAL REGULATION

Neurons are highly susceptible to any changes in translation fidelity. Various studies have shown the association of neurodegenerative diseases to errors in translational control (reviewed in (Kapur and Ackerman 2018)). Translational regulation could be either general, affecting large amount of mRNAs, or could be mRNA specific.

One major translational regulation pathway involved in neurodegeneration is phosphorylation of eIF2 $\alpha$ , which indicates activation of the integrated stress response (Pakos-Zebrucka et al. 2016). During the ISR, phosphorylation of eIF2 $\alpha$  by one of these four kinases, PKR (protein kinase R, EIF2AK2), PERK (PKR like endoplasmic reticulum kinase, EIF2AK3), GCN2 (general control non derepressible 2, EIF2AK4), and HRI (heme-regulated inhibitor, EIF2AK1) results in inhibition of general translation. Dephosphorylation is performed by two phosphatase complexes containing the catalytic subunit PP1c (protein phosphatase 1, PPP1C) and one of two regulatory subunits: CReP (constitutive repressor of eIF2a phosphorylation, PPP1R15B) or GADD34 (growth arrest and DNA damage-inducible 34, PPP1R15A). However, a subset of mRNAs is selectively translated. This includes transcription factor ATF4, which contains uORFs in its 5'UTR. Under normal conditions, translation of uORFs dominates the translation of main ORF. During stress, when eIF2 $\alpha$  is phosphorylated, there is an increased translation of main ORF resulting in the production of ATF4 proteins that promote recovery from stress (Shi et al. 1998; Harding, Zhang, and Ron 1999).

The second mechanism involved in general translational regulation is through m<sup>7</sup>G-cap recognition, thereby preventing recruitment of the translational machinery to the mRNA. As mentioned above, m<sup>7</sup>G-cap is recognized by eIF4E, however, proteins called eIF4E-binding proteins (4E-BPs) (Marcotrigiano et al. 1999) compete with eIF4G for interaction with eIF4E, preventing the formation of complex with eIF4F (Haghighat et al. 1995). The strength of binding of 4E-BPs to eIF4E is controlled by phosphorylation: hypophosphorylated 4E-BPs bind strongly, while phosphorylation of 4E-BPs by mTOR weakens the binding (reviewed in (Barbosa, Peixeiro, and Romao 2013)).

### **1.5.1 TRANSLATIONAL CONTROL IN NEURODEGENERATIVE DISEASES**

Dysregulation of eIF2 is associated with many neurodegenerative diseases. Increased levels of p-eIF2 $\alpha$  were found in cortex and hippocampus of AD mouse models (Unterberger et al. 2006) and in brain and spinal cord of patients with prion disease, ALS, PD, AD and various tauopathies (Unterberger et al. 2006; Kim et al. 2007; Ilieva et al. 2007). In accordance with these observations, eIF2 $\alpha$  kinases are activated in many models of neurodegeneration. In addition to this, reduction of p-eIF2 $\alpha$  levels by overexpression of the phosphatase GADD34 in prion infected mice restored levels of synaptic proteins and reversed synaptic dysfunction (Moreno et al. 2012). Recent studies have shown that small molecules interfering with the p-eIF2 $\alpha$  mediated translational dysfunction, rescued the pathology in these models (Halliday et al. 2017; Halliday et al. 2015).

p-eIF2 $\alpha$  levels are also increased in a *Drosophila* model of TDP-43-associated ALS that has impaired motor function. Knockdown of the fly homolog of PERK improved motor function, while knockdown of GADD34 aggravated the phenotype (Kim et al. 2014). Similarly, treatment with a PERK inhibitor diminished the toxicity of TDP-43 overexpression in rat neurons (Kim et al. 2014). In sharp contrast to this, other studies have suggested that eIF2 $\alpha$  phosphorylation in ALS may be protective. Administration of GADD34 inhibitor, guanabenz, delayed morbidity and death in SOD1G93A mice (Wang, Popko, and Roos 2014). Reduction of PERK levels genetically, in an ALS mouse model led to an accelerated phenotype and a hypomorphic GADD34 mutation slowed the disease course (Wang, Popko, and Roos 2014, 2011). Thus these observations emphasizes that ALS is a complex disease and the available animal models are diverse.

### **1.5.2. NON-CANONICAL TRANSLATION**

Microsatellite repeat expansions are known to cause a wide variety of neurodegenerative diseases including HD, C9orf72 ALS/FTD, Fragile X-associated tremor and ataxia syndrome (FXTAS), myotonic dystrophy (DM) type 1 and 2. One mechanism by which these microsatellite expansion cause disease is through production of novel toxic translational products generated from non-canonical start sites (also called repeat-associated non- ATG (RAN) translation). It was shown that



these repeat expansion mutations produce unexpected translational products from all three reading frames in the absence of an AUG initiation codon (Zu et al. 2011; Gaspar et al. 2000).

Studies have shown that C9orf72 expansion mutation undergoes RAN translation resulting in dipeptide repeat proteins (DPRs) with gly-pro (GP), gly-ala (GA), gly-arg (GR) in the sense strand and pro-arg (PR), pro-ala (PA) and gly-pro (GP) in the antisense strand (Zu et al. 2013). Several studies have shown that RAN translation is dependent on the repeat length and longer repeats are associated with accumulation of RAN proteins (Zu et al. 2013; Krauss et al. 2013; Krans, Kearse, and Todd 2016). It has also been shown that the flanking sequences affect RAN translation (Zu et al. 2011; Todd et al. 2013).

The products of RAN translation have been shown to be associated with impaired autophagy (Gupta et al. 2017). Interestingly, these proteins also interact nonspecifically with mRNAs, blocking their interactions with translation factors thereby reducing global translation (Kanekura et al. 2016). However, detailed studies are required to clearly define the mechanism of RAN translation and the effects of these RAN proteins in neurodegeneration.

## **1.6 METHODS TO STUDY TRANSLATION**

Gene expression at the translational level can be fine-tuned by a cell in response to a number of physiological and pathological situations. Translation regulation is one of the major processes governing cellular homeostasis in different conditions and biological situations such as stress or during different stages of development (Liu, Beyer, and Aebersold 2016). The correlation between transcript abundance and protein levels is poor, which is presumed to be mainly due to translational regulation. Thus, it is important to get a direct measure of translation to obtain a more accurate picture of gene expression. Some of the methods that are used to study translational regulation include polysome profiling, ribosome profiling and translating ribosome affinity purification (TRAP) (Figure 6). This section provides a brief overview of the principle aspects of each of these methods.

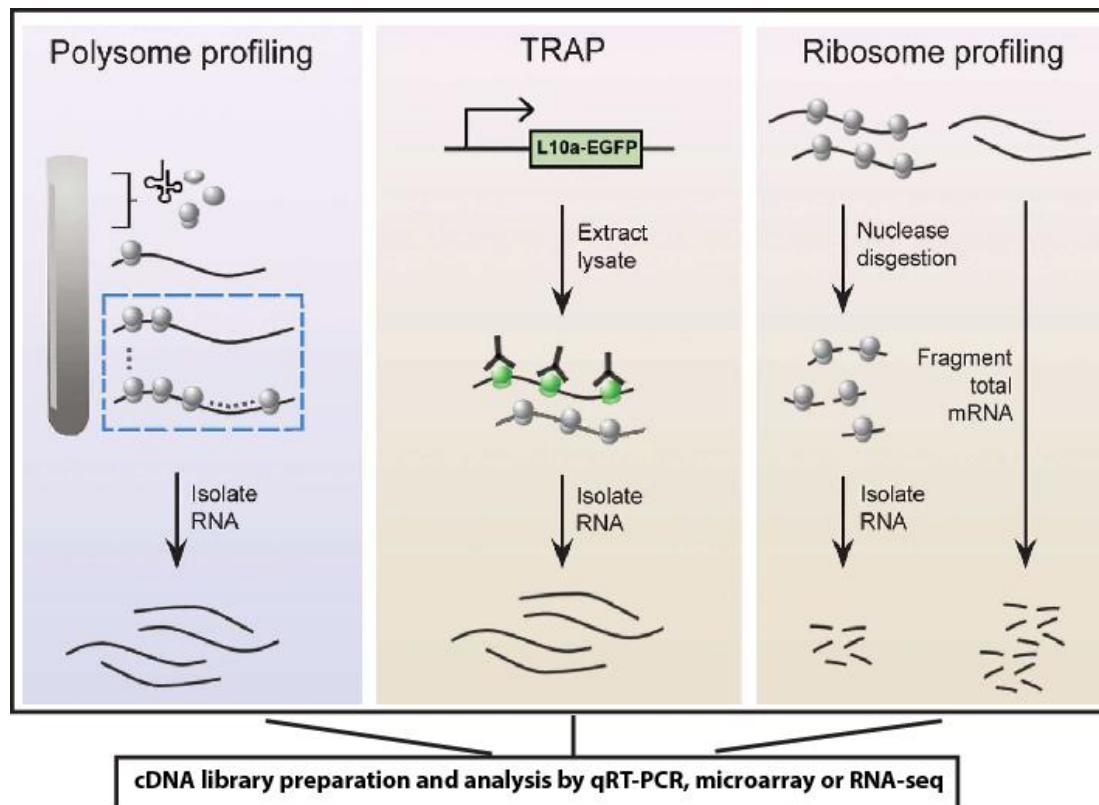


Figure 6: Methods to study translational regulation. Figure modified from (Kapeli and Yeo 2012).

### 1.6.1 POLYSOME PROFILING

In polysome profiling, translating mRNAs are separated on a sucrose gradient based on the number of ribosomes bound. This method is based on the observation that polysome-associated mRNAs are likely to be translationally active. Cells are lysed and loaded on a sucrose gradient followed by ultracentrifugation. Following ultracentrifugation, mRNAs are monitored at 254nm and the fractionated: untranslated mRNAs (top fractions) are separated from polysome-associated mRNAs (bottom fractions). mRNA extraction is carried out from these fractions. The translational status of a given mRNA species can be analyzed by northern blotting or qRT-PCR amplification, with relative quantification in each fraction. Alternatively, the content of the polysomal fractions can be identified using a global analysis approach (such as high-throughput sequencing), granting access to the cell translome (reviewed in (Chasse et al. 2017)). This method allows analysis of full length mRNAs giving access to the UTR information for isoform analysis. Polysome profiling has been widely used in studies examining changes in general translation, like studying effects of cellular stress where mRNAs shift from polysomes to non-translating lighter

fractions. A major disadvantage of this method lies in its underlying assumption that mRNAs bound by multiple ribosomes are translationally active. In fact, it has been shown that both active and stalled ribosomes co-sediment in sucrose gradients. This could be overcome by the use of puromycin which has been shown to selectively target actively translating ribosomes (Blobel and Sabatini 1971). Other drawbacks of the technique are this method is labor intensive and difficult to scale-up.

### **1.6.2. RIBOSOME PROFILING**

Ribosome profiling (Ingolia et al. 2009) provides a genome-wide measure of translation. This method involves nuclease digestion of cell lysates to obtain ~ 30 nucleotide long ribosome protected fragments (RPFs), also called “ribosome footprints”. RPFs are isolated either through sucrose gradients or cushions, followed by enzymatic manipulations and gel purification steps to generate a sequencing library. These isolated RPFs are identified by high-throughput sequencing, revealing the locations of ribosomes along transcripts at nucleotide-level resolution. Translation efficiency can be quantitatively measured using this method by ratio of ribosome density to total mRNA. This method has also been useful in identifying novel translational regulatory mechanism, like identification of new uORFs and non- AUG (non-canonical) initiation sites. This method has provided new insights into ribosomal pausing mechanism. Ribosome profiling has been implemented in many organisms including yeast, bacteria and mammalian systems. As ribosome-protected fragments are short, it is particularly challenging to deconvolve repetitive sequences or alternative transcripts in these data, and longer or paired-end sequencing reads cannot be used (reviewed in (Ingolia 2014)). Since ribosome footprints mainly map the coding sequence, this method does not provide information about translation of transcript isoforms with different 5' and 3' UTR elements.

### **1.6.3. TRANSLATING RIBOSOME AFFINITY PURIFICATION**

Translation ribosome affinity purification (TRAP) involves affinity purification of epitope-tagged ribosomes and associated mRNAs (Heiman et al. 2008). This method has proven to be a powerful technique *in vivo*, giving us a better understanding of translational control within the tissues of interest. In this method, genetically modified mice with EGFP-tagged ribosomal protein L10a driven by specific promoters are used. Polysome-associated RNA corresponding to the specific cell type is isolated by

immunoprecipitating for EGFP-L10a and can be examined different methods, for example by deep sequencing. This method could be extended to different cell types as described in (Doyle et al. 2008), but its utility is highly dependent on the availability of specific BAC driver lines.

## 2. AIMS OF THE PROJECT

TDP-43, an RBP, is heavily implicated in neurodegenerative diseases. Several studies indicate that RNA metabolism plays a crucial role in disease. More importantly, TDP-43 is usually located in the nucleus, but shuttles to the cytoplasm, and accumulates in this compartment in disease. Several lines of evidences suggest that cytoplasmic functions of TDP-43 could be relevant for the disease. In particular, previous studies have shown that TDP-43 is involved in translational regulation. However, only a few genes have been validated as translational targets of TDP-43 and all the identified targets are translationally repressed under certain circumstances. This motivates a broader investigation of TDP-43's impact on translation and how it might contribute to neurodegenerative disease. Techniques like ribosome footprint profiling and polysome profiling have substantially improved the way translational regulation is studied. For this project, I took advantage of these techniques to identify translational targets of TDP-43 and a patient mutant variant on a genome-wide scale.

Our hypothesis was that altered expression or mutation of TDP-43 affects translation of specific mRNAs in motor neurons and that this promotes disease.

My specific aims were as follows:

1. To identify specific mRNAs showing altered translation when TDP-43 is overexpressed or mutated.
2. To understand how TDP-43 affects translation of these mRNAs.
3. To learn how altered translation of these mRNAs might be disease relevant.

## 3. MATERIALS

### 3.1. CELL CULTURE MEDIUM AND REAGENTS

#### 3.1.1. MN1 CELL CULTURE REAGENTS

Reagent	Source	Final concentration
DMEM+ GlutaMAX	Gibco (61965-026)	1x (500mL)
FBS	Gibco (10270-106)	10%
Penstrep	Gibco (15140122)	1%
HEPES (1M) pH Range: 7.2-7.5	Gibco (15630-056)	2.4%

#### 3.1.2. PRIMARY NEURON CULTURE REAGENTS

Reagent	Source
poly-L-Lysine	Sigma (P2636)
Primary Neuro Basal Medium	Lonza (CC4462)
L- Glutamine	Lonza (CC4460HH)
NSF-1	Lonza (CC4459HH)
Penstrep	Gibco (15140122)
Cytosine $\beta$ -D-arabinofuranoside (Ara-C)	Sigma (C6645)

### 3.2. RIBOSOME PROFILING BUFFERS

#### 3.2.1 LYSIS BUFFER

Reagent	Source	Final concentration
Tris-Cl (pH 7.4)		20 mM
NaCl		150 mM
MgCl <sub>2</sub>		5 mM
Dithiothreitol (DTT)	Sigma (D9779)	1 mM
Cycloheximide (CHX)	Sigma (C7698)	100 $\mu$ g/mL
Triton X-100		1% (vol/vol)
Turbo DNase I	Thermo scientific (AM2239)	25 U/ ml

#### 3.2.2 GRADIENT BUFFER

Reagent	Source	Final concentration
Tris-Cl (pH 7.4)		20 mM
NaCl		150 mM
MgCl <sub>2</sub>		5 mM
Dithiothreitol (DTT)	Sigma (D9779)	1 mM
Cycloheximide (CHX)	Sigma (C7698)	100 $\mu$ g/mL
SUPERaseIn	Invitrogen (AM2694)	20 U/mL

#### 3.2.3 Poly-A SELECTION- BINDING BUFFER

Reagent	Final concentration
Tris-Cl (pH 7.5)	20 mM
LiCl	1 M
EDTA (pH 8.0)	2 mM

### 3.2.4 Poly-A SELCTION WASH BUFFER

Reagent	Final concentration
Tris-Cl (pH 7.5)	10 mM
LiCl	150 mM
EDTA (pH 8.0)	1 mM

### 3.2.5 DNA GEL EXTRACTION BUFFER

Reagent	Final concentration
Tris-Cl (pH 8.0)	10 mM
NaCl	300 mM
EDTA (pH 8.0)	1 mM

### 3.2.6 REVERSE INDEXED LIBRARY PRIMERS

Index	Sequence
ACAGTG	5'CAAGCAGAAGACGGCATAACGAGAT <b>CACTGT</b> GTGACTGGAGTTCAGACGTG TGCTCTTCCG3'
GCCAAT	5'CAAGCAGAAGACGGCATAACGAGAT <b>ATTGGC</b> GTGACTGGAGTTCAGACGTG TGCTCTTCCG3'
CTTGTA	5'CAAGCAGAAGACGGCATAACGAGAT <b>TACAAG</b> GTGACTGGAGTTCAGACGTG TGCTCTTCCG3'
GTGAAA	5'CAAGCAGAAGACGGCATAACGAGAT <b>TTTCAC</b> GGTGTGACTGGAGTTCAGACGT GTGCTCTTCCG3'
ATCAGT	5'CAAGCAGAAGACGGCATAACGAGAT <b>ACTGAT</b> GTGACTGGAGTTCAGACGTG TGCTCTTCCG3
CAGCAT	5'CAAGCAGAAGACGGCATAACGAGAT <b>ATGCTG</b> GTGACTGGAGTTCAGACGTG TGCTCTTCCG3

### 3.2.7 BIOTINYLATED OLIGOS

Oligo sequence	Reference
GGGGGGATGCGTGCATTTATCAGATCA	NR_003278.1
TTGGTGACTCTAGATAACCTCGGGCCGATCGCACG	NR_003278.1
GAGCCGCCTGGATACCGCAGCTAGGAATAATGGAAT	NR_003278.1
TCGTGGGGGGCCCAAGTCCTTCTGATCGAGGCC	NR_003279.1
GCACTCGCCGAATCCCGGGGCCGAGGGAGCGA	NR_003287.1
GGGGCCGGGCCGCCCTCCACGGCGCG	NR_003279.1
GGGGCCGGGCCACCCCTCCACGGCGCG	NR_003287.1
CCCAGTGCGCCCGGGCGTCGTCGCGCCGTCGGTCCCGG	NR_003279.1
TCCGCCGAGGGCGCACCAACGGCCCGTCTCGCC	NR_003279.1
AGGGGCTCTCGTCTTGGCGCCAAGCGT	NR_003279.1
GAGCCTCGGTTGGCCCCGGATAGCCGGTCCCGT	NR_003279.1
GAGCCTCGGTTGGCCTCGGATAGCCGGTCCCGCG	NR_003287.1
TCGCTGCGATCTATTGAAAGTCAGCCCTCGACACA	NR_003287.1
TCCTCCCGGGGCTACGCCTGTCTGAGCGTGC	NR_003280.1

## 3.3. POLYSOME PROFILING BUFFERS

### 3.3.1 LYSIS/GRADIENT BUFFER:

Reagent	Source	Final concentration
Tris-Cl (pH 7.4)		20 mM

<b>NaCl</b>		100 mM
<b>MgCl<sub>2</sub></b>		5 mM
<b>Cycloheximide (CHX)</b>	Sigma (C7698)	50 µg/mL
<b>NP-40</b>		0.4% (vol/vol)
<b>Complete mini EDTA-free protease inhibitor cocktail</b>	Roche (11836170001)	1X
<b>RNaseIn</b>	Promega, (N2615)	100 U/mL
<b>SUPERaseIN</b>	Invitrogen (AM2694)	20 U/mL

### 3.4 UV-CLIP BUFFERS

#### 3.4.1 LYSIS BUFFER

Reagent	Source	Final concentration
<b>Tris-Cl (pH 7.4)</b>		50 mM
<b>NaCl</b>		100 mM
<b>SDS</b>		0.1%
<b>Sodium deoxycholate</b>		0.5%
<b>NP-40</b>		1% (vol/vol)
<b>Complete mini EDTA-free protease inhibitor cocktail</b>	Roche (11836170001)	1X

#### 3.4.2 HIGH SALT BUFFER

Reagent	Final concentration
<b>Tris-Cl (pH 7.4)</b>	50 mM
<b>NaCl</b>	1 M
<b>SDS</b>	0.1%
<b>Sodium deoxycholate</b>	0.5%
<b>NP-40</b>	1% (vol/vol)
<b>EDTA (pH 8.0)</b>	0.1 %

#### 3.4.3 WASH BUFFER

Reagent	Final concentration
<b>Tris-Cl (pH 7.4)</b>	50 mM
<b>NaCl</b>	10 mM
<b>Tween-20</b>	0.2 % (vol/vol)

#### 3.4.4 NT2 BUFFER:

Reagent	Final concentration
<b>Tris-Cl (pH 7.4)</b>	50 mM
<b>NaCl</b>	150 mM
<b>NP-40</b>	0.05% (vol/vol)
<b>MgCl<sub>2</sub></b>	1 mM

### 3.5. WESTERN BLOT BUFFERS

#### 3.5.1 LYSIS BUFFER (RIPA BUFFER)

Reagent	Source	Final concentration
<b>Tris-Cl (pH 8)</b>		10 mM
<b>NaCl</b>		150 mM



<b>SDS</b>		0.1%
<b>EDTA (pH 8)</b>		10 mM
<b>NP-40</b>		1% (vol/vol)
<b>Complete mini EDTA-free protease inhibitor cocktail</b>	Roche (11836170001)	1X

### 3.5.2 RUNNING BUFFER

Reagent	Final concentration
<b>Tris base</b>	25 mM
<b>Glycine</b>	190 mM
<b>SDS</b>	0.1 %

### 3.5.3 TRANSFER BUFFER

Reagent	Final concentration
<b>Tris base</b>	25 mM
<b>Glycine</b>	190 mM
<b>Methanol</b>	20%

### 3.5.4 TBST (Tris- buffered saline with Tween 20)

Reagent	Final concentration
<b>Tris (pH 7.5)</b>	20 mM
<b>NaCl</b>	150 mM
<b>Tween 20</b>	0.1 %

## 3.6 SUBCELLULAR FRACTIONATION

### 3.6.1 BUFFER A

Reagent	Source	Final concentration
<b>HEPES, pH 8</b>		10 mM
<b>MgCl<sub>2</sub></b>		1.5 mM
<b>KCl</b>		10 mM
<b>DTT</b>		0.5 mM
<b>Complete mini EDTA-free protease inhibitor cocktail</b>	Roche (11836170001)	1X

### 3.6.2 BUFFER S1

Reagent	Source	Final concentration
<b>Sucrose</b>		0.25 mM
<b>MgCl<sub>2</sub></b>		10 mM
<b>Complete mini EDTA-free protease inhibitor cocktail</b>	Roche (11836170001)	1X

### 3.6.3 BUFFER S3

Reagent	Source	Final concentration
<b>Sucrose</b>		0.88 mM
<b>MgCl<sub>2</sub></b>		5 mM
<b>Complete mini EDTA-free protease inhibitor cocktail</b>	Roche (11836170001)	1X

### 3.6.4 LYSIS BUFFER (5X)

Reagent	Source	Final concentration
Tris, pH 7.4		250 mM
NaCl		750 mM
NP-40		5%
Sodium deoxycholate		2.5%
Complete mini EDTA-free protease inhibitor cocktail	Roche (11836170001)	1X

## 3.7 PRIMERS

### 3.7.1 qRT-PCR PRIMERS

mRNA	Forward primer (5'-3')	Reverse primer (5'-3')
<i>Camta1</i>	ATTCTGCGGAAGTAGCACCT	ATTTGCGGCAGACATTCAAGC
<i>Dennd4a</i>	GTCAGGGCTCTGAAAAGTGC	GTCCACAGAGCTGCATGAGA
<i>Mig12</i>	AGCACTGAGAACCAGGGGAT	GGCTGCTCTTATCTTTGGCT
<i>Gapdh</i>	TTGATGGCAACAATCTCCAC	CGTCCCGTAGACAAAATGGT
<i>Pth1r</i>	CACTAAGCTTCGGGAGACCA	GGCCATGAAGACGGTGTAGT
<i>Tardbp</i>	CGTGTCTCAGTGTATGAGAGGAGTC	CTGCAGAGGAAGCATCTGTCTCATCC
<i>18s rRNA</i>	CTTAGAGGGGACAAGTGGCG	ACGCTGAGCCAGTCAGTGTA
<i>Rluc</i>	TGGTAACGCGGCCTCTTCT	GCCTGATTTGCCCATACCAA
<i>Fluc</i>	GTTTCCAAAAAGGGGTTG	CATCGACTGAAATCCCTGGT
<i>Nfkb</i>	GAACGATAACCTTTGCAGGC	ATTTGATTCCGCTATGTGTG
<i>App</i>	GTTTACCACAGAACATGGCG	CTTGGCACTGCTCCTGCT
<i>Tcf7</i>	GTGGACTGCTGAAATGTTTCG	CTTCAATCTGCTCATGCCCT
<i>Atf5</i>	CGCTCAGTCATCCAATCAGA	TGGGCTGGCTCGTAGACTAT
<i>Myb</i>	GCGTTCACGTATTTCCGAG	TGCCTCAAAGCCTTTACCG
<i>Satb1</i>	CTTCGGATCATCGACAGGTT	GAAGCGTGCTAAAGTGTCCC
<i>Zdhhc2</i>	TAAGCCATGAGGCACACAAC	TCTACTGGATCCCGGTGGT

### 3.7.2 CLONING PRIMERS

Oligo name	Forward primer (5'-3')	Reverse primer (5'-3')
<i>Camta1</i> 5'UTR	CTAGGGGCGGCGGGGTGGCTGGGC CGGCGGCGGCGGCGGTACGAGGCG CGCGCTCGGGTCCCGTTCGCGAG GAGGAGGAGGGGTAC	CCCTCCTCCTCCTCGGACCGGGACCC CGAGCGCGCGCCTCGTACCGCCGCCG CCGCCGGCCAGCCACCCCGCCGCC
<i>Camta1</i> 3'UTR	ATAGCGGCCGCAGACATACAGCAGC ATCCCTTAGCAATGTGAC	TATACGCGTGGGGAAATTTTCTTCATTT TTAATTTACAGCAGAAAG
<i>Mig12</i> 5'UTR	ATACCTAGGATCAGGCGAGAGGCGG AGC	TATGGTACCGGTGGCCGAGCGGGC

<b><i>Mig12</i> 3'UTR</b>	ATACTCGAGTCTCGGGTCGGCTCTA CC	TATACGCGTGTTTTAAATAACAAGACA TATAACAACAGTGGA
<b><i>Dennd4a</i> 5'UTR</b>	CTACCTAGGATGGCGCCGGCCGCG	GATGGTACCCTTCCATCACAGAGTTTAT ATCCATTCAAGCAACTAATG
<b><i>Dennd4a</i> 3'UTR</b>	ATACTCGAGGACGTGTGTGTATATGT ATACATTCAATATATATTGTATAG	TATACGCGTTGAAGTAAAAATAAGTATT TATTGCCTAAAATGCTGAACC

### 3.8 PLASMIDS USED

Plasmid name	Plasmid information
pCMV sport6 FLAG-hTDP-43-V5	Plasmid encoding hTDP-43 protein with FLAG tag at N- terminus and V5 tag at C- terminus
pCMV sport6 FLAG-hTDP-43 <sup>A315T</sup> -V5	Plasmid encoding hTDP-43 mutant protein with FLAG tag at N- terminus and V5 tag at C- terminus
pCMV sport6 FLAG-hTDP-43 NES-V5	Plasmid encoding hTDP-43 protein containing extra nuclear export signal, FLAG tag at N- terminus and V5 tag at C- terminus
pCMV sport6-Fluc	Plasmid encoding firefly luciferase enzyme
pCMV sport6- Rluc	Plasmid encoding Renilla luciferase enzyme
pCMV sport6- Camta1 5'UTR Rluc	Plasmid containing Renilla luciferase sequence with 5'UTR of mouse <i>Camta1</i> mRNA
pCMV sport6- Camta1 3'UTR Rluc	Plasmid containing Renilla luciferase sequence with 3'UTR of mouse <i>Camta1</i> mRNA
pCMV sport6- Mig12 5'UTR Rluc	Plasmid containing Renilla luciferase sequence with 5'UTR of mouse <i>Mig12</i> mRNA
pCMV sport6- Mig12 3'UTR Rluc	Plasmid containing Renilla luciferase sequence with 3'UTR of mouse <i>Mig12</i> mRNA
pCMV sport6- Dennd4a 5'UTR Rluc	Plasmid containing Renilla luciferase sequence with 5'UTR of mouse <i>Dennd4a</i> mRNA
pCMV sport6- Dennd4a 3'UTR Rluc	Plasmid containing Renilla luciferase sequence with 3'UTR of mouse <i>Dennd4a</i> mRNA
pCMV sport6- Dennd4a 3'UTR Rluc 1-214	Plasmid containing Renilla luciferase sequence with 1-214 nt 3'UTR of mouse <i>Dennd4a</i> mRNA
pCMV sport6- Dennd4a 3'UTR Rluc 1-445	Plasmid containing Renilla luciferase sequence with 1-445 nt 3'UTR of mouse <i>Dennd4a</i> mRNA
pCMV sport6- Dennd4a 3'UTR Rluc 1-607	Plasmid containing Renilla luciferase sequence with 1-607 nt 3'UTR of mouse <i>Dennd4a</i> mRNA

<b>pcDNA3-FLAG-Mig12 ( kind gift from Prof. Jay Horton, UT Southwestern Medical Center, Dallas)</b>	Plasmid encoding MIG12 protein with FLAG tag at N- terminus
<b>pcDNA3-mycGFP-Mid1 (kind gift from Dr Germana Meroni, University of Trieste, Trieste, Italy)</b>	Plasmid encoding MID1 protein with myc GFP tag at N- terminus
<b>pEGFP-C1</b>	Plasmid containing enhanced GFP sequence

## 3.9 ANTIBODIES

### 3.9.1 PRIMARY ANTIBODIES USED IN WB AND ICC

Antigen	Dilution WB	Dilution ICC	Host species	Source
<b>Human TDP-43</b>	1:500		Mouse	Novus biologicals (H000023435-M01)
<b>TDP-43</b>	1:1000		Rabbit	CST (3448)
<b>GAPDH</b>	1:1000 - 1:2000		Mouse	Sigma (G8795)
<b>FLAG</b>	1:1000		Mouse	Sigma (F1804)
<b><math>\alpha</math>Tubulin</b>	1:1000		Mouse	Sigma (T5168)
<b>Cofilin</b>	1:2000		Rabbit	Abcam (ab42824)
<b>Phospho-Histone H3</b>	1:1000		Rabbit	CST (9701)
<b>V5</b>	1:1000	1:100	Mouse	Invitrogen (46-1157)
<b>MID1IP1/MIG12</b>	1:250	1:100	Rabbit	Sigma (HPA038816)
<b>CAMTA1</b>		1:100	Rabbit	Sigma (HPA036343)
<b>Tau1</b>		1:100	Mouse	Millipore (MAB3420)
<b>Acetylated-Tubulin</b>		1:750	Mouse	Sigma (T7451)

### 3.9.2 SECONDARY ANTIBODIES USED IN WB AND ICC

Antigen	Dilution WB	Dilution ICC	Host species	Conjugate	Source
<b>Rabbit IgG</b>	1:10000		Goat	HRP	Thermo Fisher Scientific (1858415)
<b>Mouse-IgG</b>	1:10000		Goat	HRP	Thermo Fisher Scientific (1858413)
<b>Rabbit-IgG</b>	1:15000		Goat	IRDye 680LT	Li-Cor (925-68021)
<b>Mouse-IgG</b>	1:15000		Goat	IRDye 680LT	Li-Cor (925-68020)
<b>Rabbit-IgG</b>	1:15000		Goat	IRDye 800CW	Li-Cor (926-68171)
<b>Mouse-IgG</b>	1:15000		Goat	IRDye 800CW	Li-Cor (925-32210)
<b>Rabbit IgG</b>		1: 300	Goat	Alexa Fluor 488	Invitrogen (A11008)

<b>Mouse-IgG</b>	1: 300	Goat	Alexa Fluor 488	Invitrogen (A11001)
<b>Rabbit-IgG</b>	1: 300	Goat	Alexa Fluor 546	Invitrogen (A11010)
<b>Mouse-IgG</b>	1: 300	Goat	Alexa Fluor 546	Invitrogen (A11003)

### 3.9.3 ANTIBODIES USED FOR UV-CLIP

<b>Antigen</b>	<b>Amount used</b>	<b>Host species</b>	<b>Source</b>
<b>TDP-43</b>	2.5 µg	Rabbit	Abcam (ab41881)
<b>IgG</b>	2.5 µg	Rabbit	Jackson Immuno

## **4. METHODS**

### **4.1. MN1 CELL CULTURING**

#### **4.1.1 MAINTENANCE OF CELL LINE**

MN1 cells were passaged twice a week when they reached around 90% confluency. Before every passage, the old medium from the flask was removed and washed briefly with 1X DPBS solution. Cells were trypsinized using 0.05% Trypsin-EDTA (Invitrogen, Cat No: 25300-054), incubating the flask for 2-3 mins in the 37°C incubator. The activity of trypsin was inhibited by the addition of pre-warmed medium containing 10% FBS. This was followed by centrifugation of cells and removal of trypsin containing medium. Finally cells were re-suspended in fresh medium and the required number of cells was added to the plates. The plates were swirled to distribute cells evenly and returned to 37°C, 5% CO<sub>2</sub>.

#### **4.1.2 DNA TRANSFECTION IN MN1 CELLS**

Transient transfection of MN1 cells were done using Qiagen Effectene transfection reagent (Cat No. 301427) according to the manufacturer's protocol. The cells were seeded on the plate 24 hours prior to transfection so that they are 60-80% confluent on the day of transfection. The suggested amount of plasmid DNA was diluted in the EC buffer. This was followed by the addition of Enhancer and brief vortexing. The mix was incubated for 5 min at room temperature. Effectene reagent was added to the above DNA-Enhancer mix. This mix was vortexed for 10 sec and incubated at room temperature for 10 mins. During this incubation, the growth media was removed from the cells, the cells were washed once with pre-warmed PBS, fresh pre-warmed growth medium was added. After the 10 mins incubation, DNA-Enhancer-Effectene mix was added to the cells dropwise. The dish was gently swirled to mix the growth media, and returned to the incubator. Cells were harvested either after 24 hours or 48 hours.

#### **4.1.3 siRNA TRANSFECTION**

ON-TARGET plus Mouse Mid1ip1 siRNA-SMART pool (L-063562-01-0005) and ON-TARGETplus Mouse Camta1 siRNA-SMART pool (L-051054-00-0005) was purchased from GE Healthcare/Dharmacon. siRNA transfections were performed using X-tremeGENE siRNA Transfection reagent (Roche) according to the

manufacturer's protocol. MN1 cells confluency were passed 24 hours prior to transfection in order to obtain 30-50% cell confluency by the time of transfection.

The protocol mentioned here is valid per well of 24-well plate. On the day of transfection, 47.5  $\mu$ L of Opti-MEM (Gibco- Cat.No- 11058021) was taken in 'Tube 1'. 2.5  $\mu$ L of Xtreme siRNA transfection reagent was added to 'Tube 1'. In another tube, 'Tube 2', 1  $\mu$ g of siRNA was added to Opti-MEM to a final volume of 50  $\mu$ L. Following this, the contents of 'Tube 1' and 'Tube 2' are mixed and incubated for 20 mins at room temperature. Transfection mixtures were added dropwise to cells, and the plates were swirled gently to distribute the solution. The cells were harvested either after 72 hours or 96 hours of transfection. Cells were grown on poly-L-Lysine coated coverslips for immunostaining as described above for immunostaining. For RNA extraction, cells grown on 24-well plates were washed with 1 $\times$  PBS and Trizol (Life tech- Cat No. 15596018) was directly added onto them. This was followed by the addition of chloroform and subsequent purification by PureLink kit according to the manufacturer's protocol (Ambion- Cat No 12183025). cDNA libraries were generated using RevertAid RT reverse transcription kit (Thermo Scientific- C at No K1691).

## 4.2 PRIMARY NEURONAL CULTURE

Primary cortical neurons were prepared from embryonic day 16 (E16) mice transgenically expressing either *hTARDBP<sup>WT</sup>* (Xu et al. 2010) or *hTARDBP<sup>A315T</sup>* (Wegorzewska et al. 2009) were obtained from the Jackson Laboratory (Bar Harbor Maine, USA) stocks 016608 and 010700 respectively on a congenic C57Bl/6J background. All mouse lines used to generate primary neurons for experiments were congenic on the C57Bl/6J background and maintained by backcrossing to this wild-type background.

Neurons were grown on dishes or glass coverslips coated with poly-L-Lysine for 12-20 hours prior to seeding. These cells were grown in Primary Neuro Basal Medium supplemented with NSF-1, 1% Penicillin/Streptomycin antibiotics and L- Glutamine. 0.5  $\mu$ M Cytosine  $\beta$ -D- arabinofuranoside (Ara-C) was added to the culture on days in vitro 4 (DIV4) to get rid of the cycling cells. Neurons were cultured for 14 days at 37°C in a 5%CO<sub>2</sub> environment prior to harvesting for ribosome profiling. Cells used for immunostaining were fixed on DIV4 without the treatment of Ara-C.

### **4.3 PLASMID CLONING**

pCMV sport6 FLAG-hTDP-43-V5, pCMV sport6 FLAG-hTDP-43A315T-V5 and pCMV sport6 FLAG-hTDP-43 NES-V5 were made by Dr. Katherine Miller for her doctoral project. pCMV Sport6-Fluc and pCMV Sport6-Rluc for reporter cloning and dual luciferase assays were generated by subcloning the CDS for Firefly or Renilla luciferase from pMTFluc or pMT-Rluc (Schleich et al. 2014) into pCMV Sport 6 using KpnI at the 5' site and XhoI at the 3' site.

All UTR Renilla luciferase reporter plasmid constructs were generated by cloning into pCMV Sport6- Rluc. UTR sequences were obtained from the ENSEMBL Mouse GRCm38.p6 database. The short 5'UTR of Camta1 was cloned using an oligo annealing technique; 5' UTRs of Mig12 and Dennd4a were polymerase chain reaction (PCR) amplified from MN1 cDNA and all 5' UTR constructs were cloned with 5' AvrII and 3' KpnI restriction sites. The 3' UTR of Camta1 was PCR amplified from mouse genomic DNA and cloned with 5' NotI and 3' MluI restriction sites. 3' UTRs of Mig12 and Dennd4a were PCR amplified from mouse genomic DNA and cloned with 5' XhoI and 3' MluI restriction sites. All plasmid sequences were confirmed by Sanger sequencing using at least two primers per plasmid. Cloning primers are listed in section 6.6.2.

### **4.4 SUBCELLULAR FRACTIONATION**

These experiments were done in 10 cm dishes. Transfected MN1 cells were harvested and spun down at 200 g for 10 mins at 4°C. The cell pellets were washed with ice cold 1X PBS and then resuspended in 1mL cold buffer A and incubated on ice for 5 mins. This was followed by homogenization using Dounce homogenizer with type A pestle. Samples were centrifuged at 200 g for 10 mins at 4°C. The supernatant contains the cytoplasmic fraction. To the 750 µL of this supernatant 200 µL of 5X lysis buffer was added. The pellet was resuspended in 1 mL of buffer S1. In a new 2 mL tube, 1 mL of buffer S3 was taken and the resuspended pellet in S1 buffer was layered carefully on buffer S3 followed by centrifugation at 2800 g for 10 mins at 4°C. This sucrose cushion removed the remaining cytoplasmic proteins and cell membrane and pelleted the nuclei. After removing the supernatant, the nuclei were resuspended in 500 µL of 1x Lysis buffer, sonicated on ice 3 x 5 sec to shear genomic DNA, and then centrifuged at 2800 g for 10 min at 4°C. This



supernatant contains the nuclear fraction and was removed to a new tube. These samples were then analysed by western blot.

## **4.5 RIBOSOME FOOTPRINT PROFILING**

The original protocol was followed (Ingolia et al. 2012) with few modifications. MN1 cells were treated with 100 µg/ml cycloheximide (CHX) for 3 min before lysis. No CHX treatment was done for primary neurons prior to lysis. Cells were washed with ice cold 1X PBS. Appropriate volume of lysis buffer was added to the dishes. Cells were scraped off the dishes and transferred to a microfuge tube. These tubes were incubated on ice for 10 mins followed by trituration ten times using a 27G needle. The lysates were centrifuged at 20000 g for 10 min at 4°C. The supernatant was collected in a new tube. For the extraction of ribosome footprints, lysate containing 1000 µg total protein was treated with 0.075 µl RNaseI (Ambion- Cat no AM2294). These RNaseI added samples were incubated at 25°C in a shaking thermomixer for 45 min. Reactions were stopped by adding 1.5 µl SUPERaseIN (Invitrogen- Cat No AM2696). During RNaseI incubation, fresh sucrose solutions with 50 and 17.5% sucrose were prepared in gradient buffer. The sucrose gradients were generated using the Gradient Master 108 programmable gradient pourer (Biocomp). Samples were then loaded onto sucrose gradients and centrifuged for 2.5 h at 35 000 rpm in a SW40Ti rotor in a Beckman L7 ultracentrifuge (Beckman Coulter). After centrifugation, gradients were fractionated and measured for RNA content using a Piston Gradient Fractionator (Biocomp) attached to a UV monitor (BioRad). Fractions containing monosome peaks were selected for footprint library preparation (Figure 16A).

RNA extraction was done by adding 40 µl of 20% SDS and 650 µl acid phenol per 600 µl of pooled fractions. These samples were incubated in a 65°C water bath for 10 mins vortexing every minute. These samples were then transferred to ice for 5 mins. Following this, 650 µl of chloroform was added, and samples were vortexed. Tubes were spun at top speed for 5 min and the aqueous supernatant was added to a new tube. 650 µl PCI were added per 600 µl of diluted extract, and tubes were vortexed, and centrifugation at top speed for 5 min. The aqueous supernatant was again taken in a new tube, and 1/9 volume of 3 M sodium acetate (NaOAc), 1 volume Isopropanol and 3 µl of GlycoBlue (Invitrogen- Cat No AM9515) were added. Samples were chilled between 30 min and overnight at -80°C. Samples were spun at top speed at

4°C for 30 min, and pellet was washed in 750 µl 80% Ethanol. Pellet was then air-dried and resuspended in 5 µl 10 mM Tris, pH 8.0. This RNA contains the footprint material.

For total RNA extraction, Trizol was added to the lysate in the ratio of 3:1 (Trizol: lysate) followed by pipetting up and down. Sample was then incubated at room temperature for 5 min. 200 µl chloroform per mL of Trizol was added to samples and the tubes were shaken vigorously by hand, and then incubated at room temperature for 3 min. Samples were then centrifuged for 15 min at 12000 g at 4°C. The aqueous supernatant was transferred to a new tube, and 2 µl of GlycoBlue and 500 µl of Isopropanol per mL of Trizol were added. Samples were incubated for 10 min -80°C, then centrifuged for 15 min at 12000 g at 4°C. The pellet was washed in 750 µl 80% Ethanol and air dried, and then resuspended in 100 µl 10 mM Tris pH 7.5.

Poly(A) selection was performed for total RNA extraction. 100 µL of binding buffer was added to the sample and the mix was incubated for 2 mins at 65°C in a shaking thermomixer. The mix was placed on ice and 0.5 µL of RNAsin was added. 200 µL Dynabeads Oligo (dT)<sub>25</sub> (Life Technologies Cat no. 610-02) was taken in a new tube and the storage buffer was removed. The beads were then washed with binding buffer. Following this, 100 µL of binding buffer was added to resuspended the beads. Denatured RNA was also added to the resuspended beads and incubated for 5 mins with rotation. The beads were then washed with wash buffer. Then, 18 µl 10 mM Tris, pH 7.5 was added to beads, and they were incubated for 2 min at 80°C in a shaking thermomixer. Elute was transferred to a PCR tube and placed ice.

Total RNA was then fragmented by adding 2 µl 10x RNA fragmentation buffer (Life Technologies- Cat no. AM8740). Reactions were incubated in a PCR machine for 5 min at 94°C. To stop the reaction, the sample was immediately placed on ice, and 2 µl 10x stop solution (Life Technologies- Cat no. AM8740) was added and mixed. 80 µL water, 11 µl 3M NaOAc, 2 µl GlycoBlue and 100 µl isopropanol were added to the sample, and the sample was chilled for 30 min to overnight at -80°C. Sample was spun at top speed at 4°C for 30 min to pellet RNA. Pellet was washed in 750 µl 80% Ethanol, air dried, and resuspended in 5 µl 10 mM Tris pH8.0. This contains the total RNA material.

Both total RNA and footprints were run on a 15% TBE/Urea/polyacrylamide gels (Life Technologies Cat no. EC68855BOX) and size selected by loading 28mer and 34mer marker mix. The part of the gel corresponding to the region of the 28/34 mers was cut out. A 0.5 ml tube was pierced with an 18.5 gauge needle and placed inside a microcentrifuge tube. The excised gel piece was placed into the smaller tube, and nested tubes were spun for 3 min at top speed to force the gel through the needle hole. 360  $\mu$ l of water was added to the gel, and it was soaked for 10 min at 70°C on a shaking thermomixer. The gel elution was added to a Spin X Zentrifugen Filtersystem CA 2.2 ml 0.22  $\mu$ m column (Fisher Scientific Cat No. 10104101) and spun for 3 min at top speed. 40  $\mu$ l 3M NaOAc, 1.5  $\mu$ l GlycoBlue and 500  $\mu$ l Isopropanol were added to the sample, and this mix was left from 30 min to overnight at -80°C. Sample was then spun at top speed at 4°C for 30 min to pellet the RNA, pellet was washed in 750  $\mu$ l 80% Ethanol, air dried, and resuspended in 10  $\mu$ l 10 mM Tris, pH 8.0.

The next step of library preparation was dephosphorylation. 33  $\mu$ l water was added to the sample, and the mix was denatured for 90s at 80°C. Samples were then placed on ice, and 7  $\mu$ l of dephosphorylation mix was added (5  $\mu$ l T4 PNK buffer, 1  $\mu$ l SUPERaseIn (RNase inhibitor), 1  $\mu$ l T4 PNK (NEB Cat no. M0201). Samples were incubated for 1 hr at 37°C, and then for 10 min at 70°C. 39  $\mu$ l H<sub>2</sub>O, 1  $\mu$ l GlycoBlue, 10  $\mu$ l 3M NaOAc, and 150  $\mu$ l isopropanol were added to samples, and samples were incubated from 30 min to overnight at -80°C. Samples were spun at 4°C for 30 min to pellet the RNA. Pellets were washed in 750  $\mu$ l 80% Ethanol, air dried, and resuspended in 8.5  $\mu$ l 10 mM Tris, pH 8.0. This step was followed by linker ligation. 1.5  $\mu$ l of preadenylated Universal miRNA Cloning Linker (NEB cat no. S1315) was added to the sample followed by denaturation for 90s at 80°C. The mix was then cooled down to room temperature. A ligation reaction was set up (RNA-linker, 2  $\mu$ l 10x T4 Rnl2 buffer, 6  $\mu$ l 50% PEG 8000, 1  $\mu$ l SUPERaseIn (RNase inhibitor), 1  $\mu$ l T4 Rnl2 (NEB cat. No. M0242)), and incubated for 2.5 hr at room temperature. Following this, 338  $\mu$ l water, 1.5  $\mu$ l GlycoBlue, 40  $\mu$ l 3 M NaOAc, and 500  $\mu$ l Isopropanol were added to samples, and samples were incubated from 30 min to overnight at -80°C. Samples were then spun at 4°C for 30 min to pellet the RNA. Pellet was washed in 750  $\mu$ l 80% Ethanol, air dried, and resuspended in 5  $\mu$ l 10 mM Tris, pH 8.0. After this step, the samples were run on a 15%

TBE/Urea/polyacrylamide gels (Life Technologies Cat no. EC68855BOX) and purified using Spin X Zentrifugen Filtersystem CA 2.2 ml 0.22 µm column (Fisher Scientific Cat no. 10104101) as mentioned above.

Samples were then reverse transcribed. 2 µl of reverse transcription primers (5' phosphate AGATCGGAAGAGCGTCGTGTAGGGAAAGAGTGTAGATCTCGGTGGT CG(Spacer18)CACTCA(Spacer18)TTCAGACGTGTGCTCTTCCGATCTATTGATGG TGCCTACAG; 1.25 µM) were added to a PCR tube and denatured for 90s at 80°C in a PCR machine. The tube was then placed in ice, and the PCR machine was cooled to 48°C. A reverse transcription reaction was then set up (Ligation + primer, 4 µl first strand buffer, 4 µl 2.5 mM dNTPs, 1 µl 100 mM DTT, 1 µl SUPERaseIn (RNase inhibitor), 1 µl SuperScript III (Life Technologies Cat no. 18080-093). and incubated for 30 min at 48°C in the PCR machine. The reaction was then hydrolyzed by adding 2.2 µl 1N Sodium hydroxide. These samples were incubated for 20 min at 90°C. 156 µl water, 2.0 µl GlycoBlue, 20 µl 3M NaOAc, and 300 µl isopropanol were added to samples, and samples were incubated from 30 min to overnight at -80°C. Samples were then spun at 4°C for 30 min to pellet the RNA. Pellet was washed in 740 µl 80% EtOH, air dried, and resuspended in 5 µl 10 mM Tris pH 8.0. These samples were then run on a 15% TBE/Urea/polyacrylamide gels (Life Technologies Cat no. EC68855BOX) and purified using Spin X Zentrifugen Filtersystem CA 2.2 ml 0.22 µm column (Fisher Scientific Cat no. 10104101) as mentioned above.

The next step was circularization. Circularization reaction (First strand cDNA, 2 µl 10x CirLigase buffer, 1 µl 1mM ATP, 1 µl MnCl<sub>2</sub>, 1 µl CirLigase (Biozym cat no. 131405)) was set up and incubated at 60°C for 1 hour. The reaction was stopped by incubating at 80°C for 10 mins. 156 µl water, 2 µl GlycoBlue, 20 µl 3 M NaOAc, and 300 µl Isopropanol were added to the sample. Sample was incubated for 30 min to overnight at -80°C. Samples were then spun at 4°C for 30 min to pellet the RNA. Pellet was washed in 750 µl 80% Ethanol, air dried, and resuspended in 5 µl 10 mM Tris, pH 8.0.

This was followed by rRNA depletion. Mix the resuspended sample from the circularization step with 1 µl of subtraction oligo pool (section 6.2.7), 1 µl of 20× SSC (Invitrogen, cat. no. AM9763) and 3 µl water in a PCR tube. Denature the mix for 90 s at 100 °C, followed by annealing at 0.1 °C/s to 37 °C. Incubate for 15 min at 37 °C.

Warm a Thermomixer to 37 °C. 25 µL of MyOne Streptavidin C1 DynaBeads (Invitrogen, cat. no. 65001) was taken in a new tube and the storage buffer was removed. The beads were washed thrice with bind/wash buffer ((for 2x) Mix 2 M NaCl, 1 mM EDTA, 5 mM Tris (pH 7.5) and 0.2% (vol/vol) Triton X-100). The beads were resuspend in 10 µL of 2X bind/wash buffer. Transfer 10 µl of subtraction reaction directly from the PCR tube in the thermal cycler to the beads. Incubate for 15 min at 37 °C with mixing at 1000 r.p.m. 17.5 µL of eluate was recovered from the mix and taken in a new tube. 74 µl water, 2 µl GlycoBlue, 6 µl % M NaCl and 150 µl Isopropanol were added to the sample. Sample was incubated for 30 min to overnight at -80°C. Samples were then spun at 4°C for 30 min to pellet the RNA. Pellet was washed in 750 µl 80% Ethanol, air dried, and resuspended in 5 µl 10 mM Tris, pH 8.0.

Samples were then PCR amplified. A PCR mixture was made with a different indexed reverse primer for each sample (20 µl 5x Phusion HF buffer, 8 µl 2.5 mM dNTPs, 0.5 µl 100 µM Forward library primer (5'-AATGATACGGCGACCACCGAGATCTACAC-3'), 0.5 µl 100 µM Reverse indexed library primer (section 6.2.6), 65 µl water, 5 µl circularized DNA template, 1 µl Phusion polymerase (NEB cat no. M0530). 16 µl aliquots of each sample were placed into 5 tubes. Tubes were thermocycled (1 cycle: 30 sec 98°C; 10-18 cycles: 10 sec 98°C, 10 sec 65°C, 5 sec 72°C). Tubes were removed after 10, 12, 15 extension cycles (Figure 16B). The PCR products were run on a 10% TBE non-denaturing gels (Invitrogen Cat no. EC62755BOX). The product band at the size of 176 nt was excised and placed into a 2 ml tube. 400 µl of DNA Gel Extraction Buffer was added. Samples were rotated on a shaker overnight. 1.5 ml GlycoBlue and 500 µl Isopropanol were added to the samples, and samples were incubated for 30 min to overnight at -80°C. Samples were then spun at top speed at 4°C for 30 min to pellet the RNA. Pellet was washed in 750 µl 80% Ethanol, air dried, and resuspended. The libraries were multiplexed sequenced on an Illumina HiSeq2500 SR 50 base run.

## **4.6 ANALYSIS OF THE RIBOSOME PROFILING DATA**

The ribosome footprinting data was analyzed by Dr. Giorgio Gonnella from Prof. Stefan Kurtz's team at the Center for Bioinformatics, University of Hamburg and

some analyses was done by Malik Alawi at the Bioinformatics Core, University Medical Center Hamburg-Eppendorf.

For the analysis of the ribosome profiling data, we implemented the open source pipeline Ribopip (<http://github.com/stepf/RiboPip>). The pipeline is implemented in Ruby and follows the protocol (Ingolia et al. 2012), with minor differences described here. For all analyses, we used the mouse genome sequence and annotation GRCm38.p4 as a reference. Adapter clipping was performed using cutadapt 1.8.1 (Martin 2011) with the parameters: `-trimmed-only -e 0`. No filtering regarding the read length was applied. Non-coding RNAs were removed by filtering out the reads which bowtie2 (Langmead and Salzberg 2012) aligned to the annotated non-coding RNAs, using a seed length and a minimum alignment length of 14. The alignment of the remaining reads to the genome was performed using TopHat2 (Kim et al. 2013) with Bowtie2 (Langmead and Salzberg 2012) as read mapper. For all alignments, we set a minimum seed length parameter to 14. To compensate for the different lengths of the remaining reads, we decided to allow a number of mismatches in the alignment to the genome, relative to the read length. However, this option is not provided by the alignment tools we used. Therefore, we split, prior to the alignment, the reads into buckets of reads of equal length. Each bucket of reads was aligned separately, allowing a maximum number of  $\text{ceil}(e \cdot l)$  mismatches, where  $e$  is the desired error rate (we set  $e$  to 0.1) and  $l$  is the read length. If  $e \cdot l$  is not an integer, we round to the smallest integer larger than  $e \cdot l$ . After the computation, the alignments of each bucket were joined. The number of hits for each annotated feature was determined using FeatureCounts 1.4.4 (Liao, Smyth, and Shi 2014). DeSeq (Anders and Huber 2010) was used for the analysis of the differential expression between samples. Details of read counts and mapping for each sample are in Appendix 1a and 1b. Mapping to UTRs versus CDS appear in Appendix 2.

## **4.7 POLYSOME PROFILING**

Transfected MN1 cells were treated with 50µg/ml CHX for 3 min prior to lysis. Cells were washed with ice cold 1X PBS. Appropriate volume of lysis buffer was added to the dishes. Cells were scraped off the dishes and transferred to a microfuge tube. Cells were lysed on ice for 10 min and cell debris was then spun down at maximum speed for 10 min at 4°C. Protein concentrations were determined by Bradford assays

and used to normalize gradient loading. Lysates were loaded onto 17.5–50% sucrose gradients. The sucrose gradients were generated using the Gradient Master 108 programmable gradient pourer (Biocomp). Samples were then loaded onto sucrose gradients and centrifuged for 2.5 hour at 35 000 rpm in a SW40Ti rotor in a Beckman L7 ultracentrifuge (Beckman Coulter). After centrifugation, gradients were fractionated and measured for RNA content using a Piston Gradient Fractionator (Biocomp) attached to a UV monitor (BioRad). For RNA isolation, fractions were pooled according to the scheme presented in Figure 18A. A fraction of the original lysate loaded onto the gradient was retained and processed in parallel as a reference for total cytoplasmic RNA.

#### **4.8 RNA EXTRACTION AND qRT PCR**

RNA was isolated from the pooled fractions using Trizol in a ratio of 3:1 followed by the addition of chloroform and subsequent purification by PureLink kit. A total of 450 ng of RNA was used to make cDNA from each fraction. cDNA libraries were generated using SuperScript® II Reverse Transcriptase (Life Technologies Ct no. 18064014) according to the manufacturer's protocol for random hexamer priming. FastStart Universal SYBR Green Master ROX (Roche Cat no. 04913914001) was used for qRT-PCR with three technical replicates per sample and reactions were run on ABI 7900HT instruments. The standard curve method was used for analysis with ABI instrument software. Primers used in this project are shown in section 6.7.1. To obtain relative distribution plots, 18S rRNA levels were measured and their relative distribution across the fraction pools was calculated.

#### **4.9 ANALYSIS OF THE FRACTION OF RIBOSOMES IN POLYSOMES**

The area under the curves representing the monosome and polysome peaks in gradient profiles was quantified using ImageJ (Schneider, Rasband, and Eliceiri 2012). The fraction of ribosomes in polysomes was calculated by dividing polysome area by the sum of polysome and monosome areas.

## 4.10. CROSSLINK IMMUNOPRECIPITATION

MN1 cells were seeded in 10 cm dishes 2 days prior to performing the assay and were ~70–80% confluent when used. Culture medium was removed and ice-cold 1x PBS was added to the cells followed by UV irradiation (200 mJ/cm<sup>2</sup>) using a Stratalinker. Cross-linked cells were lysed in 1 ml of Lysis Buffer. A fraction of the lysate corresponding to 5% of the input material (50µl) was saved to be used as a reference for calculating fraction of input material in the IP pellet. The remaining lysate was added to Protein G Dynabeads (Invitrogen Cat no. 10004D) pre-bound with either 2.5 µg TDP-43 antibody or rabbit IgG control and incubated at 4°C overnight with rotation. Beads were then washed twice for 2 min in High Salt Buffer, followed by washing twice for 2 min in wash buffer and a final wash for 2 min in NT2 buffer. For protein analysis, 1X or 6X Laemmli buffer was added directly to the beads or input fraction, respectively, followed by incubation at 95°C for 5 min. RNA was eluted by incubation with 30 µg Proteinase K (Carl Roth- Cat no. 7528.1) in NT2 Buffer for 30 min at 55°C. RNA extraction was carried out both from the eluate and input sample as mentioned above. All RNA obtained from each sample (Input or IP) was used to generate cDNA libraries using random hexamers and the RevertAid RT reverse transcription kit, following the manufacturer's protocol. FastStart Universal SYBR Green Master ROX was used for qRT-PCR with three technical replicates per sample and reactions were run on ABI 7900HT instruments. To calculate target mRNA enrichments, we first calculated the delta C<sub>t</sub> for TDP-43 IP versus Input and converted this to a linear 'Fold Change' value. These were then corrected for the reduced amount of input analyzed (i.e. divided by 20), and then multiplied by 100 to obtain '% of Input mRNA in IP'.

## 4.11 IMMUNOSTAINING

Transfected cells or neurons were grown on glass cover slips coated with poly L Lysine. Twenty-four hours after transfection for MN1 and on DIV2 for primary neurons, cells were fixed with 4% PFA for 2 min followed by ice cold methanol for 3 min and three washes with 1X PBS. Blocking was done using 5% goat serum in 1X PBS. Coverslips were incubated with primary antibodies in blocking solution at 4°C overnight. Coverslips were then washed three times with 1X PBS and incubated with secondary antibodies in blocking solution at room temperature for 2 h in dark.



Coverslips were then washed three times with 1X PBS, submerged in MilliQ water and mounted on glass microscope slides with Fluoromount-G (Southern Biotech Cat no. SB1-0100-01). Cells were imaged using an Olympus Fluoview 1000 microscope with 60X objective, using similar acquisition settings for laser power, offset and detector gain across conditions.

## 4.12 MICROSCOPY IMAGE ANALYSIS

Image analysis was done using Fiji (Schindelin et al. 2012). Transfected cells were marked with V5 (for hTDP-43 / hTDP-43A315T) and/or GFP (for GFP and MID1-GFP) as markers. The region of interest was marked with DAPI for nuclear staining. For cytoplasmic staining, the Nuclear DAPI staining region was masked in the original image and residual mean intensity for the whole cell region was calculated. For primary neurons, the mean intensity gray value of a line drawn along the neurites marked using acetylated tubulin or Tau1 was measured using Fiji. Linear adjustments of brightness and contrast were performed on images using Photoshop CS.

## 4.13 LUCIFERASE ASSAYS

Transient transfections in MN1 cells were performed in 24- well plates using Effectene Transfection Reagent (Qiagen) as mentioned above. The amounts of plasmids used were GFP/Flag-hTDP-43-V5/FlaghTDP-43<sup>A315T</sup>-V5- 180 ng/170 ng; Rluc ctrl/Camta1 5'UTR-Rluc/Camta1 3'UTR- Rluc- 17 ng; Mig12 5'UTR-Rluc/Mig12 3'UTR-Rluc/ Dennd4a 5'UTRRluc/ Dennd4a 3'UTR- Rluc – 9 ng; Fluc- 11 ng/13 ng. Cells were lysed by adding 150 µl 1X Passive Lysis Buffer (Promega, Cat No: E1910) per well of a 24-well plate and incubating in a shaking platform for 15 min. Lysate was spun down in a microfuge at maximum speed for 1 min and 10 µl of supernatant for each sample was loaded in duplicate to 96-well luminometer plates. The plate was measured in a Victor3 (TM) 1420 Multilabel counter luminometer (Perkin Elmer), set to dispense 50 µl of each Dual Luciferase Assay reagent (Promega, Cat No: E1980) per well.

For RNA extraction from transfected reporter samples, lysates were treated with Turbo DNase, to get rid of plasmid-derived signal prior to preparing RNA with Trizol reagent, as described above. A total of 250 ng of RNA was used to make cDNA for these experiments. RNA extraction and cDNA synthesis were done as shown in

section 7.9 except at the cDNA synthesis step, each sample was divided in two and incubated either in the presence or absence of Reverse Transcriptase ('no RT), to verify that signal was due to mRNA and not contaminating DNA. qPCR was performed as described above and analyzed using the  $\Delta C_t$  method. All samples used for analysis showed clear enrichment compared to the corresponding no RT control.

#### **4.14 WESTERN BLOTTING**

Cells were harvested 24 hours after transfection. Cells were lysed using RIPA buffer and protein content was quantified using Bradford assay. For every western blotting, equal amount of protein was loaded for each sample (usually 20-25  $\mu$ g) and separated on a 12% SDS-PAGE gel in 1X running buffer. Immunoblotting to nitrocellulose or polyvinylidene difluoride (PVDF) was performed either with wet transfer method for 1.5 hours in 1X running buffer at 4°C or using an iBlot rapid transfer device according to the manufacturer's guidelines. The membrane was blocked for 1 hour at room temperature using TBS-Tween containing 5% powdered milk, then overnight at 4°C, shaking, with primary antibody. The following day, membranes were washed 3 X 10 min in TBS-Tween. Membranes were incubated for 2 hour at room temperature with secondary antibody. Signals were either visualized using HRP-conjugated secondary antibodies and Super Signal Dura or Femto reagent (Thermo Fisher Scientific Cat no. 34075 or 34096) and imaged on a Fujifilm LAS-4000 luminescent image analyzer or by using fluorescent secondary antibodies and imaged on a Li-Cor Odyssey CLx (Li-Cor). Total protein staining was performed using Revert Total Protein Stain Kit (Li-Cor) according to the manufacturer's instructions and used for normalization. Western blot quantification was done using ImageJ or Image studio™ Lite (LI-COR Biosciences).

#### **4.15 STATISTICAL ANALYSIS AND PLOTS**

All statistical tests were performed in GraphPad Prism (version 5.02) or Microsoft Excel. Two-tailed unpaired t-tests were performed, unless otherwise indicated. Plots were generated either using GraphPad Prism (version 5.02), Origin-Pro 2017G or Microsoft Excel. Venn diagrams were generated online using Venny: <http://bioinfogp.cnb.csic.es/tools/venny/>

## 5. RESULTS

### 5.1 TRANSIENT TRANSFECTION OF MN1 CELLS SHOW SIMILAR EXPRESSION LEVELS OF HUMAN TDP-43 AND TDP-43<sup>A315T</sup> PROTEINS

ALS is a motor neuron disease known to affect both upper and lower motor neurons. For the major part of this project, I used the motor neuron cell line, MN1, as an experimental system. This cell line was generated by fusing mouse spinal motor neurons and neuroblastoma cells (Salazar-Grueso, Kim, and Kim 1991). MN1 cells are shown to express choline acetyl transferase (ChAT) which is a characteristic of lower motor neurons.

We used a transient transfection strategy for our experiments with this cell line. The cells were transfected with plasmids encoding wild-type or A315T mutant human TDP-43 (with FLAG as N-terminal tag and V5 as C-terminal tag) using Effectene Transfection Reagent (Qiagen) following the manufacturer's protocol. We also used GFP transfected cells as a control for all our experiments. 24 hours after transfection, cells were lysed and protein extracts were obtained to check for the transfection efficiency.

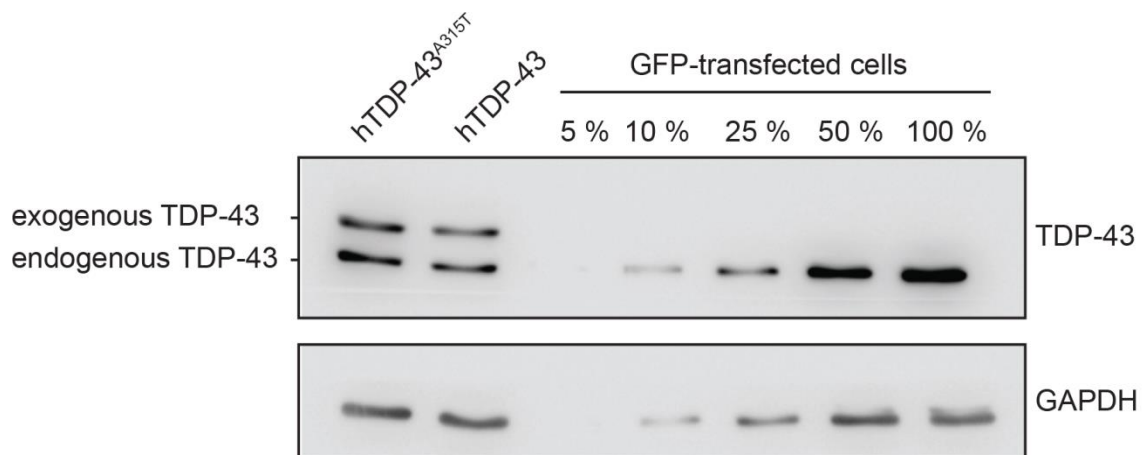


Figure 9: Lysates from transiently transfected MN1 cells were probed by western blot. Various dilution of GFP transfected lysate was used to check the expression efficiency of hTDP-43 / hTDP-43<sup>A315T</sup> protein. GAPDH was used as a loading control.

Figure (9) shows expression of hTDP-43 and hTDP-43<sup>A315T</sup> protein in transfected cells. There were two bands observed in the blot, one of which corresponds to the endogenous protein and a higher band, which corresponds to the exogenously expressed protein. It is known that expression of exogenous TDP-43 protein leads to the downregulation of endogenous protein (Ayala et al. 2011), which is also observed in our experiments. The blot shows that approximately 30-40% of endogenous TDP-43 is present upon the expression of hTDP-43/ hTDP-43<sup>A315T</sup>. GAPDH served as a loading control here. Importantly, expression levels of TDP-43 variants were similar and total TDP-43 levels in these assays suggest quite moderate overexpression (Figure 10).

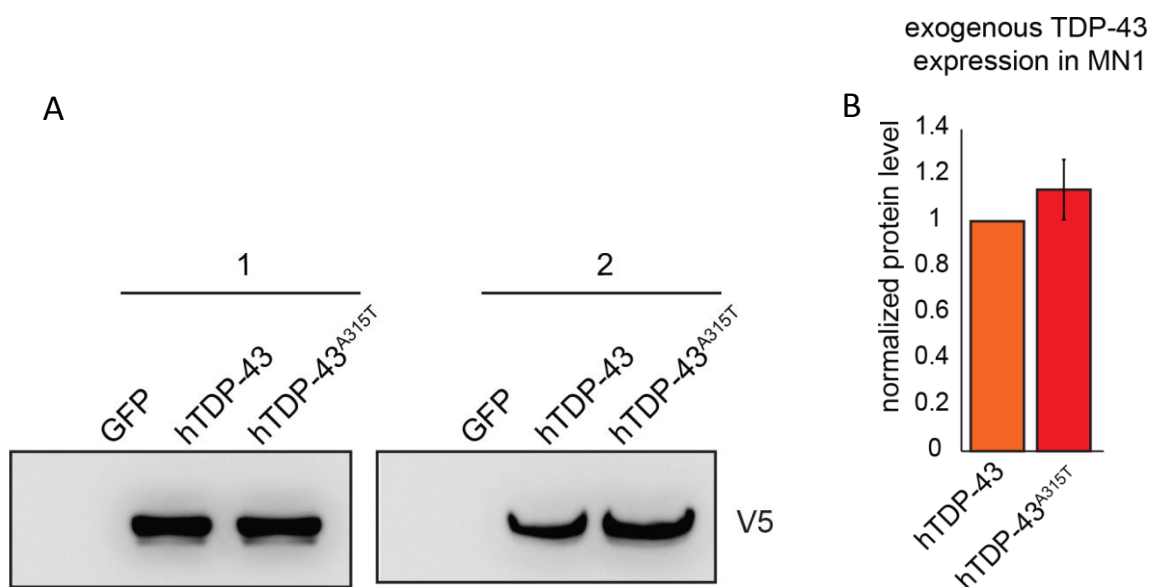


Figure 10: (A) Representative immunoblot showing similar levels of expression of transiently transfected hTDP-43-V5 and hTDP-43<sup>A315T</sup>-V5 protein in MN1 cells from two replicates. (B) Normalized protein levels of exogenous TDP-43 in transfected MN1 cells, derived from A. (n=2, error bars show deviation from the average for hTDP-43<sup>A315T</sup> samples). Note the highly similar expression levels.

## 5.2 HUMAN TDP-43<sup>A315T</sup> PROTEIN HAVE SLIGHTLY HIGHER EXPRESSION LEVEL THAN HUMAN TDP-43 IN PRIMARY CORTICAL NEURON CULTURE

We used primary cortical neurons as our experimental system for upper motor neurons, which is one of the neuronal populations affected in ALS. Primary neuronal cultures were prepared from cerebral cortices of E16 mice expressing human TDP-43 wild-type protein (Xu et al. 2010) and human TDP-43<sup>A315T</sup> protein (Wegorzewska

et al. 2009). Cells were grown for 14 days and then harvested for our experiments. Cells were lysed and protein extracts were obtained in order to check the expression of protein derived from transgene. The expression levels of hTDP-43 and hTDP-43<sup>A315T</sup> proteins were comparable as seen in the Figure (11). We used human TDP-43 specific antibody to check the expression of the transgenic proteins. A single band is seen in cells expressing hTDP-43<sup>A315T</sup> when probed against FLAG antibody, which is expected as hTDP-43<sup>A315T</sup> transgene has a FLAG tag in its N-terminus.

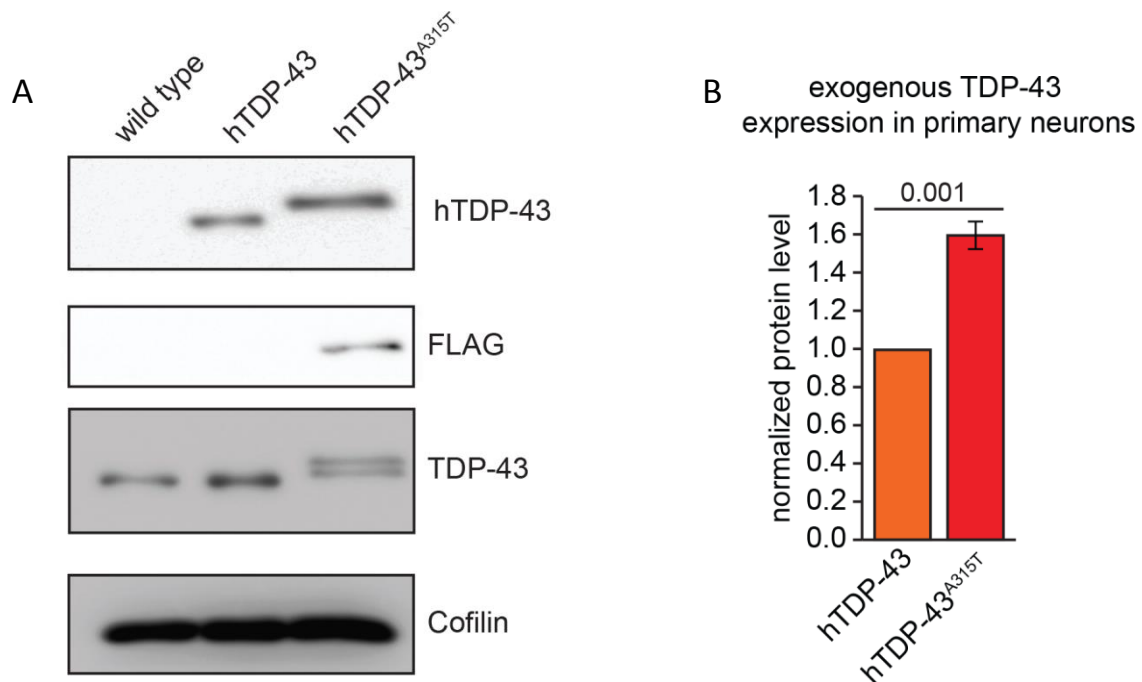


Figure 11: (A) Representative immunoblot showing expression of transgene-derived hTDP-43 and Flag-hTDP-43A315T protein, as well as total TDP-43 protein in primary cortical neurons. (B) Normalized protein levels of exogenous TDP-43 from three independent cultures generated on different days. (n=3, s.e.m error bars, *P*-values indicated).

Mutant protein levels in primary cultures were somewhat higher than the WT hTDP-43, but total overexpression levels were not especially high (Figure 11).

### 5.3 SUBCELLULAR FRACTIONATION SHOWS BOTH HUMAN WT TDP-43 AND TDP-43<sup>A315T</sup> ARE MOSTLY NUCLEAR

It is known that TDP-43 protein is mostly located in the nucleus. For this project, we were interested in translational regulation by both hTDP-43 and hTDP-43<sup>A315T</sup>. So it was important to look at the cellular localization of these transfected proteins to assess how much of the exogenous protein is involved in translational regulation in

cytoplasm. Transfected MN1 cell lysates were fractionated into nuclear and cytoplasmic components followed by western blot detection of our proteins of interest. As we transfected V5- tagged constructs of both hTDP-43 and hTDP-43<sup>A315T</sup>, we used V5 antibody to detect the transfected proteins. GAPDH, a cytoplasmic protein and phospho Histone H3, a nuclear protein was used as controls for the experiment. In addition, we also took advantage of another plasmid construct available in the lab, V5- tagged hTDP-43 with an extra NES (nuclear export signal), which leads to more cytoplasmic localization.

Both hTDP-43 and hTDP-43<sup>A315T</sup> were mostly localized in the nucleus with a small fraction in the cytoplasm which contributes to translational regulation in cytoplasm. GAPDH was found mostly in the nucleus and phospho Histone H3 was found only in the nucleus with no detectable amount in the cytoplasm. Above all, hTDP-43 NES showed more cytoplasmic localization as expected.

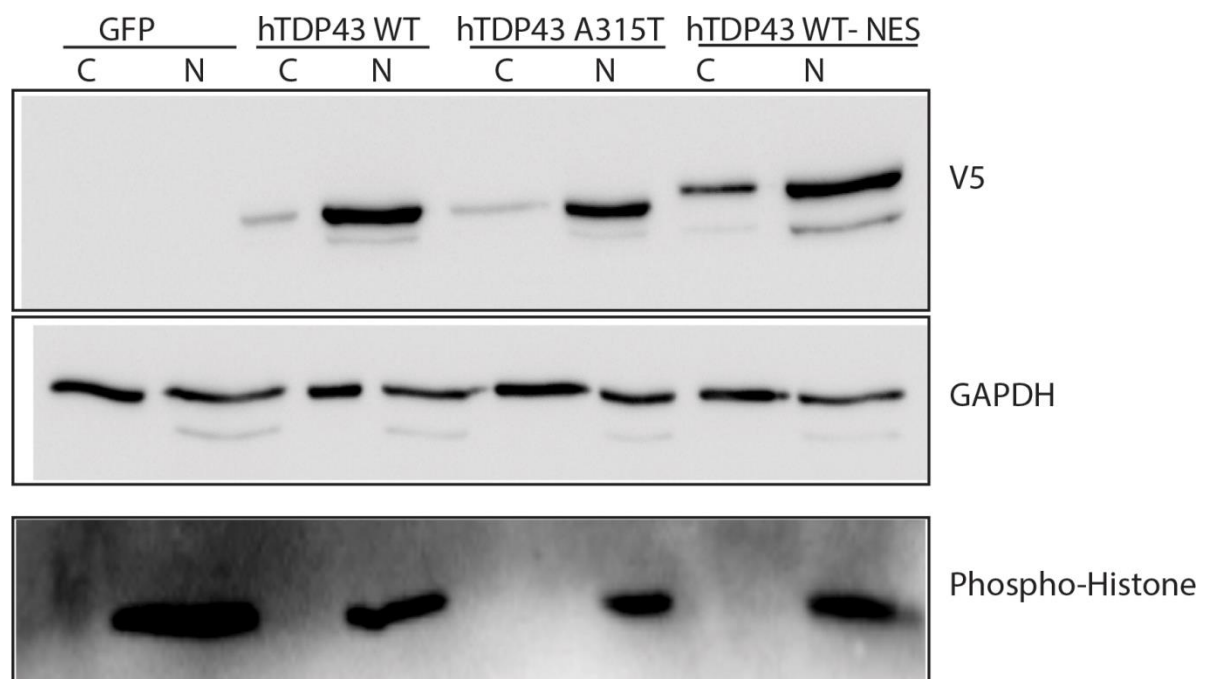


Figure 12: Transfected MN1 cells were fractionated into nuclear and cytoplasmic components followed by western blot probing. Exogenous TDP-43 detected by V5 antibody indicates nuclear localization. (C- cytoplasmic fraction, N- nuclear fraction)

## 5.4 OVEREXPRESSION OF HUMAN TDP-43 OR TDP-43<sup>A315T</sup> PROTEIN DOES NOT LEAD TO A SIGNIFICANT EFFECT ON GENERAL TRANSLATION

Previous studies have shown that TDP-43 is implicated in translational regulation and have also identified few targets that are translationally repressed. But none of these studies addressed the effects of such translational regulation in disease. We were interested in assessing the effects of WT TDP-43 and mutant TDP-43 on translational control and how this causes disease. In order to do that, it was important to know if overexpression of these proteins has effect on general translation in motor neuron-like cells. For this, we used the technique called polysome profiling.

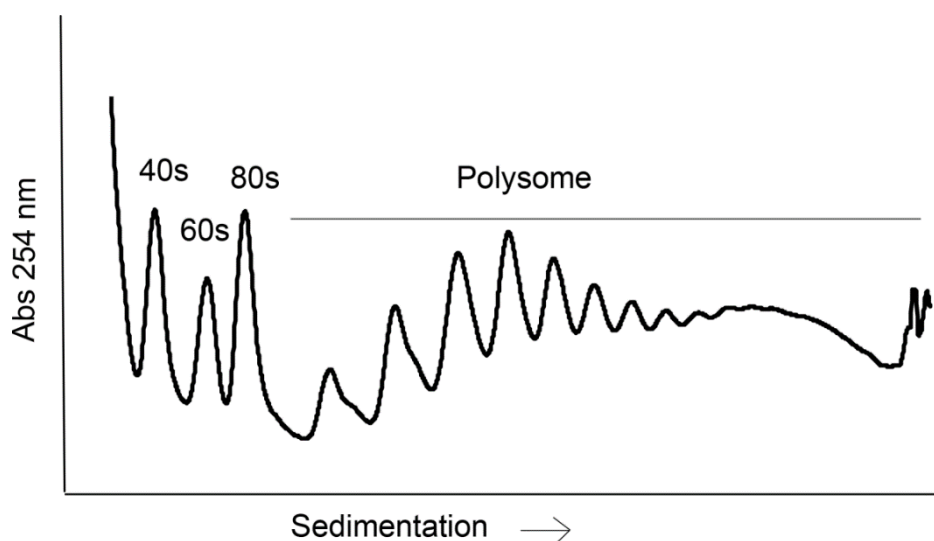


Figure 13: Representative polysome profile from untransfected MN1 cells. Gradients were fractionated to resolve the 40S and 60S ribosome subunits, 80S monosomes, and polysomes (disomes, trisomes, etc).

Polysome profiling is one of the commonly used methods to study translational regulation. Cells are treated with a translation inhibitor called cycloheximide (CHX) in order to freeze the translocating ribosomes. This gives an overview of translation at steady state. Lysate from CHX-treated cells is loaded onto a sucrose gradient and spun in an ultracentrifuge. The cellular components get separated based on their sedimentation rate. Following this, the gradient is passed through a UV monitor set at 254 nm and fractionated. The absorbance at 254 nm facilitates in visualizing the concentration of nucleic acids, which is usually represented as shown in Figure 13 in a “polysome profile”. Effects on general translation can be visualized from this graph. For instance, deviations in the relative height of the 80S and polysome peaks from the control profile indicate translation defects.

In addition to the general translation defects, this method can provide information about the translation state of specific mRNAs. Protein or RNA can be isolated from various fractions and their distribution across the gradient quantified using methods for detection of specific mRNAs (e.g. Northern blotting or qRT-PCR). mRNAs that shift from lighter fractions to heavier fractions have increased ribosome density, which frequently is due to increased translation. Conversely, movement of an mRNA to lighter fractions indicates lower ribosome density and decreased translation.

Polysome profiles from MN1 cells transfected with either hTDP-43 or hTDP-43<sup>A315T</sup> appeared similar to GFP-transfected control profiles (Figure 14 A-C), suggesting no significant impact of overexpression of either WT hTDP-43 or hTDP-43<sup>A315T</sup> on general translation. In order to quantitatively represent this, we calculated the fraction of ribosomes in polysomes from multiple experimental replicates, which revealed no statistically significant differences among the different transfections (Figure 14D). Thus, TDP-43 overexpression does not significantly affect general translation in motor neuron-like cells.

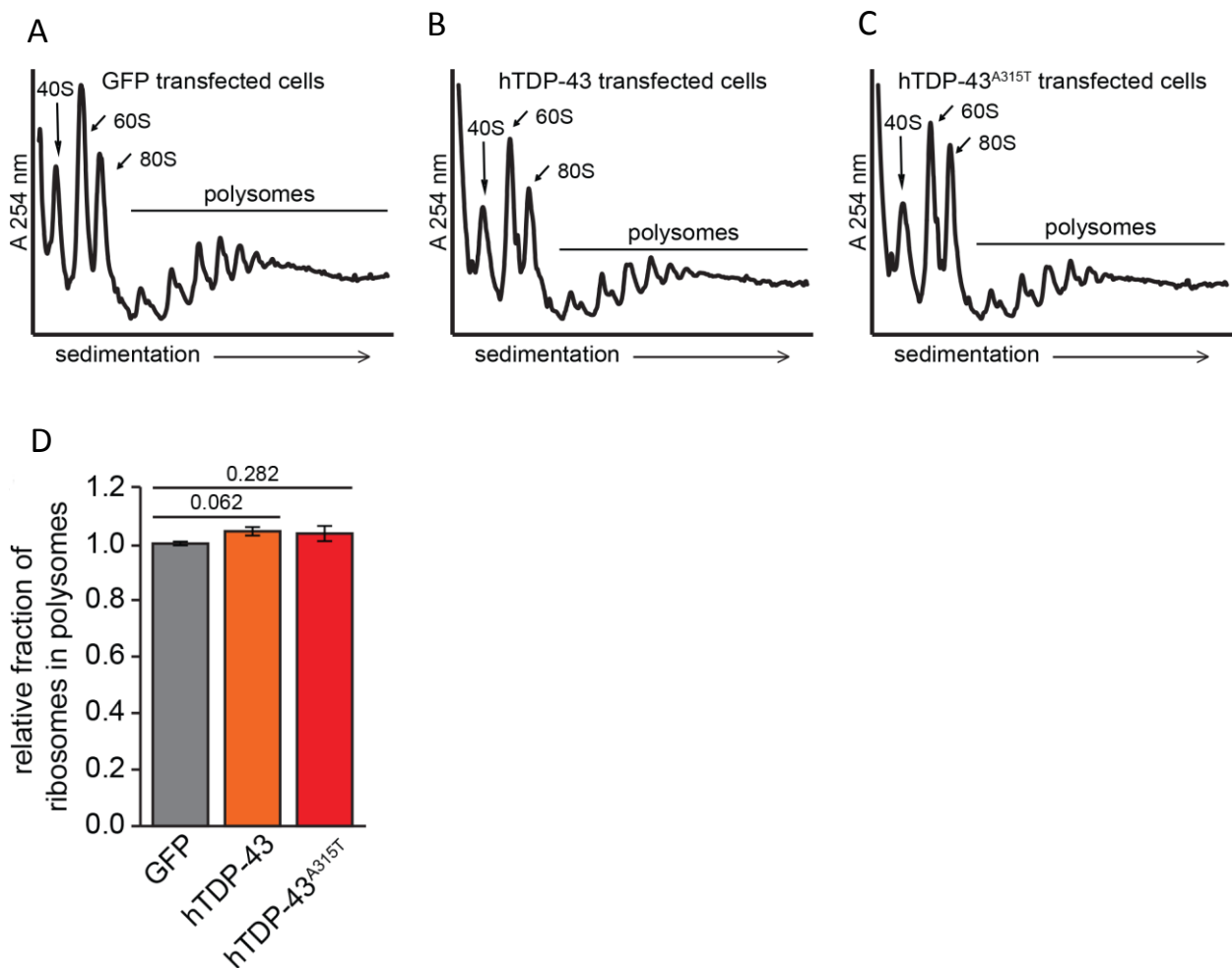




Figure 14: Representative polysome profiles are shown from MN1 cells transiently transfected with GFP (A), hTDP-43-V5 (B), or hTDP-43<sup>A315T</sup>-V5 (C). Note the similarity of the profiles. (D) Quantification of the relative fraction of ribosomes in polysomes from independent experiments reveals no statistically significant difference (n=3, s.e.m. error bars, P-value indicated, unpaired two-tailed t-test).

Having confirmed that there is no effect on general translation by overexpression of hTDP-43 or hTDP-43<sup>A315T</sup>, we hypothesized that there might be mRNA-specific effects on translation. To identify mRNAs that are translationally targeted by these proteins, we used the genome-wide technique called 'Ribosome footprint profiling' (Ingolia et al. 2012).

## **5.5 RIBOSOME FOOTPRINT PROFILING ON MN1 CELLS AND PRIMARY CORTICAL NEURONS REVEALS TRANSLATIONAL TARGETS OF TDP-43**

Ribosome footprint profiling is a genome-wide technique that monitors translation based on ribosome protected mRNA fragments. Ribosome density measurements combined with RNA-Seq measurements can be used to study translational regulation, as protein expression levels do not always correlate with transcripts levels (Liu, Beyer, and Aebersold 2016). This ribosome density is used as a more reliable measurement of gene expression as it allows the identification and quantification of mRNA fragments that were protected by the ribosome. Translating ribosomes protect ~30 nt long mRNA fragments from nuclease digestion. These ribosome-protected fragments are recovered and cDNA libraries are prepared out of these fragments. These libraries are then sequenced and these reads are used to map the positions of ribosomes on any given mRNA. In principle, this method provides information about both the number of ribosomes bound on an mRNA (ribosome density) and where ribosomes are bound on an mRNA.

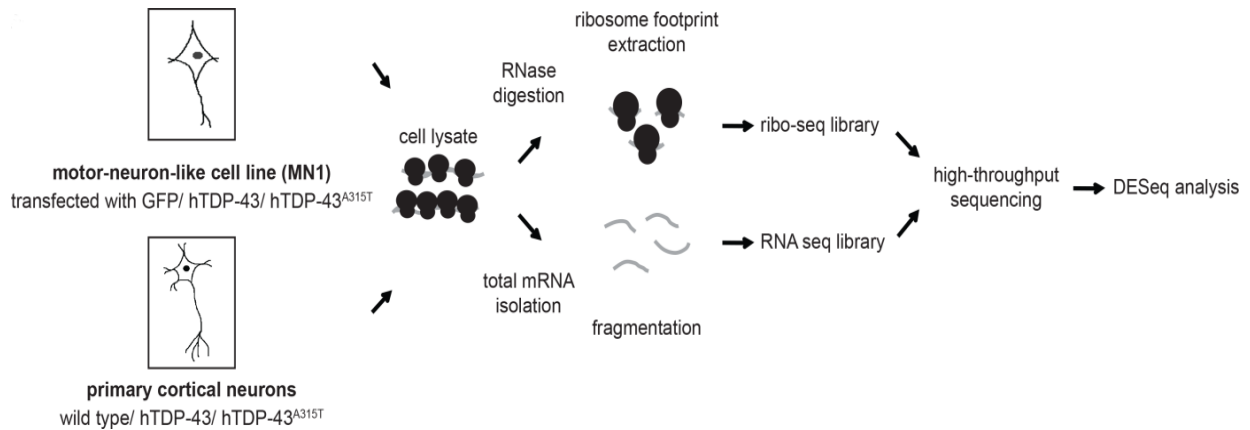


Figure 15: Overview of experimental design. MN1 cells were transfected with GFP control or human TDP-43 variants (hTDP-43-V5 or hTDP-43<sup>A315T</sup>-V5) (n=2). Primary cortical neurons were prepared from E16 wild type mice (n=2) or mice expressing human TDP-43 variants (hTDP-43 and Flag-hTDP-43<sup>A315T</sup>, n=3). Neurons were grown in culture for two weeks (DIV14). Ribosome footprints and total mRNA were extracted from each of these cell types, followed by library generation and high-throughput sequencing.

Reads obtained from ribosome footprint profiling indicate parts of genome that are actually being translated by ribosomes. In addition to quantification of translation rate, this method has been particularly helpful in identification of new short ORFs and uORFs.

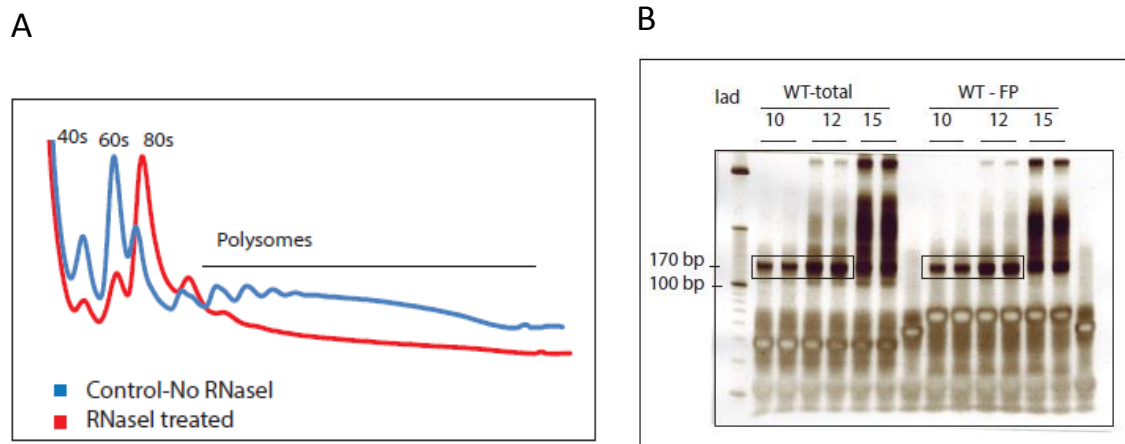
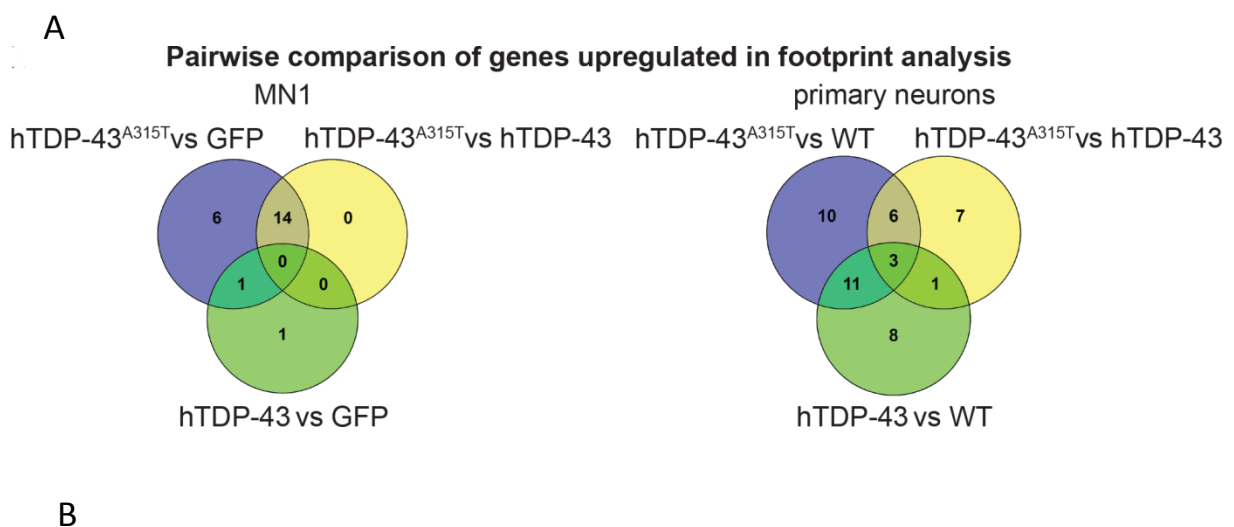


Figure 16: (A) RNaseI-digested MN1 lysate was run on a sucrose gradient and fractionated. MN1 lysate without any RNaseI digestion was run as a control. RNaseI treatment has clearly led to an increase in 80S peak and loss of polysome peaks, indicating that the polysome peaks are digested to generate monosome peaks, as expected. (B) Representative gel picture obtained from the last step of the protocol- PCR amplification. The bands within the boxes indicate the correct sized product ~175nt. These bands of the gel were cut out and purified followed by deep sequencing. (lad- ladder; WT- wild type control; total- total mRNA; FP- footprint; 10,12,15- PCR cycle numbers).

To identify specific mRNAs regulated by TDP-43 at the translational level, we performed ribosome profiling with two different cell systems: motor neuron-like MN1 cells and primary cortical neuronal cultures (Figure 15). For MN1 cells, we performed two replicates, using cells transiently transfected with plasmids encoding GFP, hTDP-43, or the mutant hTDP-43<sup>A315T</sup> protein found in a subset of ALS patients. Primary cortical neurons were obtained from hemizygous transgenic animals expressing either hTDP-43 or hTDP-43<sup>A315T</sup> mutant and non-transgenic littermate control animals. Because only the mutant animals develop disease as hemizygotes, hTDP-43 neurons serve as an important control. Changes specifically observed in cortical neurons expressing hTDP-43<sup>A315T</sup>, but not hTDP-43, correlate with disease. We followed the standard protocol for generating ribosome footprint profiling libraries (Ingolia et al. 2012) with minor modifications and also generated libraries in parallel from total mRNA to control for transcriptional vs. translational regulation. Details of sequencing library preparation, sequencing, and data analysis are described in Methods. Appendix 1a and 1b provides an overview of the mapping statistics and read counts obtained for each individual sample. Exon-mapped read numbers and mapping rates were similar to other published ribosome profiling experiments (Thoreen et al. 2012; O'Connor, Andreev, and Baranov 2016). Importantly, we also observed the expected preference in read mapping to coding sequence (CDS) vs. 3'UTRs in ribosome footprint samples, but not corresponding total mRNA samples (See Appendix 2).



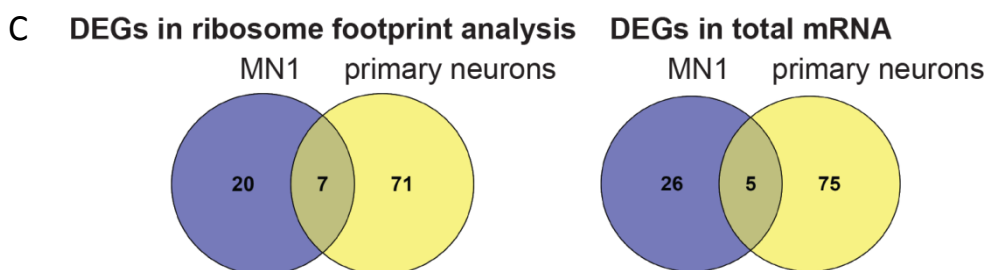
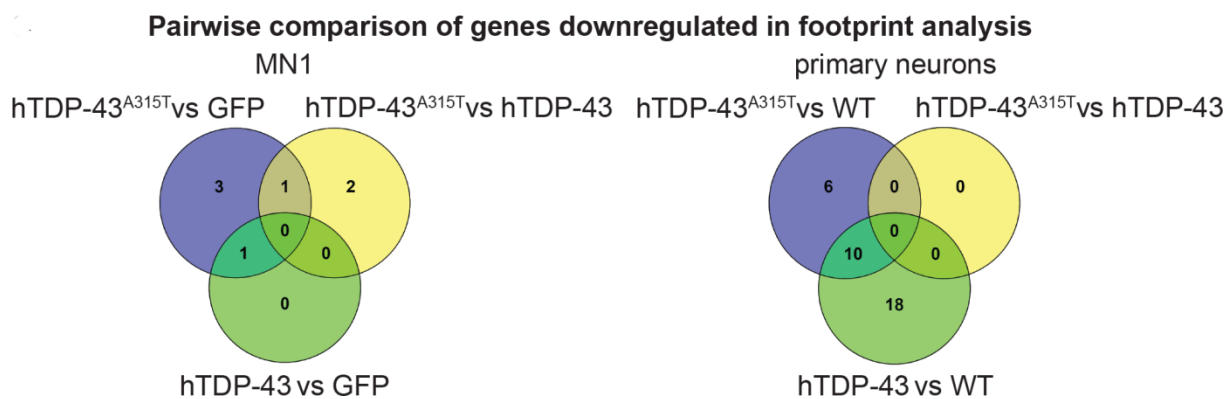


Figure 17: (A, B) Overview of differentially regulated genes. Venn diagrams show pairwise comparisons of genes that were upregulated (A) or down regulated (B) in MN1 and primary cortical neurons. (C) Venn diagrams showing Differentially Expressed Genes (DEGs) identified in MN1 cells, primary cortical neurons, or both. DEGs from ribosome footprint analysis (translation) and total mRNA sequencing (transcription/mRNA stability) are shown separately.

To identify differentially expressed mRNAs, we performed three different comparisons for each cell type: GFP/WT vs hTDP-43, hTDP-43 vs hTDP-43<sup>A315T</sup> and GFP/WT vs hTDP-43<sup>A315T</sup> (Appendix 3-6). To identify altered translation, we refined our hits to genes that show altered regulation only in the ribosome footprints, but not in total mRNA (Figure 17A, 17B). Strikingly, we identified a set of mRNAs whose translation was altered by hTDP-43<sup>A315T</sup> in both MN1 cells and primary cortical neurons (Figure 17C and Table 1).

**DEGs in both primary cortical neurons and MN1 cells in ribosome footprint analysis and the comparison(s) where these genes were identified**

Ensembl ID	Gene symbol	Primary cortical neuron	MN1
ENSMUSG00000052117	<i>D630039A03Rik</i>	hTDP-43 <sup>A315T</sup> vs hTDP-43, hTDP-43 <sup>A315T</sup> vs WT, hTDP-43 vs WT,	GFP vs hTDP-43 <sup>A315T</sup>
ENSMUSG00000032492	<i>Pth1r</i>	hTDP-43 <sup>A315T</sup> vs hTDP-43, hTDP-43 <sup>A315T</sup> vs WT	hTDP-43 vs hTDP-43 <sup>A315T</sup> , GFP vs hTDP-43 <sup>A315T</sup>

ENSMUSG00000008035	<i>Mid1ip1/Mig12</i>	hTDP-43 <sup>A315T</sup> vs hTDP-43, hTDP-43 <sup>A315T</sup> vs WT	GFP vs hTDP-43 <sup>A315T</sup>
ENSMUSG00000095738	<i>Gm25313</i>	hTDP-43 <sup>A315T</sup> vs hTDP-43	GFP vs hTDP-43 <sup>A315T</sup>
ENSMUSG00000029797	<i>Sspo</i>	hTDP-43 <sup>A315T</sup> vs hTDP-43	GFP vs hTDP-43 <sup>A315T</sup>
ENSMUSG00000046854	<i>Pip5k1l</i>	hTDP-43 vs WT	GFP vs hTDP-43 <sup>A315T</sup>
ENSMUSG00000027552	<i>E2f5</i>	hTDP-43 <sup>A315T</sup> vs WT	GFP vs hTDP-43 <sup>A315T</sup> , hTDP-43 vs hTDP-43 <sup>A315T</sup>

**DEGs found in both primary cortical neurons and MN1 cells in total mRNA analysis and the comparison(s) where these genes were identified**

Ensembl ID	Gene symbol	Primary cortical neuron	MN1
ENSMUSG00000030428	<i>Ttyh1</i>	hTDP-43 <sup>A315T</sup> vs WT	hTDP-43 vs GFP
ENSMUSG00000028195	<i>Cyr61</i>	hTDP-43 <sup>A315T</sup> vs WT	hTDP-43 vs hTDP-43 <sup>A315T</sup>
ENSMUSG00000031216	<i>Stard8</i>	hTDP-43 <sup>A315T</sup> vs WT	hTDP-43 vs hTDP-43 <sup>A315T</sup>
ENSMUSG00000018916	<i>Csf2</i>	hTDP-43 <sup>A315T</sup> vs WT	hTDP-43 vs hTDP-43 <sup>A315T</sup> , hTDP-43 vs GFP
ENSMUSG00000034883	<i>Lrr1</i>	hTDP-43 <sup>A315T</sup> vs WT	hTDP-43 vs hTDP-43 <sup>A315T</sup>

Table 1: List of genes that were differentially regulated in footprint or total mRNA from both MN1 and primary neuron datasets

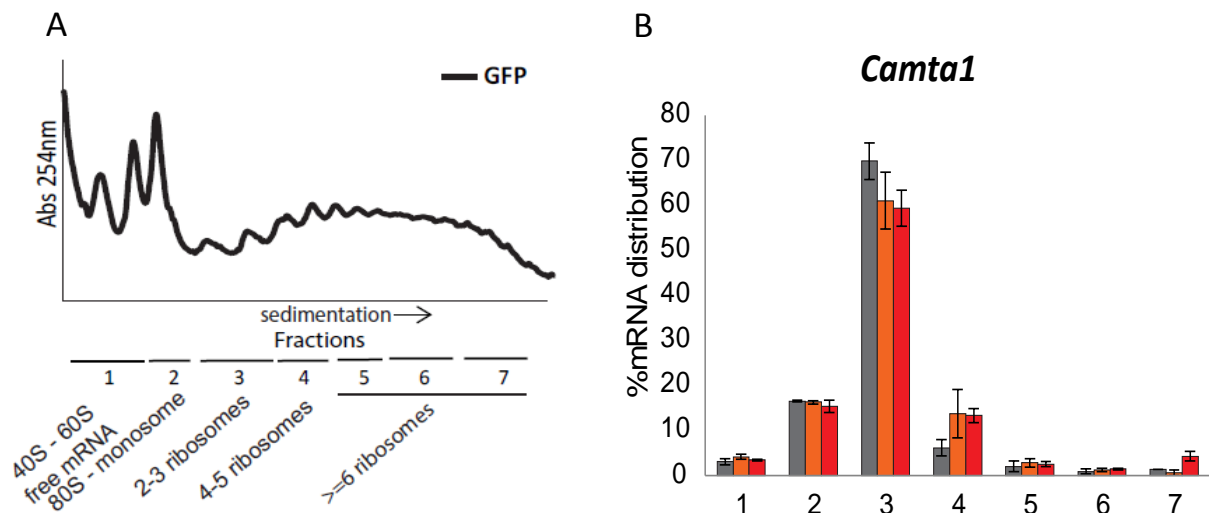
These genes are especially interesting, as they show changes in both cell populations, MN1 cells and primary cortical neurons that are affected in the disease. Thus, we have identified potential new translational targets of hTDP-43 and hTDP-43<sup>A315T</sup> proteins in MN1 cells and primary cortical neurons. To prioritize translational targets from ribosome profiling for further experiments, we first focused on mRNAs that showed altered translational regulation only upon expression of the patient mutant hTDP-43<sup>A315T</sup> protein. While it is known that overexpression of hTDP-43 WT at a sufficiently high level can cause disease-like phenotypes (Gendron and Petrucelli 2011), we know the level of expression of hTDP-43-WT in the transgenic animals that we used for primary neurons is not sufficient to cause disease (Xu et al. 2010). After applying this filter, we next selected genes for follow-up analysis that met one of two criteria: either (1) they showed strong, direct links to neurodegenerative disease based on previous studies, or (2) they were identified in both cell types. Based on these criteria, we identified three genes for further downstream analysis: *Camta1*, *Dennd4a*, and *Mig12/Mid1ip1* (Table 2).

Ensembl ID	Gene symbol	Gene name
ENSMUSG00000014592	<i>Camta1</i>	calmodulin binding transcription activator 1
ENSMUSG00000008035	<i>Mid1ip1/Mig12</i>	Mid1 interacting protein 1
ENSMUSG00000053641	<i>Dennd4a</i>	DENN domain containing 4A

Table 2: Genes selected from ribosome profiling for further validation

## 5.6 POLYSOME PROFILING CONFIRMS THAT hTDP-43<sup>A315T</sup> PROTEIN INCREASES RIBOSOME DENSITY ON *Camta1*, *Mig12*, AND *Dennd4a* mRNAs IN MN1 CELLS

Because high-throughput genome-wide methods can lead to false positives, it is important to perform independent validation experiments to verify the effects of hTDP-43<sup>A315T</sup> on translation of specific mRNAs that were identified by ribosome profiling. In order to do this, we performed sucrose density-gradient polysome profiling of specific mRNAs with transiently transfected MN1 cells. We pooled polysome gradient fractions as indicated (Figure 18 A), purified RNA, and examined the relative levels of specific mRNAs in pooled gradient fractions by qRT-PCR in two independent validation experiments.



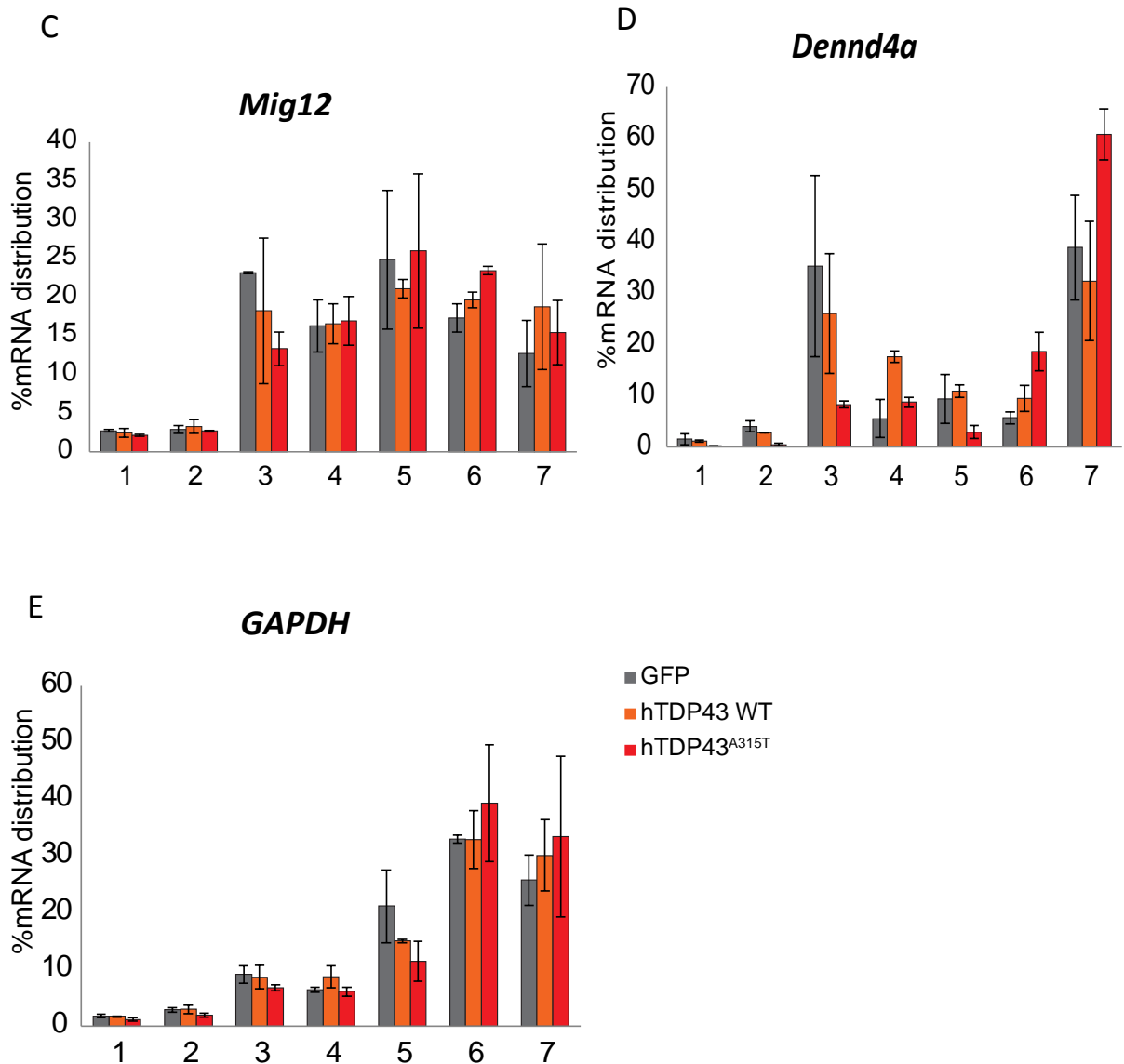


Figure 18: (A) Representative polysome profile of control MN1 cells transfected with GFP. The pooling scheme of gradient fractions used for mRNA distribution analysis is indicated. (B-E) Plots showing mRNA distribution for candidate mRNAs identified by ribosome footprint profiling: *Camta1* (B), *Mig12* (C), *Dennd4a* (D), and *GAPDH* (E). (n=2; values normalized to 18s rRNA; error bars show deviation from average in the replicates).

When hTDP-43<sup>A315T</sup> protein was expressed, *Camta1*, *Mig12*, and *Dennd4a* mRNAs all shifted to heavier gradient fractions (Figure 18 B-D), implying increased ribosome density on these mRNAs, exactly as seen in our genome-wide ribosome profiling experiments (Appendix 3 and 4). In contrast, the distribution of *GAPDH* mRNA in polysomes was not affected by either hTDP-43 or hTDP43<sup>A315T</sup> in these experiments, highlighting a specific effect on translation of the other mRNAs (Figure 18E).

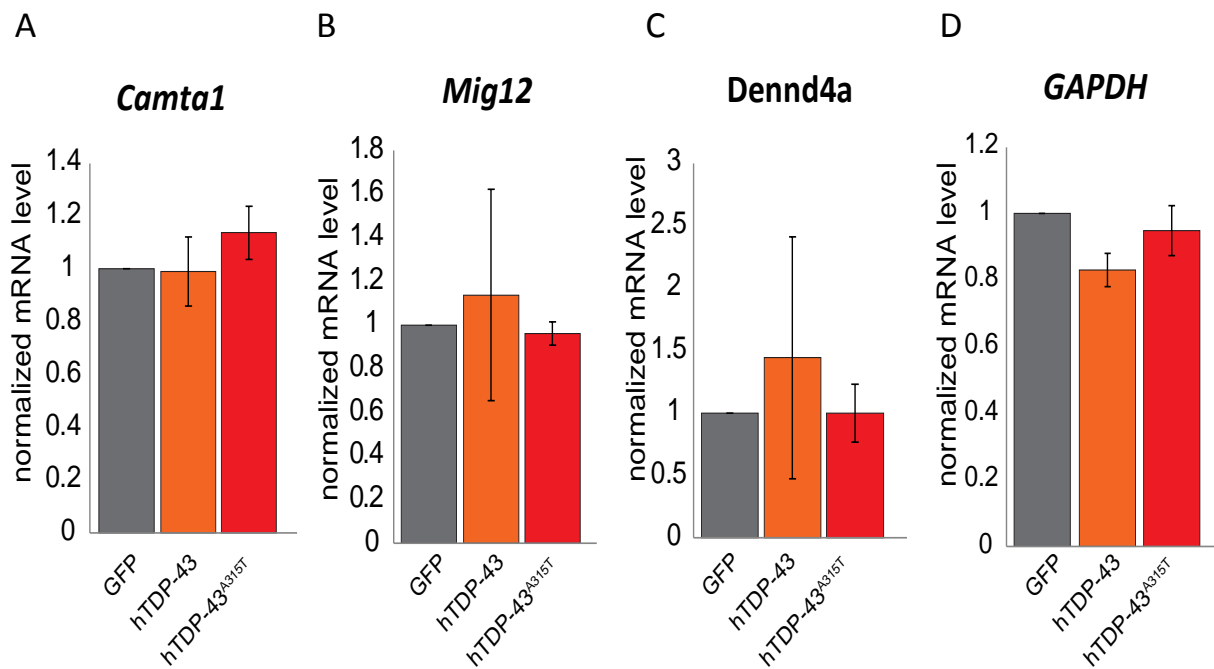
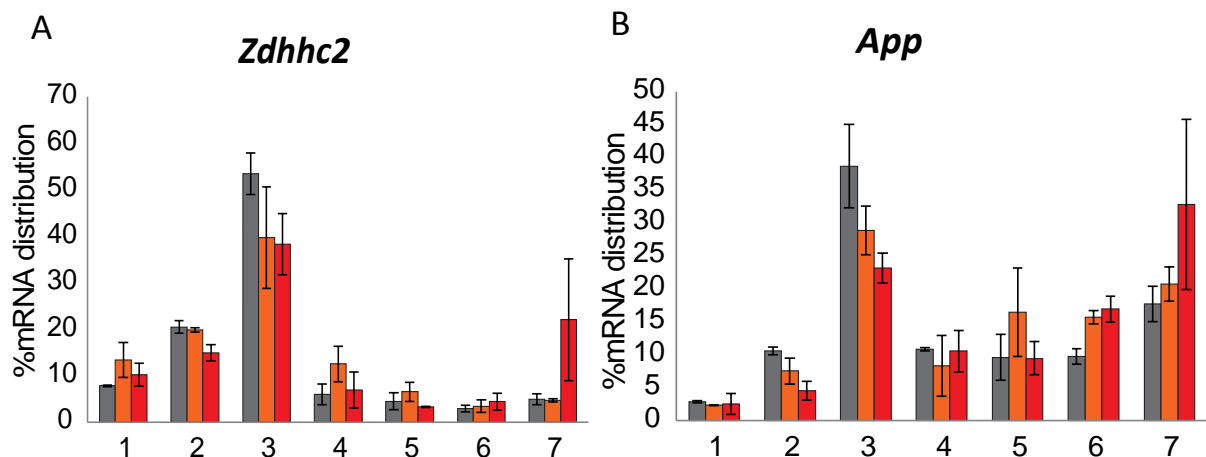


Figure 19: Graphs showing mRNA levels of *Camta1* (A), *Mig12* (B), *Dennd4a* (C) and *GAPDH* (D) in the input material for polysome profiling (n=2, error bars show deviation from average, values normalized to 18s rRNA). Note the similarity of the levels, consistent with the original ribosome profiling data for candidate mRNAs which revealed a change only in footprints.

We also checked whether total mRNA levels might be altered. Consistent with our profiling datasets, we detected no significant change in total mRNA levels for *Camta1*, *Mig12* or *Dennd4a* mRNAs (Figure 19). Taken together, these results confirm that exogenous expression of the hTDP-43<sup>A315T</sup> protein increases ribosome density on *Camta1*, *Mig12*, and *Dennd4a* mRNAs and therefore affects their translation in motor neuron-like cells.





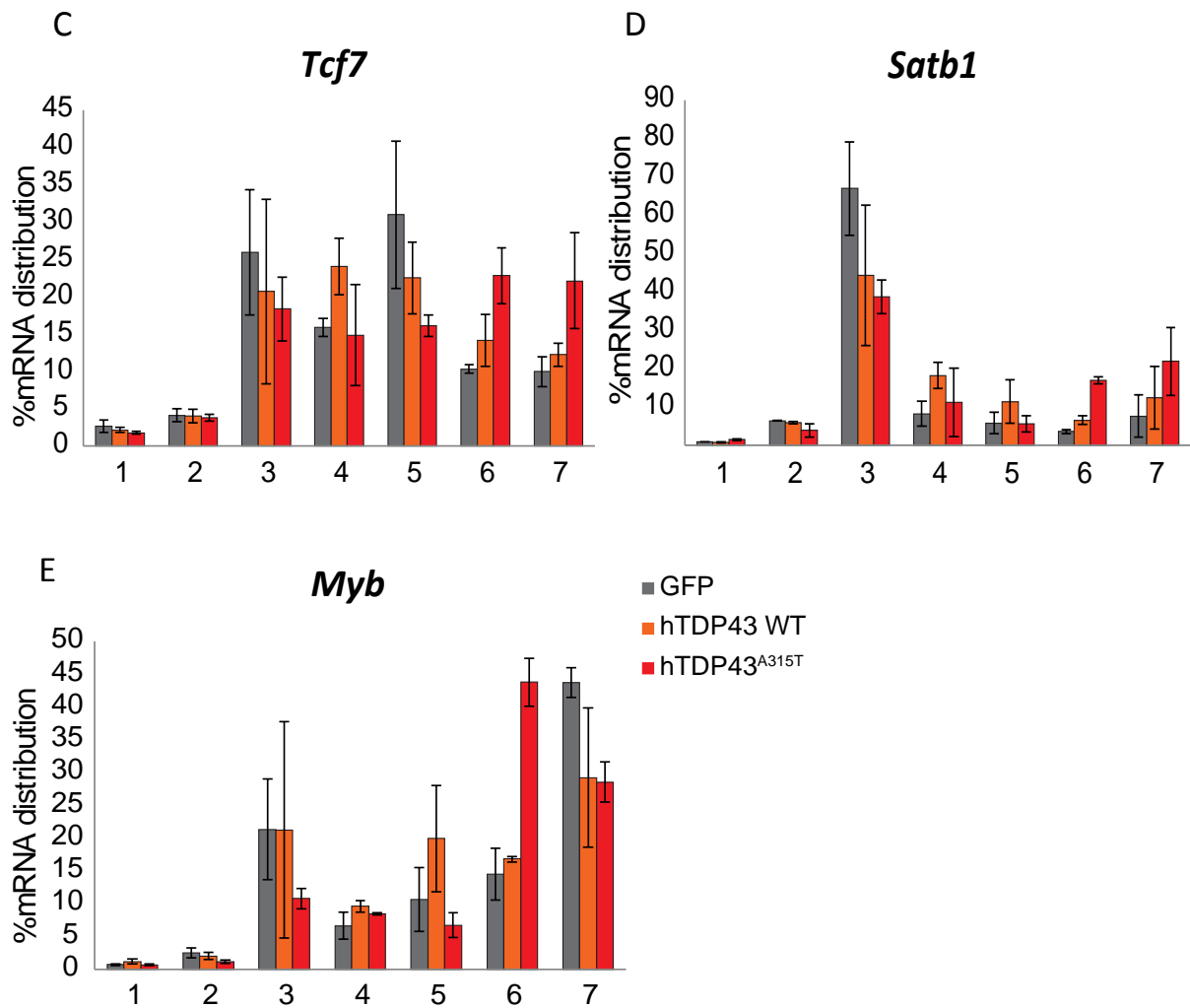


Figure 20: (A-E) Plots showing mRNA distribution for ‘Master Regulator’ mRNAs from (Ikiz et al. 2015; Brichta et al. 2015): *Zdhhc2* (A), *App* (B), *Tcf7* (C), *Satb1* (D), and *Myb* (E). (n=2; values normalized to 18s rRNA; error bars show deviation from average in the replicates). The pooling scheme for the fractions is shown in Figure 18A.

*Camta1* and *Dennd4a* have been found to be “Master Regulators” (MRs) of neurodegenerative disease transcriptional programs in an in vivo Parkinson’s disease model and a cultured motor neuron-based ALS model (Ikiz et al. 2015; Brichta et al. 2015). The Parkinson’s study identified 19 MRs and the ALS identified 23 MRs, however, only three were found in common. Remarkably, CAMTA1 and DENND4A were among these three.

## 5.7 ASSESSMENT OF NEURODEGENERATION MASTER REGULATOR FUNCTION AND REGULATION IN CELLS EXPRESSING hTDP-43/hTDP-43<sup>A315T</sup>

Our results show altered ribosome density on two MRs of neurodegeneration, CAMTA1 and DENND4A. In our ribosome profiling assays, we also performed parallel RNA-Seq experiments, which would reveal changes in mRNA levels due to transcriptional effects (Appendix 5 and 6). We detected significantly altered mRNA levels for only a relatively small number of genes. Remarkably, two of 24 mRNAs, *Cyr61* and *Elovl4*, that were significantly altered in RNA-Seq from hTDP-43<sup>A315T</sup> vs. hTDP-43 transfection were also identified as specific transcriptional targets of CAMTA1 that were deregulated in the aforementioned Parkinson's study (Brichta et al. 2015). *Cyr61* was also significantly altered in RNA-Seq from hTDP-43<sup>A315T</sup> vs. WT in primary neurons. This suggests that mutant TDP-43 expression not only leads to enhanced translation of *Camta1* mRNA, but also has functional consequences on transcriptional regulation of a subset of CAMTA1 targets. On the other hand, *Map7*, known to be a regulatory target of DENND4A from the same study was identified in our RNA-Seq analysis from hTDP-43<sup>A315T</sup> vs. hTDP-43 transfection.

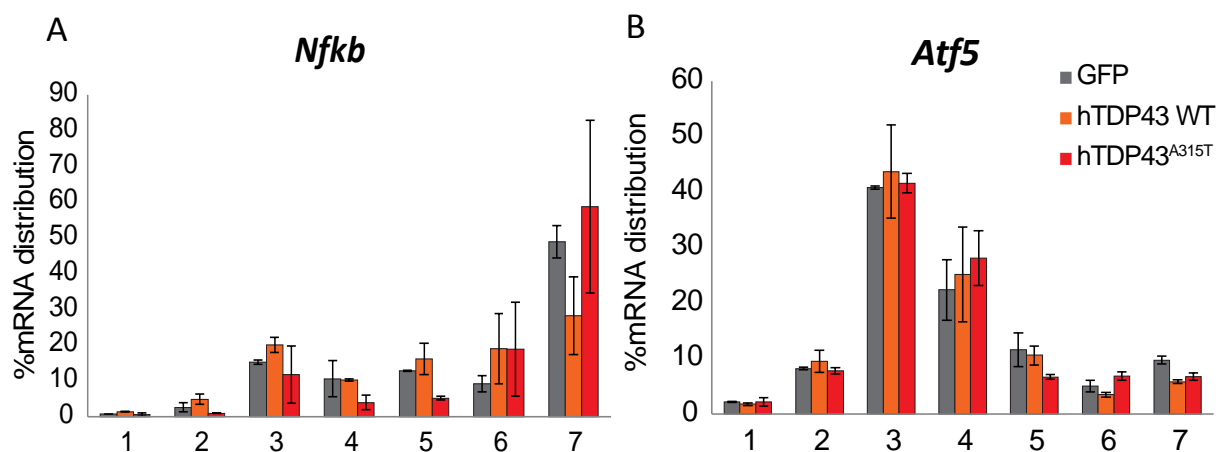


Figure 21: Plots showing mRNA distribution for 'Master Regulator' mRNAs from (Ikiz et al. 2015; Brichta et al. 2015): *Nfkb* (A), and *Atf5* (B). (n=2; values normalized to 18s rRNA; error bars show deviation from average in the replicates). The pooling scheme for the fractions is shown in Figure 18A.

As two of the MRs from the above mentioned studies (Ikiz et al. 2015; Brichta et al. 2015) showed altered translational status in our datasets, and these MRs were found to be relevant in two different neurodegenerative diseases, we were interested in

translational regulation of other MRs. Of the Master Regulators that we checked, *Zdhhc2*, *App*, *Tcf7*, *Satb1* (Figure 20 A-D) mRNAs shifted to deeper fractions upon expression of hTDP-43<sup>A315T</sup>. In contrast, expression of hTDP-43<sup>A315T</sup> caused *Myb* mRNA to shift in the opposite direction: from heavier to lighter fractions (Figure 20E). For all these mRNAs, expression of hTDP-43 protein did not lead to any change in the mRNA distribution across the gradient, as compared to the cells expressing GFP (Figure 22). MRs like *Nfkb* and *Atf5* did not show any significant shift in ribosome density upon expression of either hTDP-43 or hTDP-43<sup>A315T</sup> proteins (Figure 21).

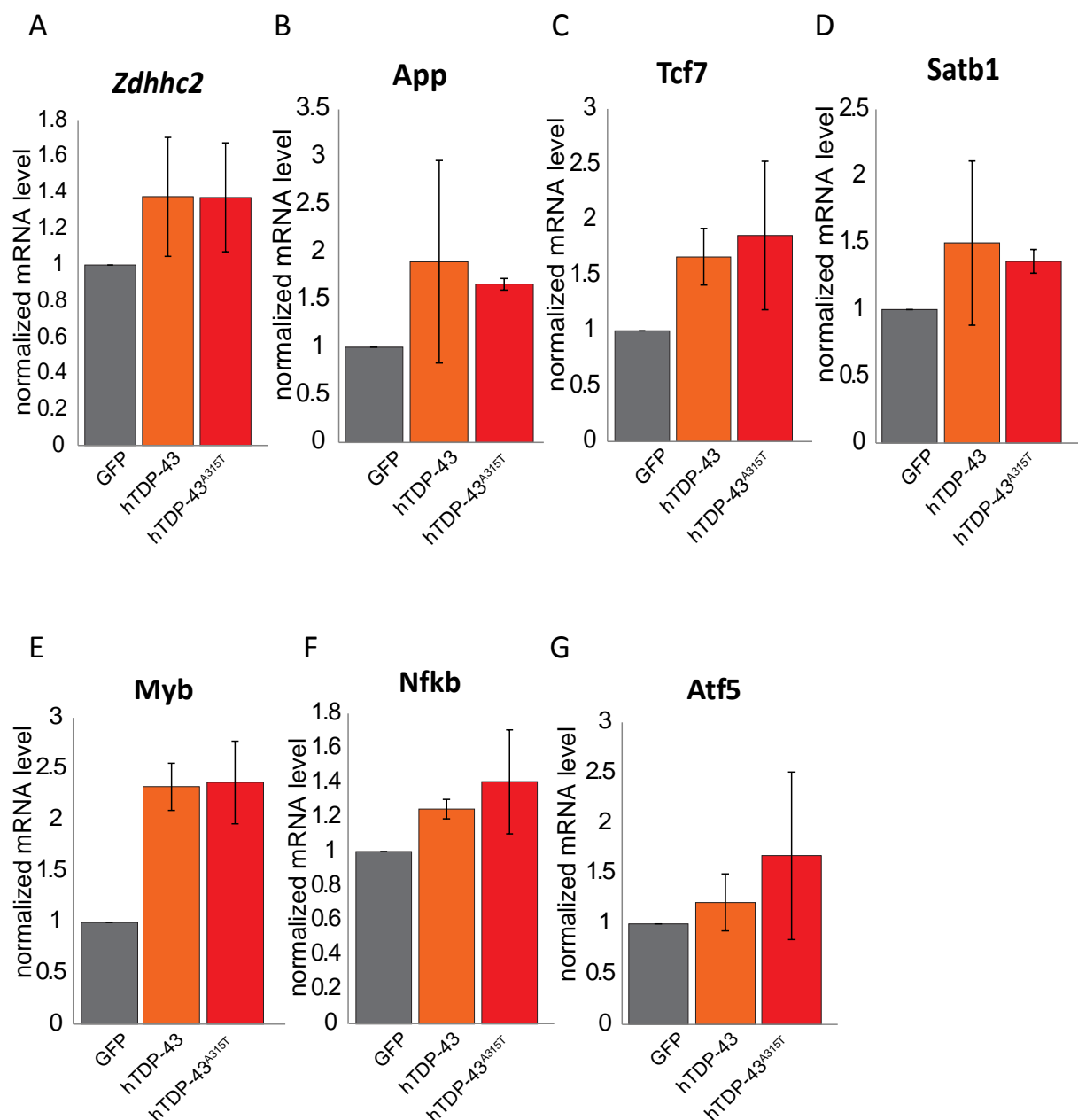


Figure 22: Graphs showing mRNA levels of 'Master Regulator' mRNAs from (Ikiz et al. 2015; Brichta et al. 2015): *Zdhhc2* (A), *App* (B), *Tcf7* (C) and *Satb1* (D), *Myb* (E), *Nfkb* (F), and *Atf5*

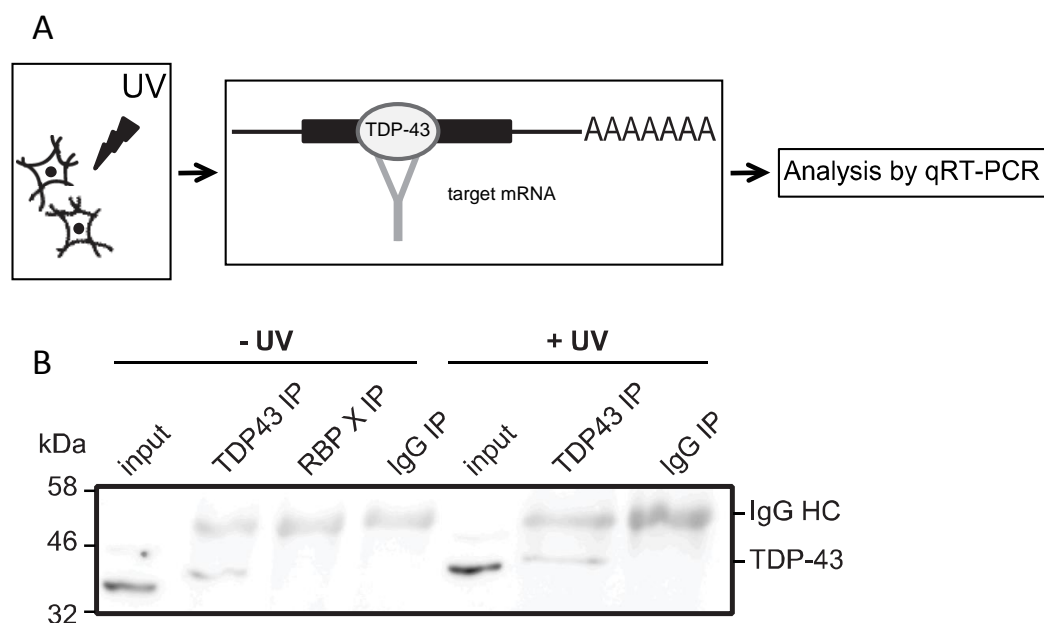
(G) in the input material for polysome profiling (n=2, error bars show deviation from average, values normalized to 18s rRNA).

We also measured total mRNA levels of these Master Regulator genes. *Zdhhc2* and *Atf5* (Figure 22A, 22G) did not show any change upon expression of either hTDP-43 or hTDP-43<sup>A315T</sup> protein. Some mRNAs, including *App* and *Satb1* (Figure 22B, 22D), show an increase in total mRNA level upon expression of hTDP-43<sup>A315T</sup>, suggesting effects on transcription or mRNA stability, in addition to translational effects. *Tcf7* (Figure 22C) shows an increase only upon expression of WT hTDP-43 protein, but not hTDP-43<sup>A315T</sup> protein. *Myb* and *Nfkb* (Figure 22E, 22F) total mRNA levels increase in cells expressing both hTDP-43 and hTDP-43<sup>A315T</sup> proteins. Interestingly, *Nfkb1* was identified as candidate from ribosome footprint in primary neurons for both WT vs hTDP-43<sup>A315T</sup> and WT vs hTDP-43 comparisons (Appendix 4). These results show that TDP-43 protein could regulate these ‘Master Regulators’, some at the mRNA level and some at the translational level, although these MRs were not identified from our ribosome profiling dataset. This could be due to the fact that we applied the standard stringent cut-off, demanding a more than two-fold change of differential expression. For most of the MRs, we observed only subtle changes in ribosome density. Presumably, this is why these MRs were not identified as TDP-43 targets in our dataset. Nevertheless, these directed experiments reveal potential effects on other MRs and suggest that more experiments should be conducted to examine neurodegeneration MR regulation by TDP-43.

## **5.8 TDP-43 PROTEIN INTERACTS DIRECTLY WITH *Camta1*, *Mig12*, AND *Dennd4a* mRNAs**

After having confirmed the altered ribosome density on target mRNAs, we then wanted to know if they are directly regulated by TDP-43 via direct binding. For this we performed crosslink immunoprecipitation (Figure 23A) (Ule et al. 2005). The protocol begins with UV crosslinking of RNA-protein complexes that are in direct contact (within angstrom distance). The cells in the culture dishes were irradiated with UV light which forms covalent bond between RNA and protein. This covalent bond allows rigorous purification including stringent washing during the downstream steps thus giving information about direct interacting targets.

We first, confirmed the specificity of immunoprecipitation of endogenous TDP-43 protein with anti-TDP-43 antibody relative to control IPs and that IP efficiency was not affected by UV treatment (Figure 23B). Following this, we used qRT-PCR to examine levels of specific mRNAs in the different IP samples, comparing *Camta1*, *Mig12*, and *Dennd4a* mRNAs to *Tdp-43* and *Gapdh* mRNAs. *Tdp-43* mRNA serves as a positive control, since TDP-43 is known to bind to its own mRNA for autoregulation (Ayala et al. 2011). Conversely, biologically significant binding of *Gapdh* mRNA by TDP-43 has not been described. We first confirmed that mRNA signals in TDP-43 IPs from UV-treated cells were greater than IgG control background in each of our three replicate experiments. Next, we quantified the percent of input mRNA that co-immunoprecipitated with TDP-43 protein. In UV-treated cells, we observed significant enrichment over *Gapdh* mRNA for *Tdp-43* and all our candidate mRNAs (Figure 23C). In the absence of UV treatment, mRNA recovery was reduced by more than 100 fold and significant enrichment relative to *Gapdh* mRNA was lost, demonstrating crosslink dependence of the detected interactions (Figure 23D). We conclude that TDP-43 protein interacts directly with *Camta1*, *Mig12*, and *Dennd4a* mRNAs in motor neuron-like MN1 cells.



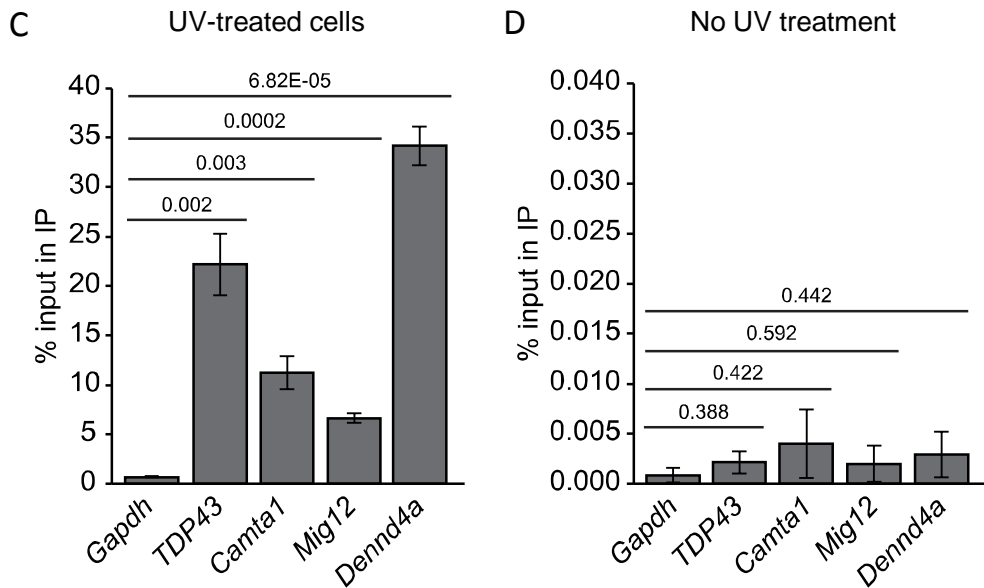


Figure 23: (A) Schematic diagram of the CLIP experiment. (B) Immunoblot showing specific IP of TDP-43 from MN1 cells under CLIP conditions. A TDP-43 band is specifically observed in the input and TDP-43 IP lanes from both untreated and UV-treated cells, but not in the IgG or anti-RBP X control lanes. RBP X is an IP of a different RNA-binding protein, which serves as an additional specificity control here. (C, D) Plots showing % of input mRNA in the TDP-43 IP for the mRNAs indicated in three separate CLIP assays from MN1 cells. Performing CLIP from UV-treated cells leads to significant recovery and enrichment relative to *Gapdh* for all mRNAs examined (C) (Figure generated by Christoph Janiesch in the Duncan lab). In the absence of UV treatment, much less mRNA is recovered and no significant enrichment relative to *Gapdh* mRNA is observed. Note that the Y-axis scale in D is 1000x smaller than in C, indicating strong crosslinking dependence of mRNA co-immunoprecipitation (n=3, s.e.m. error bars, P-values indicated in the plot, unpaired two-tailed t-test).

### 5.9 hTDP-43 AND hTDP-43<sup>A315T</sup> ENHANCE TRANSLATION OF *Camta1* AND *Mig12* mRNAs VIA THEIR 5'UTRS

We next wanted to determine which regions of the translationally targeted mRNAs might be important for regulation. First, we performed a manual search for potential TDP-43 binding sites in annotated *Camta1*, *Mig12*, and *Dennd4a* mRNAs. Long (UG) repeats strongly correlate with TDP-43 binding, and shorter motifs are neither necessary nor sufficient (Tollervey et al. 2011; Polymenidou et al. 2011). We found no repeats >5nt in these mRNAs (Table 3), suggesting that TDP-43 either recognizes these mRNAs through short motifs or other types of binding sites.

Gene name	5'UTR	CDS	3'UTR
<i>Camta1</i>	-	9	6
<i>Mig12</i>	1	-	5
<i>Dennd4a</i>	-	11	6

Table 3: TDP-43 (UG) repeat motifs in 5'UTR, CDS and 3'UTR of target mRNAs

Next, we performed dual luciferase assays to identify the mRNA regions that are necessary for translational regulation by TDP-43. 'Dual reporter assays' refers to the simultaneous use of two different reporter genes in a single system for studying gene expression. The 'experimental reporter' carries the mRNA regions of interest and 'control reporter' which is co-transfected to the same system serves as an internal control. The activity of the experimental reporter is normalized to the activity of the control reporter in order to minimize experimental variability caused by differences in cell viability or transfection efficiency.

Next, we generated plasmids encoding Renilla luciferase (RLuc) reporters with 5' or 3'UTRs from *Mig12*, *Camta1*, and *Dennd4a* mRNAs. We co-transfected MN1 cells with these reporters and a plasmid encoding hTDP-43<sup>A315T</sup> or an equivalent amount of a control plasmid encoding GFP. In parallel, we also evaluated whether the effects were indeed specific for the mutant TDP-43 protein by co-transfecting a similar amount of plasmid encoding hTDP-43, which we know gives similar protein expression levels to the mutant under our assay conditions. As shown in Figure 24, in dual luciferase assays we observed enhanced RLuc levels only from specific combinations of reporters and proteins. Importantly, under the tested conditions neither hTDP-43 nor hTDP-43<sup>A315T</sup> affected RLuc production from the control plasmid used for cloning (Figure 24A). Co-transfection of either hTDP-43 or hTDP-43<sup>A315T</sup> led to a significant increase in RLuc activity for both *Camta1* and *Mig12* 5'UTR reporters (Figure 24B, 24D). In contrast, no significant increase was observed for *Camta1* or *Mig12* 3'UTR reporters with either protein (Figure 24C, 24E). These data highlight the 5'UTRs of *Camta1* and *Mig12* mRNAs as important regions for their translational enhancement by TDP-43. They also reveal that regulation in these cases is not specific to the patient mutant allele: hTDP-43 and hTDP-43<sup>A315T</sup> were both able to stimulate RLuc output from these reporters to similar extents.

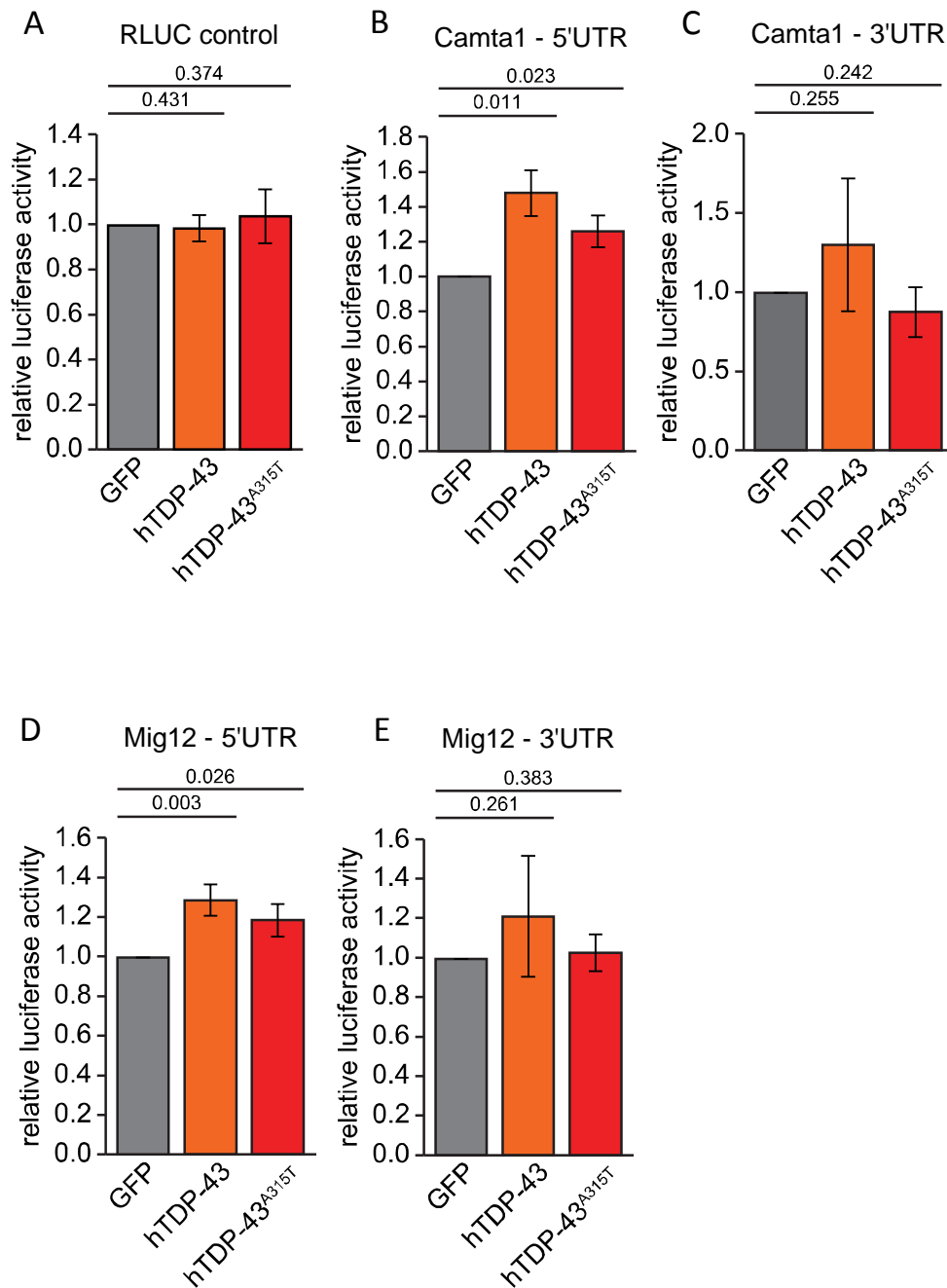


Figure 24: Relative luciferase activity measured by dual luciferase assay in MN1 cells transfected with GFP, hTDP-43, or hTDP-43<sup>A315T</sup> and co-transfected with Fluc and either Rluc vector ctrl containing no UTR of interest (A), Camta1 5'UTR (B), Camta1 3'UTR (C), Mig12 5'UTR (D), Mig12 3'UTR (E). (n=3-7; s.e.m. error bars, P-value indicated, unpaired one-tailed t-test).

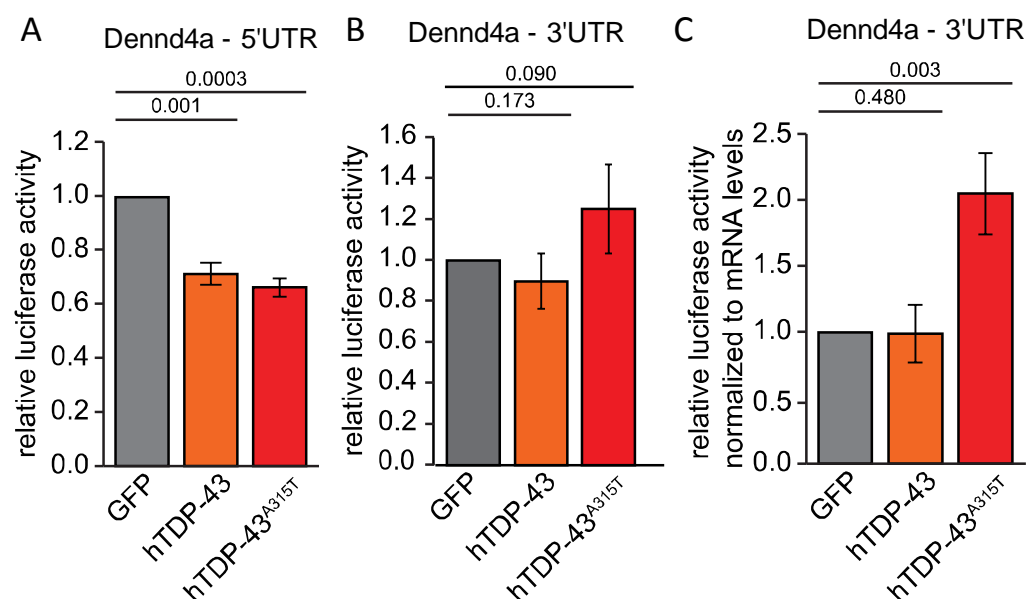
## 5.10 hTDP-43<sup>A315T</sup> ENHANCES TRANSLATION OF *Dennd4a* mRNA THROUGH A SPECIFIC 3'UTR REGION

Unlike *Camta1* and *Mig12*, the 5'UTR of *Dennd4A* mRNA appeared to confer translational repression by both hTDP-43 and hTDP-43<sup>A315T</sup> under our assay

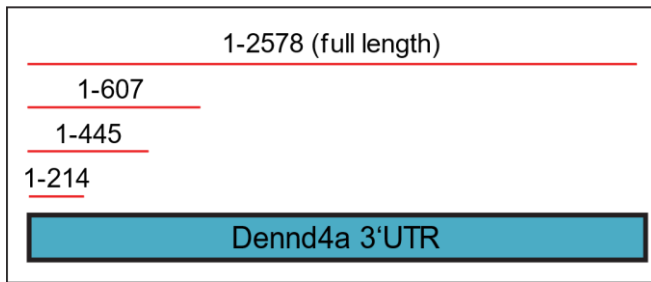


conditions (Figure 25A). This was surprising, given that hTDP-43A315T expression increased ribosome density on *Dennd4a* mRNA in both polysome assays and the original ribosome profiling screen. Standard luciferase measurements with the *Dennd4a* 3'UTR reporter showed only a trend toward increased RLuc activity in the presence of hTDP-43<sup>A315T</sup> (Figure 25B). However, normalizing luciferase activity to reporter mRNA levels revealed a significant increase in RLuc protein/mRNA that was strikingly specific for the hTDP-43<sup>A315T</sup> mutant protein (Figure 25C). These data suggest that a disease-causing allele of TDP-43 has a function that is specific for the mutant protein: selective enhancement of translation of *Dennd4a* mRNA via its 3'UTR.

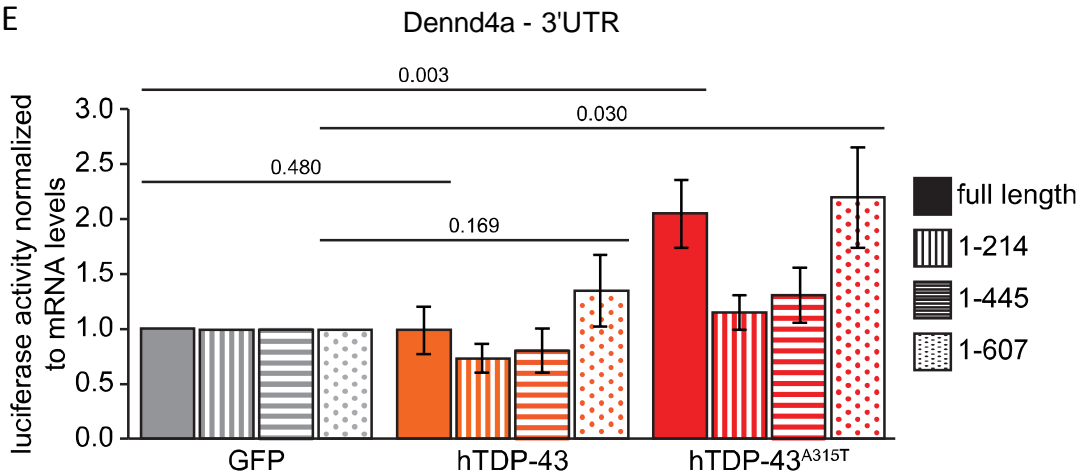
To determine which regions of the *Dennd4a* 3'UTR might be important for selective translational enhancement by hTDP-43A<sup>315T</sup>, we tested a series of truncation mutants in the same assay setup (Figure 25D, 25E). As shown in Figure 25E, hTDP-43<sup>A315T</sup> was able to enhance translation of a reporter containing nucleotides 1-607 of the *Dennd4a* mRNA 3'UTR to a level comparable to the full-length 3'UTR reporter, whereas truncating further leading to shorter 3'UTRs abolished regulation. As expected, WT hTDP-43 did not stimulate translation of any of these reporters. Importantly, this was not due to differential expression level of hTDP-43, since its mRNA levels were very similar to those for hTDP-43<sup>A315T</sup> in these assays (Figure 25F). These data suggest that a region between nucleotides 445-607 of the *Dennd4a* 3'UTR is particularly important for selective translational enhancement of this mRNA by a patient mutant allele of TDP-43.



D



E



F

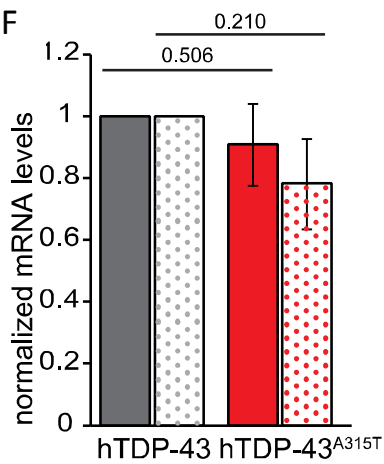
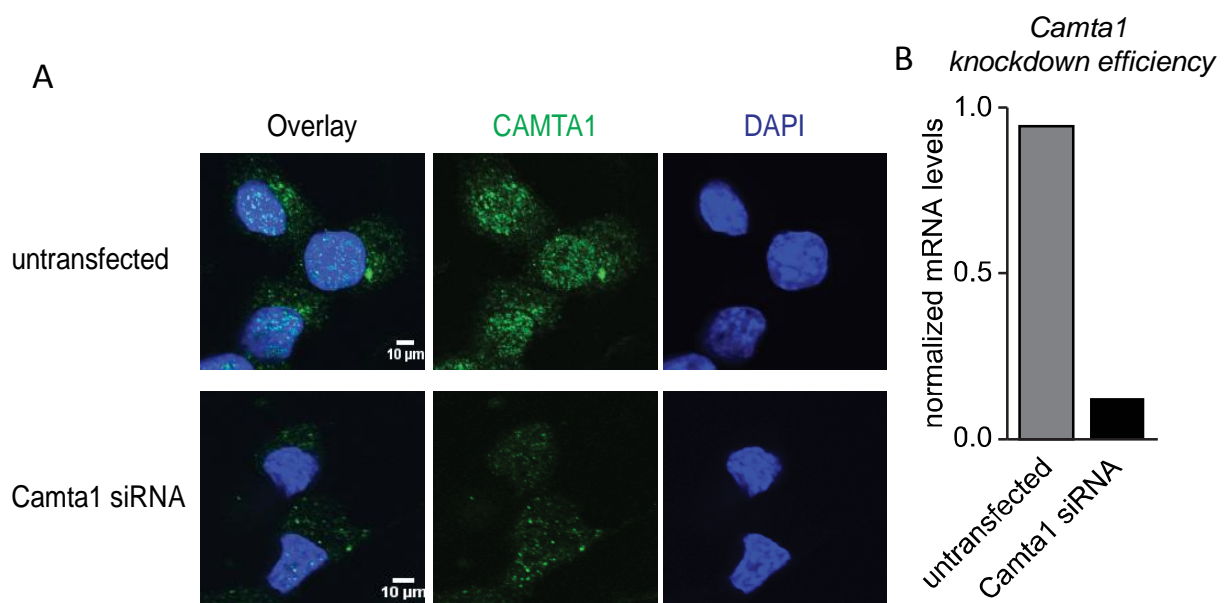


Figure 25: Relative luciferase activity measured by dual luciferase assay in MN1 cells transfected with GFP, hTDP-43, or hTDP-43<sup>A315T</sup> and co-transfected with Fluc and either Rluc vector containing *Dennd4a* 5'UTR (A), *Dennd4a* 3'UTR (B). (C) Relative luciferase activity normalized to mRNA levels in cells cotransfected with *Dennd4a* 3'UTR. (D) Schematic of *Dennd4a* 3'UTR-derived constructs used for this study. (E) Relative luciferase activity normalized to mRNA levels in cells co-transfected with GFP, hTDP-43, or hTDP-43<sup>A315T</sup>, Fluc, and the indicated *Dennd4a* 3'UTR constructs shown in D (n=3-7; s.e.m. error bars, P-value indicated, unpaired one-tailed t-test). (F) Comparison of hTDP-43 mRNA

expression levels in the MN1 cells transiently co-transfected with hTDP-43 or hTDP-43<sup>A315T</sup>. Lack of a significant difference implies that specific regulation of the *Dennd4a* reporters by hTDP-43<sup>A315T</sup> is not due to differential expression vs. hTDP-43 (n=3-7; s.e.m. error bars, P-values indicated, unpaired two tailed t-test).

## 5.11 VALIDATION OF CAMTA1 AND MIG12 ANITIBODIES

Having established that TDP-43 binds directly to *Camta1*, *Mig12*, and *Dennd4a* mRNAs and can enhance translation via their UTRs, we next sought to determine the potential functional impact of altered translation of these mRNAs on levels of the encoded proteins. In order to do that we first validated antibodies targeting these proteins using knockdown experiments. For these experiments we used MN1 cells and XtremeGene siRNA transfection reagent (Roche), ON-TARGET plus Mouse *Mid1ip1* siRNA-SMART pool) and ON-TARGETplus Mouse *Camta1* siRNA-SMART pool from GE Healthcare/ Dharmacon.



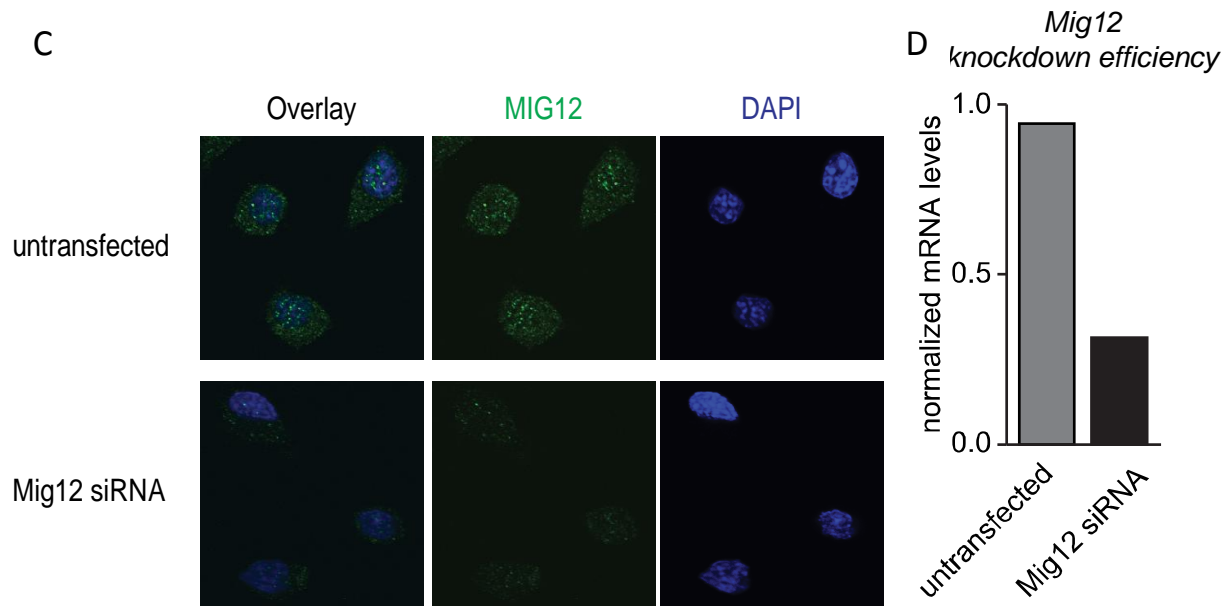


Figure 26: (A) Immunostaining of MN1 untransfected control and cells transfected with *Camta1* siRNA after 72 hours of knock down stained for CAMTA1 (green) and DAPI (blue). (B) Knockdown efficiency of *Camta1* mRNA measured by qRT-PCR and normalized to *Gapdh*. (C) Immunostaining of MN1 untransfected control and cells transfected with *Mig12* siRNA after 72 hours of knock down stained for MIG12 (green) and DAPI (blue). (D) Knockdown efficiency of MIG12 measured by qRT-PCR and normalized to *Gapdh*. Note the significant decrease in IF signal for both CAMTA1 and MIG12 after siRNA knockdown, implying specific detection of these proteins in MN1 cells under our IF conditions.

We achieved 80% knockdown for CAMTA1 and 70% knockdown for MIG12 proteins (Figure 26). These results show that the antibodies we used gave specific signal for our proteins of interest in immunostaining experiments.

## 5.12 hTDP-43 OVEREXPRESSION LEADS TO INCREASED CAMTA1 AND MIG12 PROTEIN LEVELS IN MN1 CELLS

In order to assess the effect of TDP-43 on MIG12 protein levels, we first performed a western blot, one of the standard assays used for this purpose. We transfected MN1 cells with GFP control vector, hTDP-43-V5 and hTDP-43<sup>A315T</sup>-V5 plasmids. 24 hours after transfection, cells were lysed and standard western blot was performed (see methods for lysis and western blot protocols). Upon quantification of these blots, we observed a trend towards increase in protein level upon expression of both hTDP-43 and hTDP-43<sup>A315T</sup> proteins (Figure 27).

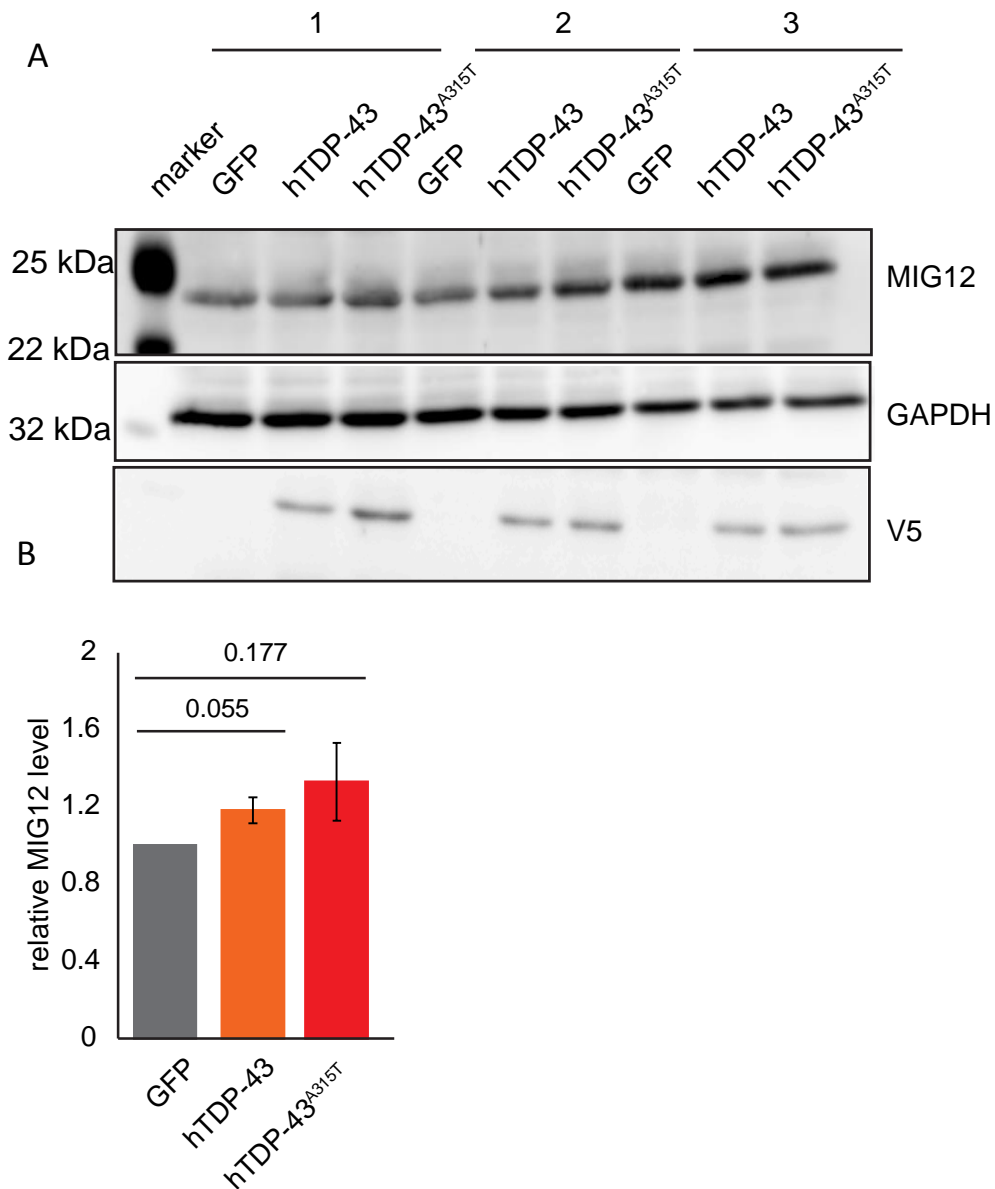


Figure 27: (A) MN1 cells were transfected with GFP control, hTDP-43-V5 or hTDP-43-A315T-V5. Three independent transfections are shown. Immunoblotting was performed for MIG12, GAPDH, or the V5 tag. (B) Normalized MIG12 protein levels were quantified and are shown relative to GFP-transfected controls (n=3, s.e.m error bars, P-values indicated; unpaired two-tailed t-test). Note the trend toward increased levels after transfection of hTDP-43-V5 or hTDP-43-A315T-V5, but lack of significance ( $P > 0.05$ ).

Subsequently, we performed immunostaining experiments, reasoning that this might be more sensitive and could provide information about potential spatial effects of altered protein synthesis. We transfected MN1 cells with V5-tagged hTDP-43 variants and examined the impact on endogenous CAMTA1 and MIG12 immunofluorescence signal intensity in confocal microscopy images. Transfection efficiencies were around 70% in these assays, allowing us to compare protein levels in transfected (V5+) cells

to neighboring untransfected (V5-) cells from the same coverslip. Since these untransfected (V5-) cells have been processed and imaged in parallel, they serve as an ideal internal control. Consistent with the reporter assay results, we observed increased levels of CAMTA1 protein in cells transfected with either hTDP-43 WT or hTDP-43<sup>A315T</sup> protein (Figure 28A, 28B) and this was manifested in both the nucleus and cytoplasm (Figure 28C, 28D).

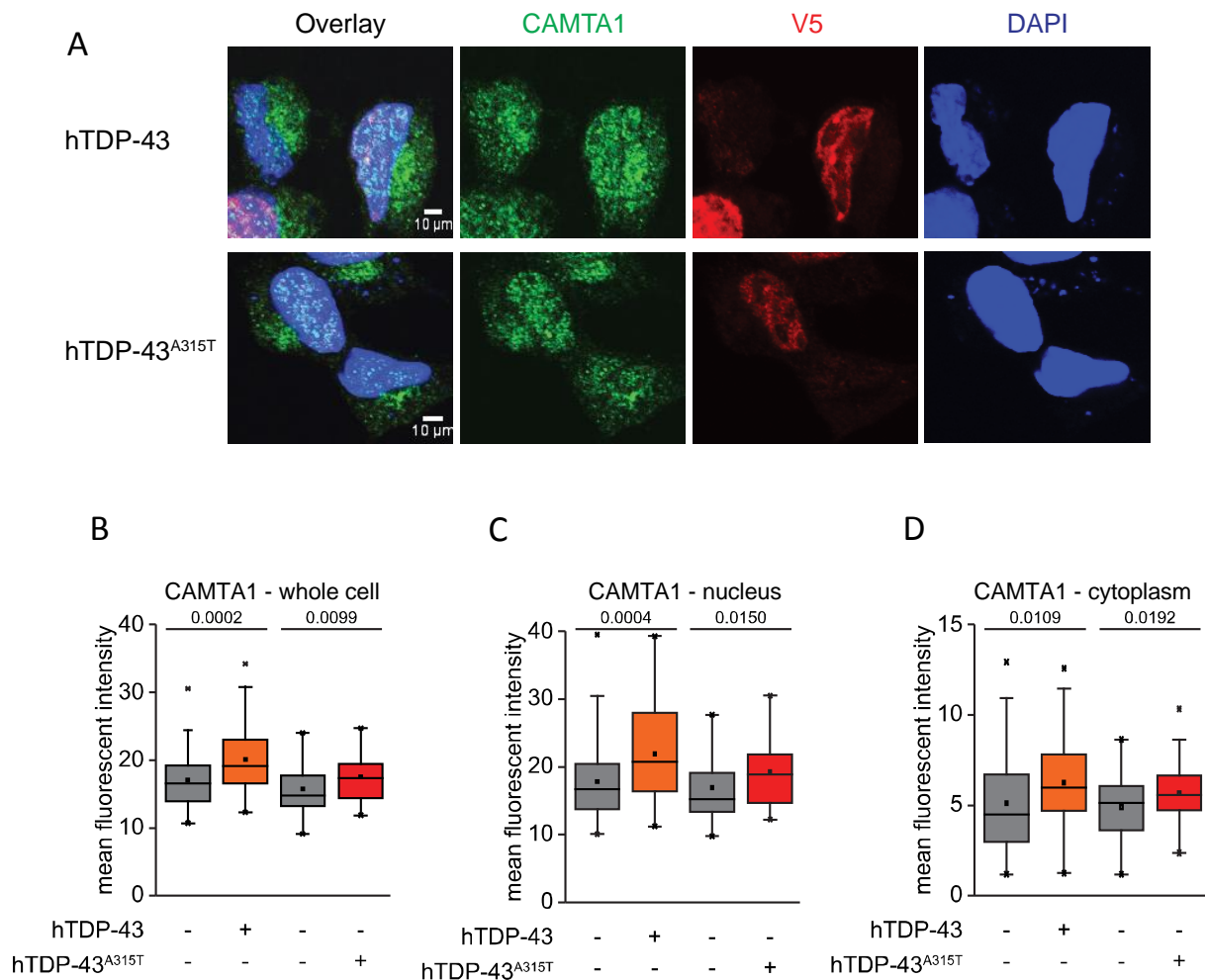


Figure 28: (A) Immunofluorescence of MN1 cells transiently transfected with hTDP-43-V5 or hTDP-43<sup>A315T</sup>-V5 and stained for CAMTA1 (green), V5 (red), and DAPI (blue); Scale bar represents 10  $\mu$ m. Intensity of CAMTA1 in whole cell (B), nucleus (C), and cytoplasm (D); (n= 40-60 cells each; P-value indicated in each plot; unpaired two-tailed t-test).

MIG12 protein levels were also increased in cells transfected with either hTDP-43-V5 or hTDP-43<sup>A315T</sup>-V5 protein relative to neighboring untransfected (V5-) control cells (Figure 29A, 29B). However, a significant increase in MIG12 protein levels appeared

only in the nucleus, even though specific MIG12 protein signal was present in both the nucleus and cytoplasm (Figure 29C, 29D).

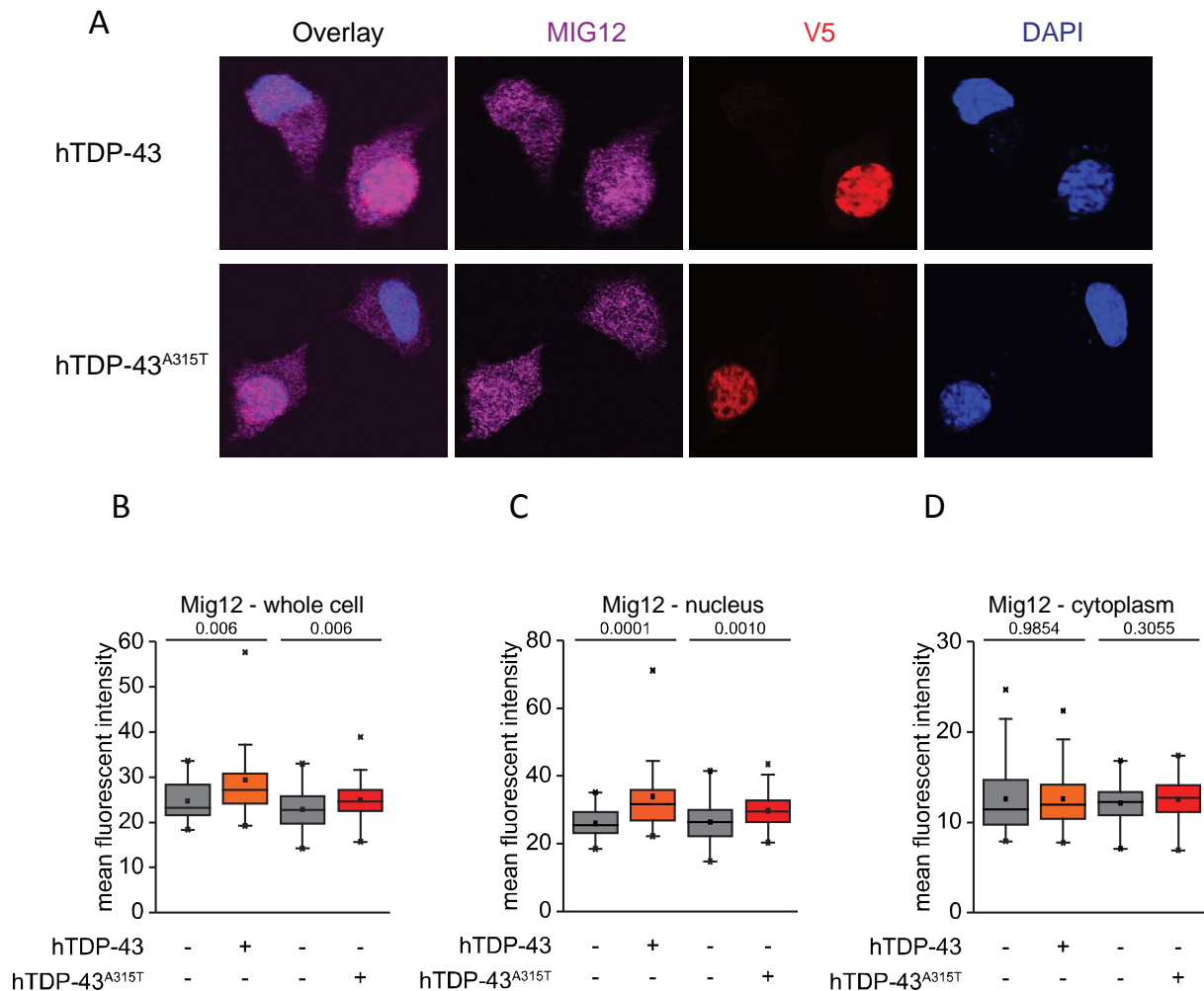


Figure 29 (A) Immunofluorescence of MN1 cells transiently transfected with hTDP-43-V5 or hTDP-43<sup>A315T</sup>-V5 and stained for MIG12 (magenta), V5 (red), and DAPI (blue); Scale bar represents 10  $\mu$ m. Intensity of MIG12 in whole cell (B), nucleus (C), and cytoplasm (D); (n= 30-70 cells each; P-value indicated in each plot; unpaired two-tailed t-test).

As an additional control for these studies, we transfected a plasmid encoding EGFP instead of TDP-43 and compared GFP+ cells to their GFP- neighbors. CAMTA1 and MIG12 protein levels were not changed between GFP+ and GFP- cells (Figure 30), highlighting a specific role for TDP-43 in this assay. These data indicate that increased levels of TDP-43 can enhance protein levels encoded by two of its directly bound translational targets. Moreover, as for translational enhancement of *Camta1* and *Mig12* 5'UTR reporters in luciferase assays, these effects on endogenous protein levels are observed with either WT or mutant TDP-43.

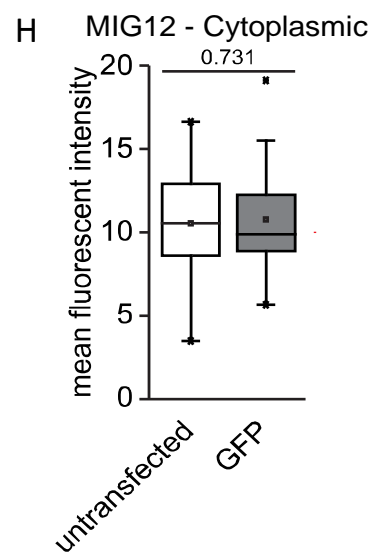
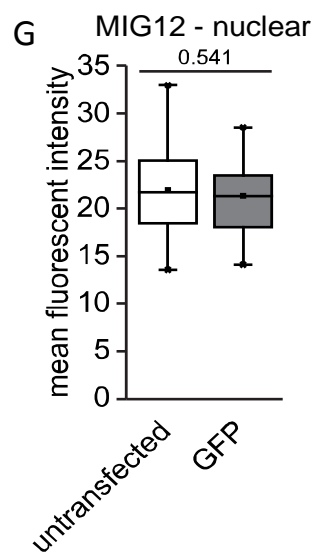
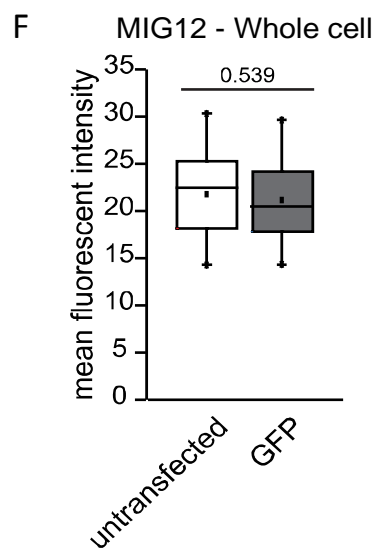
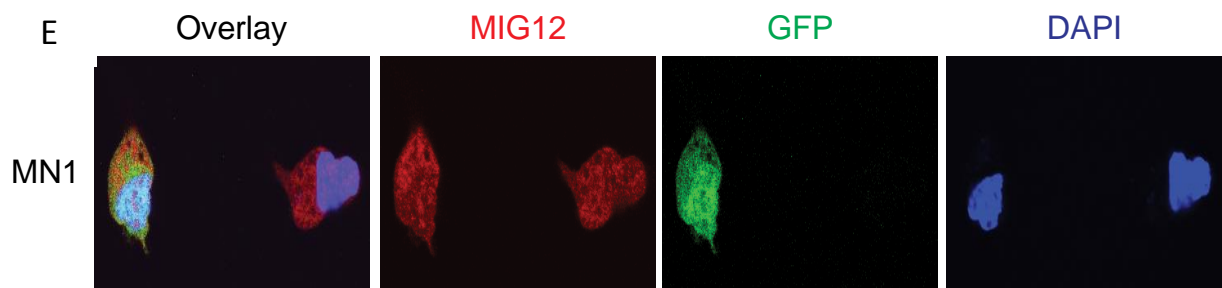
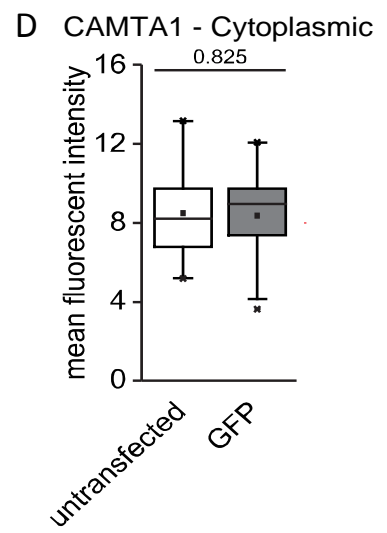
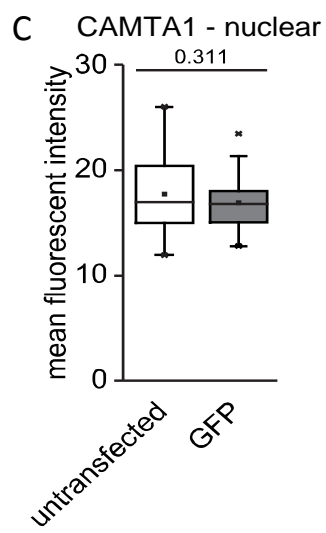
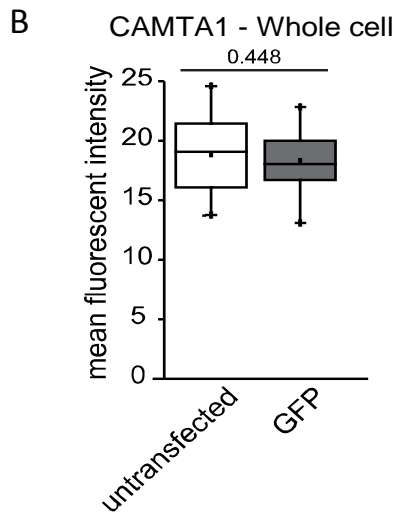
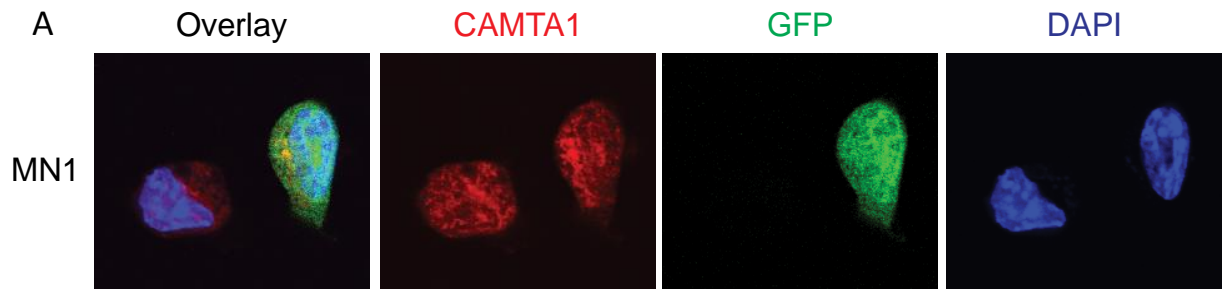




Figure 30: (A-D) Immunostaining for CAMTA1 with MN1 cells transfected with pEGFP-C1 plasmid. (A) Representative images showing staining for CAMTA1 (red) and DAPI (blue). Intensity of CAMTA1 in the whole cell (B), nucleus (C), and cytoplasm (D) (n= 30-35 cells each; P-value indicated in each plot; unpaired two-tailed t-test). (E-H) Immunostaining for MIG12 with MN1 cells transfected with pEGFPC1 plasmid. (E) Representative images showing staining for MIG12 (red) and DAPI (blue). Intensity of MIG12 in the whole cell (F), nucleus (G) and in cytoplasm (H) (n= 36, 40 cells; P-values indicated in each plot; unpaired two-tailed t-test).

### **5.13 hTDP-43<sup>A315T</sup> EXPRESSION LEADS TO INCREASED MIG12 PROTEIN LEVELS IN PROCESSES OF PRIMARY CORTICAL NEURONS**

In our ribosome profiling experiments, MIG12 was identified as an hTDP-43<sup>A315T</sup> target in both MN1 cells and primary neuronal cultures (Table 1). Thus, we next investigated the effect of mutant hTDP-43 expression on MIG12 protein levels in primary cortical neurons obtained from the same transgenic mouse ALS model expressing hTDP-43<sup>A315T</sup> (Wegorzewska et al. 2009). As in MN1 cells, MIG12 was present in both the nucleus and cytosol of cultured cortical neurons. Moreover, we also detected MIG12 staining in neuronal processes marked by Tau1 antibody staining (Figure 31A, 31B). In contrast to MN1 cells, we did not observe any change in nuclear MIG12 intensity in cultured cortical neurons expressing hTDP-43<sup>A315T</sup> relative to non-transgenic littermate controls (Figure 31C). However, quantification of MIG12 signal intensity in neuronal processes revealed a significant increase in the MIG12 protein level in neurites of cells expressing hTDP-43<sup>A315T</sup> protein as compared to non-transgenic wild type cells (Figure 31D). In contrast, levels of phosphorylated Tau protein (Tau1 staining) in neuronal processes were not significantly altered (Figure 31B, 31E), supporting a specific effect on MIG12 protein levels. Thus, our immunostaining data shows that MIG12 protein levels are also affected by hTDP-43<sup>A315T</sup> protein in primary cultures of cortical neurons. Intriguingly, the effect here is also cellular compartment-specific, but manifests in neuronal processes, rather than in the nucleus.

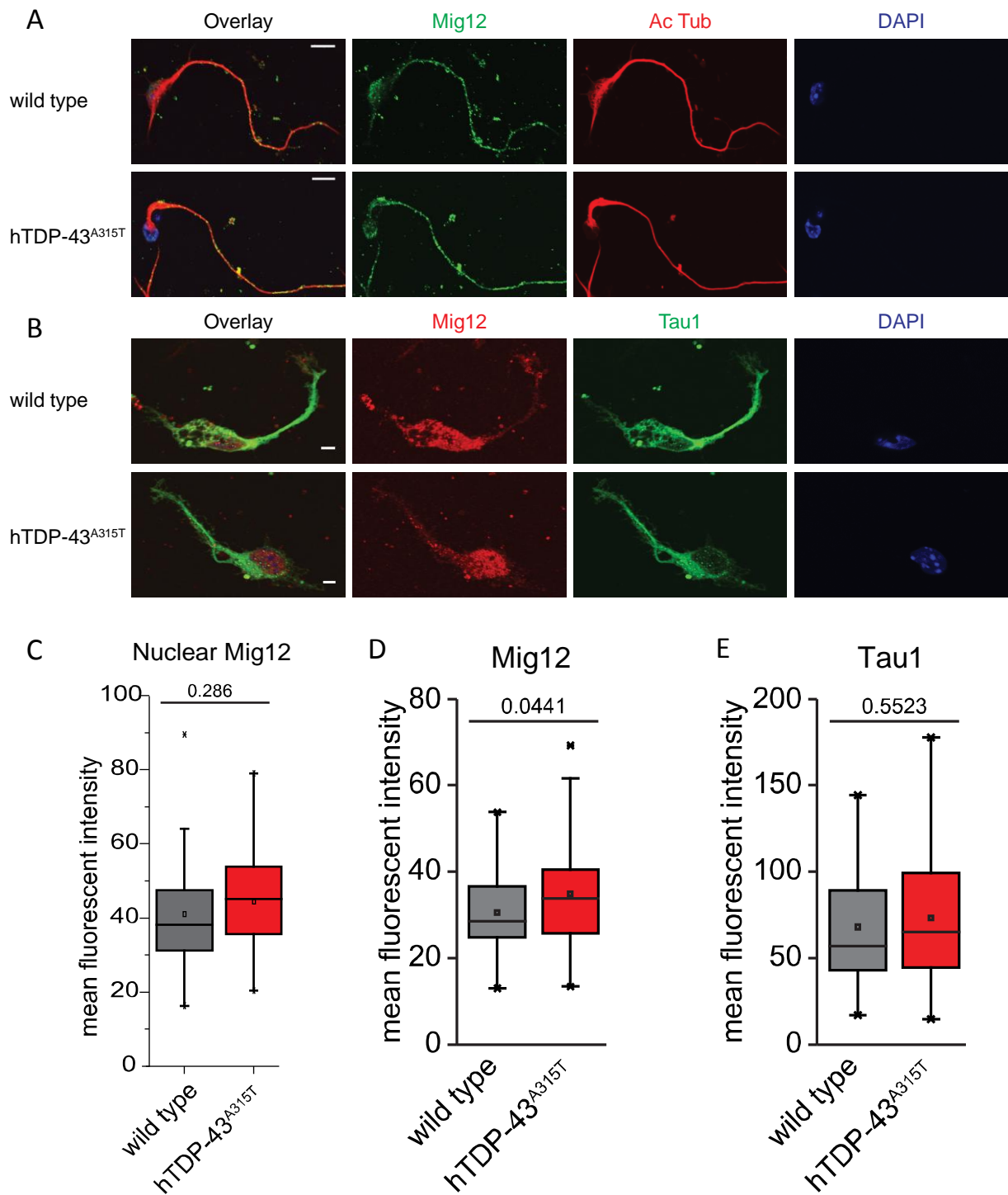


Figure 31: (A, B) Representative immunofluorescence images of DIV2 primary cortical neurons from mice expressing the hTDP-43<sup>A315T</sup> protein or non-transgenic wild type littermates. Scale bar represents 10  $\mu$ m. (A) MIG12 (green), Acetylated tubulin (red) and DAPI (blue). (B) MIG12 (red), TAU (using Tau1 antibody, red) and DAPI (blue); (C) Mean fluorescence intensity of MIG12 in the nuclei of DIV-2 primary cortical neurons (two-tailed t-test, P-values indicated in the plot). (D) Quantification of mean fluorescent intensity of MIG12 in neurites. (n= 37-40 cells from three independent cultures; unpaired two-tailed t-test, P-values indicated in plot). (E) Quantification of mean fluorescent intensity of Tau1

immunoreactivity in neurites (n=30-33 cells from three independent cultures; unpaired two-tailed t-test, P-values indicated in plot).

#### **5.14 MID1, A DISEASE-ASSOCIATED MIG12 BINDING PARTNER, MODIFIES TDP-43'S EFFECTS ON MIG12 PROTEIN**

Unlike CAMTA1 and DENND4A, no direct connection between MIG12 and neurodegenerative disease has previously been described. However, several lines of evidence support a role for MIG12's protein-protein interaction partner, MID1, in both neurodevelopmental disorders and neurodegenerative disease (Winter et al. 2016). MID1 is a cytoplasmic protein whose molecular functions include E3 ubiquitin ligase activity and regulation of translation through direct and indirect mechanisms (Zanchetta et al. 2017; Winter et al. 2016; Trockenbacher et al. 2001; Krauss et al. 2013). This suggests that MID1 binding to MIG12 could affect MIG12 protein levels, and that this could be a potential connection between altered Mig12 mRNA translation and neurodegenerative disease. To examine this possibility, we asked whether increasing cytoplasmic MID1 levels had any impact on how TDP-43 affects MIG12 protein levels. Specifically, we transfected MN1 cells with either hTDP-43 or hTDP-43<sup>A315T</sup> and co-transfected equivalent amounts of either pcDNA3 empty vector control or myc-GFPMID1 (Figure 32A, 32B, respectively). When pcDNA3 empty vector was co-transfected, we observed the expected increased protein levels driven by hTDP-43 or hTDP-43<sup>A315T</sup> (Fig 32A, 32C). In striking contrast, co-transfection of a myc-GFP-MID1 plasmid led to expression of myc-GFP-MID1 in the cytoplasm and completely abolished TDP-43's effects on nuclear MIG12 levels (Fig. 32B, 32C). Cytoplasmic MIG12 levels were not affected by hTDP-43 or hTDP-43<sup>A315T</sup> when either pCDNA3.1 or myc-GFP-MID1 was co-transfected (Figure 32D). Thus, overexpression of MID1 can mitigate the effect of overexpressing hTDP-43 proteins on MIG12 protein levels in MN1 cells. These results suggest that cytoplasmic MID1 levels can determine whether altered ribosome density on Mig12 mRNA leads to altered MIG12 protein levels in the nucleus.

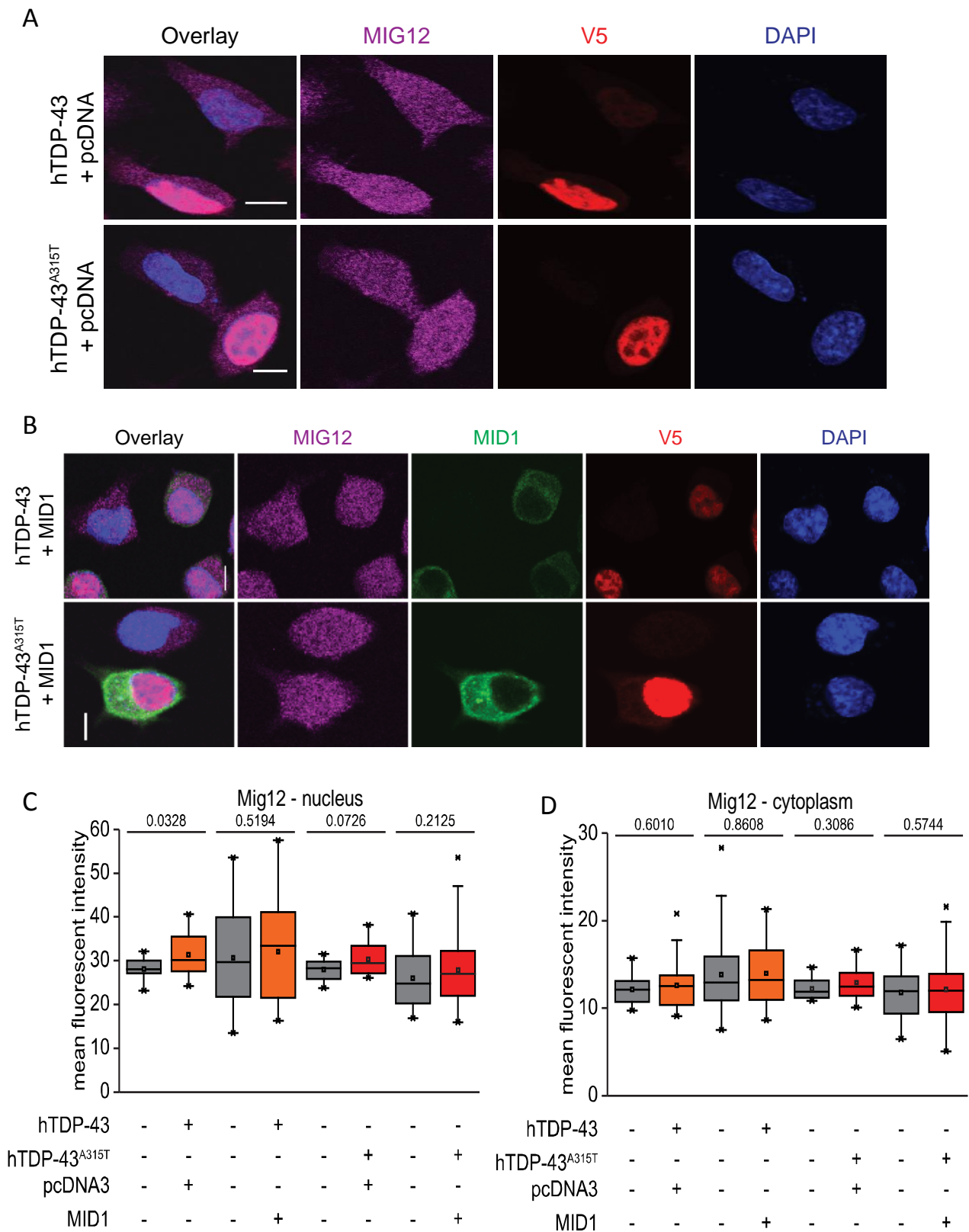


Figure 32: Immunofluorescence of MN1 cells transiently transfected with (A) Flag-hTDP-43-V5/ Flag- hTDP- 43<sup>A315T</sup>-V5 and pcDNA control plasmid stained for MIG12 (Magenta), V5 (red) and DAPI (blue). Immunofluorescence of MN1 cells transiently transfected with (B) Flag-hTDP-43- V5/ Flag- hTDP- 43<sup>A315T</sup>-V5 and MycGFP Mid1 plasmid stained for MIG12 (Magenta), MID1 (green from GFP), V5 (red) and DAPI (blue). Scale bar represents 10  $\mu$ m.

Intensity of MIG12 in nucleus (C) and cytoplasm (D) (n= 10-24 cells for hTDP-43/ hTDP-43<sup>A315T</sup> and pcDNA3 transfection; n= 42-72 cells for hTDP-43/hTDP-43<sup>A315T</sup> and MycGFP-Mid1 transfection; P-value indicated in each plot; unpaired two-tailed t-test).

## 5.15 OPTIMIZATION OF RIBOSOME PROFILING PROTOCOL FOR BETTER DATA QUALITY

Ribosome footprint profiling can provide much more information than simply ribosome density on the coding sequence since it also provides positional information on where ribosomes are bound on an mRNA and can even delineate which reading frame is being used. In principle, ribosome positional information can be useful for identifying new uORFs, alternative start sites, and regulated use of alternative open reading frames. After having identified new translational targets of TDP-43, we wanted to use our datasets to study the effects of TDP-43 in uORF utilization and/or alternative translation start sites. However, the quality of the data required for robust analysis of positional information is much higher than for standard differential expression analysis. Our dataset gave results compared to other published datasets in both Pearson correlation analysis (Table 4) and mapping statistics (Appendix 2), implying that it was suitable for differential expression analysis. For positional analyses a different set of quality control measures are required. This section of my thesis examines our original dataset using these measures, leading to the conclusion that we cannot use it for positional analyses on individual mRNAs. It further describes the steps I took to try to establish improved ribosome profiling conditions with our neurodegeneration models that would enable such analyses.

	GFP_f1	GFP_f2	GFP_t1	GFP_t2	a315_t_f1	a315_t_f2	a315_t_t1	a315_t_t2	wt_f_1	wt_f_2	wt_t_1	wt_t_2
GFP_f1	1.00	0.93	0.89	0.89	0.94	0.92	0.89	0.88	0.93	0.90	0.89	0.88
GFP_f2	0.93	1.00	0.88	0.89	0.93	0.92	0.88	0.87	0.92	0.91	0.88	0.88
GFP_t1	0.89	0.88	1.00	0.95	0.89	0.87	0.96	0.94	0.89	0.85	0.95	0.94
GFP_t2	0.89	0.89	0.95	1.00	0.89	0.88	0.96	0.96	0.89	0.86	0.95	0.95
a315_t_f1	0.94	0.93	0.89	0.89	1.00	0.92	0.90	0.88	0.93	0.90	0.89	0.88
a315_t_f2	0.92	0.92	0.87	0.88	0.92	1.00	0.88	0.87	0.91	0.90	0.88	0.88
a315_t_t1	0.89	0.88	0.96	0.96	0.90	0.88	1.00	0.96	0.90	0.86	0.96	0.95

<b>a315 t_t2</b>	0.88	0.87	0.94	0.96	0.88	0.87	<b>0.96</b>	<b>1.00</b>	0.88	0.85	0.95	0.95
<b>wt_f 1</b>	0.93	0.92	0.89	0.89	0.93	0.91	0.90	0.88	<b>1.00</b>	<b>0.90</b>	0.90	0.89
<b>wt_f 2</b>	0.90	0.91	0.85	0.86	0.90	0.90	0.86	0.85	<b>0.90</b>	<b>1.00</b>	0.86	0.85
<b>wt_t 1</b>	0.89	0.88	0.95	0.95	0.89	0.88	0.96	0.95	0.90	0.86	<b>1.00</b>	<b>0.94</b>
<b>wt_t 2</b>	0.88	0.88	0.94	0.95	0.88	0.88	0.95	0.95	0.89	0.85	<b>0.94</b>	<b>1.00</b>

Table 4: Pearson correlation for MN1 samples sequenced at lower sequencing depth. GFP-GFP control transfected cells; wt- hTDP-43 transfected cells; a315t- hTDP-43<sup>A315T</sup> transfected cells; t- Total mRNA; f- footprint samples; 1, 2- replicate number. Replicate samples are highlighted in green. Note that the correlation between the replicates is high.

Our sequencing depth for the above mentioned study was between 10 and 15 million total reads yielding around one million mapped reads. This, however is too low to obtain any of the information mentioned above. Besides low read count the reproducibility of the data indicated by pearson correlation was high with values >0.93 for most samples (Table 4). We also observed the expected preference in reads mapping to coding sequence (CDS) vs. 3'UTRs in ribosome footprint samples, but not corresponding total mRNA samples (Appendix 2). This implies that the footprint data is OK by these quality metrics. Nevertheless, we obtained very few genes that are found to be differentially regulated upon DESeq analysis. This could either mean that very few things are regulated or that relatively low sequencing depth prevented their detection.

	<b>a_t_f 1</b>	<b>a_t_f 2</b>	<b>a_t_t 1</b>	<b>a_t_t 2</b>	<b>GFP _f1</b>	<b>GFP _f2</b>	<b>GFP _t1</b>	<b>GFP _t2</b>	<b>hwt_ f1</b>	<b>hwt_ f2</b>	<b>hwt_ t1</b>	<b>hwt_ t2</b>
<b>a_t_f 1</b>	<b>1.00</b>	<b>0.97</b>	0.82	0.83	0.95	0.96	0.83	0.85	0.97	0.96	0.85	0.85
<b>a_t_f 2</b>	<b>0.97</b>	<b>1.00</b>	0.83	0.87	0.95	0.99	0.85	0.89	0.97	0.99	0.86	0.89
<b>a_t_t 1</b>	0.82	0.83	<b>1.00</b>	<b>0.97</b>	0.77	0.82	0.96	0.95	0.78	0.83	0.97	0.95
<b>a_t_t 2</b>	0.83	0.87	<b>0.97</b>	<b>1.00</b>	0.80	0.86	0.97	0.98	0.81	0.88	0.98	0.98
<b>GFP _f1</b>	0.95	0.95	0.77	0.80	<b>1.00</b>	<b>0.95</b>	0.79	0.83	0.96	0.95	0.81	0.83
<b>GFP _f2</b>	0.96	0.99	0.82	0.86	<b>0.95</b>	<b>1.00</b>	0.84	0.89	0.97	0.99	0.85	0.89
<b>GFP _t1</b>	0.83	0.85	0.96	0.97	0.79	0.84	<b>1.00</b>	<b>0.95</b>	0.81	0.85	0.97	0.95
<b>GFP _t2</b>	0.85	0.89	0.95	0.98	0.83	0.89	<b>0.95</b>	<b>1.00</b>	0.85	0.91	0.96	0.99

<b>hwt_</b> <b>f1</b>	0.97	0.97	0.78	0.81	0.96	0.97	0.81	0.85	<b>1.00</b>	<b>0.97</b>	0.82	0.84
<b>hwt_</b> <b>f2</b>	0.96	0.99	0.83	0.88	0.95	0.99	0.85	0.91	<b>0.97</b>	<b>1.00</b>	0.87	0.90
<b>hwt_</b> <b>t1</b>	0.85	0.86	0.97	0.98	0.81	0.85	0.97	0.96	0.82	0.87	<b>1.00</b>	<b>0.96</b>
<b>hwt_</b> <b>t2</b>	0.85	0.89	0.95	0.98	0.83	0.89	0.95	0.99	0.84	0.90	<b>0.96</b>	<b>1.00</b>

Table 5: Pearson correlation for MN1 samples resequenced at higher sequencing depth. GFP- GFP control transfected cells; hwt- hTDP-43 transfected cells; a\_t- hTDP-43<sup>A315T</sup> transfected cells; t- Total mRNA; f- footprint samples; 1, 2- replicate number. Replicate samples are highlighted in green. Note that the correlation between the replicates are high.

In an attempt to improve sequencing depth, we resequenced the same samples with greater sequencing depth aiming for more mappable reads and thereby potentially identifying more candidate genes. Upon resequencing, the raw reads were around 50 million and the mapped reads were ranging between three and five million. One reason for this big disconnect between raw reads and mapped reads could be rRNA contamination. Nevertheless, the resequenced samples also had a higher Pearson correlation for the biological replicates with values >0.95 (Table 5). Following this we performed some of the quality checking for both of the original and the resequenced datasets, including read length analysis, subcodon analysis (frame preference analysis), and read mapping position. Dr. Lorenzo Calviello, who was then a PhD student with Prof. Dr. Uwe Ohler, performed some of these quality control analyses using their standard pipeline.

Typical ribosome footprint reads are known to be 28-29nt long. But read length analysis shows that all of our footprint reads were longer. Figure 33 shows that footprint samples from both rounds of sequencing are 33-35 nt long. This is most likely explained by inefficient RNase I digestion, one of the important steps in generating ribosome-protected fragments.

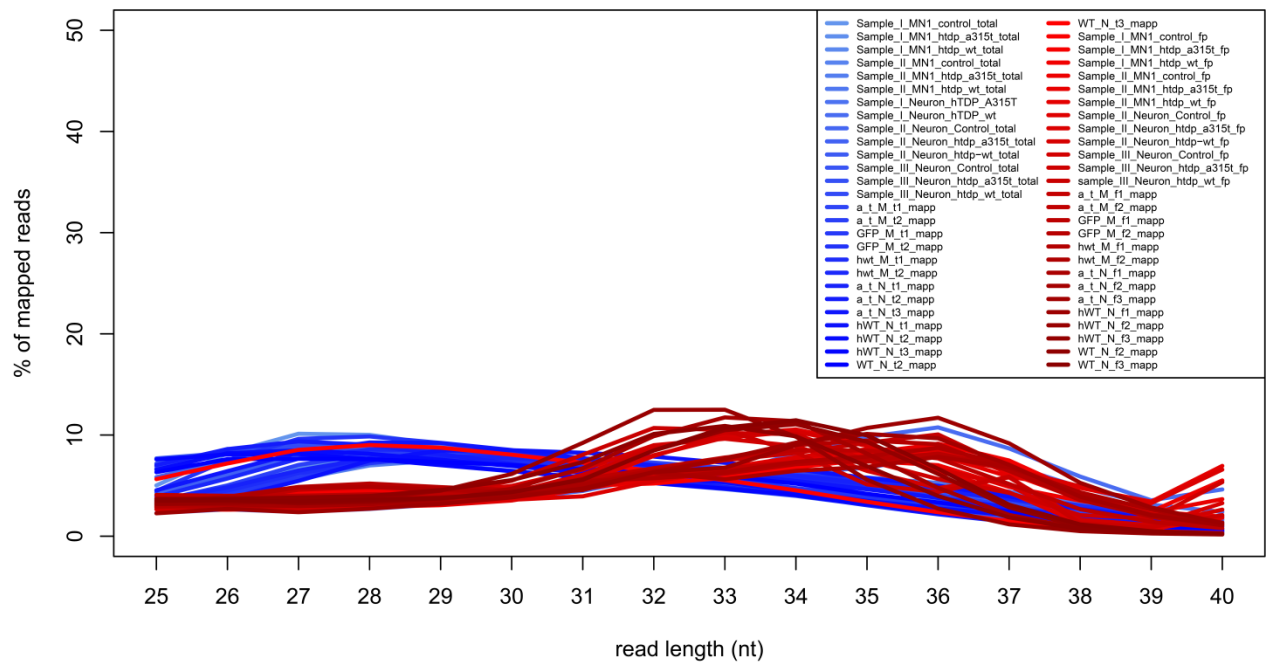


Figure 33: Read length analysis for MN1 and primary neuron samples from both rounds of sequencing. Samples labelled in different shades of blue indicate total mRNA and samples in different shades of red indicate ribosome footprint samples. Note that the footprint samples are 33-35 nt long. GFP- GFP control transfected cells; hwt- hTDP-43 transfected cells; a\_t- hTDP-43<sup>A315T</sup> transfected cells; t, total- Total mRNA; f, fp- footprint samples; I,II, 1, 2- replicate number.

Next, Dr. Calviello analyzed the mapping position of both total and footprint reads across the whole genome. Gratifyingly, this analysis shows that the ratio of percentage of reads mapped to CDS to percentage of reads mapped to UTRs is very high for footprint samples as expected. This illustrates that this data could be used for differential expression analysis as these are real footprint reads. This analysis also revealed that, although we have a greater percentage of reads being mapped to CDS, we have a prominent amount of reads mapped to the intergenic regions in our footprint samples than expected (Figure 34).



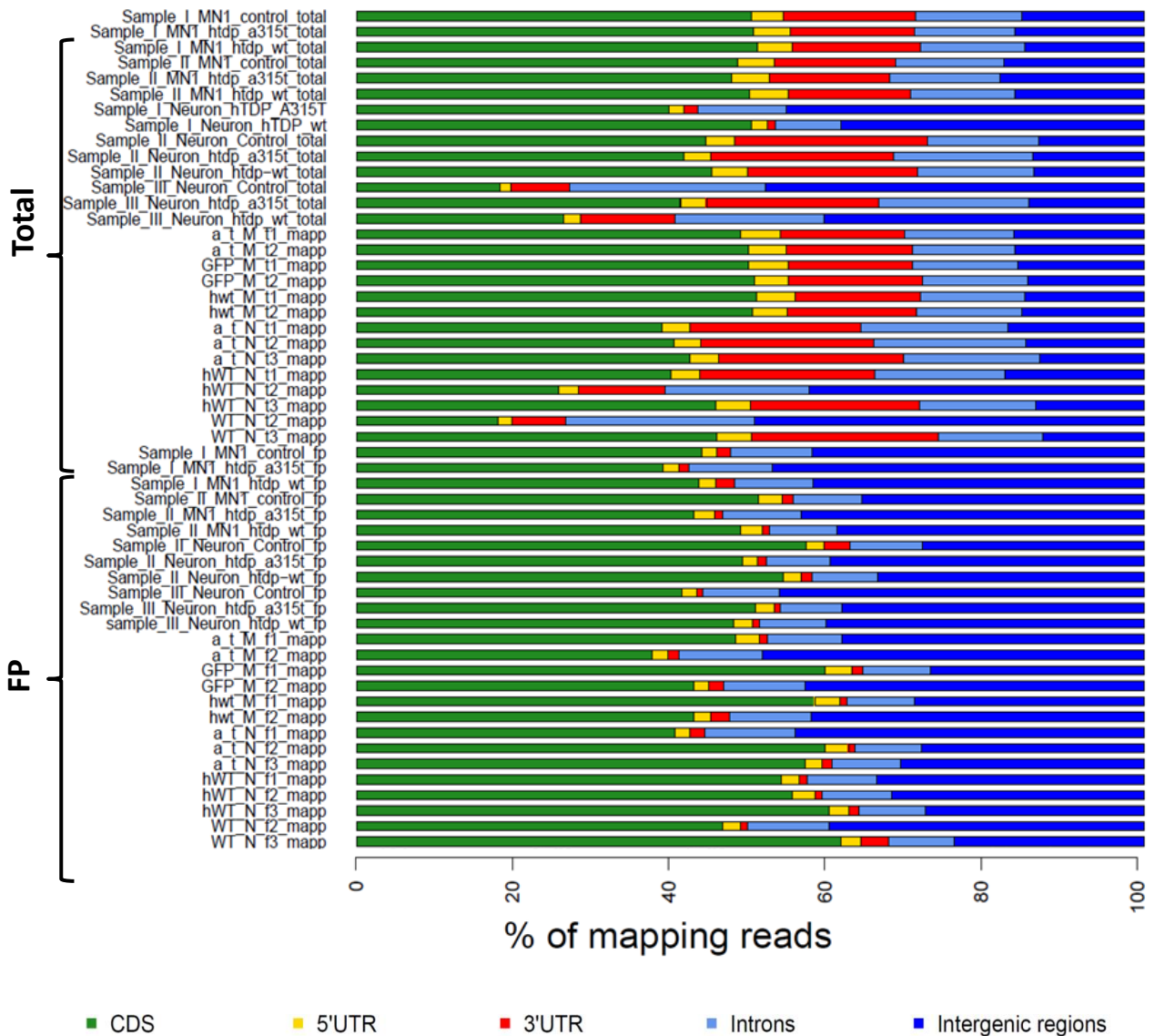


Figure 34: Mapping positions of total and footprint reads across genome. Note that footprint samples have a high fraction of reads mapping to intergenic region. GFP- GFP control transfected cells; hwt- hTDP-43 transfected cells; a\_t- hTDP-43<sup>A315T</sup> transfected cells; t, total- Total mRNA; f, fp- footprint samples; I,II, 1, 2- replicate number Figure generated by Dr. Calviello in Uwe Ohler's lab..

It is well known that the 5' end of the ribosome footprint fragments start 12-13nt upstream of start codon and 18 nt upstream of stop codon and it is expected to show a clear 3nt periodicity (Ingolia et al. 2009). Thus reads covered by ribosome footprints indicate the reading frame being translated and this gives us the idea of frame preference of translation. Also it is well established that these ribosome protected fragments started on the first nucleotide of a codon (Ingolia et al. 2009) (Figure 35).

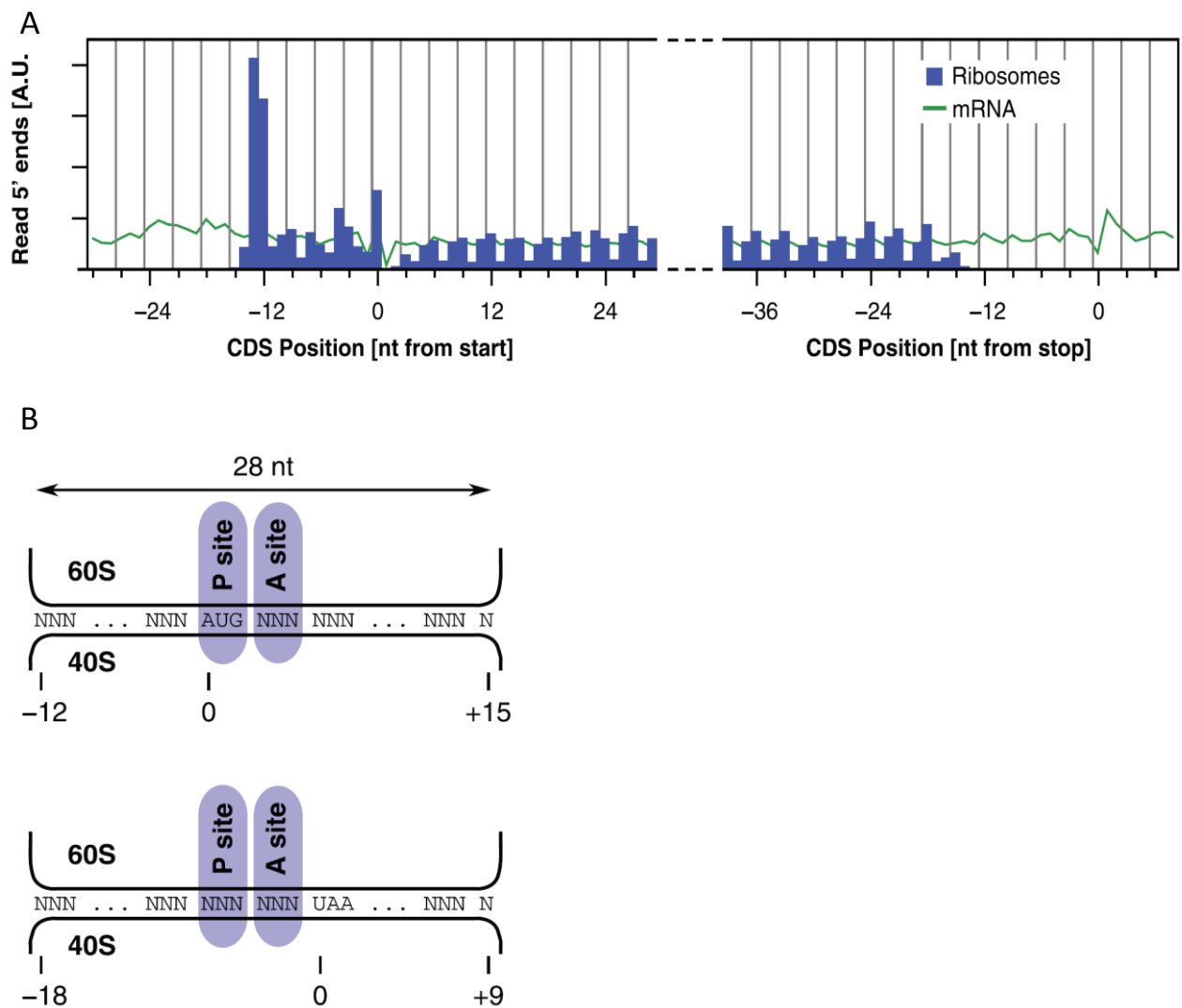


Figure 35: (A). Plot showing the distribution of ribosome footprint reads at the start and stop codon of mRNA. (B). Graph showing the distance between 5' end of footprint reads and P site of the ribosome at the start codon and stop codon. (Figure from (Ingolia et al. 2009)).

Next, we wanted to look at these parameters in our datasets. This was performed by Malik Alawi, from Bioinformatics Core, University Medical Center Hamburg-Eppendorf (UKE). These analyses show that in our datasets, there is no codon periodicity for footprint reads that are 29nt long, whereas reads that are 35-36nt long maintain the codon periodicity which means the main reading frame preference is maintained (Figure 36). This holds true for both MN1 and primary neuron datasets. This again indicates that the real footprint reads in our datasets are longer than they should be, implying that the RNaseI treatment was inefficient.

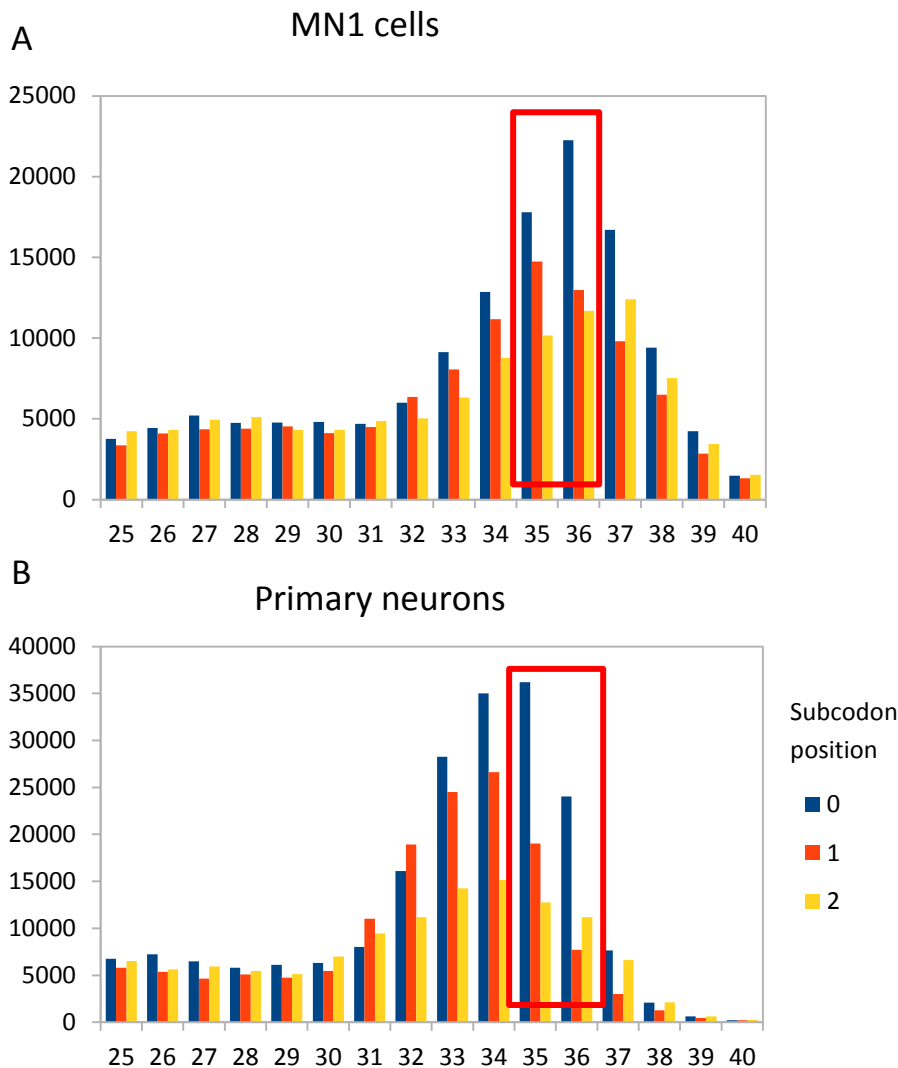


Figure 36: (A). Triplet periodicity analysis for MN1 footprint reads. (B). Triplet periodicity analysis for primary neurons footprint reads. Note that the longer reads of 35-36nt have clear main reading frame preference. (x-axis indicate read length; y-axis indicate number of mapped reads) Figure generated by Malik Alawi at the Bioinformatics core of UKE, Hamburg.

Taken together, all these analyses show that these data cannot be used for positional analyses and needs further optimization. Most of the above mentioned issues with these data arise from inefficient RNaseI treatment. Another drawback of these data is very high amount of ribosomal RNA contaminantion.

Now that we have identified some of the major issues with these datasets, we decided to optimize the protocol to get better data. First we optimized the RNaseI digestion by using different amount of the enzyme. Next, we included rRNA depletion step by hybridization of first strand cDNAs to biotinylated sense-strand

oligonucleotides followed by removal of the duplexes using streptavidin beads. The depletion oligos sequences and the protocol were obtained from (Ingolia et al. 2012). For these optimization experiments, we used untransfected MN1 cells. We used three different amounts of RNaseI- 12 U/ 30  $\mu$ g RNA, 15 U/ 30  $\mu$ g RNA and 17 U/ 30  $\mu$ g RNA. To check if our rRNA depletion protocol worked, we included negative controls where we skipped this step.

As this was optimization experiment, we performed sequencing on NextSeq 500, SR 75 cycles- single reads platform that gives upto 400 million reads. We obtained a wide range of raw read counts with a minimum of 11 million reads and a maximum of 50 million reads (Appendix 7). There was a very minimal enrichment for reads aligned to CDS in samples where rRNA depletion step was included. Nevertheless, we proceeded with further quality control analysis.

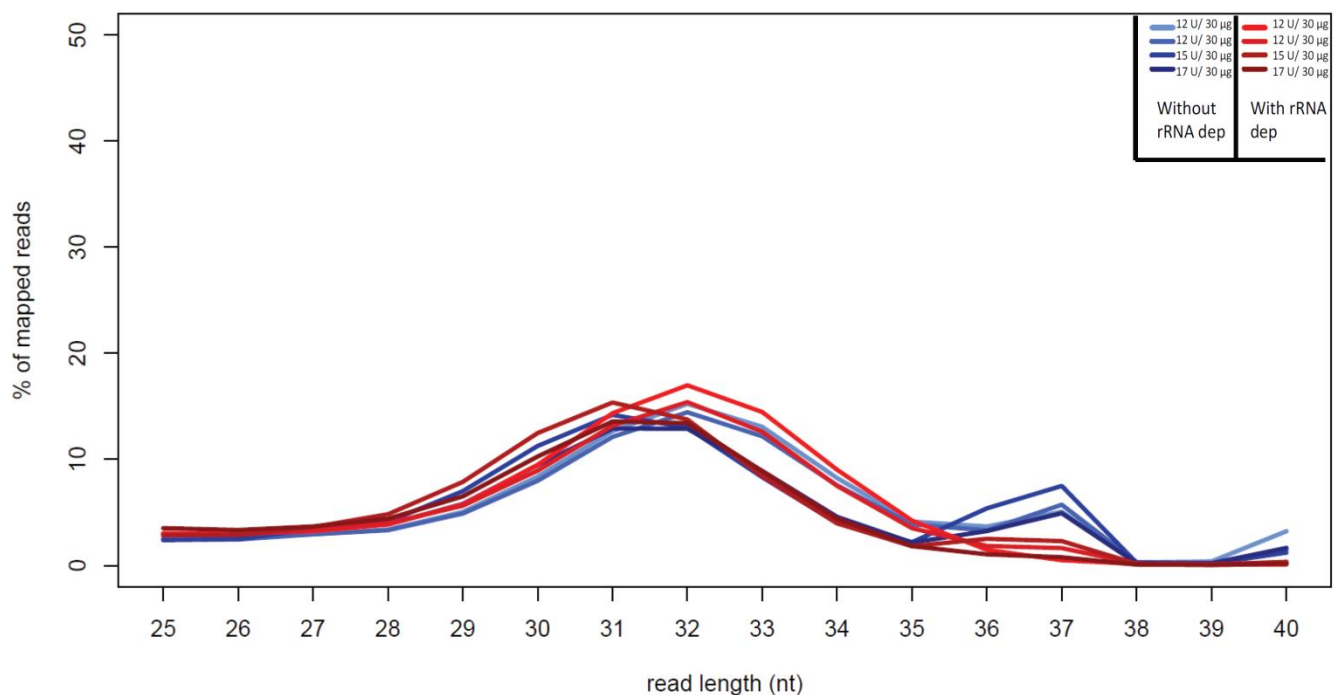


Figure 37: Read length analysis for optimization samples with various RNaseI amount and with/without rRNA depletion. Samples labelled in different shades of blue indicate samples without rRNA depletion and samples labelled in different shades of red indicate samples with rRNA depletion.

Read length analysis show that the fragment length was indeed dependent upon RNaseI amount. Samples with 12U / 30 $\mu$ g RNA yielded 32-33 nt long fragments, whereas samples with 15 U/ 30  $\mu$ g RNA and 17 U/ 30  $\mu$ g RNA resulted in slightly

shorter 31 nt long fragments (Figure 37). Interestingly, for samples where rRNA depletion step was excluded, there was a prominent peak at 37nt which could imply that these might be derived from ribosomal RNA fragments.

Upon analyzing the mapping positions in these samples, we saw a significant improvement over the previous datasets.

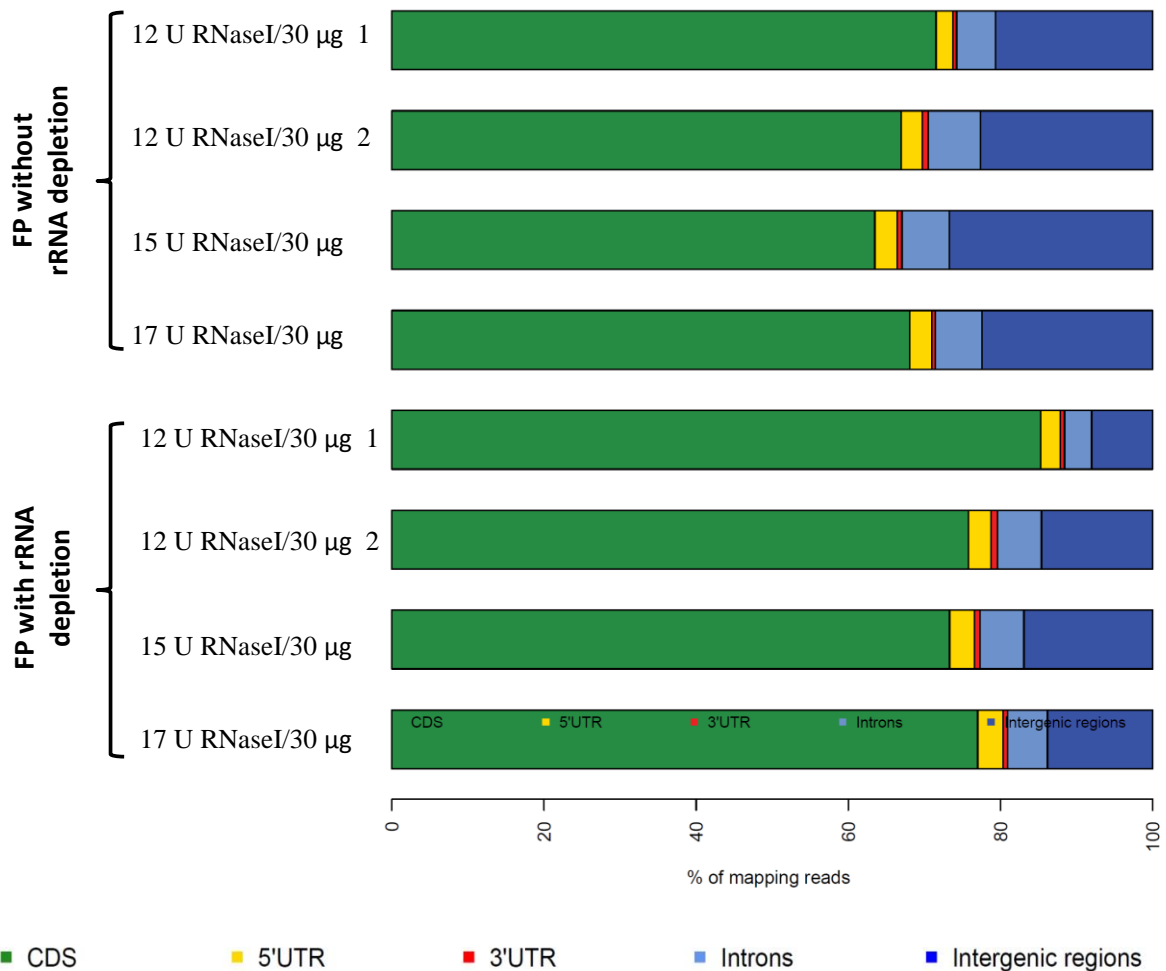


Figure 38: Mapping positions of optimized footprint reads with various RNaseI amount and with/without rRNA depletion. Note that 80% of reads were mapped to CDS in samples with rRNA depletion.

We observed few differences between samples with and without rRNA depletion. In samples without rRNA depletion we observed 30% of reads mapping to intergenic region, where as this was further reduced in samples with rRNA depletion where we had 15-20% of reads mapping to intergenic region (Figure 38). Additionally, reduced intergenic reads contamination resulted in advantage of more reads mapping to CDS. In these samples we observed 75-80% of reads mapping to CDS, which implies that

we have made some parts of the protocol work better than in the previous experiments.

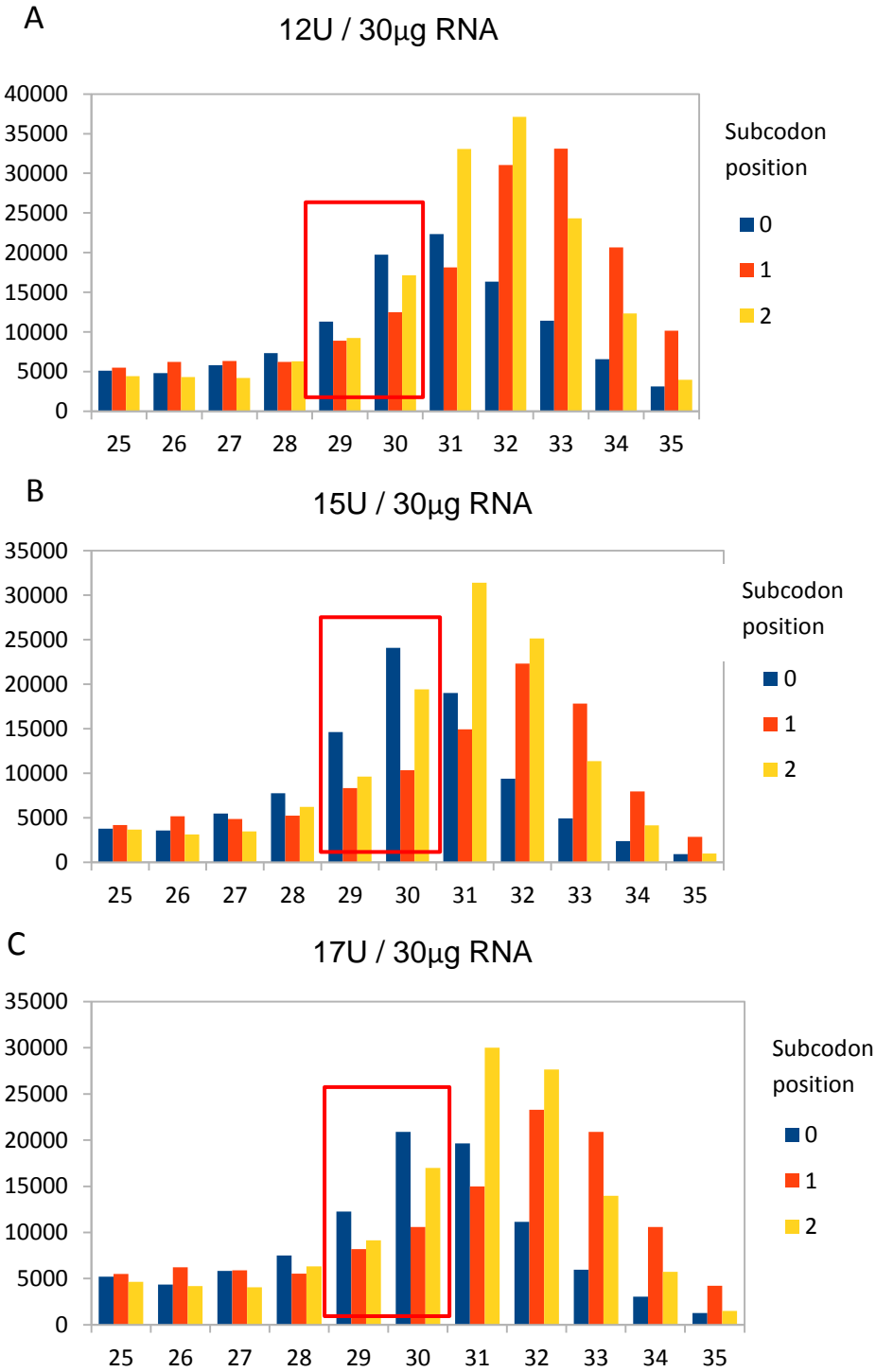


Figure 39: (A-C). Triplet periodicity analysis for optimized footprint reads with various RNaseI amount and with rRNA depletion; 12 U/ 30  $\mu$ g RNA (A), 15 U/ 30  $\mu$ g RNA (B) and 17 U/ 30  $\mu$ g RNA (C) (x-axis indicate read length; y-axis indicate number of mapped reads).

Following this we performed subcodon analysis on these datasets. In samples treated with 12 U/ 30  $\mu$ g RNA, we did not see the expected frame preference. In samples with more RNaseI amount, we observed the main reading frame preference to some extent, for reads that are 29-30 nt long. Besides that, replicating the results observed in Figure 37, we found more reads that are 34-35 nt long in sample with least amount of RNaseI (12 U/ 30  $\mu$ g RNA). And the distribution shifts more towards shorter fragments as the RNaseI amount increases.

To summarize, although the new protocol appears to be an improvement over the previous protocol we used, there were few drawbacks. We enriched for the correct sized fragments and we also obtained reading frame preference to some degree. Nevertheless, this could be further improved, perhaps by using even higher amounts of RNase I, titrating the duration or temperature of RNaseI treatment, or perhaps switching to a different nuclease. Additionally, we still had a major fraction of contaminating ribosomal RNA reads, which implies that the rRNA depletion step should further be improved. Despite this, mapping statistics were greatly improved by our modifications, with 80% of reads now mapping to CDSs. Although this refined protocol worked better than the previous experiments, it needs further optimization if we want to generate data where positional information can be reliably analyzed

## 6. DISCUSSION

TDP-43 is known to be one of the key players in ALS and FTD and many efforts have been undertaken to study the role of this RNA-binding protein both in healthy cells and in disease (Reviewed in (Zu et al. 2013; Ratti and Buratti 2016; Lee, Lee, and Trojanowski 2012). Studies have shown that TDP-43 affects various steps of mRNA metabolism both in nucleus and cytoplasm during disease. Most of these studies have focussed on its role in nucleus and there are fewer studies addressing its role in the cytoplasm.

Here, we used a genome wide method 'ribosome profiling' to study the effects of TDP-43 in translational regulation. In this study, we used two cell culture models of the types of neurons that are affected in ALS and FTD: 1. Motor neuron-like cell line-MN1 for modelling lower motor neurons, 2. Primary cortical neurons for modelling upper motor neurons and related neurons affected in both diseases. This led us to the identification of three new translational target mRNAs of human TDP-43 protein: *Camta1*, *Dennd4a*, and *Mig12*. Interestingly, *Mig12* mRNA was found to be translationally targeted by TDP-43 in both MN1 cells and primary neurons. Ribosome profiling experiments show that these mRNAs have increased ribosome density when a mutated form of human TDP-43 is expressed. Cross-linking IP experiments demonstrate that these mRNAs are directly bound by TDP-43. Moreover these mRNAs are previously implicated in neurodegenerative diseases. Using reporter assays we have identified the mRNA regions that are important for this translational regulation by TDP-43. Our results show that TDP-43 functions as an **mRNA-specific translational enhancer**. They also reveal that the impact of such altered mRNA translation can be dynamically regulated in a cell type-specific manner and by binding partners of the protein encoded.

### 6.1 TDP-43 IS REGULATING TRANSLATION OF SPECIFIC mRNAs

TDP-43 shuttles between nucleus and cytoplasm, but is and it is known to be more localized towards cytoplasm during disease. Moreover, the majority of TDP-43 appears to relocate to the cytoplasm as a response to neuronal injury and nuclear localization is reestablished upon recovery (Moisse et al. 2009). These results raise the possibility that an enhancement of cytoplasmic TDP-43 functions may be involved in the regulation of neuronal function as part of an injury response. One of the main



unanswered question is whether the disease is the result of loss of nuclear function, gain of cytoplasmic function, or some combination of the two (Lee, Lee, and Trojanowski 2012).

In this project, we focussed on a potential cytoplasmic role of TDP-43. As mentioned earlier (section 1.5.4.4.), there are few studies addressing the effect of TDP-43 in translational regulation. These directed studies with individual mRNAs indicate that TDP-43 represses translation of specific mRNAs under certain conditions. We were interested in assessing whether human TDP-43 wildtype or mutant protein might have an effect on general translation in MN1 cells. Polysome profiles generated from MN1 cells transfected with GFP control/ hTDP-43/ hTDP-43<sup>A315T</sup> protein show that there were no effects on general translation. It is very likely that TDP-43 has no role in global translation, rather it is involved in translational regulation of specific mRNAs.

## **6.2 CELL BASED MODELS TO STUDY EARLY EFFECTS OF WILDTYPE AND MUTANT hTDP-43**

As mentioned earlier, the MN1 cell line was generated by fusing mouse spinal motor neurons and neuroblastoma cells (Salazar-Grueso, Kim, and Kim 1991). MN1 cells express choline acetyl transferase (ChAT), a lower motor neuron marker. We performed transient transfections with hTDP-43/ hTDP-43<sup>A315T</sup>. It is important to note that the expression of these proteins themselves did not lead to any visible phenotypes in these cells. To study the effect of hTDP-43<sup>A315T</sup> on translation in primary cortical neurons we used E16 transgenic mice expressing the mutant human TDP-43 under the control of the prion promoter (Wegorzewska et al. 2009). In order to examine how the translational landscape is affected in cells expressing hTDP-43 WT protein we used E16 mice transgenic mice expressing the human TDP-43 WT under the control of prion promoter (Xu et al. 2010). As an additional negative control, we used primary cortical cultures from pure wildtype animals (littermates).

It is noteworthy that neither MN1 cells nor these cultured neurons exhibit any overt phenotypes at the stage we used them for our experiments. Accordingly, we consider these cells as systems to study the early molecular changes resulting from the expression of hTDP-43/hTDP-43<sup>A315T</sup> proteins.

### **6.3 IDENTIFICATION OF NEW TRANSLATIONAL TARGET mRNAs OF HUMAN TDP-43<sup>A315T</sup> PROTEIN**

We performed ribosome footprint profiling (Ingolia et al. 2012) on transfected MN1 cells and primary cortical neurons from E16 embryos grown for 14 days in culture. We obtained a very small set of genes for both transcriptional and translational targets (Appendix 3-6). We applied the cutoff of minimum two-fold change in gene expression for any gene to be considered as a real candidate to be a regulatory target of TDP-43. Replicate numbers were two for MN1 cells and three for primary neuronal cells. Our mapping statistics shown in Appendix 1, are similar to many published ribosome profiling experiments. However, they are lower than in some studies and this could be why we identified very few mRNAs as candidates.

Another possible explanation is that in our MN1 cell experiments, we performed mild overexpression of hTDP-43WT or the A315T mutant for only 24 hours (Figure 10). However, our primary neuron cultures were made from embryos that overexpress the transgene for longer period. Nevertheless, the expression levels are not high enough to cause any striking phenotype at this stage. Based on this, we conclude that, although there are steps where the protocol could be improved, these candidates that we obtained are real. Moreover, we used ribosome profiling as a primary screening technique to identify translational targets; we are not trying to claim that we have identified every mRNA that is regulated by TDP-43 under these conditions.

We used two criteria to prioritize candidates to follow up in further experiments. (1) they showed strong, direct links to neurodegenerative disease based on previous studies, or (2) they were identified in both cell types. Upon applying the above criteria, we identified three genes for further downstream analysis: *Camta1*, *Dennd4a*, and *Mig12/Mid1ip*.

### **6.4 CAMTA1 AND DENND4A ARE WELL-KNOWN MASTER REGULATORS OF NEURODEGENERATION**

Two of the three identified translational targets- CAMTA1 and DENND4A have already shown to be implicated in ALS. CAMTAs comprise a conserved family of transcription factors that could possibly be regulated by calcium signaling through direct binding of calmodulin (Bouche et al. 2002). It was also found that CAMTA protein binds to CG-rich motifs on its target DNAs. Additionally, loss of CAMTA1

leads to dysregulation of many genes in the cerebellum (Long et al. 2014). The same study shows that *Camta1* KO animals, where CAMTA1 is removed throughout the nervous system, display significant deficits in motor performance on the rotarod at the age of 6 weeks. These animals develop ataxia and show Purkinje cell degeneration along with significant cerebellar atrophy at the age of 3 months. A GWAS in sporadic ALS patients identified a *CAMTA1* locus that significantly affects survival, causing a reduction of about four months (Fogh et al. 2016). Intragenic mutations in human *CAMTA1* have also been implicated in neurobehavioral abnormalities like intellectual disability and speech problems (Shinawi et al. 2015). Furthermore, a SNP in the *CAMTA1* locus is associated with human episodic memory performance (Huentelman et al. 2007). Another study showed that CAMTA1 plays a regulatory role in long-term memory formation in mice (Bas-Orth et al. 2016).

DENND4A is known to function as a GEF specifically for Rab10 in HeLa cells (Yoshimura et al. 2010). Interestingly, bioinformatics analysis has shown that the protein encoded by the *C9orf72* gene, which is heavily implicated in ALS and FTD, show strong structural homology with DENN-like superfamily (Levine et al. 2013).

In further support of an important causal role in neurodegenerative disease, CAMTA1 and DENND4A were found to be “Master Regulators” (MRs) of neurodegenerative disease transcriptional programs by two independent studies (Zu et al. 2013; Ikiz et al. 2015; Brichta et al. 2015). One of these studies was based on an MPTP-induced Parkinson’s disease model. In this study, TRAP-seq was performed from midbrain SNpc and VTA DA neurons on *Dat* BacTRAP animals. These *Dat* bacTRAP animals express EGFP-L10a transgene under the control of the *Dat* (Dopamine transporter) promoter. The other study involved an in vitro ALS model where purified ES-MNs were used following exposure to astrocyte-conditioned medium (ACM) from either Non-Tg/SOD1<sup>WT</sup> animals or SOD1<sup>G93A</sup> animals. RNA-seq analyses were performed on these cells. Both of these studies used the algorithm ARACNe (Margolin et al. 2006) to generate regulatory networks that are affected in these animals from the genes that are identified to be differentially regulated. Following this, both studies used the algorithm called MARINa (Lefebvre et al. 2010; Carro et al. 2010) along with the regulatory network constructed, to identify the ‘Master Regulators (MRs)’ that are upstream regulatory genes that could potentially be the most important causative factors. Strikingly, both CAMTA1 and DENND4A were two of the three genes found

from both of these studies. In addition to that, the *in vitro* ALS study showed that DENND4A is a motor neuron ‘death driver’ (MNDD), as knockdown of this *Dennd4a* mRNA has led to a significant increase in the survival of cultured spinal motor neurons. However, the authors concluded that this role was independent of ALS, as this gene did not specifically enhance survival of neurons cultured with mutant Astrocytes in the ALS model used. This indicates that enhanced translation of *Dennd4a* mRNA might lead to increased motor neuronal death. Interestingly, although both of these studies conclude that the activity of CAMTA1 and DENND4A proteins is altered in neurodegeneration, both also found that their mRNA expression levels were not altered. This raises the question of what leads to altered activity of the MRs themselves to trigger the neurodegenerative transcriptional program. The authors speculate that post-translational effects would be responsible, but they did not provide direct evidence for this hypothesis. While this could certainly be true, our results raise the possibility that a translational mechanism could be important, since we found that the translational status of mRNAs encoding CAMTA1 and DENND4A is altered by a patient mutant TDP-43 that causes disease in humans, rodents, and cell-culture models.

Importantly, both of our models were designed to reflect pre-symptomatic stages of disease, since our goal was to identify early molecular changes that could trigger disease, rather than secondary effects caused by disease. Thus, altered MR translational status may not be sufficient for induction of the full neurodegenerative transcriptional program. For this reason, we conclude that the effects on translation we observe are probably among the earliest effects in motor neurons with mutant TDP-43.

## **6.5 EFFECT OF HUMAN TDP-43 PROTEIN ON TRANSLATIONAL STATUS OF OTHER MASTER REGULATORS OF NEURODEGENERATION**

Apart from the ones we identified from our ribosome profiling datasets, we also checked the ribosome density and total mRNA levels of other MRs identified in our transfected MN1 model. These results have been summarized below along with the original observation made in both studies (Table 6) (Ikiz et al. 2015; Brichta et al. 2015). It was shown in Parkinson’s study that regulatory activities of SATB1 and ZDHHC2 are reduced in dopaminergic neurons at an early stage of degeneration.

The ALS study confirmed the activation of NF- $\kappa$ B pathway leading to neurodegeneration. *Zdhhc2* mRNA is the only mRNA that behaves similar to *Camta1* and *Dennd4a* mRNAs, showing a shift towards heavier fractions in our polysome profiling experiments upon expression of hTDP-43<sup>A315T</sup> protein with no change in total mRNA levels. This is striking, since *Zdhhc2* was the third common MR identified in both the Parkinson's and ALS studies. Moreover, this protein was found to be an "ALS-related motor neuron death driver" (ALS-related MNDD) (Ikiz et al. 2015). Another ALS-related MNDD, *Tcf7* showed an increase in ribosome density upon expression of hTDP-43<sup>A315T</sup> protein, but an increase in mRNA level in hTDP-43 expressing cells. *App* and *Satb1* mRNAs showed an increase in total mRNA levels upon expression of hTDP-43<sup>A315T</sup> and shifted to heavier fractions, implying potential combined effects on transcription and/or stability, as well as translation. The gene *Atf5* was unchanged in our experiments.

Overall, these results indicate that other neurodegeneration MRs are deregulated by TDP-43 overexpression, sometimes in a manner that is patient mutant-specific. In principle, these could be "false-negatives" from our original genome-wide assay. However, in most cases the effects are not as strong as for *Camta1* and *Dennd4a* mRNAs, and so presumably these genes would have escaped detection for this reason. Interestingly, except for *Zdhhc2*, regulation is not always exclusively at the translational level. For most, corresponding effects on both translation and mRNA levels were observed. In the case of *Myb*, there seems to be a strong (>2x) increase in mRNA levels with an antagonistic effect on ribosome density (i.e. shift to lighter fractions). Thus, *Myb* mRNA seems to be a *bona fide* target of TDP-43 overexpression that was missed in our original screen. Collectively, our results reveal that a subset of reported neurodegeneration MRs is deregulated by TDP-43 overexpression in a complex manner. How exactly TDP-43 regulates these mRNAs and whether it does so directly remains to be determined.

What could be the biological significance of deregulation of additional MRs besides CAMTA1 and DENND4A upon TDP-43 overexpression? The original neurodegeneration MR studies implied that multiple MRs are deregulated in disease (Ikiz et al. 2015; Brichta et al. 2015). Thus, effects on some other MRs might actually be expected in our models. At the same time, only three MRs were identified to be common factors for the Parkinson's and ALS studies. This implies that the common

regulatory component exists, but also supports significant differences involving regulatory pathways that contribute in a disease-specific manner. Together with the original studies, our data motivates further experiments in disease models to examine how deregulation of these MRs occurs and how functional effects on specific MR downstream targets ultimately leads to disease. Nevertheless, one of the most intriguing ideas that emerges from my thesis is that the mRNAs that encode the three “common” MRs all show enhanced ribosome density in response to overexpression of a patient mutant variant of TDP-43. This highlights a potential role for altered translation of these MRs in driving disease in ALS and also raises the possibility that this could be relevant in other neurodegenerative diseases as well.

MR	Initial observation	Validation (Ikiz et al. 2015; Brichta et al. 2015)	Ribosome density change (polysome profiling)	Total mRNA change	Motor neuron survival
<b>Zdhhc2</b>	Reduced activity in (Brichta et al. 2015) Increased activity in (Ikiz et al. 2015)	Both	Shifts deeper	No change	ALS-related MNDD
<b>App</b>	Increased activity in (Ikiz et al. 2015)	(Ikiz et al. 2015)	Shifts deeper	hTDP-43 <sup>A315T</sup> - specific increase	No effect
<b>Tcf7</b>	Increased activity in (Ikiz et al. 2015)	(Ikiz et al. 2015)	Shifts deeper	hTDP-43-specific increase	ALS-related MNDD
<b>Satb1</b>	Reduced activity in (Brichta et al. 2015)	(Brichta et al. 2015)	Shifts deeper	hTDP-43 <sup>A315T</sup> - specific increase	No data available
<b>Myb</b>	Increased activity in (Ikiz et al. 2015)	(Ikiz et al. 2015)	Shifts lighter	Both hTDP-43 and hTDP-43 <sup>A315T</sup> caused increase	No effect
<b>Nfkb</b>	Increased activity in (Ikiz et al. 2015)	(Ikiz et al. 2015)	No change	Both hTDP-43 and hTDP-43 <sup>A315T</sup> caused increase	ALS-related MNDD
<b>Atf5</b>	Increased activity in (Ikiz et al. 2015)	(Ikiz et al. 2015)	No change	No change	No effect

Table 6: Summary of results obtained for MRs from various studies. Initial observation indicates the original results obtained from MARINA analyses; Validation indicates the validation experiments performed in the study these genes were originally identified as MR; Ribosome density change indicates the results of our polysome profiling experiments; Motor neuron survival indicates the effect of these MRs on survival rate of motor neurons.

## **6.6 POTENTIAL ROLE OF MID1IP1/MIG12 IN NEURODEGENERATION**

The third candidate, Mid1ip1/Mig12, was identified to be a translational target from both MN1 and primary neurons. MIG12's nuclear function has yet to be identified, but two cytoplasmic functions for MIG12 have been described: regulating fatty acid synthesis (Inoue et al. 2011) via effects on the acetyl-CoA carboxylase complex (Kim et al. 2010) and binding Mid1 to affect microtubule stabilization (Berti et al. 2004). In principle, either or both of these functions might be affected by expression of TDP-43 in cortical neurons and spinal motor neurons in vivo. Changes in fatty acid metabolism (Bazinet and Laye 2014) and microtubule dynamics are both implicated in neurodegeneration (Dubey, Ratnakaran, and Koushika 2015; Clark et al. 2016). Thus, our work motivates future use of ALS animal models to test whether altered MIG12 protein levels are indeed affecting these processes and to evaluate their potential contributions to disease phenotypes.

The *Mid1* gene is strongly implicated in Opitz syndrome, a congenital disorder affecting the ventral midline (Quaderi et al. 1997; Li, Zhou, and Zou 2016). Additionally, a recent study has shown that *Mid1* is transcriptionally regulated by Rac1 and that the Rac1/Mid1/mTOR complex might play a role in cerebellar development (Nakamura et al. 2017). Although *Mig12* is not directly involved in neurodegeneration, some studies have shown that MID1 is. In vitro studies have shown that, Mid1-complex enhances the translation of BACE1 mRNA, which is heavily implicated in AD, by activating/phosphorylating the ribosomal protein S6. Moreover, MID1-PP2A complex activity was shown to be important for phosphorylation of Tau at AD-specific sites in primary neurons (Kickstein et al. 2010). In silico analysis of BACE1 mRNA revealed the presence of MID1-associated sequence (MIDAS) (Aranda-Orgilles et al. 2011) motifs (Hettich et al. 2014). The MID1 complex is known to bind the CAG repeat motifs of *Huntingtin* (*HTT*) mRNA,

inducing its translation and this interaction is length dependent, with stronger interaction for longer CAG repeats (Krauss et al. 2013).

Moreover, the MID1 protein has been identified to be an E3 ubiquitin ligase and some of its targets have already been identified (Zanchetta et al. 2017; Trockenbacher et al. 2001; Schweiger et al. 2014). In our studies, we show that the level of MID1 protein influences the level of MIG12 protein. This could imply that MIG12 is targeted by MID1 for degradation by the ubiquitin-proteasome system.

## **6.7 SUCCESSFUL VALIDATION OF TDP-43 TRANSLATIONAL TARGETS USING POLYSOME PROFILING**

It is important to realize that genome-wide experiments are subject to false positives. Consequently, it is crucial to perform independent validation. We used polysome profiling on MN1 cells transfected with GFP/hTDP-43/hTDP-43<sup>A315T</sup>. This gives us the distribution of any mRNA of interest across a polysome sucrose gradient, which reflects the ribosome density on that mRNA. We isolated mRNAs from various fractions and performed qRT-PCR for candidate genes and *Gapdh*, as a control.

These experiments showed that all the candidate mRNAs shifted to heavier fractions in MN1 cells expressing hTDP-43<sup>A315T</sup> protein (Figure 18). In contrast, we did not find any change in the total mRNA level for the candidate mRNAs tested (Figure 19). These results confirm the results obtained from ribosome profiling. Alteration in ribosome density could be due to various reasons. When an mRNA shifts to heavier fractions, it is presumably due to more ribosomes associating with it. This increase in ribosome density could mean either: 1. an increase in translation and protein level, or 2. More ribosome being stalled on an mRNA, presumably leading to a reduction in protein levels. In order to distinguish between these possibilities, one could do these experiments including puromycin treatment, as this drug selectively affects actively translating ribosomes (Blobel and Sabatini 1971). Alternatively, one could assess the effects on protein level by performing western blot or immunostaining.

## **6.8 IDENTIFICATION OF mRNA REGIONS IMPORTANT FOR TDP-43 TRANSLATIONAL REGULATION**

Following validation by polysome profiling, we wanted to find how TDP-43 enhances translation of these mRNAs to get more mechanistic insights. In principle, hTDP-



43<sup>A315T</sup> could affect translation of specific mRNAs through direct or indirect mechanisms. To distinguish between these possibilities, we used UV-crosslink immunoprecipitation (CLIP), to determine whether TDP-43 can interact directly with these mRNAs in MN1 cells. These experiments confirm that TDP-43 binds directly to all three target mRNAs.

Dual luciferase assays were carried out to identify the cis-region on the candidates that are important for this translational regulation. Overexpressing either WT or mutant hTDP-43 similarly affected luciferase reporters derived from 5'UTR of *Camta1* and *Mig12* mRNAs. These reporter data also highlight the 5'UTRs of these mRNAs as a key cis-element for their translational enhancement by TDP-43. Taken together with our CLIP data demonstrating that TDP-43 binds directly to both mRNAs, this suggests that TDP-43 regulates these mRNAs through the 5'UTRs to stimulate translation. Manual inspection of these UTRs does not reveal obvious similarities, raising the possibility that the underlying mechanisms might nevertheless be different, despite both involving 5'UTRs. Thus, for *Camta1* and *Mig12* mRNAs, our data suggest a gain-of function mechanism operating through their 5'UTRs.

Translational enhancement of *Dennd4a* mRNA appears to involve a fundamentally different mechanism. In this case, overexpression of the hTDP-43<sup>A315T</sup> mutant, but not WT hTDP-43, selectively increased the translation, via the *Dennd4a* 3'UTR as observed in our dual luciferase assays. Moreover, using CLIP, we found that WT TDP-43 exhibits direct binding to this mRNA as well. This suggests that differential translational enhancer activity, rather than binding per se underlies the mutant-specific effect. Further experiments involving a systematic comparison of the impact of other TDP-43 patient alleles on *Dennd4a* translation would be interesting. Such experiment would help us to know if this translational enhancement of *Dennd4a* is specific for this patient mutant or if this is a general effect observed in more patient mutants. It will also be important to map the exact regions that mediate TDP-43 interaction with these mRNAs and compare in detail the translational enhancer mechanisms operating via their UTRs.

## 6.9 IMPACT OF ALTERED mRNA TRANSLATION ON ENCODED PROTEIN LEVELS CAN BE DYNAMICALLY REGULATED

Immunostaining experiments in MN1 cells using a specific antibody to CAMTA1 protein showed that there is an increase in the steady state protein level in transfected MN1 cells. More detailed analysis showed that there is a significant increase in protein levels in both nucleus and cytoplasm. A specific antibody to MIG12 enabled us to analyze the impact of altered translational status on steady-state protein levels in this case as well. Immunostaining revealed that MIG12 was present in both nucleus and cytoplasm of all cells we examined, consistent with a previous report (Berti et al. 2004). An *In vitro* study using HEK cells showed that TDP-43 aggregation might lead to compartment specific changes in steady state level of certain proteins (Prpar Mihevc et al. 2016). Similarly, TDP-43's effects on MIG12 protein levels were cell compartment-specific and varied with cell type, and levels of a MIG12 interaction partner, MID1. In MN1 cells, TDP-43 transfection led to a significant increase in MIG12 protein levels only in the nucleus.

Notably, we observed these effects whether we transfected wild-type hTDP-43 or hTDP-43<sup>A315T</sup>, even though *Mig12* and *Camta1* mRNAs were identified as a specific target of mutant TDP-43 in our ribosome profiling screen. One reason could be that hTDP-43 actually had an effect on ribosome footprints, but this was not detected in our differential expression analysis, because its fold-change was below the standard cutoff of two. Importantly, this observation does not call into question potential disease relevance, since overexpression of hTDP-43, as we do here, is sufficient to cause disease phenotypes in a host of animal and cell models (Xu et al. 2010; Wils et al. 2010; Berti et al. 2004)

In primary cortical neurons, we also observed compartment-specific effects of TDP-43<sup>A315T</sup> expression on MIG12 protein levels, but here we saw more MIG12 protein in neurites, whereas levels in nucleus and cell body were unchanged. Overexpression of MID1, a binding partner of MIG12 in MN1 cells abolished the increase in nuclear MIG12 protein levels caused by hTPD-43 transfection. Taken together, these results highlight dynamic regulation of MIG12 protein levels in response to TDP-43, which varies with cell type and binding partners. Since MID1 is an E3 ubiquitin ligase (Zanchetta et al. 2017; Trockenbacher et al. 2001; Schweiger et al. 2014) and binds directly to MIG12, this could imply that newly synthesized MIG12 is targeted by MID1

for degradation by the ubiquitin-proteasome system. In this view, newly synthesized MIG12 protein fails to reach the nucleus due to interaction with MID1 and undergoes rapid turnover, but the pre-existing nuclear pool is stable and unchanged over the time frame of the experiment. Regardless of how MID1 itself is regulated, our study reveals that MID1 levels can have a profound influence on whether altered translational status of *Mig12* mRNA is manifest on the protein level.

In addition to this, expression level of Mid1-targeting miR-19b-3p (Unterbruner et al. 2018) is altered by TDP-43 as shown already (Chen et al. 2017) where downregulation of TDP-43 increased the level of miR-19b-3p. Other studies have shown that the level of this miRNA is altered in neurodegeneration (Wu et al. 2017; Marcuzzo et al. 2014). Further studies focusing on the level of other miRNAs regulating Mid1 would lead to a better understanding of the disease. Also it is important to study the regulation of these miRNAs which in turn would regulate MID1 levels, by hTDP-43 mutant variants. Thus it emerges from our study the level of MID1 is crucial for MIG12 expression and leading to disease.

Finally, although DENND4A was successfully validated in polysome profiling experiments for increased ribosome density and showed increased translation in our dual luciferase assays, this target needs further experimentations to monitor protein level changes. Commercial antibody used in our immunostaining experiments resulted in non specific staining in cells where Dennd4a was knocked down. This part of the project still needs further experiments. Unfortunately, any method to study specific protein level is dependent on the availability of specific antibody. In principle, we could perform quantitative proteomics, but that would be excessive for our need. Nevertheless, one could do it, if one is interested in other information from the method. The table below summarized the results we obtained with the TDP-43 translational target mRNAs.

Genes	Cell type	Ribosome profiling	Validation (Polysome profiling)	Direct binding (CLIP)	mRNA region (Reporter assay)	Effects on Protein level (Immunostaining)
<i>Camtal</i>	MN1	↑	+	+	5'UTR	+

<b><i>Mig12</i></b>	MN1 and Primary Neurons	↑	+	+	5'UTR	+
<b><i>Dennd4a</i></b>	MN1	↑	+	+	3'UTR	No data available

Table 7: Summary of results from this work. ↑ indicates increased footprint reads indicating increased ribosome density; + indicates positive results in various experiments as shown above. All three mRNAs show increased ribosome density in polysome profiling validation experiments and display direct binding to TDP-43 in CLIP experiments. Both CAMTA1 and MIG12 protein levels were increased upon expression of both hTDP-43 and hTDP-43<sup>A315T</sup>. We also identified the mRNA region involved in this translational regulation by TDP-43.

## 6.10 EFFECTS OF ALTERED TRANSLATIONAL REGULATION OF TDP-43 TARGETS AND THEIR IMPLICATION IN NEURODEGENERATION

How does altered translational regulation of the *Camta1* and *Dennd4a* mRNAs lead to disease? Our results ultimately show that altered MR translational status may not be sufficient for induction of the full neurodegenerative transcriptional program. Importantly, both of our models were designed to reflect pre-symptomatic stages of disease, since our goal was to identify early molecular changes that could trigger disease, rather than secondary effects caused by disease. Hence, these altered translational regulation shown here are probably some of the earliest effects in motor neurons with overexpression of wildtype or mutant TPD-43.

Similar to cancer, where oncogene expression is rarely sufficient on its own to cause disease, neurodegenerative diseases are hypothesized to follow a ‘multiple hit model’ (Dormann and Haass 2011). One common idea is that specific lesions combine with chronic activation of cellular stress pathways to push cells over a “stressor threshold” (Saxena and Caroni 2011). According to this view, altered translational status of MR-encoding mRNAs due to cytoplasmic TDP-43 would be a “first hit” and a currently unknown “second hit” would lead to activation of the MR degenerative transcriptional program. Clearly, identifying the relevant second hit will be crucial to understanding whether this model is correct and better defining the contribution of altered translational control of Master Regulators to neurodegenerative disease mechanisms. Signalling pathways that converge on eIF2α phosphorylation and lead

to stress granule formation are prime candidates (Ramaswami, Taylor, and Parker 2013; Kim et al. 2014; Li et al. 2013).

The role of MIG12 in neurodegeneration is not well understood yet. However, our results show that the translational status of this mRNA is affected in both MN1 cells and primary neurons. This indicates that this gene could be a common signature from both cell types that are affected in the disease. However there are reports linking its interacting partner MID1 to various neurological phenotypes. Further studies are needed to investigate the effects of human TDP-43 on these genes and identify if there is involvement of any common pathway associated in driving the disease. However there are reports linking its interacting partner MID1 to various neurological phenotypes.

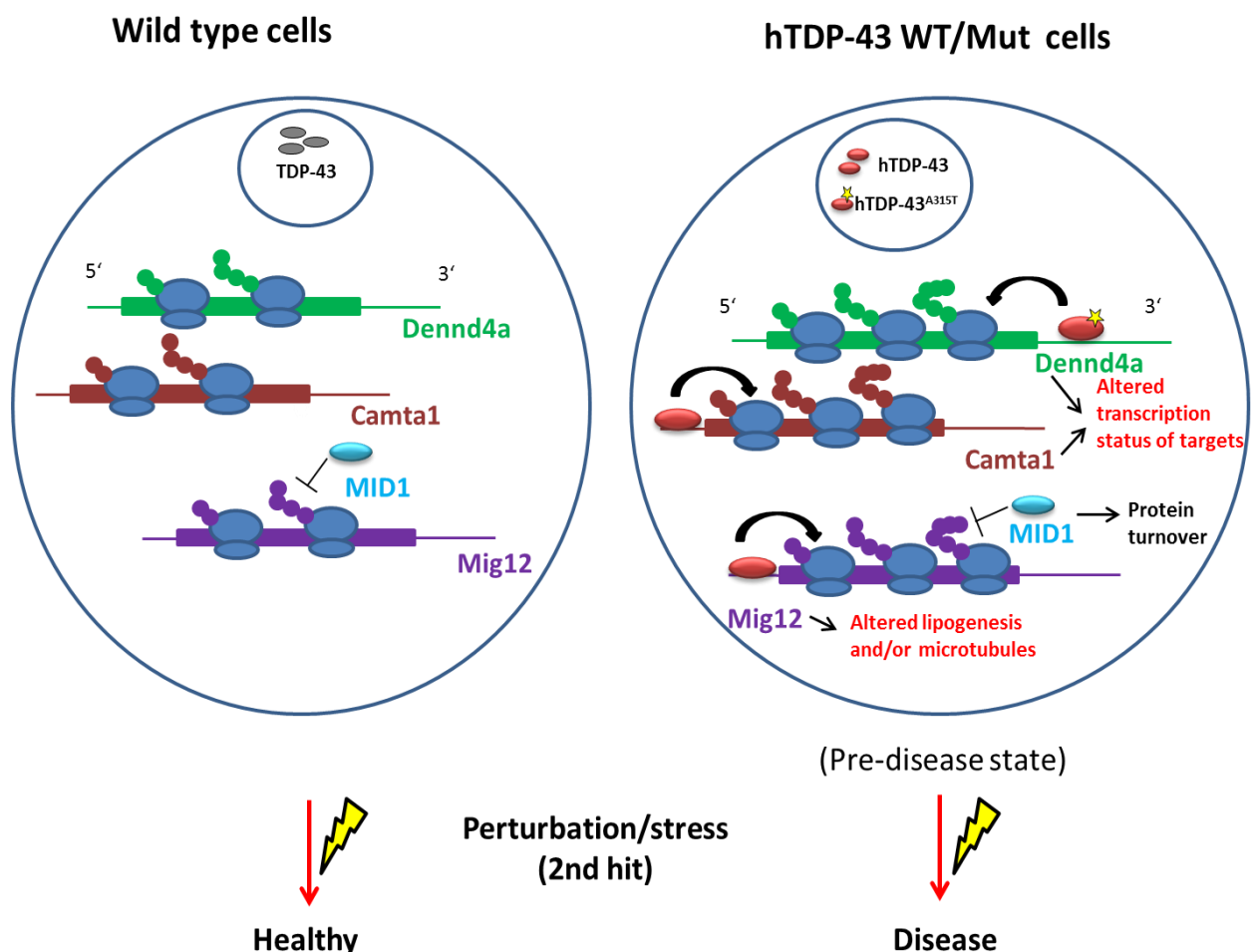


Figure 40: **Working model for TDP-43 as a translational enhancer and its role in neurodegeneration.** In wildtype cells with expression of endogenous TDP-43, the targets genes undergo ‘normal’ translation. In cells expressing wildtype human TDP-43, (which is

equivalent to sALS cases without mutations, but accumulation of TDP-43 aggregates) there is an increased translation of *Camta1* and *Mig12* mRNAs via their 5'UTRs, thereby leading to an increase in their protein level. In cells expressing human TDP-43<sup>A315T</sup> protein, there is an increase in translation of *Camta1*, *Mig12* and *Dennd4a* mRNAs. These increased translation and protein levels define the basal state in these cells. In case of CAMTA1 and DENND4A, both being transcription factors, this leads to an increase in transcription of their downstream target genes. In case of MIG12, this leads to altered lipogenesis and microtubule dynamics. MIG12 protein level is regulated by its binding partner MID1. All these molecular changes occur during pre-symptomatic phase when there are no overt disease symptoms yet. Upon any perturbation, aging or environmental stress, the wildtype cells maintain homeostasis and remain healthy, whereas hTDP-43/hTDP-43<sup>A315T</sup> cells develop disease. This study shows that TDP-43 is an 'mRNA-specific translational enhancer' and this altered translational regulation might be disease relevant.

## **6.11 FURTHER OPTIMIZATION OF RIBOSOME PROFILING IS REQUIRED TO GET MORE INSIGHTS INTO TDP-43- MEDIATED TRANSLATIONAL REGULATION**

Ribosome profiling is a very powerful technique to study translational regulation. In addition to counting ribosomes on mRNA coding sequences, it can be used to identify novel uORFs, initiation start sites, termination sites, and alternative reading frames, and provide insights on ribosome movement and ribosome pausing events (Reviewed in (Ingolia, Hussmann, and Weissman 2018)). Although, we had hoped to be able to understand how TDP-43 might affect these aspects of translation, our ribosome profiling experiments lacked the necessary read depth and precise footprint lengths needed for these analyses (Section 3.14).

Although we successfully identified some of the new translational targets of TDP-43 protein, the information we obtained was limited in various aspects. In the first place, we identified very few genes that were differentially regulated in the footprints (Appendix 3, 4). This might have been driven by our limited number of mapped reads (Appendix 1). Our sequencing depth was not very high overall and we had very high amount of contaminating ribosomal RNA reads. This limited our gene coverage, which could be a reason why we detected few differentially regulated genes. Consequently, we could not perform other standard analyses for large gene datasets such as Gene Ontology (GO)-term analysis, pathway analysis, or PPI network to gain insights into which pathways or processes are affected on a global scale. We also

obtained more reads mapping to intergenic regions than is typically observed for ribosome footprint read datasets. Why exactly this is the case is not clear at the moment. In addition to this, we obtained longer footprint reads that limited our capacity to make any conclusions about codon-level ribosome positioning in these experiments, as this affected the mapping of P- and A-sites

We performed another set of experiments with the aim of generating better datasets. Despite a few improvements, the issue of rRNA contamination still persisted. Ribosome footprint reads of the correct size were enriched with around 70 – 80% of reads mapping to CDS leading to isolation of true ribosome footprints. In addition to this, we were also able to significantly reduce the intergenic reads in our datasets.

In summary, further optimization should still be performed in order to get ideal dataset from these experiments. In order to remove rRNA reads more efficiently and get more mappable reads, one option is to use kits available commercially. Therefore, in order to get a broader view of all potential translational targets of TDP-43, and additional insight into how exactly they may be regulated, these experiments should be repeated with an optimized protocol.

## 7. FUTURE PERSPECTIVES

We have identified new translational targets of TDP-43 and shown that TDP-43 acts as an mRNA-specific translational enhancer. These experiments were performed on cell systems where we do not observe any overt phenotypes. Thus, we conclude that the altered translational control that we identified reflects early changes that are due to the over expression of hTDP-43/hTDP-43<sup>A315T</sup> protein, rather than secondary effects. Notably, some of the targets we identified were previously found to be 'Master Regulators' of neurodegeneration in two different disease models.

It would be interesting to examine whether expression of the mRNAs and proteins identified in these in vitro studies is altered in animal models of ALS and to see how this correlates with the timing of disease. The hTDP-43<sup>A315T</sup> mice that we used for cortical neurons preparation in this project, develop motor neuron phenotypes (rotarod test) at the age of 8 weeks in males and 12 weeks in females. This has been established by Rita Marques as a part of her Doctoral thesis (*Identification of potential disease-driving proteins in mouse models of ALS caused by mutant TDP-43*). Thus, it would be relevant to see if these targets are regulated in adult animals during disease progression. Based on my data, we would predict changes in translation would be present early on, but there might not be major protein level changes until later, perhaps at disease onset. Moreover, mRNA levels would presumably not be changed. Additionally, it would be more interesting to study the regulation of these targets in human patient samples – patient derived iPSCs (Sances et al. 2016). This could help to show that these changes in translation also occur in human cells with mutated TDP-43 expressed from the endogenous chromosome. These studies would all have the potential to strengthen the case that altered translational control of these mRNAs is relevant to disease.

A second interesting aspect would be to focus on the 'multiple-hit model' and screen for the second hit that presumably pushes these cells into the disease state. Cellular stresses such as heat shock, oxidative stress or endoplasmic reticulum (ER) stress have all been implicated in ALS (reviewed in (Farley and Watkins 2018)). Figure 41 shows the various stress pathways that are shown to be important for various neurodegenerative diseases.



A recent study has shown that in ALS, the UPR signalling pathway is affected. Furthermore, this study has shown that these alterations lead to differential expression of downstream gene targets of two ER proteins, IRE1 and ATF6 (Montibeller and de Bellerocche 2018). Another study has shown pharmacologically that reducing ER stress is neuroprotective in *C. elegans* and Zebrafish models of ALS (Vaccaro et al. 2013). eIF2 $\alpha$  phosphorylation is also implicated in various forms of ALS (Kim et al. 2014; Cheng et al. 2018). Hence it would be important to examine which of these pathways is relevant to drive disease in this case. In order to do this, one could induce these pathways by adding stressors like sodium arsenite or thapsigargin, in addition to overexpressing wildtype or mutant TDP-43 and study the effects on the target mRNAs and proteins.

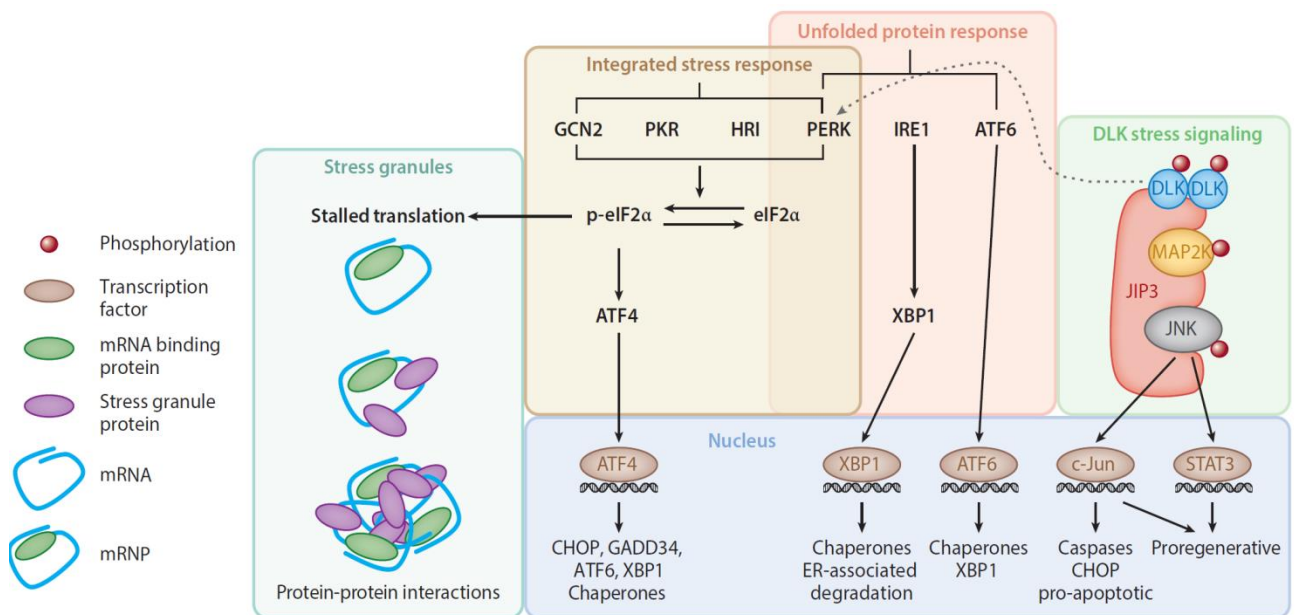


Figure 41: Overview of various stress response mechanisms implicated in neurons. Figure from (Farley and Watkins 2018)

Another direction would be to study how these candidates are affected in other disease associated mutations. Various mutations of TDP-43 protein have been identified in disease, some of them being shown in Figure 8. This would provide an insight into the question of whether there is a common link connecting different forms of disease that converges on the targets described in this thesis. Furthermore, answering this question is very important as it could influence treatment options.

Identifying common downstream disease-causing molecules would be ideal therapeutic targets.

Finally, exploring the effects of CAMTA1 and DENND4A in regulating their downstream target mRNAs and how this is connected to disease would be crucial, especially given the fact that these are 'Master Regulators' of neurodegeneration. As these two are transcription factors, one could perform ChIP-Seq for these in order to get more details about their mode of action. These experiments would give us information about the downstream gene signatures affected and this would in turn be informative in finding common linking factors in various neurodegenerative diseases. In principle, these studies could be done with the cellular models described here, as well as with animal models and patient iPSCs.

## REFERENCES

- Alami, N. H., R. B. Smith, M. A. Carrasco, L. A. Williams, C. S. Winborn, S. S. W. Han, E. Kiskinis, B. Winborn, B. D. Freibaum, A. Kanagaraj, A. J. Clare, N. M. Badders, B. Bilican, E. Chaum, S. Chandran, C. E. Shaw, K. C. Eggan, T. Maniatis, and J. P. Taylor. 2014. 'Axonal transport of TDP-43 mRNA granules is impaired by ALS-causing mutations', *Neuron*, 81: 536-43.
- Anders, S., and W. Huber. 2010. 'Differential expression analysis for sequence count data', *Genome Biol*, 11: R106.
- Arai, T., M. Hasegawa, H. Akiyama, K. Ikeda, T. Nonaka, H. Mori, D. Mann, K. Tsuchiya, M. Yoshida, Y. Hashizume, and T. Oda. 2006. 'TDP-43 is a component of ubiquitin-positive tau-negative inclusions in frontotemporal lobar degeneration and amyotrophic lateral sclerosis', *Biochem Biophys Res Commun*, 351: 602-11.
- Aranda-Orgilles, B., D. Rutschow, R. Zeller, A. I. Karagiannidis, A. Kohler, C. Chen, T. Wilson, S. Krause, S. Roepcke, D. Lilley, R. Schneider, and S. Schweiger. 2011. 'Protein phosphatase 2A (PP2A)-specific ubiquitin ligase MID1 is a sequence-dependent regulator of translation efficiency controlling 3-phosphoinositide-dependent protein kinase-1 (PDK-1)', *J Biol Chem*, 286: 39945-57.
- Arnold, E. S., S. C. Ling, S. C. Huelga, C. Lagier-Tourenne, M. Polymenidou, D. Ditsworth, H. B. Kordasiewicz, M. McAlonis-Downes, O. Platoshyn, P. A. Parone, S. Da Cruz, K. M. Clutario, D. Swing, L. Tessarollo, M. Marsala, C. E. Shaw, G. W. Yeo, and D. W. Cleveland. 2013. 'ALS-linked TDP-43 mutations produce aberrant RNA splicing and adult-onset motor neuron disease without aggregation or loss of nuclear TDP-43', *Proc Natl Acad Sci U S A*, 110: E736-45.
- Ayala, Y. M., L. De Conti, S. E. Avendano-Vazquez, A. Dhir, M. Romano, A. D'Ambrogio, J. Tollervey, J. Ule, M. Baralle, E. Buratti, and F. E. Baralle. 2011. 'TDP-43 regulates its mRNA levels through a negative feedback loop', *EMBO J*, 30: 277-88.
- Barbosa, C., I. Peixeiro, and L. Romao. 2013. 'Gene expression regulation by upstream open reading frames and human disease', *PLoS Genet*, 9: e1003529.
- Barmada, S. J., G. Skibinski, E. Korb, E. J. Rao, J. Y. Wu, and S. Finkbeiner. 2010. 'Cytoplasmic mislocalization of TDP-43 is toxic to neurons and enhanced by a mutation associated with familial amyotrophic lateral sclerosis', *J Neurosci*, 30: 639-49.
- Bas-Orth, C., Y. W. Tan, A. M. Oliveira, C. P. Bengtson, and H. Bading. 2016. 'The calmodulin-binding transcription activator CAMTA1 is required for long-term memory formation in mice', *Learn Mem*, 23: 313-21.
- Bazinet, R. P., and S. Laye. 2014. 'Polyunsaturated fatty acids and their metabolites in brain function and disease', *Nat Rev Neurosci*, 15: 771-85.
- Berti, C., B. Fontanella, R. Ferrentino, and G. Meroni. 2004. 'Mig12, a novel Opitz syndrome gene product partner, is expressed in the embryonic ventral midline and co-operates with Mid1 to bundle and stabilize microtubules', *BMC Cell Biol*, 5: 9.
- Blobel, G., and D. Sabatini. 1971. 'Dissociation of mammalian polyribosomes into subunits by puromycin', *Proc Natl Acad Sci U S A*, 68: 390-4.

- Bouche, N., A. Scharlat, W. Snedden, D. Bouchez, and H. Fromm. 2002. 'A novel family of calmodulin-binding transcription activators in multicellular organisms', *J Biol Chem*, 277: 21851-61.
- Brichta, L., W. Shin, V. Jackson-Lewis, J. Blesa, E. L. Yap, Z. Walker, J. Zhang, J. P. Roussarie, M. J. Alvarez, A. Califano, S. Przedborski, and P. Greengard. 2015. 'Identification of neurodegenerative factors using translome-regulatory network analysis', *Nat Neurosci*, 18: 1325-33.
- Brown, V., P. Jin, S. Ceman, J. C. Darnell, W. T. O'Donnell, S. A. Tenenbaum, X. Jin, Y. Feng, K. D. Wilkinson, J. D. Keene, R. B. Darnell, and S. T. Warren. 2001. 'Microarray identification of FMRP-associated brain mRNAs and altered mRNA translational profiles in fragile X syndrome', *Cell*, 107: 477-87.
- Buratti, E. 2018. 'TDP-43 post-translational modifications in health and disease', *Expert Opin Ther Targets*, 22: 279-93.
- Buratti, E., and F. E. Baralle. 2001. 'Characterization and functional implications of the RNA binding properties of nuclear factor TDP-43, a novel splicing regulator of CFTR exon 9', *J Biol Chem*, 276: 36337-43.
- Carro, M. S., W. K. Lim, M. J. Alvarez, R. J. Bollo, X. Zhao, E. Y. Snyder, E. P. Sulman, S. L. Anne, F. Doetsch, H. Colman, A. Lasorella, K. Aldape, A. Califano, and A. Iavarone. 2010. 'The transcriptional network for mesenchymal transformation of brain tumours', *Nature*, 463: 318-25.
- Chasse, H., S. Boulben, V. Costache, P. Cormier, and J. Morales. 2017. 'Analysis of translation using polysome profiling', *Nucleic Acids Res*, 45: e15.
- Chen, X., Z. Fan, W. McGee, M. Chen, R. Kong, P. Wen, T. Xiao, X. Chen, J. Liu, L. Zhu, R. Chen, and J. Y. Wu. 2017. 'TDP-43 regulates cancer-associated microRNAs', *Protein Cell*.
- Cheng, W., S. Wang, A. A. Mestre, C. Fu, A. Makarem, F. Xian, L. R. Hayes, R. Lopez-Gonzalez, K. Drenner, J. Jiang, D. W. Cleveland, and S. Sun. 2018. 'C9ORF72 GGGGCC repeat-associated non-AUG translation is upregulated by stress through eIF2alpha phosphorylation', *Nat Commun*, 9: 51.
- Chou, C. C., Y. Zhang, M. E. Umoh, S. W. Vaughan, I. Lorenzini, F. Liu, M. Sayegh, P. G. Donlin-Asp, Y. H. Chen, D. M. Duong, N. T. Seyfried, M. A. Powers, T. Kukar, C. M. Hales, M. Gearing, N. J. Cairns, K. B. Boylan, D. W. Dickson, R. Rademakers, Y. J. Zhang, L. Petrucelli, R. Sattler, D. C. Zarnescu, J. D. Glass, and W. Rossoll. 2018. 'TDP-43 pathology disrupts nuclear pore complexes and nucleocytoplasmic transport in ALS/FTD', *Nat Neurosci*, 21: 228-39.
- Clark, J. A., E. J. Yeaman, C. A. Blizzard, J. A. Chuckowree, and T. C. Dickson. 2016. 'A Case for Microtubule Vulnerability in Amyotrophic Lateral Sclerosis: Altered Dynamics During Disease', *Front Cell Neurosci*, 10: 204.
- Colombrita, C., E. Zennaro, C. Fallini, M. Weber, A. Sommacal, E. Buratti, V. Silani, and A. Ratti. 2009. 'TDP-43 is recruited to stress granules in conditions of oxidative insult', *J Neurochem*, 111: 1051-61.
- Coyne, A. N., I. Lorenzini, C. C. Chou, M. Torvund, R. S. Rogers, A. Starr, B. L. Zaepfel, J. Levy, J. Johannesmeyer, J. C. Schwartz, H. Nishimune, K. Zinsmaier, W. Rossoll, R. Sattler, and D. C. Zarnescu. 2017. 'Post-transcriptional Inhibition of Hsc70-4/HSPA8

- Expression Leads to Synaptic Vesicle Cycling Defects in Multiple Models of ALS', *Cell Rep*, 21: 110-25.
- Coyne, A. N., B. B. Siddegowda, P. S. Estes, J. Johannesmeyer, T. Kovalik, S. G. Daniel, A. Pearson, R. Bowser, and D. C. Zarnescu. 2014. 'Futsch/MAP1B mRNA is a translational target of TDP-43 and is neuroprotective in a Drosophila model of amyotrophic lateral sclerosis', *J Neurosci*, 34: 15962-74.
- Darnell, J. C., and E. Klann. 2013. 'The translation of translational control by FMRP: therapeutic targets for FXS', *Nat Neurosci*, 16: 1530-6.
- Darnell, J. C., S. J. Van Driesche, C. Zhang, K. Y. Hung, A. Mele, C. E. Fraser, E. F. Stone, C. Chen, J. J. Fak, S. W. Chi, D. D. Licatalosi, J. D. Richter, and R. B. Darnell. 2011. 'FMRP stalls ribosomal translocation on mRNAs linked to synaptic function and autism', *Cell*, 146: 247-61.
- Davis, S. A., K. A. Gan, J. A. Dowell, N. J. Cairns, and M. A. Gitcho. 2017. 'TDP-43 expression influences amyloidbeta plaque deposition and tau aggregation', *Neurobiol Dis*, 103: 154-62.
- de Planell-Saguer, M., D. G. Schroeder, M. C. Rodicio, G. A. Cox, and Z. Mourelatos. 2009. 'Biochemical and genetic evidence for a role of IGHMBP2 in the translational machinery', *Hum Mol Genet*, 18: 2115-26.
- DeJesus-Hernandez, M., I. R. Mackenzie, B. F. Boeve, A. L. Boxer, M. Baker, N. J. Rutherford, A. M. Nicholson, N. A. Finch, H. Flynn, J. Adamson, N. Kouri, A. Wojtas, P. Sengdy, G. Y. Hsiung, A. Karydas, W. W. Seeley, K. A. Josephs, G. Coppola, D. H. Geschwind, Z. K. Wszolek, H. Feldman, D. S. Knopman, R. C. Petersen, B. L. Miller, D. W. Dickson, K. B. Boylan, N. R. Graff-Radford, and R. Rademakers. 2011. 'Expanded GGGGCC hexanucleotide repeat in noncoding region of C9ORF72 causes chromosome 9p-linked FTD and ALS', *Neuron*, 72: 245-56.
- Dever, T. E., and R. Green. 2012. 'The elongation, termination, and recycling phases of translation in eukaryotes', *Cold Spring Harb Perspect Biol*, 4: a013706.
- Dewey, C. M., B. Cenik, C. F. Sephton, D. R. Dries, P. Mayer, 3rd, S. K. Good, B. A. Johnson, J. Herz, and G. Yu. 2011. 'TDP-43 is directed to stress granules by sorbitol, a novel physiological osmotic and oxidative stressor', *Mol Cell Biol*, 31: 1098-108.
- Dharmadasa, T., and M. C. Kiernan. 2018. 'Riluzole, disease stage and survival in ALS', *Lancet Neurol*, 17: 385-86.
- Dormann, D., A. Capell, A. M. Carlson, S. S. Shankaran, R. Rodde, M. Neumann, E. Kremmer, T. Matsuwaki, K. Yamanouchi, M. Nishihara, and C. Haass. 2009. 'Proteolytic processing of TAR DNA binding protein-43 by caspases produces C-terminal fragments with disease defining properties independent of progranulin', *J Neurochem*, 110: 1082-94.
- Dormann, D., and C. Haass. 2011. 'TDP-43 and FUS: a nuclear affair', *Trends Neurosci*, 34: 339-48.
- Doyle, J. P., J. D. Dougherty, M. Heiman, E. F. Schmidt, T. R. Stevens, G. Ma, S. Bupp, P. Shrestha, R. D. Shah, M. L. Doughty, S. Gong, P. Greengard, and N. Heintz. 2008. 'Application of a translational profiling approach for the comparative analysis of CNS cell types', *Cell*, 135: 749-62.

- Dubey, J., N. Ratnakaran, and S. P. Koushika. 2015. 'Neurodegeneration and microtubule dynamics: death by a thousand cuts', *Front Cell Neurosci*, 9: 343.
- Fan, Z., X. Chen, and R. Chen. 2014. 'Transcriptome-wide analysis of TDP-43 binding small RNAs identifies miR-NID1 (miR-8485), a novel miRNA that represses NRXN1 expression', *Genomics*, 103: 76-82.
- Farley, M. M., and T. A. Watkins. 2018. 'Intrinsic Neuronal Stress Response Pathways in Injury and Disease', *Annu Rev Pathol*, 13: 93-116.
- Fiesel, F. C., A. Voigt, S. S. Weber, C. Van den Haute, A. Waldenmaier, K. Gerner, M. Walter, M. L. Anderson, J. V. Kern, T. M. Rasse, T. Schmidt, W. Springer, R. Kirchner, M. Bonin, M. Neumann, V. Baekelandt, M. Alunni-Fabbroni, J. B. Schulz, and P. J. Kahle. 2010. 'Knockdown of transactive response DNA-binding protein (TDP-43) downregulates histone deacetylase 6', *EMBO J*, 29: 209-21.
- Fiesel, F. C., S. S. Weber, J. Supper, A. Zell, and P. J. Kahle. 2012. 'TDP-43 regulates global translational yield by splicing of exon junction complex component SKAR', *Nucleic Acids Res*, 40: 2668-82.
- Fogh, I., K. Lin, C. Tiloca, J. Rooney, C. Gellera, F. P. Diekstra, A. Ratti, A. Shatunov, M. A. van Es, P. Proitsi, A. Jones, W. Sproviero, A. Chio, R. L. McLaughlin, G. Soraru, L. Corrado, D. Stahl, R. Del Bo, C. Cereda, B. Castellotti, J. D. Glass, S. Newhouse, R. Dobson, B. N. Smith, S. Topp, W. van Rheenen, V. Meininger, J. Melki, K. E. Morrison, P. J. Shaw, P. N. Leigh, P. M. Andersen, G. P. Comi, N. Ticozzi, L. Mazzini, S. D'Alfonso, B. J. Traynor, P. Van Damme, W. Robberecht, R. H. Brown, J. E. Landers, O. Hardiman, C. M. Lewis, L. H. van den Berg, C. E. Shaw, J. H. Veldink, V. Silani, A. Al-Chalabi, and J. Powell. 2016. 'Association of a Locus in the CAMTA1 Gene With Survival in Patients With Sporadic Amyotrophic Lateral Sclerosis', *JAMA Neurol*, 73: 812-20.
- Fratta, P., P. Sivakumar, J. Humphrey, K. Lo, T. Ricketts, H. Oliveira, J. M. Brito-Armas, B. Kalmar, A. Ule, Y. Yu, N. Birsa, C. Bodo, T. Collins, A. E. Conicella, A. Mejia Maza, A. Marrero-Gagliardi, M. Stewart, J. Mianne, S. Corrochano, W. Emmett, G. Codner, M. Groves, R. Fukumura, Y. Gondo, M. Lythgoe, E. Pauws, E. Peskett, P. Stanier, L. Teboul, M. Hallegger, A. Calvo, A. Chio, A. M. Isaacs, N. L. Fawzi, E. Wang, D. E. Housman, F. Baralle, L. Greensmith, E. Buratti, V. Plagnol, E. M. Fisher, and A. Acevedo-Arozena. 2018. 'Mice with endogenous TDP-43 mutations exhibit gain of splicing function and characteristics of amyotrophic lateral sclerosis', *EMBO J*, 37.
- Freibaum, B. D., R. K. Chitta, A. A. High, and J. P. Taylor. 2010. 'Global analysis of TDP-43 interacting proteins reveals strong association with RNA splicing and translation machinery', *J Proteome Res*, 9: 1104-20.
- Freibaum, B. D., Y. Lu, R. Lopez-Gonzalez, N. C. Kim, S. Almeida, K. H. Lee, N. Badders, M. Valentine, B. L. Miller, P. C. Wong, L. Petrucelli, H. J. Kim, F. B. Gao, and J. P. Taylor. 2015. 'GGGGCC repeat expansion in C9orf72 compromises nucleocytoplasmic transport', *Nature*, 525: 129-33.
- Gan, L., M. R. Cookson, L. Petrucelli, and A. R. La Spada. 2018. 'Converging pathways in neurodegeneration, from genetics to mechanisms', *Nat Neurosci*, 21: 1300-09.
- Gaspar, C., M. Jannatipour, P. Dion, J. Laganier, J. Sequeiros, B. Brais, and G. A. Rouleau. 2000. 'CAG tract of MJD-1 may be prone to frameshifts causing polyalanine accumulation', *Hum Mol Genet*, 9: 1957-66.

- Gendron, T. F., K. A. Josephs, and L. Petrucelli. 2010. 'Review: transactive response DNA-binding protein 43 (TDP-43): mechanisms of neurodegeneration', *Neuropathol Appl Neurobiol*, 36: 97-112.
- Gendron, T. F., and L. Petrucelli. 2011. 'Rodent models of TDP-43 proteinopathy: investigating the mechanisms of TDP-43-mediated neurodegeneration', *J Mol Neurosci*, 45: 486-99.
- Gijselinck, I., T. Van Langenhove, J. van der Zee, K. Sleegers, S. Philtjens, G. Kleinberger, J. Janssens, K. Bettens, C. Van Cauwenberghe, S. Pereson, S. Engelborghs, A. Sieben, P. De Jonghe, R. Vandenberghe, P. Santens, J. De Bleeker, G. Maes, V. Baumer, L. Dillen, G. Joris, I. Cuijt, E. Corsmit, E. Elinck, J. Van Dongen, S. Vermeulen, M. Van den Broeck, C. Vaerenberg, M. Mattheijssens, K. Peeters, W. Robberecht, P. Cras, J. J. Martin, P. P. De Deyn, M. Cruts, and C. Van Broeckhoven. 2012. 'A C9orf72 promoter repeat expansion in a Flanders-Belgian cohort with disorders of the frontotemporal lobar degeneration-amyotrophic lateral sclerosis spectrum: a gene identification study', *Lancet Neurol*, 11: 54-65.
- Grammatikakis, I., A. C. Panda, K. Abdelmohsen, and M. Gorospe. 2014. 'Long noncoding RNAs(lncRNAs) and the molecular hallmarks of aging', *Aging (Albany NY)*, 6: 992-1009.
- Grohmann, K., M. Schuelke, A. Diers, K. Hoffmann, B. Lucke, C. Adams, E. Bertini, H. Leonhardt-Horti, F. Muntoni, R. Ouvrier, A. Pfeufer, R. Rossi, L. Van Maldergem, J. M. Wilmshurst, T. F. Wienker, M. Sendtner, S. Rudnik-Schoneborn, K. Zerres, and C. Hubner. 2001. 'Mutations in the gene encoding immunoglobulin mu-binding protein 2 cause spinal muscular atrophy with respiratory distress type 1', *Nat Genet*, 29: 75-7.
- Gupta, R., M. Lan, J. Mojsilovic-Petrovic, W. H. Choi, N. Safren, S. Barmada, M. J. Lee, and R. Kalb. 2017. 'The Proline/Arginine Dipeptide from Hexanucleotide Repeat Expanded C9ORF72 Inhibits the Proteasome', *eNeuro*, 4.
- Haeusler, A. R., C. J. Donnelly, and J. D. Rothstein. 2016. 'The expanding biology of the C9orf72 nucleotide repeat expansion in neurodegenerative disease', *Nat Rev Neurosci*, 17: 383-95.
- Haghighat, A., S. Mader, A. Pause, and N. Sonenberg. 1995. 'Repression of cap-dependent translation by 4E-binding protein 1: competition with p220 for binding to eukaryotic initiation factor-4E', *EMBO J*, 14: 5701-9.
- Halliday, M., H. Radford, Y. Sekine, J. Moreno, N. Verity, J. le Quesne, C. A. Ortori, D. A. Barrett, C. Fromont, P. M. Fischer, H. P. Harding, D. Ron, and G. R. Mallucci. 2015. 'Partial restoration of protein synthesis rates by the small molecule ISRIB prevents neurodegeneration without pancreatic toxicity', *Cell Death Dis*, 6: e1672.
- Halliday, M., H. Radford, K. A. M. Zents, C. Molloy, J. A. Moreno, N. C. Verity, E. Smith, C. A. Ortori, D. A. Barrett, M. Bushell, and G. R. Mallucci. 2017. 'Repurposed drugs targeting eIF2 $\alpha$ -P-mediated translational repression prevent neurodegeneration in mice', *Brain*, 140: 1768-83.
- Harding, H. P., Y. Zhang, and D. Ron. 1999. 'Protein translation and folding are coupled by an endoplasmic-reticulum-resident kinase', *Nature*, 397: 271-4.
- Heiman, M., A. Schaefer, S. Gong, J. D. Peterson, M. Day, K. E. Ramsey, M. Suarez-Farinas, C. Schwarz, D. A. Stephan, D. J. Surmeier, P. Greengard, and N. Heintz.

2008. 'A translational profiling approach for the molecular characterization of CNS cell types', *Cell*, 135: 738-48.
- Hentze, M. W., A. Castello, T. Schwarzl, and T. Preiss. 2018. 'A brave new world of RNA-binding proteins', *Nat Rev Mol Cell Biol*, 19: 327-41.
- Hettich, M. M., F. Matthes, D. P. Ryan, N. Griesche, S. Schroder, S. Dorn, S. Kraubeta, and D. Ehninger. 2014. 'The anti-diabetic drug metformin reduces BACE1 protein level by interfering with the MID1 complex', *PLoS One*, 9: e102420.
- Higashi, S., T. Kabuta, Y. Nagai, Y. Tsuchiya, H. Akiyama, and K. Wada. 2013. 'TDP-43 associates with stalled ribosomes and contributes to cell survival during cellular stress', *J Neurochem*, 126: 288-300.
- Hinnebusch, A. G. 2014. 'The scanning mechanism of eukaryotic translation initiation', *Annu Rev Biochem*, 83: 779-812.
- Huentelman, M. J., A. Papassotiropoulos, D. W. Craig, F. J. Hoerndli, J. V. Pearson, K. D. Huynh, J. Corneveaux, J. Hanggi, C. R. Mondadori, A. Buchmann, E. M. Reiman, K. Henke, D. J. de Quervain, and D. A. Stephan. 2007. 'Calmodulin-binding transcription activator 1 (CAMTA1) alleles predispose human episodic memory performance', *Hum Mol Genet*, 16: 1469-77.
- Ikeda, K., and Y. Iwasaki. 2015. 'Edaravone, a Free Radical Scavenger, Delayed Symptomatic and Pathological Progression of Motor Neuron Disease in the Wobbler Mouse', *PLoS One*, 10: e0140316.
- Ikiz, B., M. J. Alvarez, D. B. Re, V. Le Verche, K. Politi, F. Lotti, S. Phani, R. Pradhan, C. Yu, G. F. Croft, A. Jacquier, C. E. Henderson, A. Califano, and S. Przedborski. 2015. 'The Regulatory Machinery of Neurodegeneration in In Vitro Models of Amyotrophic Lateral Sclerosis', *Cell Rep*, 12: 335-45.
- Ilieva, E. V., V. Ayala, M. Jove, E. Dalfo, D. Cacabelos, M. Povedano, M. J. Bellmunt, I. Ferrer, R. Pamplona, and M. Portero-Otin. 2007. 'Oxidative and endoplasmic reticulum stress interplay in sporadic amyotrophic lateral sclerosis', *Brain*, 130: 3111-23.
- Ingolia, N. T. 2014. 'Ribosome profiling: new views of translation, from single codons to genome scale', *Nat Rev Genet*, 15: 205-13.
- Ingolia, N. T., G. A. Brar, S. Rouskin, A. M. McGeachy, and J. S. Weissman. 2012. 'The ribosome profiling strategy for monitoring translation in vivo by deep sequencing of ribosome-protected mRNA fragments', *Nat Protoc*, 7: 1534-50.
- Ingolia, N. T., S. Ghaemmaghami, J. R. Newman, and J. S. Weissman. 2009. 'Genome-wide analysis in vivo of translation with nucleotide resolution using ribosome profiling', *Science*, 324: 218-23.
- Ingolia, N. T., J. A. Hussmann, and J. S. Weissman. 2018. 'Ribosome Profiling: Global Views of Translation', *Cold Spring Harb Perspect Biol*.
- Inoue, J., K. Yamasaki, E. Ikeuchi, S. Satoh, Y. Fujiwara, T. Nishimaki-Mogami, M. Shimizu, and R. Sato. 2011. 'Identification of MIG12 as a mediator for stimulation of lipogenesis by LXR activation', *Mol Endocrinol*, 25: 995-1005.



- Kabashi, E., L. Lin, M. L. Tradewell, P. A. Dion, V. Bercier, P. Bourgouin, D. Rochefort, S. Bel Hadj, H. D. Durham, C. Vande Velde, G. A. Rouleau, and P. Drapeau. 2010. 'Gain and loss of function of ALS-related mutations of TARDBP (TDP-43) cause motor deficits in vivo', *Hum Mol Genet*, 19: 671-83.
- Kabashi, E., P. N. Valdmanis, P. Dion, D. Spiegelman, B. J. McConkey, C. Vande Velde, J. P. Bouchard, L. Lacomblez, K. Pochigaeva, F. Salachas, P. F. Pradat, W. Camu, V. Meininger, N. Dupre, and G. A. Rouleau. 2008. 'TARDBP mutations in individuals with sporadic and familial amyotrophic lateral sclerosis', *Nat Genet*, 40: 572-4.
- Kanekura, K., T. Yagi, A. J. Cammack, J. Mahadevan, M. Kuroda, M. B. Harms, T. M. Miller, and F. Urano. 2016. 'Poly-dipeptides encoded by the C9ORF72 repeats block global protein translation', *Hum Mol Genet*, 25: 1803-13.
- Kapeli, K., and G. W. Yeo. 2012. 'Genome-wide approaches to dissect the roles of RNA binding proteins in translational control: implications for neurological diseases', *Front Neurosci*, 6: 144.
- Kapur, M., and S. L. Ackerman. 2018. 'mRNA Translation Gone Awry: Translation Fidelity and Neurological Disease', *Trends Genet*, 34: 218-31.
- Kapur, M., C. E. Monaghan, and S. L. Ackerman. 2017. 'Regulation of mRNA Translation in Neurons-A Matter of Life and Death', *Neuron*, 96: 616-37.
- Kawahara, Y., and A. Mieda-Sato. 2012. 'TDP-43 promotes microRNA biogenesis as a component of the Drosha and Dicer complexes', *Proc Natl Acad Sci U S A*, 109: 3347-52.
- Kickstein, E., S. Krauss, P. Thornhill, D. Rutschow, R. Zeller, J. Sharkey, R. Williamson, M. Fuchs, A. Kohler, H. Glossmann, R. Schneider, C. Sutherland, and S. Schweiger. 2010. 'Biguanide metformin acts on tau phosphorylation via mTOR/protein phosphatase 2A (PP2A) signaling', *Proc Natl Acad Sci U S A*, 107: 21830-5.
- Kim, C. W., Y. A. Moon, S. W. Park, D. Cheng, H. J. Kwon, and J. D. Horton. 2010. 'Induced polymerization of mammalian acetyl-CoA carboxylase by MIG12 provides a tertiary level of regulation of fatty acid synthesis', *Proc Natl Acad Sci U S A*, 107: 9626-31.
- Kim, D., G. Pertea, C. Trapnell, H. Pimentel, R. Kelley, and S. L. Salzberg. 2013. 'TopHat2: accurate alignment of transcriptomes in the presence of insertions, deletions and gene fusions', *Genome Biol*, 14: R36.
- Kim, H. J., A. R. Raphael, E. S. LaDow, L. McGurk, R. A. Weber, J. Q. Trojanowski, V. M. Lee, S. Finkbeiner, A. D. Gitler, and N. M. Bonini. 2014. 'Therapeutic modulation of eIF2alpha phosphorylation rescues TDP-43 toxicity in amyotrophic lateral sclerosis disease models', *Nat Genet*, 46: 152-60.
- Kim, H. S., Y. Choi, K. Y. Shin, Y. Joo, Y. K. Lee, S. Y. Jung, Y. H. Suh, and J. H. Kim. 2007. 'Swedish amyloid precursor protein mutation increases phosphorylation of eIF2alpha in vitro and in vivo', *J Neurosci Res*, 85: 1528-37.
- King, I. N., V. Yartseva, D. Salas, A. Kumar, A. Heidersbach, D. M. Ando, N. R. Stallings, J. L. Elliott, D. Srivastava, and K. N. Ivey. 2014. 'The RNA-binding protein TDP-43 selectively disrupts microRNA-1/206 incorporation into the RNA-induced silencing complex', *J Biol Chem*, 289: 14263-71.

- Kozak, M. 1987. 'At least six nucleotides preceding the AUG initiator codon enhance translation in mammalian cells', *J Mol Biol*, 196: 947-50.
- Krans, A., M. G. Kearse, and P. K. Todd. 2016. 'Repeat-associated non-AUG translation from antisense CCG repeats in fragile X tremor/ataxia syndrome', *Ann Neurol*, 80: 871-81.
- Krauss, S., N. Griesche, E. Jastrzebska, C. Chen, D. Rutschow, C. Achmuller, S. Dorn, S. M. Boesch, M. Lalowski, E. Wanker, R. Schneider, and S. Schweiger. 2013. 'Translation of HTT mRNA with expanded CAG repeats is regulated by the MID1-PP2A protein complex', *Nat Commun*, 4: 1511.
- Kwiatkowski, T. J., Jr., D. A. Bosco, A. L. Leclerc, E. Tamrazian, C. R. Vanderburg, C. Russ, A. Davis, J. Gilchrist, E. J. Kasarskis, T. Munsat, P. Valdmanis, G. A. Rouleau, B. A. Hosler, P. Cortelli, P. J. de Jong, Y. Yoshinaga, J. L. Haines, M. A. Pericak-Vance, J. Yan, N. Ticozzi, T. Siddique, D. McKenna-Yasek, P. C. Sapp, H. R. Horvitz, J. E. Landers, and R. H. Brown, Jr. 2009. 'Mutations in the FUS/TLS gene on chromosome 16 cause familial amyotrophic lateral sclerosis', *Science*, 323: 1205-8.
- Kwon, S., E. Barbarese, and J. H. Carson. 1999. 'The cis-acting RNA trafficking signal from myelin basic protein mRNA and its cognate trans-acting ligand hnRNP A2 enhance cap-dependent translation', *J Cell Biol*, 147: 247-56.
- Laferriere, F., and M. Polymenidou. 2015. 'Advances and challenges in understanding the multifaceted pathogenesis of amyotrophic lateral sclerosis', *Swiss Med Wkly*, 145: w14054.
- Lagier-Tourenne, C., and D. W. Cleveland. 2009. 'Rethinking ALS: the FUS about TDP-43', *Cell*, 136: 1001-4.
- Lagier-Tourenne, C., M. Polymenidou, and D. W. Cleveland. 2010. 'TDP-43 and FUS/TLS: emerging roles in RNA processing and neurodegeneration', *Hum Mol Genet*, 19: R46-64.
- Langmead, B., and S. L. Salzberg. 2012. 'Fast gapped-read alignment with Bowtie 2', *Nat Methods*, 9: 357-9.
- Lee, E. B., V. M. Lee, and J. Q. Trojanowski. 2012. 'Gains or losses: molecular mechanisms of TDP43-mediated neurodegeneration', *Nat Rev Neurosci*, 13: 38-50.
- Lee, E. K., H. H. Kim, Y. Kuwano, K. Abdelmohsen, S. Srikantan, S. S. Subaran, M. Gleichmann, M. R. Mughal, J. L. Martindale, X. Yang, P. F. Worley, M. P. Mattson, and M. Gorospe. 2010. 'hnRNP C promotes APP translation by competing with FMRP for APP mRNA recruitment to P bodies', *Nat Struct Mol Biol*, 17: 732-9.
- Lefebvre, C., P. Rajbhandari, M. J. Alvarez, P. Bandaru, W. K. Lim, M. Sato, K. Wang, P. Sumazin, M. Kustagi, B. C. Bisikirska, K. Basso, P. Beltrao, N. Krogan, J. Gautier, R. Dalla-Favera, and A. Califano. 2010. 'A human B-cell interactome identifies MYB and FOXM1 as master regulators of proliferation in germinal centers', *Mol Syst Biol*, 6: 377.
- Levine, T. P., R. D. Daniels, A. T. Gatta, L. H. Wong, and M. J. Hayes. 2013. 'The product of C9orf72, a gene strongly implicated in neurodegeneration, is structurally related to DENN Rab-GEFs', *Bioinformatics*, 29: 499-503.

- Li, B., T. Zhou, and Y. Zou. 2016. 'Mid1/Mid2 expression in craniofacial development and a literature review of X-linked opitz syndrome', *Mol Genet Genomic Med*, 4: 95-105.
- Li, W., Y. Jin, L. Prazak, M. Hammell, and J. Dubnau. 2012. 'Transposable elements in TDP-43-mediated neurodegenerative disorders', *PLoS One*, 7: e44099.
- Li, Y. R., O. D. King, J. Shorter, and A. D. Gitler. 2013. 'Stress granules as crucibles of ALS pathogenesis', *J Cell Biol*, 201: 361-72.
- Liao, Y., G. K. Smyth, and W. Shi. 2014. 'featureCounts: an efficient general purpose program for assigning sequence reads to genomic features', *Bioinformatics*, 30: 923-30.
- Ling, J. P., O. Pletnikova, J. C. Troncoso, and P. C. Wong. 2015. 'TDP-43 repression of nonconserved cryptic exons is compromised in ALS-FTD', *Science*, 349: 650-5.
- Liu-Yesucevitz, L., A. Bilgutay, Y. J. Zhang, T. Vanderweyde, A. Citro, T. Mehta, N. Zaarur, A. McKee, R. Bowser, M. Sherman, L. Petrucelli, and B. Wolozin. 2010. 'Tar DNA binding protein-43 (TDP-43) associates with stress granules: analysis of cultured cells and pathological brain tissue', *PLoS One*, 5: e13250.
- Liu, X., D. Li, W. Zhang, M. Guo, and Q. Zhan. 2012. 'Long non-coding RNA gadd7 interacts with TDP-43 and regulates Cdk6 mRNA decay', *EMBO J*, 31: 4415-27.
- Liu, Y., A. Beyer, and R. Aebersold. 2016. 'On the Dependency of Cellular Protein Levels on mRNA Abundance', *Cell*, 165: 535-50.
- Long, C., C. E. Grueter, K. Song, S. Qin, X. Qi, Y. M. Kong, J. M. Shelton, J. A. Richardson, C. L. Zhang, R. Bassel-Duby, and E. N. Olson. 2014. 'Ataxia and Purkinje cell degeneration in mice lacking the CAMTA1 transcription factor', *Proc Natl Acad Sci U S A*, 111: 11521-6.
- Mackenzie, I. R., E. H. Bigio, P. G. Ince, F. Geser, M. Neumann, N. J. Cairns, L. K. Kwong, M. S. Forman, J. Ravits, H. Stewart, A. Eisen, L. McClusky, H. A. Kretzschmar, C. M. Monoranu, J. R. Highley, J. Kirby, T. Siddique, P. J. Shaw, V. M. Lee, and J. Q. Trojanowski. 2007. 'Pathological TDP-43 distinguishes sporadic amyotrophic lateral sclerosis from amyotrophic lateral sclerosis with SOD1 mutations', *Ann Neurol*, 61: 427-34.
- Mackenzie, I. R., M. Neumann, A. Baborie, D. M. Sampathu, D. Du Plessis, E. Jaros, R. H. Perry, J. Q. Trojanowski, D. M. Mann, and V. M. Lee. 2011. 'A harmonized classification system for FTLTDP pathology', *Acta Neuropathol*, 122: 111-3.
- Mackenzie, I. R., A. M. Nicholson, M. Sarkar, J. Messing, M. D. Purice, C. Pottier, K. Annu, M. Baker, R. B. Perkerson, A. Kurti, B. J. Matchett, T. Mittag, J. Temirov, G. R. Hsiung, C. Krieger, M. E. Murray, M. Kato, J. D. Fryer, L. Petrucelli, L. Zinman, S. Weintraub, M. Mesulam, J. Keith, S. A. Zivkovic, V. Hirsch-Reinshagen, R. P. Roos, S. Zuchner, N. R. Graff-Radford, R. C. Petersen, R. J. Caselli, Z. K. Wszolek, E. Finger, C. Lippa, D. Lacomis, H. Stewart, D. W. Dickson, H. J. Kim, E. Rogaeva, E. Bigio, K. B. Boylan, J. P. Taylor, and R. Rademakers. 2017. 'TIA1 Mutations in Amyotrophic Lateral Sclerosis and Frontotemporal Dementia Promote Phase Separation and Alter Stress Granule Dynamics', *Neuron*, 95: 808-16 e9.
- MacNair, L., S. Xiao, D. Miletic, M. Ghani, J. P. Julien, J. Keith, L. Zinman, E. Rogaeva, and J. Robertson. 2016. 'MTHFSD and DDX58 are novel RNA-binding proteins abnormally regulated in amyotrophic lateral sclerosis', *Brain*, 139: 86-100.

- Majumder, P., Y. T. Chen, J. K. Bose, C. C. Wu, W. C. Cheng, S. J. Cheng, Y. H. Fang, Y. L. Chen, K. J. Tsai, C. C. Lien, and C. K. Shen. 2012. 'TDP-43 regulates the mammalian spinogenesis through translational repression of Rac1', *Acta Neuropathol*, 124: 231-45.
- Majumder, P., J. F. Chu, B. Chatterjee, K. B. Swamy, and C. J. Shen. 2016. 'Co-regulation of mRNA translation by TDP-43 and Fragile X Syndrome protein FMRP', *Acta Neuropathol*, 132: 721-38.
- Marcotrigiano, J., A. C. Gingras, N. Sonenberg, and S. K. Burley. 1999. 'Cap-dependent translation initiation in eukaryotes is regulated by a molecular mimic of eIF4G', *Mol Cell*, 3: 707-16.
- Marcuzzo, S., D. Kapetis, R. Mantegazza, F. Baggi, S. Bonanno, C. Barzago, P. Cavalcante, N. Kerlero de Rosbo, and P. Bernasconi. 2014. 'Altered miRNA expression is associated with neuronal fate in G93A-SOD1 ependymal stem progenitor cells', *Exp Neurol*, 253: 91-101.
- Margolin, A. A., I. Nemenman, K. Basso, C. Wiggins, G. Stolovitzky, R. Dalla Favera, and A. Califano. 2006. 'ARACNE: an algorithm for the reconstruction of gene regulatory networks in a mammalian cellular context', *BMC Bioinformatics*, 7 Suppl 1: S7.
- Martin, Marcel. 2011. 'Cutadapt removes adapter sequences from high-throughput sequencing reads', 2011, 17.
- McDonald, K. K., A. Aulas, L. Destroismaisons, S. Pickles, E. Beleac, W. Camu, G. A. Rouleau, and C. Vande Velde. 2011. 'TAR DNA-binding protein 43 (TDP-43) regulates stress granule dynamics via differential regulation of G3BP and TIA-1', *Hum Mol Genet*, 20: 1400-10.
- Miller, R. G., J. D. Mitchell, and D. H. Moore. 2012. 'Riluzole for amyotrophic lateral sclerosis (ALS)/motor neuron disease (MND)', *Cochrane Database Syst Rev*: CD001447.
- Moisse, K., K. Volkening, C. Leystra-Lantz, I. Welch, T. Hill, and M. J. Strong. 2009. 'Divergent patterns of cytosolic TDP-43 and neuronal progranulin expression following axotomy: implications for TDP-43 in the physiological response to neuronal injury', *Brain Res*, 1249: 202-11.
- Montibeller, L., and J. de Belleruche. 2018. 'Amyotrophic lateral sclerosis (ALS) and Alzheimer's disease (AD) are characterised by differential activation of ER stress pathways: focus on UPR target genes', *Cell Stress Chaperones*, 23: 897-912.
- Moreno, J. A., H. Radford, D. Peretti, J. R. Steinert, N. Verity, M. G. Martin, M. Halliday, J. Morgan, D. Dinsdale, C. A. Ortori, D. A. Barrett, P. Tsaytler, A. Bertolotti, A. E. Willis, M. Bushell, and G. R. Mallucci. 2012. 'Sustained translational repression by eIF2alpha-P mediates prion neurodegeneration', *Nature*, 485: 507-11.
- Nakamura, T., T. Ueyama, Y. Ninoyu, H. Sakaguchi, N. Chojookhuu, Y. Hishikawa, H. Kiyonari, M. Kohta, M. Sakahara, I. de Curtis, E. Kohmura, Y. Hisa, A. Aiba, and N. Saito. 2017. 'Novel role of Rac-Mid1 signaling in medial cerebellar development', *Development*, 144: 1863-75.
- Nakashima-Yasuda, H., K. Uryu, J. Robinson, S. X. Xie, H. Hurtig, J. E. Duda, S. E. Arnold, A. Siderowf, M. Grossman, J. B. Leverenz, R. Woltjer, O. L. Lopez, R. Hamilton, D. W. Tsuang, D. Galasko, E. Masliah, J. Kaye, C. M. Clark, T. J. Montine, V. M. Lee,

- and J. Q. Trojanowski. 2007. 'Co-morbidity of TDP-43 proteinopathy in Lewy body related diseases', *Acta Neuropathol*, 114: 221-9.
- Nalavadi, V. C., R. S. Muddashetty, C. Gross, and G. J. Bassell. 2012. 'Dephosphorylation-induced ubiquitination and degradation of FMRP in dendrites: a role in immediate early mGluR-stimulated translation', *J Neurosci*, 32: 2582-7.
- Neumann, M., D. M. Sampathu, L. K. Kwong, A. C. Truax, M. C. Micsenyi, T. T. Chou, J. Bruce, T. Schuck, M. Grossman, C. M. Clark, L. F. McCluskey, B. L. Miller, E. Masliah, I. R. Mackenzie, H. Feldman, W. Feiden, H. A. Kretzschmar, J. Q. Trojanowski, and V. M. Lee. 2006. 'Ubiquitinated TDP-43 in frontotemporal lobar degeneration and amyotrophic lateral sclerosis', *Science*, 314: 130-3.
- O'Connor, P. B., D. E. Andreev, and P. V. Baranov. 2016. 'Comparative survey of the relative impact of mRNA features on local ribosome profiling read density', *Nat Commun*, 7: 12915.
- Okano, H., T. Imai, and M. Okabe. 2002. 'Musashi: a translational regulator of cell fate', *J Cell Sci*, 115: 1355-9.
- Olney, N. T., S. Spina, and B. L. Miller. 2017. 'Frontotemporal Dementia', *Neurol Clin*, 35: 339-74.
- Ou, S. H., F. Wu, D. Harrich, L. F. Garcia-Martinez, and R. B. Gaynor. 1995. 'Cloning and characterization of a novel cellular protein, TDP-43, that binds to human immunodeficiency virus type 1 TAR DNA sequence motifs', *J Virol*, 69: 3584-96.
- Pakos-Zebrucka, K., I. Koryga, K. Mnich, M. Lujic, A. Samali, and A. M. Gorman. 2016. 'The integrated stress response', *EMBO Rep*, 17: 1374-95.
- Perry, E. K., M. Johnson, A. Ekonomou, R. H. Perry, C. Ballard, and J. Attems. 2012. 'Neurogenic abnormalities in Alzheimer's disease differ between stages of neurogenesis and are partly related to cholinergic pathology', *Neurobiol Dis*, 47: 155-62.
- Philips, T., and J. D. Rothstein. 2015. 'Rodent Models of Amyotrophic Lateral Sclerosis', *Curr Protoc Pharmacol*, 69: 5 67 1-21.
- Piazzon, N., F. Rage, F. Schlotter, H. Moine, C. Branlant, and S. Massenet. 2008. 'In vitro and in cellulo evidences for association of the survival of motor neuron complex with the fragile X mental retardation protein', *J Biol Chem*, 283: 5598-610.
- Polymenidou, M., and D. W. Cleveland. 2017. 'Biological Spectrum of Amyotrophic Lateral Sclerosis Prions', *Cold Spring Harb Perspect Med*, 7.
- Polymenidou, M., C. Lagier-Tourenne, K. R. Hutt, S. C. Huelga, J. Moran, T. Y. Liang, S. C. Ling, E. Sun, E. Wancewicz, C. Mazur, H. Kordasiewicz, Y. Sedaghat, J. P. Donohue, L. Shiue, C. F. Bennett, G. W. Yeo, and D. W. Cleveland. 2011. 'Long pre-mRNA depletion and RNA missplicing contribute to neuronal vulnerability from loss of TDP-43', *Nat Neurosci*, 14: 459-68.
- Prpar Mihevc, S., M. Baralle, E. Buratti, and B. Rogelj. 2016. 'TDP-43 aggregation mirrors TDP-43 knockdown, affecting the expression levels of a common set of proteins', *Sci Rep*, 6: 33996.

- Quaderi, N. A., S. Schweiger, K. Gaudenz, B. Franco, E. I. Rugarli, W. Berger, G. J. Feldman, M. Volta, G. Andolfi, S. Gilgenkrantz, R. W. Marion, R. C. Hennekam, J. M. Opitz, M. Muenke, H. H. Ropers, and A. Ballabio. 1997. 'Opitz G/BBB syndrome, a defect of midline development, is due to mutations in a new RING finger gene on Xp22', *Nat Genet*, 17: 285-91.
- Ramaswami, M., J. P. Taylor, and R. Parker. 2013. 'Altered ribostasis: RNA-protein granules in degenerative disorders', *Cell*, 154: 727-36.
- Ratti, A., and E. Buratti. 2016. 'Physiological functions and pathobiology of TDP-43 and FUS/TLS proteins', *J Neurochem*, 138 Suppl 1: 95-111.
- Renton, A. E., E. Majounie, A. Waite, J. Simon-Sanchez, S. Rollinson, J. R. Gibbs, J. C. Schymick, H. Laaksovirta, J. C. van Swieten, L. Myllykangas, H. Kalimo, A. Paetau, Y. Abramzon, A. M. Remes, A. Kaganovich, S. W. Scholz, J. Duckworth, J. Ding, D. W. Harmer, D. G. Hernandez, J. O. Johnson, K. Mok, M. Ryten, D. Trabzuni, R. J. Guerreiro, R. W. Orrell, J. Neal, A. Murray, J. Pearson, I. E. Jansen, D. Sondervan, H. Seelaar, D. Blake, K. Young, N. Halliwell, J. B. Callister, G. Toulson, A. Richardson, A. Gerhard, J. Snowden, D. Mann, D. Neary, M. A. Nalls, T. Peuralinna, L. Jansson, V. M. Isoviita, A. L. Kaivorinne, M. Holtta-Vuori, E. Ikonen, R. Sulkava, M. Benatar, J. Wu, A. Chio, G. Restagno, G. Borghero, M. Sabatelli, Italsgen Consortium, D. Heckerman, E. Rogaeva, L. Zinman, J. D. Rothstein, M. Sendtner, C. Drepper, E. E. Eichler, C. Alkan, Z. Abdullaev, S. D. Pack, A. Dutra, E. Pak, J. Hardy, A. Singleton, N. M. Williams, P. Heutink, S. Pickering-Brown, H. R. Morris, P. J. Tienari, and B. J. Traynor. 2011. 'A hexanucleotide repeat expansion in C9ORF72 is the cause of chromosome 9p21-linked ALS-FTD', *Neuron*, 72: 257-68.
- Roberts, T. C., K. V. Morris, and M. J. Wood. 2014. 'The role of long non-coding RNAs in neurodevelopment, brain function and neurological disease', *Philos Trans R Soc Lond B Biol Sci*, 369.
- Rosen, D. R., T. Siddique, D. Patterson, D. A. Figlewicz, P. Sapp, A. Hentati, D. Donaldson, J. Goto, J. P. O'Regan, H. X. Deng, and et al. 1993. 'Mutations in Cu/Zn superoxide dismutase gene are associated with familial amyotrophic lateral sclerosis', *Nature*, 362: 59-62.
- Rothstein, J. D. 2017. 'Edaravone: A new drug approved for ALS', *Cell*, 171: 725.
- Salazar-Gruesso, E. F., S. Kim, and H. Kim. 1991. 'Embryonic mouse spinal cord motor neuron hybrid cells', *Neuroreport*, 2: 505-8.
- Sances, S., L. I. Bruijn, S. Chandran, K. Eggan, R. Ho, J. R. Klim, M. R. Livesey, E. Lowry, J. D. Macklis, D. Rushton, C. Sadegh, D. Sareen, H. Wichterle, S. C. Zhang, and C. N. Svendsen. 2016. 'Modeling ALS with motor neurons derived from human induced pluripotent stem cells', *Nat Neurosci*, 19: 542-53.
- Saxena, S., and P. Caroni. 2011. 'Selective neuronal vulnerability in neurodegenerative diseases: from stressor thresholds to degeneration', *Neuron*, 71: 35-48.
- Schindelin, J., I. Arganda-Carreras, E. Frise, V. Kaynig, M. Longair, T. Pietzsch, S. Preibisch, C. Rueden, S. Saalfeld, B. Schmid, J. Y. Tinevez, D. J. White, V. Hartenstein, K. Eliceiri, P. Tomancak, and A. Cardona. 2012. 'Fiji: an open-source platform for biological-image analysis', *Nat Methods*, 9: 676-82.
- Schleich, S., K. Strassburger, P. C. Janiesch, T. Koledachkina, K. K. Miller, K. Haneke, Y. S. Cheng, K. Kuechler, G. Stoecklin, K. E. Duncan, and A. A. Teleman. 2014. 'DENR-

- MCT-1 promotes translation re-initiation downstream of uORFs to control tissue growth', *Nature*, 512: 208-12.
- Schludi, M. H., L. Becker, L. Garrett, T. F. Gendron, Q. Zhou, F. Schreiber, B. Popper, L. Dimou, T. M. Strom, J. Winkelmann, A. von Thaden, K. Rentzsch, S. May, M. Michaelson, B. M. Schwenk, J. Tan, B. Schoser, M. Dieterich, L. Petrucelli, S. M. Holter, W. Wurst, H. Fuchs, V. Gailus-Durner, M. H. de Angelis, T. Klopstock, T. Arzberger, and D. Edbauer. 2017. 'Spinal poly-GA inclusions in a C9orf72 mouse model trigger motor deficits and inflammation without neuron loss', *Acta Neuropathol*, 134: 241-54.
- Schneider, C. A., W. S. Rasband, and K. W. Eliceiri. 2012. 'NIH Image to ImageJ: 25 years of image analysis', *Nat Methods*, 9: 671-5.
- Schuller, A. P., and R. Green. 2018. 'Roadblocks and resolutions in eukaryotic translation', *Nat Rev Mol Cell Biol*.
- Schweiger, S., S. Dorn, M. Fuchs, A. Kohler, F. Matthes, E. C. Muller, E. Wanker, R. Schneider, and S. Krauss. 2014. 'The E3 ubiquitin ligase MID1 catalyzes ubiquitination and cleavage of Fu', *J Biol Chem*, 289: 31805-17.
- Shang, J., T. Yamashita, Y. Nakano, R. Morihara, X. Li, T. Feng, X. Liu, Y. Huang, Y. Fukui, N. Hishikawa, Y. Ohta, and K. Abe. 2017. 'Aberrant distributions of nuclear pore complex proteins in ALS mice and ALS patients', *Neuroscience*, 350: 158-68.
- Shi, Y., K. M. Vattam, R. Sood, J. An, J. Liang, L. Stramm, and R. C. Wek. 1998. 'Identification and characterization of pancreatic eukaryotic initiation factor 2 alpha-subunit kinase, PEK, involved in translational control', *Mol Cell Biol*, 18: 7499-509.
- Shinawi, M., R. Coorg, J. S. Shimony, D. K. Grange, and H. Al-Kateb. 2015. 'Intragenic CAMTA1 deletions are associated with a spectrum of neurobehavioral phenotypes', *Clin Genet*, 87: 478-82.
- Singh, G., G. Pratt, G. W. Yeo, and M. J. Moore. 2015. 'The Clothes Make the mRNA: Past and Present Trends in mRNP Fashion', *Annu Rev Biochem*, 84: 325-54.
- Sreedharan, J., I. P. Blair, V. B. Tripathi, X. Hu, C. Vance, B. Rogelj, S. Ackerley, J. C. Durnall, K. L. Williams, E. Buratti, F. Baralle, J. de Belleruche, J. D. Mitchell, P. N. Leigh, A. Al-Chalabi, C. C. Miller, G. Nicholson, and C. E. Shaw. 2008. 'TDP-43 mutations in familial and sporadic amyotrophic lateral sclerosis', *Science*, 319: 1668-72.
- Thoreen, C. C., L. Chantranupong, H. R. Keys, T. Wang, N. S. Gray, and D. M. Sabatini. 2012. 'A unifying model for mTORC1-mediated regulation of mRNA translation', *Nature*, 485: 109-13.
- Todd, P. K., S. Y. Oh, A. Krans, F. He, C. Sellier, M. Frazer, A. J. Renoux, K. C. Chen, K. M. Scaglione, V. Basrur, K. Elenitoba-Johnson, J. P. Vonsattel, E. D. Louis, M. A. Sutton, J. P. Taylor, R. E. Mills, N. Charlet-Berguerand, and H. L. Paulson. 2013. 'CGG repeat-associated translation mediates neurodegeneration in fragile X tremor ataxia syndrome', *Neuron*, 78: 440-55.
- Tollervey, J. R., T. Curk, B. Rogelj, M. Briese, M. Cereda, M. Kayikci, J. Konig, T. Hortobagyi, A. L. Nishimura, V. Zupunski, R. Patani, S. Chandran, G. Rot, B. Zupan, C. E. Shaw, and J. Ule. 2011. 'Characterizing the RNA targets and position-dependent splicing regulation by TDP-43', *Nat Neurosci*, 14: 452-8.

- Trockenbacher, A., V. Suckow, J. Foerster, J. Winter, S. Krauss, H. H. Ropers, R. Schneider, and S. Schweiger. 2001. 'MID1, mutated in Opitz syndrome, encodes an ubiquitin ligase that targets phosphatase 2A for degradation', *Nat Genet*, 29: 287-94.
- Turner, M. R., O. Hardiman, M. Benatar, B. R. Brooks, A. Chio, M. de Carvalho, P. G. Ince, C. Lin, R. G. Miller, H. Mitsumoto, G. Nicholson, J. Ravits, P. J. Shaw, M. Swash, K. Talbot, B. J. Traynor, L. H. Van den Berg, J. H. Veldink, S. Vucic, and M. C. Kiernan. 2013. 'Controversies and priorities in amyotrophic lateral sclerosis', *Lancet Neurol*, 12: 310-22.
- Ule, J., K. Jensen, A. Mele, and R. B. Darnell. 2005. 'CLIP: a method for identifying protein-RNA interaction sites in living cells', *Methods*, 37: 376-86.
- Unterberger, U., R. Hoffberger, E. Gelpi, H. Flicker, H. Budka, and T. Voigtlander. 2006. 'Endoplasmic reticulum stress features are prominent in Alzheimer disease but not in prion diseases in vivo', *J Neuropathol Exp Neurol*, 65: 348-57.
- Unterbruner, K., F. Matthes, J. Schilling, R. Nalavade, S. Weber, J. Winter, and S. Krauss. 2018. 'MicroRNAs miR-19, miR-340, miR-374 and miR-542 regulate MID1 protein expression', *PLoS One*, 13: e0190437.
- Vaccaro, A., S. A. Patten, D. Aggad, C. Julien, C. Maios, E. Kabashi, P. Drapeau, and J. A. Parker. 2013. 'Pharmacological reduction of ER stress protects against TDP-43 neuronal toxicity in vivo', *Neurobiol Dis*, 55: 64-75.
- van Es, Michael A., Orla Hardiman, Adriano Chio, Ammar Al-Chalabi, R. Jeroen Pasterkamp, Jan H. Veldink, and Leonard H. van den Berg. 2017. 'Amyotrophic lateral sclerosis', *The Lancet*, 390: 2084-98.
- Van Langenhove, T., J. van der Zee, and C. Van Broeckhoven. 2012. 'The molecular basis of the frontotemporal lobar degeneration-amyotrophic lateral sclerosis spectrum', *Ann Med*, 44: 817-28.
- Vance, C., B. Rogelj, T. Hortobagyi, K. J. De Vos, A. L. Nishimura, J. Sreedharan, X. Hu, B. Smith, D. Ruddy, P. Wright, J. Ganesalingam, K. L. Williams, V. Tripathi, S. Al-Saraj, A. Al-Chalabi, P. N. Leigh, I. P. Blair, G. Nicholson, J. de Belleruche, J. M. Gallo, C. C. Miller, and C. E. Shaw. 2009. 'Mutations in FUS, an RNA processing protein, cause familial amyotrophic lateral sclerosis type 6', *Science*, 323: 1208-11.
- Voigt, A., D. Herholz, F. C. Fiesel, K. Kaur, D. Muller, P. Karsten, S. S. Weber, P. J. Kahle, T. Marquardt, and J. B. Schulz. 2010. 'TDP-43-mediated neuron loss in vivo requires RNA-binding activity', *PLoS One*, 5: e12247.
- Wang, L., B. Popko, and R. P. Roos. 2011. 'The unfolded protein response in familial amyotrophic lateral sclerosis', *Hum Mol Genet*, 20: 1008-15.
- . 2014. 'An enhanced integrated stress response ameliorates mutant SOD1-induced ALS', *Hum Mol Genet*, 23: 2629-38.
- Wang, W., L. Wang, J. Lu, S. L. Siedlak, H. Fujioka, J. Liang, S. Jiang, X. Ma, Z. Jiang, E. L. da Rocha, M. Sheng, H. Choi, P. H. Lerou, H. Li, and X. Wang. 2016. 'The inhibition of TDP-43 mitochondrial localization blocks its neuronal toxicity', *Nat Med*, 22: 869-78.



- Wegorzewska, I., S. Bell, N. J. Cairns, T. M. Miller, and R. H. Baloh. 2009. 'TDP-43 mutant transgenic mice develop features of ALS and frontotemporal lobar degeneration', *Proc Natl Acad Sci U S A*, 106: 18809-14.
- Wils, H., G. Kleinberger, J. Janssens, S. Pereson, G. Joris, I. Cuijt, V. Smits, C. Ceuterick-de Groote, C. Van Broeckhoven, and S. Kumar-Singh. 2010. 'TDP-43 transgenic mice develop spastic paralysis and neuronal inclusions characteristic of ALS and frontotemporal lobar degeneration', *Proc Natl Acad Sci U S A*, 107: 3858-63.
- Winter, J., M. F. Basilicata, M. P. Stemmler, and S. Krauss. 2016. 'The MID1 protein is a central player during development and in disease', *Front Biosci (Landmark Ed)*, 21: 664-82.
- Wu, Y., J. Xu, J. Xu, J. Cheng, D. Jiao, C. Zhou, Y. Dai, and Q. Chen. 2017. 'Lower Serum Levels of miR-29c-3p and miR-19b-3p as Biomarkers for Alzheimer's Disease', *Tohoku J Exp Med*, 242: 129-36.
- Xu, Y. F., T. F. Gendron, Y. J. Zhang, W. L. Lin, S. D'Alton, H. Sheng, M. C. Casey, J. Tong, J. Knight, X. Yu, R. Rademakers, K. Boylan, M. Hutton, E. McGowan, D. W. Dickson, J. Lewis, and L. Petrucelli. 2010. 'Wild-type human TDP-43 expression causes TDP-43 phosphorylation, mitochondrial aggregation, motor deficits, and early mortality in transgenic mice', *J Neurosci*, 30: 10851-9.
- Yamashita, T., T. Hideyama, K. Hachiga, S. Teramoto, J. Takano, N. Iwata, T. C. Saido, and S. Kwak. 2012. 'A role for calpain-dependent cleavage of TDP-43 in amyotrophic lateral sclerosis pathology', *Nat Commun*, 3: 1307.
- Yoshimura, S., A. Gerondopoulos, A. Linford, D. J. Rigden, and F. A. Barr. 2010. 'Family-wide characterization of the DENN domain Rab GDP-GTP exchange factors', *J Cell Biol*, 191: 367-81.
- Youmans, K. L., and B. Wolozin. 2012. 'TDP-43: a new player on the AD field?', *Exp Neurol*, 237: 90-5.
- Zanchetta, M. E., L. M. R. Napolitano, D. Maddalo, and G. Meroni. 2017. 'The E3 ubiquitin ligase MID1/TRIM18 promotes atypical ubiquitination of the BRCA2-associated factor 35, BRAF35', *Biochim Biophys Acta*, 1864: 1844-54.
- Zu, T., B. Gibbens, N. S. Doty, M. Gomes-Pereira, A. Huguet, M. D. Stone, J. Margolis, M. Peterson, T. W. Markowski, M. A. Ingram, Z. Nan, C. Forster, W. C. Low, B. Schoser, N. V. Somia, H. B. Clark, S. Schmechel, P. B. Bitterman, G. Gourdon, M. S. Swanson, M. Moseley, and L. P. Ranum. 2011. 'Non-ATG-initiated translation directed by microsatellite expansions', *Proc Natl Acad Sci U S A*, 108: 260-5.
- Zu, T., Y. Liu, M. Banez-Coronel, T. Reid, O. Pletnikova, J. Lewis, T. M. Miller, M. B. Harms, A. E. Falchook, S. H. Subramony, L. W. Ostrow, J. D. Rothstein, J. C. Troncoso, and L. P. Ranum. 2013. 'RAN proteins and RNA foci from antisense transcripts in C9ORF72 ALS and frontotemporal dementia', *Proc Natl Acad Sci U S A*, 110: E4968-77.

# Appendix 1a

	wt_fp_1	wt_fp_2	wt_total_1	wt_total_2	hwt_fp_1	hwt_fp_2	hwt_fp_3	hwt_total_1	hwt_total_2	hwt_total_3	a315_fp_1	a315_fp_2	a315_fp_3	a315_total_1	a315_total_2	a315_total_3
Name	#Reads	#Reads	#Reads	#Reads	#Reads	#Reads	#Reads	#Reads	#Reads	#Reads	#Reads	#Reads	#Reads	#Reads	#Reads	#Reads
n_total	17746085	9832209	17550926	4830006	2533986	2785088	24010119	5173567	6691831	36714853	7183368	17307566	32906918	11393273	18409966	32529582
n_posttrim	16854149	9329002	15627377	40553904	2495372	2582964	23698096	5019507	6263766	36235606	6830426	16460812	32406392	10788733	16997503	32305941
n_ncrna_contaminants	6177176	3365098	6296459	17225929	859531	1053736	4212743	1816949	2762751	8274102	1369466	6303453	7636479	2895995	6268336	9238885
n_reads_of_interest	10676973	5963904	9330918	23327975	1635841	1529228	19485353	3202558	3501015	27961504	5460960	10157359	24769913	7892738	10729167	23067056
n_mapped_multi	4729750	2721738	6293448	13426602	719436	690167	7622582	1982040	2001139	14751864	1772980	4672345	8863861	4726974	6876287	11827235
n_mapped_uni	1809156	1236253	1313303	5784884	289020	285308	2844694	482655	785522	3805295	726815	2068276	3689904	1098055	1602159	3050269
n_mapped_uni_4err	2920594	1485485	4980145	7641718	430416	404859	4777888	1499385	1215617	10946569	1046165	2604069	5173957	3628919	5274128	8776966
n_mapped_uni_3err	50923	50349	10462	38952	12710	13446	69403	4437	6547	36133	37669	104868	26374	15935	16014	31226
n_mapped_uni_2err	132184	85742	51439	211042	24396	22122	232625	22831	33264	253172	51422	153341	225422	66239	82499	203180
n_mapped_uni_1err	158966	82234	136611	401295	25154	20852	214680	50048	63780	487386	57790	148110	232476	139012	155833	405827
n_mapped_uni_0err	753145	397297	968504	2025582	119732	104244	1562667	309351	310074	2286012	341073	832979	2035950	717142	930356	1973458
n_assigned_pc	1825376	869863	3813129	4964847	248424	244195	2698513	1112718	801952	7883866	558211	1364771	2653735	2690591	4089426	6163275
	1304116	575476	3609519	3206139	192008	166064	2389229	986092	600385	6969578	473805	1042983	2528820	2353325	3456956	5395138
	1249518	525794	3515283	2866086	180122	147189	2263228	953083	548437	6661359	442153	906093	2379213	2263934	3345664	5118898

## Appendix 1b

Name	control_fp		control_fp		control_		control_		a315_fp_		a315_total		hwt_fp_1		hwt_total	
	#Reads	#Reads	#Reads	#Reads	#Reads	#Reads	#Reads	#Reads	#Reads	#Reads	#Reads	#Reads	#Reads	#Reads	#Reads	#Reads
n_total	10149706	13278394	8011534	1.2E+07	15096843	9111530	17305020	12437698	5881432	4996996	7749899	6113229				
n_posttrim	10114152	13130197	7882656	1.2E+07	14577603	8945876	16342011	11972494	5862879	4951312	7706814	6067703				
n_ncrna_																
contamina																
nts	1792892	2264562	4000498	4280714	3131399	1499136	7007136	5060412	713953	1008605	2894637	1801327				
n_reads_of																
_interest	8321260	10865635	3882158	7513543	11446204	7446740	9334875	6912082	5148926	3942707	4812177	4266376				
n_mapped	3396726	3427540	2826127	4879135	4549446	2265054	6154481	4156877	2125502	1321331	3388803	2727263				
n_mapped	1480606	1570278	767994	1342916	1944831	1025209	1685560	1162759	892812	578290	903668	728595				
n_mapped	1916120	1857262	2058133	3536219	2604615	1239845	4468921	2994118	1232690	743041	2485135	1998668				
n_mapped	7524	55568	1167	24378	13248	12866	16912	22397	6799	26305	4093	14157				
n_mapped	78442	87246	23107	99726	140582	48900	97768	81452	53471	35346	43038	53991				
n_mapped	76250	112982	70222	212894	100356	55056	212426	170984	51972	44211	109078	114988				
n_mapped	800813	774163	474126	1097036	1191244	611028	1116441	916880	500841	324242	599577	606299				
n_mapped	953091	827303	1489511	2102185	1159185	511995	3025374	1802405	619607	312937	1729349	1209233				
n_assigned	940822	849125	1462713	2329298	1219222	521904	2988339	1912457	631354	332370	1720465	1328528				
n_assigned	879205	773380	1411590	2198608	1110305	489789	2834508	1800769	590016	301208	1647130	1258453				
_pc																

## Appendix 2

Sample info	5UTR_Total lLength	5UTR_Total Count	5UTR_Counts PerKb	CDS_Total Length	CDS_Total Count	CDS_Counts PerKb	3UTR_Total Length	3UTR_Total Count	3UTR_Counts PerKb
MN1-control-totalmRNA 1	6393671	136902	21.41	36291559	872743	24.05	30684926	554967	18.09
MN1-control-FP 1	6393671	98187	15.36	36291559	733910	20.22	30684926	153305	5
MN1-hTDP-43-total mRNA 1	6393671	170740	26.7	36291559	1028078	28.33	30684926	630110	20.53
MN1-hTDP-43- FP 1	6393671	70369	11.01	36291559	481576	13.27	30684926	107796	3.51
MN1-hTDP-43 <sup>A315T</sup> - total mRNA 1	6393671	315156	49.29	36291559	1762534	48.57	30684926	1067689	34.8
MN1-hTDP-43 <sup>A315T</sup> - FP 1	6393671	136056	21.28	36291559	904164	24.91	30684926	174727	5.69
MN1-control-totalmRNA 2	6393671	245778	38.44	36291559	1359803	37.47	30684926	840582	27.39
MN1-control-FP 2	6393671	109436	17.12	36291559	685931	18.9	30684926	120147	3.92
MN1-hTDP-43-total mRNA 2	6393671	148291	23.19	36291559	790665	21.79	30684926	463929	15.12
MN1-hTDP-43- FP 2	6393671	45657	7.14	36291559	269427	7.42	30684926	39289	1.28
MN1-hTDP-43 <sup>A315T</sup> - total mRNA 2	6393671	209394	32.75	36291559	1096185	30.2	30684926	685817	22.35
MN1-hTDP-43 <sup>A315T</sup> - FP 2	6393671	68903	10.78	36291559	414769	11.43	30684926	72500	2.36
Primary neuron- hTDP-43-total mRNA 1	6393671	547880	85.69	36291559	3537011	97.46	30684926	3117201	101.59
Primary neuron-hTDP-43- FP 1	6393671	205167	32.09	36291559	2046110	56.38	30684926	282700	9.21
Primary neuron- hTDP-43 <sup>A315T</sup> - total mRNA 1	6393671	416491	65.14	36291559	2694234	74.24	30684926	2409804	78.53
Primary neuron- hTDP-43 <sup>A315T</sup> - FP 1	6393671	219309	34.3	36291559	2035937	56.1	30684926	364865	11.89
Primary neuron-control-totalmRNA 2	6393671	297753	46.57	36291559	1981032	54.59	30684926	1559437	50.82
Primary neuron-control-FP 2	6393671	110815	17.33	36291559	1089045	30.01	30684926	203346	6.63
Primary neuron- hTDP-43-total mRNA 2	6393671	97451	15.24	36291559	543264	14.97	30684926	396801	12.93
Primary neuron-hTDP-43- FP 2	6393671	16985	2.66	36291559	161958	4.46	30684926	23131	0.75
Primary neuron- hTDP-43 <sup>A315T</sup> - total mRNA 2	6393671	189336	29.61	36291559	1234323	34.01	30684926	1038832	33.85
Primary neuron- hTDP-43 <sup>A315T</sup> - FP 2	6393671	39327	6.15	36291559	400308	11.03	30684926	54851	1.79
Primary neuron-control-totalmRNA 3	6393671	219163	34.28	36291559	1325671	36.53	30684926	1425590	46.46
Primary neuron-control-FP 3	6393671	53599	8.38	36291559	459173	12.65	30684926	66940	2.18
Primary neuron- hTDP-43-total mRNA 3	6393671	43534	6.81	36291559	273867	7.55	30684926	262586	8.56
Primary neuron-hTDP-43- FP 3	6393671	16060	2.51	36291559	129718	3.57	30684926	18681	0.61
Primary neuron- hTDP-43 <sup>A315T</sup> - total mRNA 3	6393671	284857	44.55	36291559	1892342	52.14	30684926	1458179	47.52
Primary neuron- hTDP-43 <sup>A315T</sup> - FP 3	6393671	97083	15.18	36291559	829939	22.87	30684926	102327	3.33

## Appendix 3

GFP vs A315T	GFP vs hTDP-43	hTDP vs A315T
Rnu5g	Gm23143	Mir6236
Gm25313	Mir6236	E2f5
Gm23143	Crx	Crx
Gm23287		Cybb
E2f5		Pip5kl1
Jmjd6		Srxn1
Sspo		Epha8
Srxn1		Adarb2
Rpph1		Jmjd6
D630039A03Rik		Gm24270
Plxdc2		Tspan5
Cybb		Camta1
Epha8		Pth1r
Mid1ip1		Dennd4a
Adarb2		Epha5
Pip5kl1		Sorbs3
Sorbs3		Ttll11
Gm24270		
Pth1r		
Zfp36		
Crx		
Tspan5		
Dennd4a		
Epha5		
Ttll11		
Camta1		

## Appendix 4

WT vs A315T	WT vs hTDP-43	hTDP vs A315T
Nfkb1	Nfkb1	3110007F17Rik
Gm12896	Rfx1	Peo1
Stag3	Gpr45	Sspo
Tma16	B4galt2	Tnfrsf11a
Gm12054	mt-Tf	Slc7a3
Grk1	Bbc3	Itgal
mt-Tf	Pip5k11	Rny3
Gpr45	Gon4l	Rfc1
Pcdhb10	Ip6k3	Mid1ip1
Rfx1	Ankrd60	Gm25313
Tma7	Cyp26b1	Mcm7
Rer1	Grk1	Gm25099
Rspo2	Mettl23	Irf8
Atic	Kl	Fgg
Slc46a1	Slc46a1	Pth1r
Cyp26b1	Slc44a2	Dnajc21
Fam167a	Tollip	D630039A03Rik
Rny3	Rfxap	
Rnf214	Rer1	
Ttyh1	Stag3	
Egr1	Slc25a38	
Fos	Tlx3	
Mir6240	Lzts3	
Npas4	Till6	
Rfc1	Gm12054	
Car9	Taf5l	
Arc	Rassf3	
Hes7	Peo1	
Nr4a1	Gm12896	
Mid1ip1	Car9	
Gm37608	3110007F17Rik	
Epb4.2	Mcm7	
Rnf157	Fgg	
Pth1r	Tfrc	
Mcm7	Acan	
E2f5	Gm37608	
Fgg	Hes7	
Dnajc21	Fos	
Irf8	Pcsk1	
Nthl1	Nptx2	
Rn7s6	Pcdhgc5	
H2-BI	Fam167a	
RP24-274H19.3	Plagl1	
Gm24514	Arc	
Rnu12	H2-BI	
D630039A03Rik	Slc2a1	
	Gm24514	
	Rn7s6	
	RP24-274H19.3	
	Rnu12	
	D630039A03Rik	

## Appendix 5

GFP vs A315T	GFP vs hTDP-43	hTDP vs A315T
Gm25732	Csf2	Dek
Kif21b	Ttyh1	Kif5b
Irf2bp1	Camta1	Ddx51
Fchsd2	Tardbp	Fam167a
Gm14236	Gm13886	Lrr1
Gm15189		Lzts3
Rnf157		Opn3
Gm13886		Rassf3
		Elovl4
		Map7
		Ngef
		Irf2bp1
		Adamts1
		Ilvbl
		Kif21b
		Dpy19l1
		Cyr61
		Gm38198
		Gm15189
		Fchsd2
		Micalcl
		Dach1
		Csf2
		Stard8

## Appendix 6

WT vs A315T	WT vs hTDP-43	hTDP vs A315T
Tecrl	RP23-162P5.1	RP23-227D7.1
Gm4825	Dlk1	Lhx9
Lhx9	Gm28043	Sspo
RP23-227D7.1	Gm24265	Rfc1
Sspo	mt-Tc	Neil2
4930595D18Rik	mt-Tf	Col17a1
RP23-162P5.1	1200014J11Rik	Nid1
Neil2	mt-Ta	Fgg
Gm12830	Hes7	RP24-274H19.3
Cd82	Car9	n-R5-8s1
Rfc1	4930595D18Rik	
Gm15280	Ccdc36	
Nid1	Vaultrc5	
Ndufs7	1700067K01Rik	
Il18rap	Tll6	
Col17a1	B230208H11Rik	
Gm28043	Tecrl	
B230208H11Rik	Nuak2	
Nek11	Nid1	
mt-Tf	Gm12830	
mt-Tc	lp6k3	
Lrp4	Neil2	
mt-Ta	Gm15280	
Efna1	Cd82	
Fgg	Lhx9	
Casr	Fgg	
Car9	Pdzd7	
Vaultrc5	Aim1l	
1700067K01Rik	Casr	
Rictor	Rictor	
RP24-274H19.3	Col17a1	
Aim1l	RP23-227D7.1	
Irf8	Il18rap	
Ttyh1	Gm4825	
Fam186a	Nek11	
Hes7	RP24-141D20.1	
Gm24265	Lrp4	
RP24-141D20.1	Efna1	
Nuak2	Fosb	
4933413G19Rik		
Mir1983		
1200014J11Rik		
Tlx3		
Adarb2		
Csf2		
Zfyve26		



Blm
Ip6k3
mt-Tw
Prkch
Gm23153
Myh8
Cyr61
Cybb
mt-Tv
Pdzd7
Sema3e
Sfrp2
Dnah17
Stard8
Rmrp
mt-Tp
Gm37608
Gm11649
Dlk1
Cbx8
Zcchc3
Rnf113a2
Zkscan5
Gm24359
Lrr1
Man2b2
Jade2
RP24-378G4.3
Rfxap
Ccdc36
Stag3

## Appendix 7

	sequenced	after trimming		after rRNA subtraction		after rRNA+ncRNA subtr.		aligning to CDS	
<b>Ia</b>	31,636,444	27,671,702	87.47%	13,059,427	47.19%	12,178,261	44.01%	2,013,600	16.53%
<b>Ib</b>	26,775,828	22,553,492	84.23%	11,288,658	50.05%	10,550,555	46.78%	1,761,926	16.70%
<b>IIa</b>	51,969,888	42,605,626	81.98%	20,817,893	48.86%	19,520,283	45.82%	3,084,361	15.80%
<b>IIb</b>	29,354,794	24,383,011	83.06%	12,828,683	52.61%	12,057,923	49.45%	1,909,552	15.84%
<b>IIIa</b>	19,195,857	17,873,708	93.11%	3,022,331	16.91%	2,677,910	14.98%	537,460	20.07%
<b>IIIb</b>	28,841,523	25,746,260	89.27%	12,105,912	47.02%	11,222,724	43.59%	2,905,987	25.89%
<b>IVa</b>	23,504,673	21,120,595	89.86%	3,870,154	18.32%	3,522,190	16.68%	537,938	15.27%
<b>IVb</b>	19,706,098	17,126,048	86.91%	5,564,538	32.49%	5,195,791	30.34%	893,660	17.20%
<b>Va</b>	30,100,069	28,210,581	93.72%	5,068,007	17.96%	4,477,695	15.87%	655,226	14.63%
<b>Vb</b>	11,856,454	10,368,174	87.45%	3,099,952	29.90%	2,826,403	27.26%	481,263	17.03%
<b>VIa</b>	30,192,366	24,778,729	82.07%	4,594,232	18.54%	4,084,712	16.48%	767,408	18.79%
<b>VIb</b>	16,247,557	11,019,984	67.83%	4,086,742	37.08%	3,760,208	34.12%	834,307	22.19%

## **Eidesstattliche Versicherung**

Declaration on oath

**Hiermit erkläre ich an Eides statt, dass ich die vorliegende Dissertationsschrift selbst verfasst und keine anderen als die angegebenen Quellen und Hilfsmittel benutzt habe.**

I hereby declare, on oath, that I have written the present dissertation by my own and have not used other than the acknowledged resources and aids.

Hamburg, den

Unterschrift



Universitätsklinikum Hamburg-Eppendorf  
Zentrum für Molekulare Neurobiologie Hamburg  
Forschungsgruppe:  
Neuronale Translationskontrolle

Dr. Kent Duncan  
Forschungsgruppenleiter  
Martinistraße 52  
D-20246 Hamburg  
Gebäude S50, Raum 3.23  
Telefon: +49 (0) 40 7410-56274  
Fax: +49 (0) 40 7410-53436  
Kent.Duncan@zmnh.uni-hamburg.de  
www.uke.de/zmnh  
Hausanschrift:  
Falkenried 94 / Martinistr. 85  
D-20251 Hamburg

Universitätsklinikum Hamburg-Eppendorf | Martinistraße 52 | 20246 Hamburg  
Zentrum für Molekulare Neurobiologie | Forschungsgruppe Dr. Kent Duncan

## English Language Thesis Certification: Nagammal Neelagandan

Hamburg, 09.01.2019

To whom it may concern:

**Nagammal Neelagandan**, who was born on 10<sup>th</sup> June 1992 and has matriculation number 6749678, is submitting her doctoral dissertation in English. The title of her thesis is: ***'Genome-wide ribosome profiling reveals a translational enhancer function for TDP-43 in cellular models of neurodegenerative disease'***.

I hereby certify as a native speaker and molecular biologist that the English language used in this thesis is sufficiently correct for submission.

Yours truly,

**Kent Duncan, Ph.D.**

Universität Hamburg  
Universitätsklinikum Hamburg-Eppendorf  
Zentrum für Molekulare Neurobiologie  
AG Duncan  
Falkenried 94 · D-20251 Hamburg



Universitätsklinikum Hamburg-Eppendorf  
Körperschaft des öffentlichen Rechts  
Gerichtsstand: Hamburg  
USI-ID-Nr.: DE21 8618 948

Vorstandsmitglieder:  
Prof. Dr. Burkhard Göke (Vorsitzender)  
Prof. Dr. Dr. Uwe Koch-Gromus  
Joachim Pröls | Rainer Schoppik

Bankverbindung:  
HSH Nordbank  
IBAN-Nr.: DE97210500000104364000  
BIC: HSHNDEHH